Dynamics and variability of SMAD signaling in single cells-

The activity of MAP kinases determines long-term dynamics of SMAD signaling

DISSERTATION

zur Erlangung des akademischen Grades

d o c t o r r e r u m n a t u r a l i u m

(Dr. rer. nat.)

im Fach Biologie

eingereicht an der

Lebenswissenschaftlichen Fakultät

der Humboldt-Universität zu Berlin

von

Diplom-Biologin Henriette Sophie Strasen

Präsidentin der Humboldt-Universität zu Berlin

Prof. Dr.-Ing. Dr. Sabine Kunst

Dekan der Lebenswissenschaftlichen Fakultät

Prof. Dr. Bernhard Grimm

Gutachter/innen:	Prof. Dr. Alexander Löwer
	Prof. Dr. Andreas Herrmann
	Prof. Dr. Dr. h.c. Edda Klipp
Tag der mündlichen Prüfung:	06.06.2019

“Überall geht ein frühes Ahnen dem späteren Wissen voraus.”

- Alexander von Humboldt

Table of Contents

1 ABSTRACT

The TGFβ pathway is a multi-functional signaling system regulating cellular processes ranging from proliferation and migration to differentiation and cell death. Upon ligand binding and receptor activation, SMAD proteins translocate to the nucleus and induce expression of numerous target genes. While many components of the TGFβ pathway have been identified, we are still challenged to understand how pathway activation is translated into distinct cellular responses. As the cellular response to a given stimulus often varies even in genetically identical cells, I focused on measuring pathway activity on the single cell level. By combining fluorescent reporter cell lines with time-lapse live-cell microscopy and automated image analysis, I monitored the cytoplasmic to nuclear translocation of SMADs with high temporal and spatial resolution in hundreds of individual cells. Our experiments demonstrated that pathway activity can be divided into a first synchronous phase of SMAD translocation, followed by adaptation and a second signaling phase with high variability in the extent and duration of nuclear accumulation. Furthermore, I observed that cells clustered into subpopulations according to their dynamic features show different phenotypic responses. I was interested in identifying the network interactions that shape these dynamics and focus on crosstalk with non-canonical components of the TGFβ pathway. I could show that inhibition of the MAP kinases p38 and ERK specifically abrogates the second signaling phase. This dynamic remodeling led to changes in target gene expression and cell fate decisions. I explored the molecular mechanisms underlying this interaction of the canonical and non-canonical pathways. This will provide a deeper understanding of the molecular networks regulating TGFβ signaling and open opportunities to modulate it in diseased cells.

1.1 Zusammenfassung

Der TGFβ-Signalweg ist ein multifunktionales System, das zelluläre Prozesse reguliert, die von Proliferation und Migration bis zu Differenzierung und Zelltod reichen. Nach Ligandenbindung und Rezeptoraktivierung translozieren SMAD-Proteine zum Zellkern und induzieren die Expression zahlreicher Zielgene. Während viele Komponenten des TGFβ-Signalweges identifiziert wurden, verstehen wir noch nicht genau, wie die Aktivierung des Signalwegs in verschiedene zelluläre Antworten übersetzt wird. Da die zelluläre Antwort auf einen gegebenen Stimulus oft sogar in genetisch identischen Zellen variiert, konzentrierte ich mich auf die Messung der Signalwegaktivität auf der Einzelzellebene. Durch die Kombination fluoreszierender Reporterzelllinien mit Zeitraffer-Lebendzellmikroskopie und automatisierter Bildanalyse beobachtete ich die zytoplasmatische und

nukleäre Translokation von SMADs mit hoher zeitlicher und räumlicher Auflösung in Hunderten einzelner Zellen. Unsere Experimente zeigten, dass die Signalwegaktivität in eine erste synchrone Phase der SMAD-Translokation, gefolgt von einer Adaption und einer zweiten Signalphase mit hoher Variabilität in Stärke und Dauer der nuklearen Akkumulation unterteilt werden kann. Darüber hinaus beobachtete ich, dass Zellen, die aufgrund ihrer dynamischen Eigenschaften in Subpopulationen gruppiert sind, unterschiedliche phänotypische Reaktionen zeigen. Ich war nun daran interessiert, die Netzwerkinteraktionen zu identifizieren, die diese Dynamiken formen und fokussierte mich auf den Crosstalk mit nicht-kanonischen Komponenten des TGFβ-Signalweges. Ich konnte zeigen, dass die Hemmung der MAP Kinasen p38 und ERK die zweite Signalphase spezifisch aufhebt. Diese dynamische Remodellierung führt zu Veränderungen in der Zielgenexpression und den Zellschicksalen. Ich untersuchte außerdem die molekularen Mechanismen, die dieser Wechselwirkung der kanonischen und nicht-kanonischen Wege zugrunde liegen. Dies wird zu einem tieferen Verständnis der molekularen Netzwerke führen, die die TGFβ-Signaltransduktion regulieren und Möglichkeiten eröffnen, es in erkrankten Zellen zu modulieren.

2 INTRODUCTION

2.1 Signaling dynamics in individual cells

A fundamental property of living cells is the ability to detect, process and respond appropriately to altering environmental conditions and numerous other stimuli. Recent studies reveal that cells can send and receive information by controlling the temporal behavior ("dynamics") of their signaling proteins, which subsequently induce corresponding programs of gene expression that modulate cell behavior (Purvis & Lahav, 2013). Characterizing the quantity, localization and activity of proteins with high temporal and spatial resolution is therefore critical for understanding molecular mechanisms of cellular processes, including those involved in disease progression, and for targeted discovery and development of novel therapeutics, vaccines and diagnostics. This mode of signaling encodes information in the frequency, amplitude, duration or other features of the temporal signal. It is therefore richer and more complex than transmitting information through the state of a signaling molecule at only a single point in time (Purvis & Lahav, 2013). These data are complementary to the information provided by genetics, genomics and proteomics of describing the structure of biological networks and have great potential to provide new insight into the relationship between network architecture and function. One promising technique to measure the *dynamics* of key proteins within the network is using high-resolution live-cell imaging of fluorescent reporters (Spiller *et al*, 2010). This technology allows to determine the quantity and even the subcellular localization of specific proteins in living cells. The dynamics of signaling proteins can be investigated across a population of cells or in individual cells. Cells are heterogeneous in nature and hence, population-averaged data can mask the underlying molecular mechanisms, since genetically identical cells differ widely in their dynamical behaviors even when challenged with the same external stimulus (Cohen *et al,* 2008; Lee *et al,* 2009; Batchelor *et al*, 2009; Spiller *et al*, 2010). A well-known example is the response of bacteria to antibiotics, at certain doses some cells live while others die (Cohen *et al,* 2008).

Moreover, one of the unanswered questions in cancer therapy has been why essentially identical cells respond differently to a drug. Single-cell level analyses of proteins have already revealed valuable insight into mechanisms that dictate heterogeneity in cellular response to drugs and other external stimuli (Paek *et al*, 2016).

For instance, it was shown that dynamics of tumor suppressor protein p53 in response to DNA damage derived from population studies measured by western blot was misleading (Lev Bar-Or *et al*, 2000; Batchelor *et al*, 2009). Instead of damped oscillations seen in population- averaged data, observation

of single cells revealed series of undamped p53 pulses with fixed height and duration, independent of the amount of γ-irradiation (Lahav *et al*, 2004).

Similarly, the transcription factor nuclear factor kappa B (NF-κB) in single cells shows variability in the oscillatory dynamics of nuclear localization upon stimulation (Hoffmann *et al*, 2002; Nelson *et al*, 2004).

Moreover, single cell analyses are crucial for stem cell research as decisions in individual cells determines their cellular outcome. For instance, in hematopoietic stem cells it is reported, by studying the varying levels of Sca-1 protein in individual cells, that Sca-1 protein abundance determines the timing and type of differentiation (Chang *et al*, 2008).

Hence, single cell analyses of signaling systems have already revealed important information about the role of dynamics in regulating various cellular fates. It has been reported that the dynamics of p53 play a role in the specificity of the response with pulsed p53 favoring DNA repair and cell-cycle arrest genes, and sustained p53 triggering activation of senescence and apoptotic genes (Batchelor *et al*, 2011; Purvis *et al*, 2012). Another example is found in the dynamics of ERK activity, where two separate growth factors trigger different ERK dynamics and thus different cell fates of rat neuronal precursors. Specifically, epidermal growth factor (EGF) triggers a transient response leading to cell proliferation, whereas nerve growth factor (NGF) induces sustained ERK activation leading to differentiation (Marshall, 1995). Similarly, different inflammatory stimuli induce distinct temporal dynamics of the transcription factor NF-κB. Thus, activation by tumor necrosis factor-α (TNFα) generates oscillations of transcriptionally active NF- kB and single cell analysis of luciferase expression from a synthetic NF-κB responsive promoter suggested that the pulses determine the degree and timing of downstream gene expression (Hoffmann *et al*, 2002; Nelson *et al*, 2004; Sung *et al*, 2009; Tay *et al*, 2010). On the other hand, bacterial lipopolysaccharide (LPS) leads to slower accumulation and a single prolonged wave of NF-κB activity (Covert *et al*, 2005; Lee *et al*, 2009; Werner *et al*, 2005). Moreover, stimulus strength and patterns influence the dynamics of NF-κB activity. Increasing the concentration of TNFα reveals a shortened delay in NF-κB nuclear translocation (Cheong *et al*, 2006; Tay *et al*, 2010) and increasing the frequency of TNFα stimulation reveals smaller amplitude oscillations (Ashall *et al*, 2009).

These different outcomes might reflect differences in the initial state of the cell, including cell cycle stage, external influences such as the local environment, basal level of network components or stochastic intracellular events (Loewer & Lahav, 2011; Snijder & Pelkmans, 2011), which in turn lead to variation in the quantitative behavior of the information-processing network. By visualizing the dynamical behavior and identifying how it varies among cells (or cell types), we might be able to explain varying behaviors both within cell populations and in different cell types.

Thus, cellular fates upon TGFβ (transforming growth factor beta) stimulation are manifold and vary amongst various cell types and environmental conditions (Sporn *et al*, 2006). Even though the main molecular components of the canonical and the non-canonical TGFβ signaling pathways have been largely studied, the mechanism that underlies the well-established context dependent physiological responses remains largely unexplored. Therefore, recent studies quantitatively characterized several mechanisms shaping the temporal dynamics of SMAD signaling, the main components of TGFβ signaling transduction (Clarke & Liu, 2008; Schmierer *et al*, 2008; Zi *et al*, 2012). The duration and pattern of SMAD signaling response are context dependent. Thus, it has been reported that keratinocyte epithelial cells reveal sustained phospho-SMAD responses to TGFβ stimulation, while some fibroblast and tumor cells expose transient SMAD activation (Nicolas & Hill, 2003; Ahn *et al*, 2011). It was hypothesized that sustained TGFβ signaling may be required for cell cycle arrest, while transient signaling may cause the resistance to anti-proliferative effects of TGFβ in certain tumor cells (Nicolas & Hill, 2003). However, previous quantitative studies of SMAD dynamics mainly focused on the average behavior of a cell population at defined time points, whereas the long-term response at the level of single cells with high temporal und spatial resolution is not well characterized. Recent studies showed that SMAD nuclear translocation of fluorescently labeled SMAD proteins revealed high variability in individual cells (Warmflash *et al*, 2012; Zieba *et al*, 2012).

However, to understand how TGFβ signaling elicits defined responses in a cell-specific and concentration-dependent manner, we need to systematically characterize its dynamics on the single-cell level and detect the underlying molecular interactions that shape the dynamic response. This would allow us to predict how single cells respond to specific inputs and to design targeted perturbations of the TGFβ pathway to exploit its role for therapeutic treatments, such as personalized cancer medicine (Strasen *et al*, 2018).

2.2 Diverse effects of TGFβ signaling and a dual role in cancer

Members of the TGFβ superfamily are multifunctional cytokines and important regulators of many fundamental cellular and developmental processes, including cell cycle arrest, differentiation, morphogenesis and apoptosis, as well as cancer progression (Massagué, 1998; Whitman, 1998, Piek *et al*, 1999, Siegel & Massagué, 2003). The TGFβ superfamily is subdivided into two branches: (1) the TGFβ branch and (2) the Bone Morphogenetic Protein (BMP) branch.

Considering TGFβ signaling, the effects vary according to the cell type and the environmental and physiological conditions (Moustakas & Heldin, 2005; Massagué *et al*, 2000).

Thus, TGFβ is a potent growth inhibitor to most normal epithelial cells, however it can also promote proliferation of some fibroblastic cell lines, such as NIH 3T3 (Koskinen *et al*, 1991). One key event that

leads to TGFβ induced growth arrest is the induction of expression of the CDK inhibitors $p15^{INK4B}$ (Hannon & Beach, 1994; Reynisdóttir *et al,* 1995) and/or $p21^{CIP1}$(Datto *et al*, 1995).

Furthermore, TGFβ can mediate apoptosis in epithelial cells, hepatocytes (Herzer *et al*, 2005; Perlman *et al*, 2001) and induces expression and activation of the Fas receptor, leading to caspase-8 activation and apoptosis of gastric carcinoma cells (Kim *et al*, 2004). On the other hand, TGFβ has an anti-apoptotic function and can promote cell survival and differentiation (Derynck *et al*, 2001). Thus, abrogation of TGFβ signaling in T cells leads to spontaneous T-cell differentiation and autoimmune disease, indicating that TGFβ signaling is required for T-cell homeostasis (Gorelik, *et al*, 2000).

Morphogenetic responses to TGFβ members include epithelial -mesenchymal transitions (EMT) and cell migration, which are crucial during embryogenesis, development of fibrotic diseases and advanced carcinoma spreading. EMT is characterized by the disassembly of cell–cell contacts, remodeling of the actin cytoskeleton and separation of cells, which generates fibroblast-like cells that express mesenchymal markers and become more motile and invasive (Hay, 1995; Shook *et al*, 2003; Baum *et al*, 2008; Guan *et al*, 2009).

Whether cells undergo EMT or apoptosis in response to TGFβ is dependent on their cell cycle state, and TGFβ regulates the cell cycle via survivin (Lee *et al*, 2013).

TGFβ also plays a paradoxical dual role in tumorigenesis. During normal development and early stages of tumor formation, TGFβ exhibits a suppressive role by inducing cell cycle arrest, apoptosis and inhibiting tumor growth. However later on, with tumor progression, dedifferentiated tumor cells become refractory to the growth inhibition mediated by TGFβ, either because of genetic loss of TGFβ signaling components or downstream perturbation of the signaling pathway (Waite & Eng, 2003). Moreover, late-stage tumors often display increased TGFβ expression (Dalal *et al*, 1993) and secreted TGFβ protein enhances tumor immunosuppression and facilitates tumor angiogenesis, invasion and metastasis (Walker & Dearing, 1992, Connolly *et al*, 2012). Thus, TGFβ signaling plays a dual role in breast cancer, acting as a tumor suppressor in early carcinomas while promoting tumor metastasis in more advanced breast carcinoma (Hachim *et al*, 2016).

Studying the signaling mechanisms through which the diverse effects of TGFβ are mediated is therefore crucial to better understand various cellular processes and can form the basis for new disease treatments.

2.3 TGFβ signaling and SMAD translocation

There exist three different TGFβ isoforms in mammals, TGFβ1, 2 and 3, which are encoded by different genes and which all function through the same receptor signaling systems (Massagué, 1998). TGFβ1 is the prototypical ligand of the TGFβ superfamily and is translated into a proprotein that is

proteolytically cleaved into noncovalently linked mature TGFβ and latency-associated protein (LAP) (Annes *et al*, 2003, Blobe *et al*, 2000). The inactive LAP-TGFβ complex is bound to another protein called Latent TGFβ Binding Protein (LTBP) during the secretion process. LTBP binds the extracellular matrix and sequesters LAP-TGFβ (Annes *et al*, 2003). Thus, the matrix acts as a reservoir from which TGFβ can readily be mobilized without the need for new synthesis (Taipale *et al*, 1998). Through the activities of various proteases LAP and LTBP are cleaved to release the highly stable, bioactive TGFβ (Shi & Massagué, 2003). Thus, the inactive complex can be activated for example by the metalloproteases MMP-9 and MMP-2, which are frequently expressed by malignant cells, especially at sites of tumor cell invasion (Yu & Stamenkovic, 2000; Stamenkovic, 2000; Stetler-Stevenson, 2001). Therefore, various mechanisms regulate TGFβ activation in different physiological contexts. The active TGFβ1 ligand is a 25 kDa dimer, covalently linked by a disulfide bond between cysteine residues from each monomeric peptide.

TGFβ signals through association with a complex of two types of transmembrane serine/threonine kinases and binds first a homodimer of TGFβ type II receptors (TGFβRII) (Massagué, 1998). Binding of the ligand causes bridging of the preformed dimers of type II receptors and dimers of type I receptors to form heterotetrameric, active receptor complexes (Feng & Derynck, 2005). Within the active receptor complex, the TGFβRII, which is a constitutively active kinase, undergoes autophosphorylation, as well as catalyzes transphosphorylation of TGFβRI at several Ser and Thr residues in a domain that is rich in Glycine and Serine (Shi & Massagué, 2003). Phosphorylation of this GS-domain enables the recruitment of the receptor-regulated SMADs (R-SMADs) SMAD2 and SMAD3. Transphosphorylation of the TGFβRI activates kinase activity and the type I receptor then phosphorylates the R-SMADs at a C-terminal SSXS motif. Once phosphorylated, the R-SMADs form homotrimeric complexes or heterotrimeric complexes with the common mediator SMAD4 (Heldin *et al*, 1997, Shi & Massagué, 2003). Trimers of one SMAD4 molecule and two receptor-phosphorylated R-SMAD molecules are the predominant effectors. The complexes then translocate to the nucleus, where they regulate the transcription of TGFβ target genes, like PAI-1, SMAD7, SMAD6, TIEG, SnoN, c-myc, p21, Snail, in conjunction with other transcription factors to coordinate the cellular response. (Schmierer & Hill, 2007; Peinado *et al*, 2003; Subramaniam *et al*, 1995; Deheuninck & Luo, 2009; Boehm *et al*, 1999; Yan *et al*, 2009; Moustakas *et al*, 2002). A scheme is shown in **Figure 1**.

Within the nucleus, the SMAD complexes reversibly dissociate and the monomeric phospho-R-SMADs are dephosphorylated by a nuclear phosphatase (Lin *et al*, 2006), upon which they join the pool of R-SMADs available for nuclear export. The cycle of SMAD activation and deactivation persists for as long as receptors are active (Inman *et al*, 2002b).

In the basal state, R-SMADs are predominantly localized in the cytoplasm, whereas SMAD4 is distributed in both the cytoplasm and the nucleus. SMAD proteins consist of two well-conserved domains connected by a proline-rich linker that differs substantially between the different SMAD classes. The main function of the SMAD N-terminal domain, or "Mad homology 1" (MH1) domain, is to bind DNA, except for SMAD2 which cannot bind DNA directly (Massagué, 1998; Yagi *et al*, 1999; Chai *et al*, 2003; Shi *et al*, 1998). The C-terminal domain, or MH2 domain, mediates protein- protein interaction with numerous regulator and effector proteins, including the TGFβ receptors, certain cytoplasmic anchor proteins, lineage-specific DNA-binding cofactors and chromatin modifiers (Massagué, 1998). Whereas the MH1 and MH2 domains are functionally well characterized, much less is known about the role of the interdomain linker region. The linker region is phosphorylated by kinases such as mitogen-activated protein kinases (MAPKs), glycogen synthase kinase-3 (GSK-3) and cyclin-dependent kinases (cDKs) and is thus thought to integrate positive and negative regulatory inputs from other signaling pathways. Thus, CDK8/9-mediated phosphorylation in the linker region maximizes the transcriptional activity of R-SMADs by favoring interactions with co-activators (Alarcón *et al,* 2009). Likewise, in SMAD4, the region of the linker is involved in transcriptional activation, mediated by the coactivator histone acetyltransferase p300/ CBP (de Caestecker *et al,* 1997, de Caestecker *et al*, 2000). Moreover, GSK3 switches the linker region from a binding site for co- activators to a binding site for HECT family E3 ubiquitin ligases that mark R-SMADs for proteasome-mediated degradation (Aragón *et al,* 2011; Gao *et al*, 2009). Furthermore, phosphorylation of the R-SMADs in the linker region by extracellular signal-regulated kinases (ERKs) leads to sequestration of at least a proportion of the R-SMADs in the cytoplasm, even in the presence of a TGFβ signal (Kretzschmar *et al*, 1997; Kretzschmar *et al*, 1999). Therefore, the linker region has a function in regulating the subcellular localization of SMADs.

In conclusion, these phosphorylation events lead R-SMADs to peak transcriptional activity followed by degradation, constituting an activation-turnover switch in the SMAD signaling cycle.

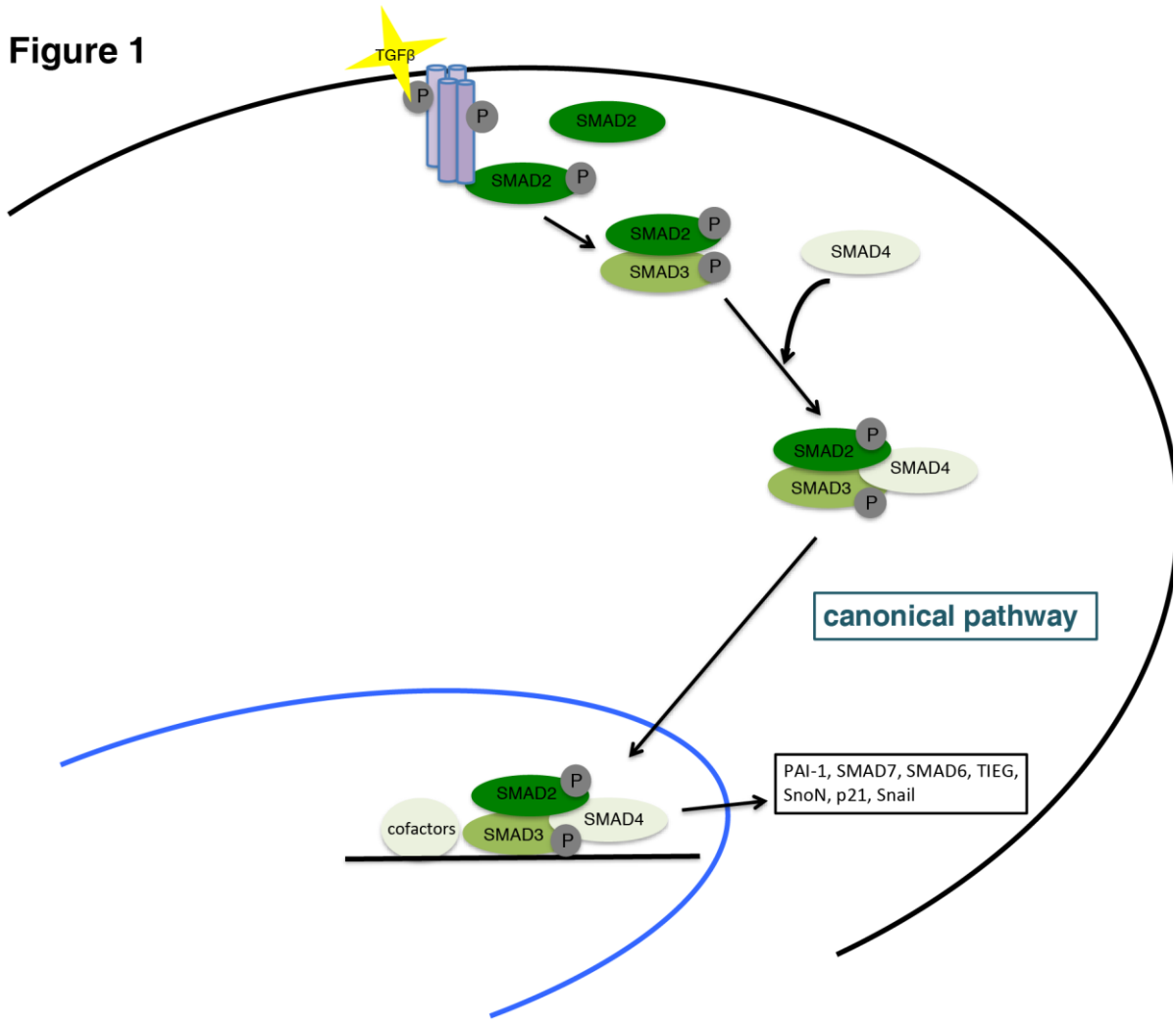

2.3 Figure 1. Scheme of canonical TGFβ pathway activation.
Scheme of the canonical TGFβ pathway. Extracellular TGFβ binds to TGFβ-receptors, thereby creating a binding platform for the proteins SMAD2 and 3. Binding of SMADs to the TGFβ receptors results in their phosphorylation and this leads to formation of complexes with SMAD4. These complexes then accumulate in the nucleus and regulate the expression of their target genes, like PAI-1, SMAD7, SMAD6, TIEG, SnoN, p21 and Snail.

2.4 Regulatory mechanisms and dynamics of SMADs

The fundamental step in TGFβ signaling is the translocation of the SMADs from the cytoplasm to the nucleus, however many regulatory mechanisms are involved to induce appropriate programs of gene expression, which in turn modulate cell behavior.

The responses of cells to TGFβ depend on the ligand concentration to which they are exposed (Clarke *et al*, 2008). Therefore, cells are somehow able to sense the concentration of TGFβ ligands at the exterior of the cell and orchestrate a specific response. How cells read, interpret and respond to TGFβ concentration is thus a question of important relevance to understanding TGFβ signaling.

In contrast to the rapid kinetics of signaling by tyrosine kinase receptors, the kinetics of SMAD phosphorylation are slow with SMAD2 phosphorylation peaking about 1 hour after ligand exposure,

then declining over the next hours (Schmierer & Hill, 2007, Inman *et al*, 2002b). Several mechanisms have been proposed to explain the signal intensity and duration (Itoh & ten Dijke, 2007).

The recognition of R-SMADs by the receptors are facilitated by auxiliary proteins. Thus, a membrane-associated protein, SARA (SMAD anchor for receptor activation), binds SMAD2 and SMAD3 in the cytoplasm and presents them to the activated type I receptors for phosphorylation and therefor promotes TGFβ signaling (Qing *et al*, 2000; Di Guglielmo *et al*, 2003; Hocevar *et al*, 2001; Tsukazaki *et al*, 1998). The interactions occur between a peptide sequence of SARA and an extended hydrophobic surface area on SMAD2/SMAD3 (Wu *et al*, 2000). SARA contains a phospholipid binding FYVE domain, which targets the molecule also to the membrane of early endosomes (Tsukazaki *et al,* 1998). These interactions allow more efficient recruitment of SMAD2 or SMAD3 to the receptors, since the activated receptor complex is internalized in SARA-rich early endosomes via clathrin- coated pits (Di Guglielmo *et al*, 2003; Hayes *et al*, 2002; Lu *et al*, 2002; Tsukazaki *et al*, 1998).

Indeed, TGFβ signaling intensity and duration can be regulated through the control of receptor trafficking. The ligand bound activated receptor complex is internalized via endocytosis, although receptors are internalized constitutively with similar efficiencies in the absence and presence of a signal (Di Guglielmo *et al*, 2003; Chen, 2009). They internalize by two distinct, competing routes: either by clathrin-dependent internalization into EEA1-positive endosomes; or by a clathrin-independent, lipid-raft–caveolin-dependent pathway into a distinct endocytic compartment. Because EEA1-positive endosomes also contain SARA, internalization through clathrin-coated pits is thought to facilitate signaling. Ligand-bound receptor complexes in the early endosomes are further sorted to late endosomes, where TGFβ and the receptors are separated. Some of the unbound receptors can be recycled to the plasma membrane, while others are degraded, along with TGFβ, upon fusion with the lysosomes (Di Guglielmo *et al*, 2003). In contrast, endocytosis through caveolae shuffles TGFβ receptors into a distinct endocytic compartment that promotes receptor degradation. Multiple protein interactions are likely to control subcellular receptor localization and cell-surface receptor availability. These parameters may in turn control the duration of SMAD phosphorylation and activation, and thus give rise to qualitatively different responses resulting to a given TGFβ stimulus.

Since TGFβ is not recycled, internalization of TGFβ by endocytosis is the primary means of removing active TGFβ from the cell surface, and lysosomal degradation is the primary means of termination of TGFβ signaling (Clarke *et al*, 2009; Zi *et al*, 2011).

Once activated, the TGFβ family receptors are negatively regulated by the I-SMADs (inhibitory SMADs), SMAD6 and SMAD7 (Itoh & ten Dijke, 2007). I-SMADs have a clearly recognizable MH2 domain but are more divergent from the other SMADs in the N-terminal and central regions. I-SMADs are transcriptionally induced in response to TGFβ in a SMAD-dependent manner and can inhibit signaling

by distinct and diverse mechanisms. Both SMAD6 and SMAD7 can interact with type I receptors, thus competitively preventing R-SMADs from being phosphorylated. Furthermore, SMAD7 controls SMAD signaling by inducing receptor complex degradation through the recruitment of ubiquitin-ligases, SMURF1 and SMURF2. The TGFβ receptor-SMAD7-SMURF complex is internalized via caveolin-positive vesicles toward the proteasome for degradation (Di Guglielmo *et al*, 2003; Hayashi *et al*, 1997; Kavsak *et al*, 2000; Ebisawa *et al*, 2001; Zhang *et al*, 2001). In addition, SMAD7 was also shown to recruit and stabilize GADD34, a regulatory subunit of protein phosphatase-1 (PP1) to the activated TGFβ receptors, thereby inducing receptor dephosphorylation and deactivation (Shi *et al*, 2004). Moreover, SMAD7 has been proposed to bind to SMAD-responsive elements through its MH2 domain and to inhibit SMAD-dependent promoter activation, indicating a nuclear role for SMAD7 (Zhang *et al*, 2007).

Moreover, phosphatases such as PPM1A can deactivate phospho-R-SMADs, resulting in the disassembly of the SMAD complex and providing a means for negative regulation of TGFβ signaling in the nucleus (Clarke & Liu, 2008).

The TGFβ dependent recruitment of Smad complexes to the transcription machinery also allows the accumulation of additional coactivators or corepressors, which regulate the amplitude of transcriptional activation. Besides the interaction of the SMAD complex with CBP/p300, SMAD4 can also engage another coactivator named MSG1 into the transcription complex to enhance the SMAD response (Shioda *et al*, 1998; Yahata *et al*, 2000).

By contrast, recruitment of a corepressor decreases the SMAD and TGFβ responsiveness. The corepressors c-Ski or SnoN antagonize TGF- signaling through direct interactions with SMAD4 and the R-SMADs (Luo *et al*, 1999; Akiyoshi *et al*, 1999; Stroschein *et al*, 1999; Liu *et al*, 2001; Wang *et al*, 2000). SnoN-mediated negative regulation on the SMAD proteins is removed during TGFβ signaling by at least two distinct ways. In the presence of TGFβ signaling, SMAD2 interacts with both SnoN and SMURF2, allowing the HECT domain of SMURF2 to target SnoN for ubiquitin- mediated degradation by the proteasome (Bonni *et al*, 2001). SMAD2 and SMAD3 can also recruit the E3 ubiquitin ligase anaphase promoting complex (APC), resulting in the ubiquitination and degradation of SMAD bound SnoN (Stroschein *et al*, 2001; Wan *et al*, 2001).

Furthermore, ubiquitin–proteasome-mediated degradation controls the levels of SMADs posttranslationally. Thus, C-terminally phosphorylated SMAD2 or SMAD3 can form a stable complex with SMURF2 and undergo proteasomal degradation that regulates nuclear R-Smad levels (Bonni *et al*, 2001). Therefore, inhibition of proteasomal degradation enhances its nuclear accumulation (Lo & Massagué, 1999). However, only a small fraction of SMAD2 and SMAD3, in the absence or presence of TGFβ, is ubiquitinated. Thus, the bulk of nuclear SMAD2 or SMAD3 is not targeted for degradation, but

dephosphorylated and relocated to the cytoplasm (Inman *et al*, 2002b; Xu *et al*, 2002). Interestingly, sumoylation of SMAD4 enhances its stability (Lee *et al,* 2003).

In conclusion, the cell has various means to regulate SMAD signal intensity and duration and positive and negative signals are equally important in controlling TGFβ signaling responses.

2.5 Non- canonical TGFβ signaling and crosstalk with MAPK pathways

The complexity of TGFβ signaling responses is influenced not only by core pathway components including ligands, receptors, SMADs and SMAD-dependent transcription factors, but also by the ability of TGFβ receptors to activate other SMAD-independent (non- canonical) pathways, including the mitogen-activated protein kinase (MAPK) pathways. Indeed, SMAD signaling interacts with a complex network of cross-talks with other signaling pathways that modify the initial SMAD signals and result in the multitude of effects induced by TGFβ. Thus, TGFβ has been shown to activate MAPK pathways in many cell types (Wakefield and Roberts, 2002; Derynck and Zhang, 2003). The MAPK cascades are key membrane-to-nucleus signaling modules that respond to various stimuli resulting in the phosphorylation and regulation *of* transcription factors*,* co-regulatory proteins and chromatin proteins required for gene expression. They mainly comprise three subfamilies: the extracellular signal-regulated kinases (ERKs), the c-Jun N-terminal kinases (JNKs) and the p38/MAPKs (Chang and Karin, 2001). The mechanisms of crosstalk cover among others regulation of co-activators and co-repressors recruited during the process of transcription, regulation of R-SMADs activity through phosphorylation, regulation of I-SMADs (SMAD6,7) expression and other interactions that could activate or inhibit certain molecules in the pathways (Zhang & Derynck, 1999). Downstream activation of distinct MAPK pathways by TGFβ occur either with slow or rapid kinetics. Slow activation of these pathways is mediated by SMAD-dependent transcription responses whilst the rapid activation is mediated by SMAD-independent responses (Hartsough & Mulder, 1995).

The p38 MAPK pathway is activated by several stresses such as heat shock, osmotic shock and hypoxia and plays diverse roles in cell proliferation, differentiation, survival and migration in different cell types. Moreover, p38 MAPK is involved in sustaining tumor growth (Fang & Richardson, 2005). p38 is at the tertiary layer of MAPK cascades, as it is activated by MAP kinase kinases (MKKs) through phosphorylation: specifically by MKK3 and MKK6 and sometimes by MKK4 (Yamashita *et al*, 2008; Sorrentino *et al*, 2008; Hanafusa *et al*, 1999; Sano *et al*, 1999; Yu *et al*, 2002). Further upstream, MKKs are activated by the MAP3Ks, like MAP3K 4, 10 and the TGFβ-activated kinase 1 (TAK1). A scheme is shown in **Figure 2A.** A direct physical interaction between TGFβ type II receptor and TAK1 was found (Watkins *et al,* 2006). TRAF6, which plays an important role in the activation of TAK1, was reported to be essential for TGFβ-induced activation of the TAK1/p38 pathways (Yamashita *et al*, 2008; Sorrentino

et al, 2008). Besides SMAD-dependent pathways, the TRAF6-TAK1-p38 pathway is fundamental for TGFβ- induced apoptosis and EMT. Thus, knockdown of TRAF6 inhibited TGFβ-mediated EMT (Yamashita *et al*, 2008). TGFβ induces both a rapid and a late activation of p38 in a cell-type-specific manner. Rapid and transient p38 activation has been observed in numerous cell types including human neutrophils, HEK293 and C2C12 cells, and may be mediated by activation of TAK1. In contrast, the delayed and sustained p38 activation reported in pancreatic carcinoma cells, hepatocytes or osteoblasts, requires SMAD-mediated expression of Gadd45b, an upstream activator of MKK4 (Takekawa *et al*, 2002). Furthermore, cooperation with the p38 pathway enables TGFβ-induced growth arrest (Kamaraju and Roberts, 2005) through phosphorylation of the R-SMAD linker region, resulting in an increased transactivation potential of R-SMADs, finally leading to cell cycle arrest. Moreover, MAPKs may indirectly influence SMAD signaling by controlling SMAD7 expression depending on the cell type (Uchida *et al*, 2001; Dowdy *et al*, 2003). Interestingly, the p38 pathway regulates post-translational modifications of SMADs, since p38 is involved in sumoylation of SMAD4, contributing to enhanced SMAD4-dependent transcription (Ohshima and Shimotohno, 2003).

The ERK 1/2 pathway is known to promote cell growth and survival (Lu & Xu, 2006), but under certain conditions it can have pro-apoptotic effects. Since the initial reports that TGFβ activates ERK1/2 in epithelial cells and breast cancer cells (Hartsough and Mulder, 1995), ERK1/2 activation has been linked to a number of TGFβ-regulated cellular events, including $p21^{Cip1}$ gene expression and growth arrest (Hartsough *et al*, 1996; Frey and Mulder, 1997), EMT (Zavadil *et al,* 2001) and breast cancer development (Dumont *et al*, 2003). The kinetics of ERK phosphorylation induced by TGFβ depend on the cell type and physiological state of the cell. In diverse cell lines, a delayed response of ERK to TGFβ was found, typically with the peak of ERK phosphorylation occurring hours after ligand stimulation, suggesting an indirect response requiring protein translation (Simeone *et al*, 2001). In contrast, in epithelial cells, breast cancer cells and fibroblasts, activation can occur rapidly within 5–10 min of TGFβ stimulation, which is comparable to the time course of ERK activation by mitogenic factors such as EGF (Olsson *et al*, 2001; Frey & Mulder, 1997). TGFβ receptors directly participates in the activation of ERK by recruiting and phosphorylating Src Homology 2 Domain-Containing Transforming Protein 1 (ShcA) on its serine and tyrosine residues. The phosphorylated ShcA then associates with TGFβR1 via its phosphotyrosine-binding domain and recruits growth factor receptor binding protein 2 (Grb2) and Sos proteins, that activates the Ras–Raf–MEK1/2–ERK1/2 cascade pathways (Lee *et al*, 2007; Rojas *et al*, 2009). A scheme is shown in **Figure 2B.** ERK and Ras then regulate target gene transcription through their downstream transcription factors in conjunction with SMADs to control the cellular response (Lee *et al*, 2007). Moreover, it has been shown that activation of ERK result in the phosphorylation of the linker segments of SMAD1, SMAD2 and SMAD3, which blocks their nuclear translocation (Kretzschmar

et al, 1997, 1999). This could explain how oncogenic Ras overrides TGFβ-mediated growth arrest in cancer cells (Kretzschmar *et al*, 1999). Other studies have not found impaired nuclear translocation of SMADs in Ras-transformed cells or in cells with activated MAPK signaling (de Caestecker *et al*, 1998; Funaba *et al*, 2002; Engel *et al*, 1999). The TGFβRs also play an important role in the ERK-TGFβ crosstalk. Mainly, the expression levels and the ratio of TGFβR2/ TGFβR1 hetero-oligomers contribute to different downstream signaling modules (Huang *et al*, 2011]. Furthermore, TGFβ-induced activation of Ras/ERK MAPK signaling can induce TGFβ1 expression, thereby amplifying the TGFβ response and inducing secondary TGFβ responses (Yue & Mulder, 2000). Furthermore, cooperativity between Ras/MAP kinase signaling and TGFβ signaling has been reported during tumor development (Oft *et al*, 1996; Lehmann *et al*, 2000). In kidney epithelial cells, activation of Raf confers protection against TGFβ-induced apoptosis while enhancing its pro invasive effects (Lehmann *et al*, 2000), and induction of EMT in breast tumor cells is dependent on the presence both of activated Ras and of a functional TGFβ autocrine loop that is enhanced by Ras (Lehmann *et al*, 2000; Xie *et al*, 2004).

The c-Jun N-terminal kinase (JNK) cascade controls several transcription and non-transcription factors in response to external stimuli and is involved in various biological processes including cell proliferation, apoptosis and tumor development. TGFβ stimulation rapidly increased JNK activity (within 5–10min) (Yue *et al*, 2004). JNKs are a third layer of MAPK cascade activated by upstream MKKs—MKK4 and MKK7. The rapid SMAD-independent activation of JNK through TGFβ is accomplished specifically through a MKK4–TAK1 axis (Yamashita *et al*, 2008; Sorrentino *et al*, 2008). The TRAF6–TAK1–JNK cascade, in cooperation with SMADs, is reported to regulate TGFβ-mediated apoptosis and EMT (Sorrentino *et al*, 2008; Liu *et al*, 2012) suggesting a close conjunction between these cellular outcomes. Moreover, overexpression of SMAD7 has been shown to induce persistent JNK activation in HepG2 cells (Mazars *et al*, 2001). Also, the JNK pathway may contribute to regulate autocrine TGFβ1 expression, as JNK-deficient fibroblasts constitutively express TGFβ1 expression that can be repressed by complementation of the cells with JNK (Ventura *et al*, 2004).

Thus, the balance between direct activation of SMADs and MAPK pathways determines the outcome of cellular response to TGFβ.

Figure 2

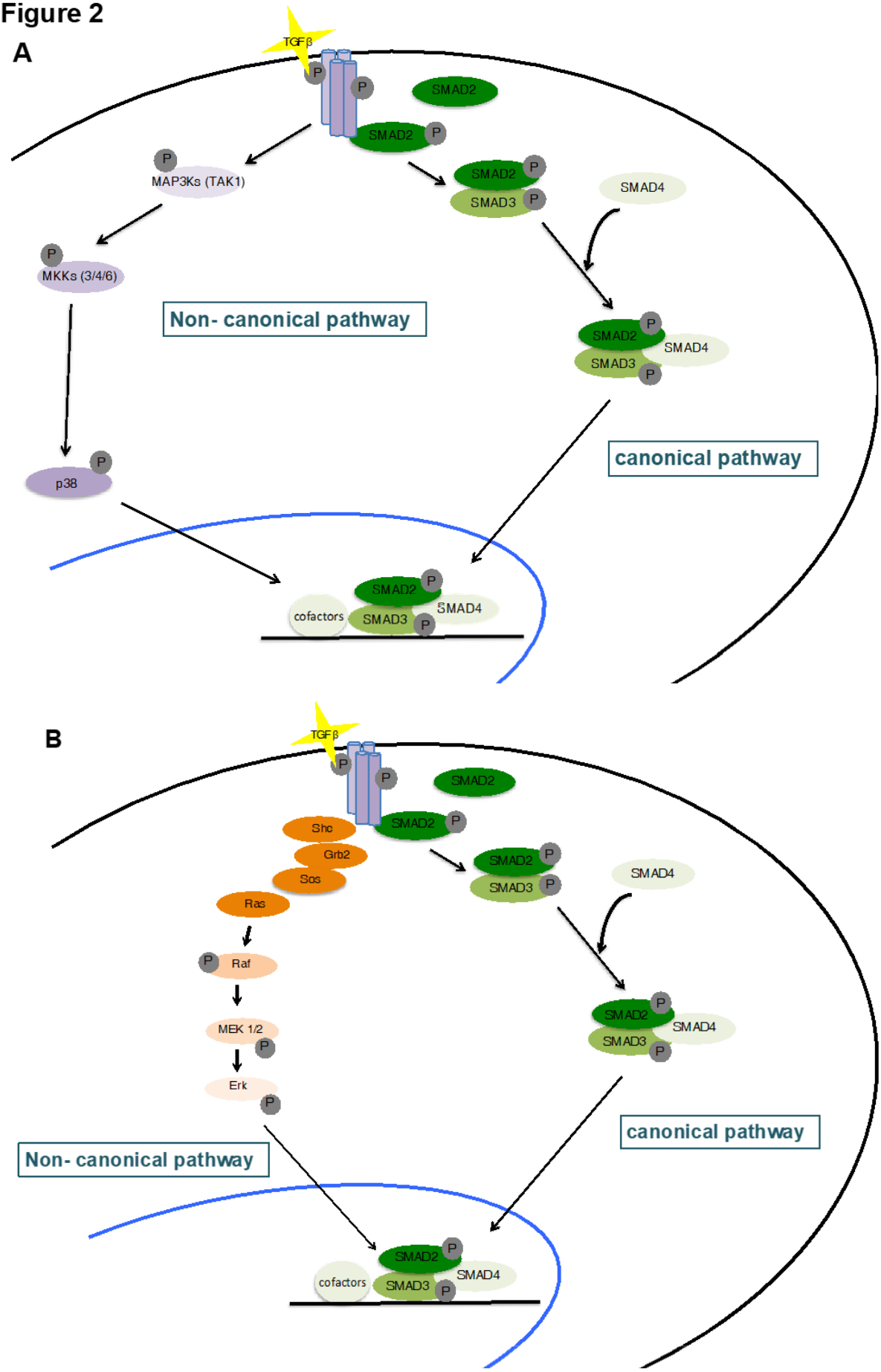
A
TGFβ
P
SMAD2
SMAD2
P
MAP3Ks (TAK1)
SMAD2
SMAD3
SMAD4
MKKs (3/4/6)
Non- canonical pathway
SMAD2
SMAD4
SMAD3
canonical pathway
p38
cofactors
SMAD2
SMAD4
SMAD3
B
TGFβ
SMAD2
Shc
SMAD2
Grb2
Sos
SMAD2
SMAD3
SMAD4
Ras
Raf
SMAD2
SMAD4
SMAD3
MEK 1/2
Erk
canonical pathway
Non- canonical pathway
SMAD2
cofactors
SMAD4
SMAD3

2.5 Figure 2. Scheme of non-canonical TGFβ pathway activation.
A Scheme of the non-canonical p38 MAP Kinase pathway upon TGFβ activation. TGFβ receptors activate MAP3Ks (Mitogen-activated protein kinase kinase kinases or MEKKs) like TAK1 (Transforming growth factor beta-activated kinase 1 or MAP3K7), which in turn activates MKKs (Mitogen-activated protein kinase kinases) like 3, 4, 6 and finally phosphorylate p38.
B Scheme of the non-canonical ERK MAP Kinase pathway upon TGFβ activation. TGFβ can induce phosphorylation of the receptors I and II and on Shc, which leads to recruiting of Grb2/Sos to activate Erk 1/2 (pp44/pp42) through Ras, Raf, and MEK1 (Mitogen-activated protein kinase kinase 1) and 2.

2.6 Aim of the study

The TGFβ pathway is a multi-functional signaling system regulating various cellular processes. Moreover, TGFβ signaling plays a dual role in cancer. The mechanisms underlying the basis of these wide range of physiological effects to TGFβ have not been elucidated in detail. Therefore, I aimed to clarify to what extent signaling dynamics determine the cellular fate upon TGFβ stimulation.

As the cellular response to a given stimulus often varies even in genetically identical cells, my approach will be to study TGFβ dynamics at the level of single cells. I am using the cellular model system MCF10A, a human non-cancerous breast epithelial cell line. By combining fluorescent reporter cell lines with live-cell microscopy and automated image analysis, I monitor the cytoplasmic to nuclear translocation of SMADs with high temporal and spatial resolution in hundreds of individual cells. Using this approach, I investigate how SMAD signaling encode information in individual cells over time and study how the TGFβ network architecture shape its dynamic response.

Moreover, I focus on understanding dynamic network interactions and thus, I examine the function of distinct interaction partners in the networks and investigate how the canonical and non- canonical pathways interact to determine long-term dynamics and specify cellular decisions.

I plan to investigate how dynamics are translated into physiological responses to predict these and understand how a misregulated pathway can lead to cancer.

3 RESULTS

3.1 Dynamics and variability of SMAD signaling in single cells

3.1.1 Live-cell reporter for TGFβ pathway activation

In order to get a systematic view of TGFβ dynamics and to follow pathway activation in single cells by monitoring the translocation of SMADs from the cytoplasm to the nucleus with high temporal and spatial resolution, I combined fluorescent reporter cell lines with live-cell microscopy and automated image analysis. First, I established stable clonal reporter cell lines for SMAD2 and SMAD4 by expressing a fusion of the corresponding cDNA with the yellow fluorescent protein mVenus (YFP) under the control of a constitutive promoter (UbCp) in the TGFβ-responsive breast epithelial cell line MCF10A (**Figure 3A**, 6.2, Soule *et al*, 1990; Debnath *et al*, 2003). A constitutive promoter can be used, because neither SMAD2 nor SMAD4 are transcriptionally regulated upon TGFβ treatment and translocation of the YFP-SMAD2 or YFP-SMAD4 fusion protein into the nucleus acts as a surrogate for the activity of the pathway. In addition, the cell lines also stably express the nuclear marker histone H2B-CFP under the control of UbCp to track the nucleus over time and enable automated image analysis **(Figure 3A)**. Next, to measure SMAD nuclear translocation quantitatively in hundreds of individual living cells, I performed time-lapse microscopy imaging every five minutes over a 24h time interval after stimulation with a saturating TGFβ concentration of 100pM. As expected (Nicolás *et al*, 2004; Schmierer & Hill, 2005), initially SMADs are predominantly located in the cytoplasm, followed by strong accumulation into the nucleus after TGFβ treatment until adaptation mechanisms and negative feedback loops terminated pathway activation and SMADs shuttled back to the cytoplasm. I employed automated image analysis to measure the changing fluorescent intensities of the fusion proteins (YFP-SMADs) over time in the nucleus by tracking the nuclear H2B-CFP marker. Furthermore, cytoplasmic SMAD intensities were taken as the average YFP intensities in a ring around the nuclear area (6.6). Finally, I determined the signaling pathway activity as the ratio of the average nuclear and cytoplasmic intensities (nuc/cyto SMAD ratio), as this measure was robust against correlated fluctuations due to heterogeneity of transgene expression or measurement aberrations such as photobleaching or unequal illumination. In **Figure 3B & C,** one individually tracked cell of the YFP-SMAD2- reporter cell line was analyzed and the resulting trajectories of nuclear, cytoplasmic and ratio SMAD2 levels are presented. Before TGFβ treatment SMAD2 was located in the cytoplasm and accumulated in the nucleus within 1h of stimulation. Followed then by a strong adaption phase where SMAD2 re-localized to the cytoplasm, before it accumulated again in the nucleus around 8h after the initial response and re- localized to the cytoplasm. **Figure 3D & E** represent one individual tracked and analyzed cell of the

YFP-SMAD4- reporter cell line. After TGFβ stimulation SMAD4 shuttled from the cytoplasm to the nucleus within 1h, followed by a short adaption phase and a second re-location in the nucleus with a subsequent re-localization to the cytoplasm.

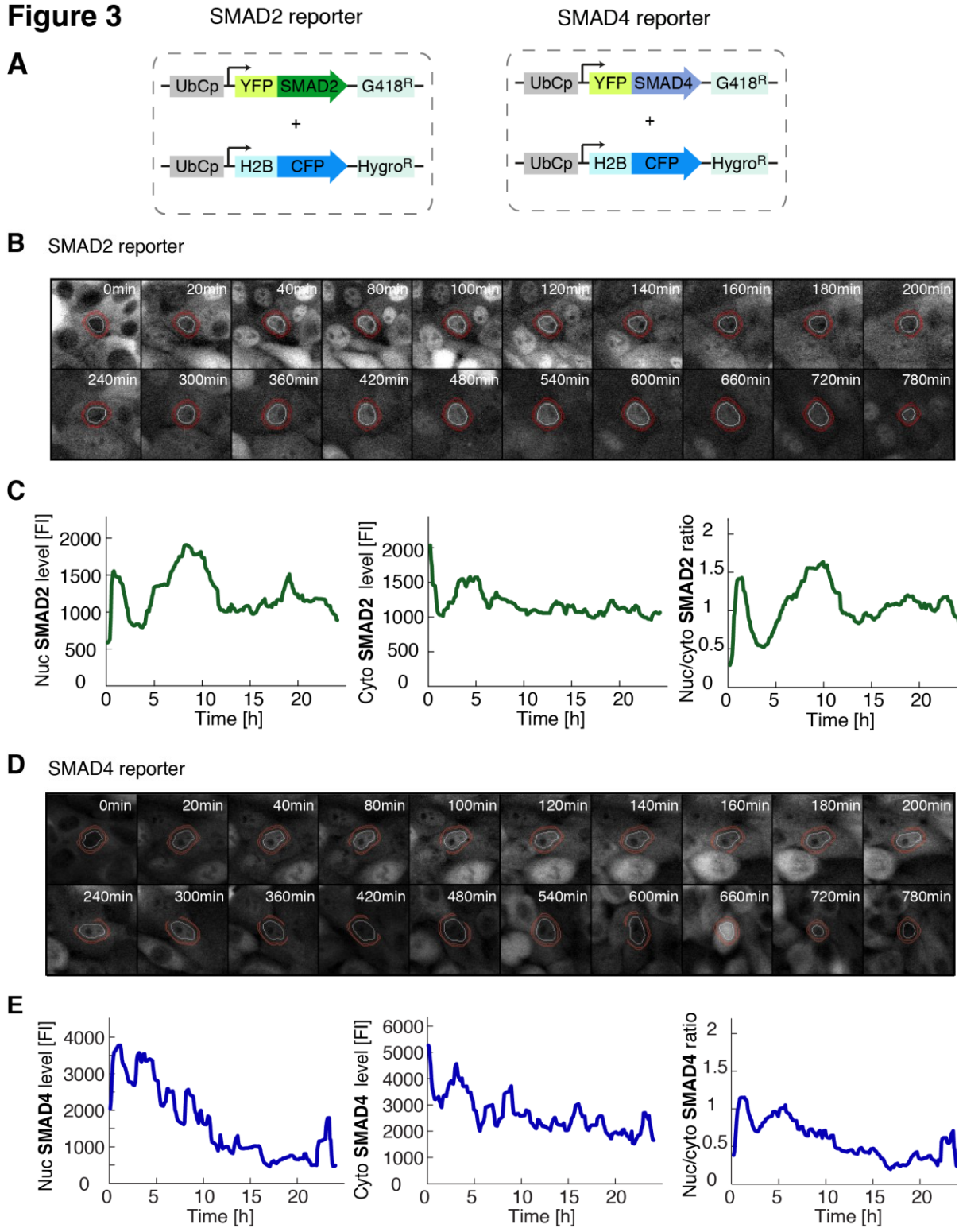

3.1.1 Figure 3. Live-cell time-lapse microscopy of the reporter cell lines.
A Fluorescent reporter system to measure SMAD signaling dynamics in individual cells. SMAD2 was fused to the yellow fluorescent protein mVenus (YFP) under the control of the human ubiquitin C promoter (UbCp) with the selection marker

G418 (Geneticin). As a nuclear marker, histone 2B (H2B) was fused to the cyan fluorescent protein mCerulean (CFP) under the control of UbCp with the selection marker hygromycin.
B Live-cell time-lapse microscopy images of MCF10A cells expressing SMAD2-YFP following treatment with 100pM TGFβ. White circles indicate the segmented nucleus, and the estimated cytoplasmic area is represented by red annuli.
C The indicated cell in (A) was tracked over 24 hours (h) and the corresponding nuclear (nuc) level, cytoplasmic (cyto) level and the nuclear-to-cytoplasmic (nuc/cyto) SMAD2-YFP ratio was plotted over time.
D Live-cell time-lapse microscopy images of MCF10A cells expressing SMAD4-YFP following treatment with 100pM TGFβ. White circles indicate the segmented nucleus, and the estimated cytoplasmic area is represented by red annuli.
E The indicated cell in (C) was tracked over 24 hours (h) and the corresponding nuclear (nuc) level, cytoplasmic (cyto) level and the nuclear-to-cytoplasmic (nuc/cyto) SMAD4-YFP ratio was plotted over time.

3.1.2 Verification of these reporters by comparing kinetics of endogenous and tagged proteins

The next step was to validate these reporter cell lines to make sure that the dynamics and cellular response of TGFβ signaling are not disturbed. As shown in **Figure 4A** Western Blot experiments revealed that the YFP-SMAD2 or YFP-SMAD4 fusion proteins are expressed at lower levels, corresponding to approximately 65% or 32.5% of endogenous proteins in the parental WT cell line, respectively. Data points for 0h, 2h and 3h post TGFβ stimulation are shown. This overexpression apparently did not change the dynamics of SMAD signaling, since I observed similar TGFβ- induced phosphorylation profiles of endogenous SMAD2 in the parental WT and YFP-SMAD2 reporter cell line by Western Blot analysis **(Figure 4B)**. Immunofluorescence experiments indicated that the kinetics of endogenous SMADs at fixed time points in the parental WT cell line reflected changes at the corresponding time points in the nuc/cyto ratio of the SMAD2 or SMAD4 reporter cell lines measured by live- cell imaging **(Figure 4C)**. By staining the nucleus of the fixed cells with Hoechst, nuclear SMAD2 or SMAD4 intensities could be calculated over time. Furthermore, cytoplasmic SMAD intensities were taken as the average YFP intensities in a ring around the nuclear area. Exemplary fixed cells for 0, 1 and 8h post TGFβ stimulus are shown in **Figure 4D**.

Finally, I checked the induction of well-characterized SMAD2/4 target genes (SMAD7, SnoN and PAI-1) in response to TGFβ stimulation by RT-PCR and observed essentially no differences between the parental WT and reporter cell lines **(Figure 5A & B)**.

In conclusion the validation experiments showed comparable dynamics of endogenous and tagged proteins and did not alter the cellular response to TGFβ stimulus. Therefore, the SMAD2 and SMAD4 reporter faithfully represents the activity of the pathway.

Figure 4

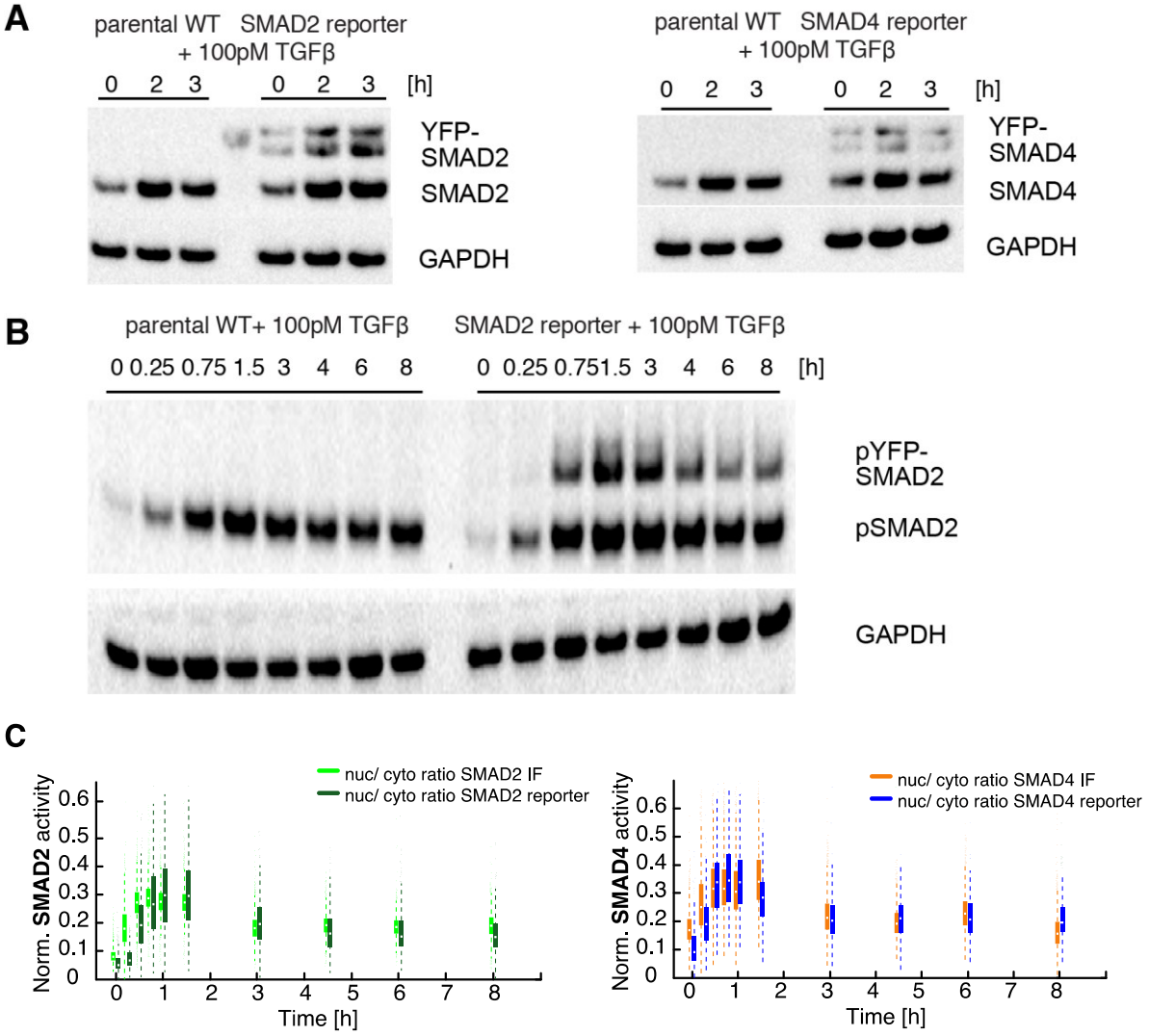
A
parental WT SMAD2 reporter
+ 100pM TGFβ
0 2 3 0 2 3 [h]
YFP-SMAD2
SMAD2
GAPDH
parental WT SMAD4 reporter
+ 100pM TGFβ
0 2 3 0 2 3 [h]
YFP-SMAD4
SMAD4
GAPDH
B
parental WT+ 100pM TGFβ
SMAD2 reporter + 100pM TGFβ
0 0.25 0.75 1.5 3 4 6 8 0 0.25 0.75 1.5 3 4 6 8 [h]
pYFP-SMAD2
pSMAD2
GAPDH
C
nuc/ cyto ratio SMAD2 IF
nuc/ cyto ratio SMAD2 reporter
Norm. SMAD2 activity
Time [h]
nuc/ cyto ratio SMAD4 IF
nuc/ cyto ratio SMAD4 reporter
Norm. SMAD4 activity
Time [h]

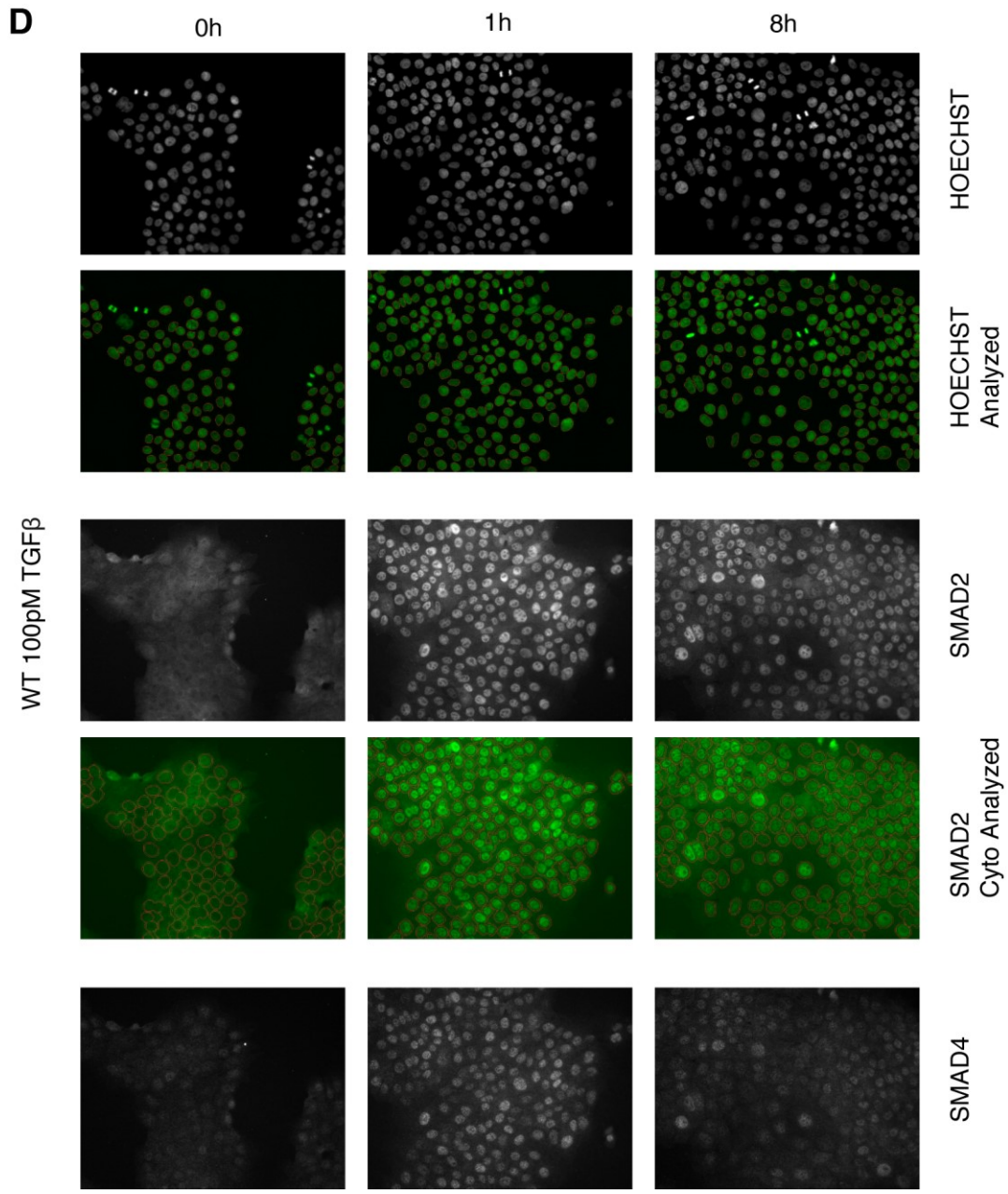

3.1.2 Figure 4. Verification of the reporter cell lines by comparing kinetics of endogenous and tagged proteins.
A Western blot analysis of endogenous and YFP-tagged SMAD2 or SMAD4 in stable clonal reporter cell lines and the corresponding parental cell line. Cells were stimulated with 100pM TGFβ and analyzed after 2 and 3 h. GAPDH was used as a loading control.
B Western blot analysis of SMAD2 activation in SMAD2-YFP reporter and parental MCF10A cells. Cells were stimulated with 100pM TGFβ, and SMAD2 phosphorylation was analyzed at indicated time points. GAPDH was used as a loading control.
C Comparison of endogenous SMAD2 and SMAD2-YFP translocation or SMAD4 and SMAD4-YFP translocation. The nuc/cyto ratio of SMAD-YFP upon 100pM TGFβ stimulation was measured in reporter cells by time-lapse microscopy at the indicated time points; the nuc/cyto ratio of endogenous SMAD2 and SMAD4 was measured in parental MCF10A WT cells by immunofluorescence under the same conditions. Data was normalized by minimum subtraction and division through the overall maximum.
D Exemplary MCF10A WT cells for immunofluorescence analyzed in (A). The nucleus was stained with Hoechst and labeled with a red ring. For SMAD2, the secondary antibody Alexa Fluor 488 and for SMAD4 Alexa Fluor 647 were used. Cytoplasmic SMAD2 area is represented by red annuli.

Figure 5

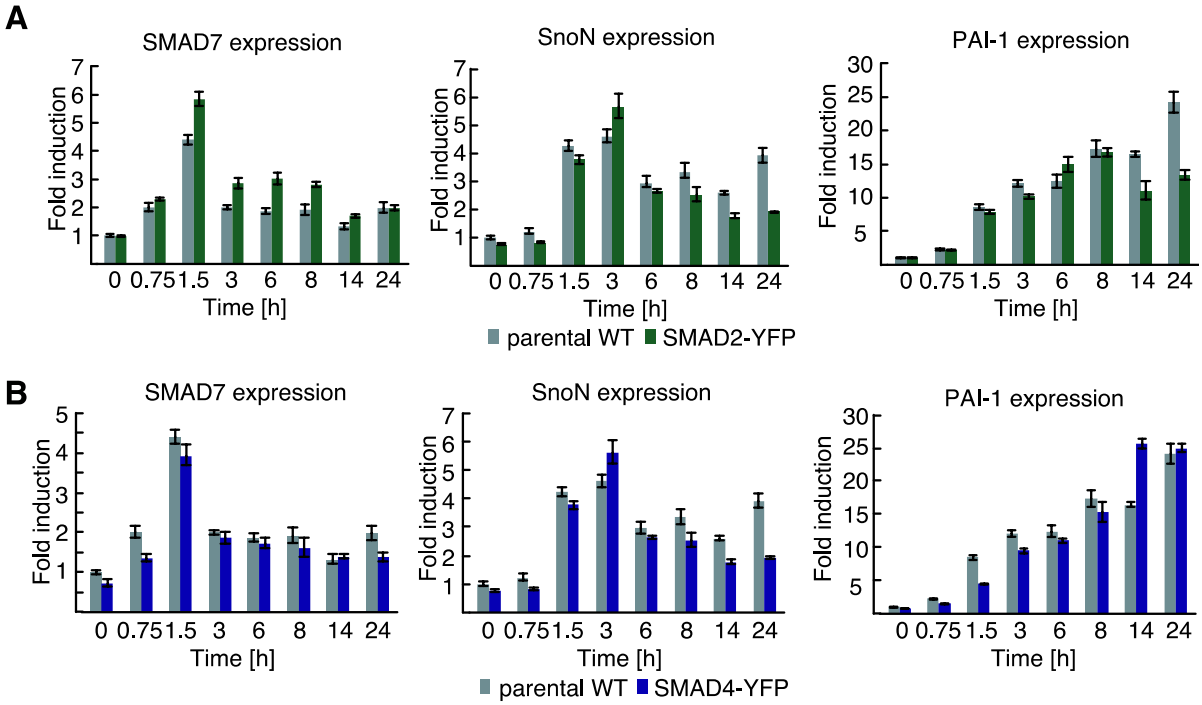

3.1.2 Figure 5. Verification of the reporter cell lines by comparing kinetics of target genes by RT-qPCR
A Expression of SMAD target genes in parental and SMAD2 reporter cell lines. Expression kinetics of SMAD7, SnoN and PAI-1 upon 100pM TGFβ stimulation were measured by RT-qPCR at indicated time points. β-Actin was used as an internal control. Error bars indicate standard deviation of technical triplicates.
B Expression of SMAD target genes in parental and SMAD4 reporter cell lines. Expression kinetics of SMAD7, SnoN and PAI-1 upon 100pM TGFβ stimulation were measured by RT-qPCR at indicated time points. β-Actin was used as an internal control. Error bars indicate standard deviation of technical triplicates.

3.1.3 Average SMAD dynamics are TGFβ dose dependent

In order to investigate TGFβ pathway activity I examined the dynamics of SMAD2 and SMAD4 under varying TGFβ concentrations (0, 1, 2.5, 5, 25 and 100pM TGFβ) over a 24h time period of hundreds of cells by time-lapse imaging **(Figure 6A)**. By analyzing the median nuc/cyto SMAD2 ratio of the cell population, one synchronous initial response of SMAD translocation at 1h, followed by adaptation could be monitored. Specifically, I observed that a decrease in the TGFβ concentration lowers the peak amplitude, renders signaling more transient and leads to rapid adaptation to the pre-stimulus level. Cells stimulated with 100pM TGFβ are characterized by a saturated amplitude, strong adaption phase and a second lower signaling plateau afterwards. The nuclear and cytoplasmic SMAD2 level reflected the ratio values. The SMAD4 reporter showed a comparable median response when cells treated with varying TGFβ doses, although with a lower amplitude of the initial response **(Figure 6B)**. In summary, the average SMAD dynamics are TGFβ dose dependent.

As shown in **Figure 6C** the median nuc/ cyto ratio of the cell population was very reproducible between biological replicates for 2.5pM and 100pM TGFβ treated cells.

Figure 6

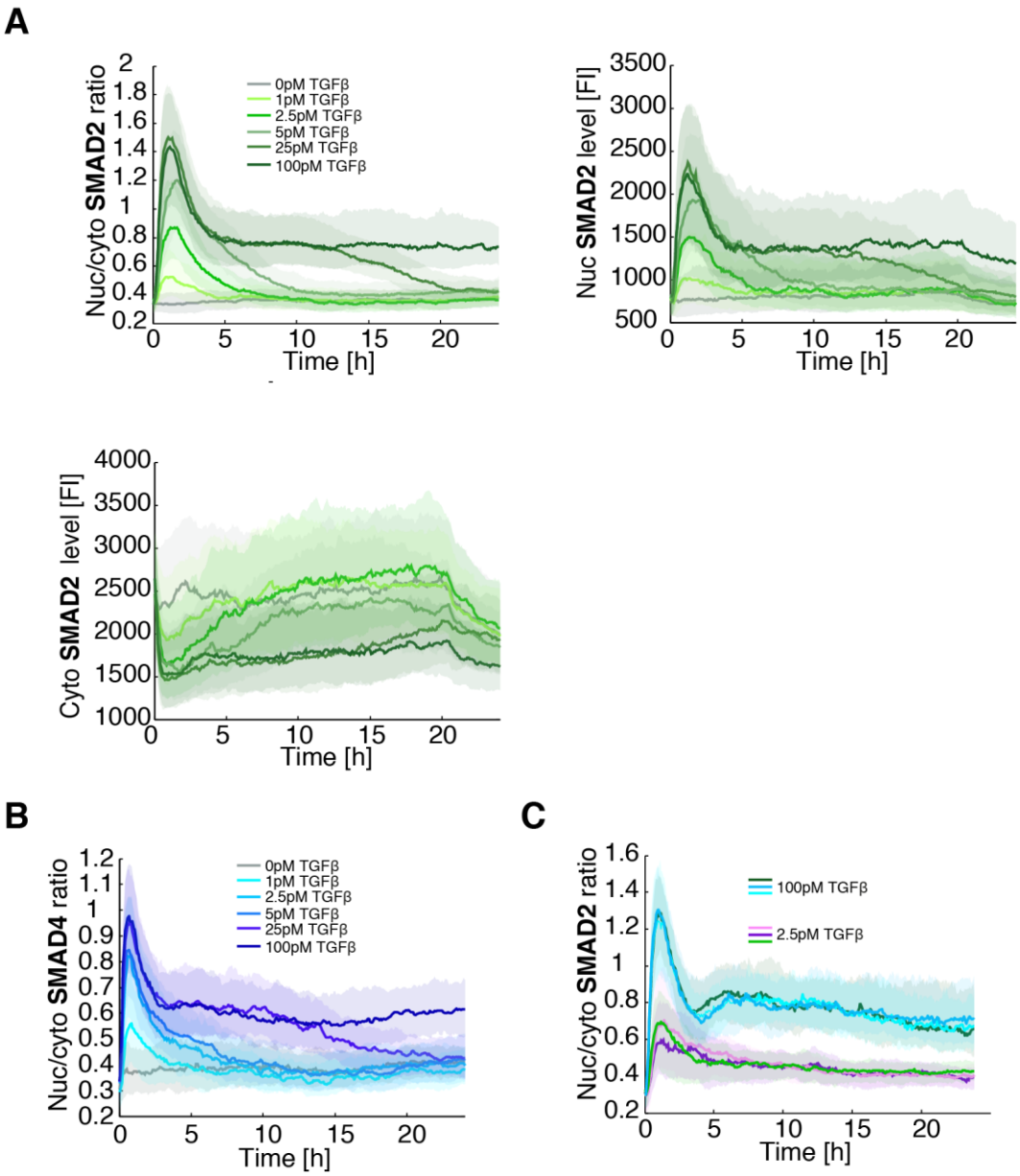

3.1.3 Figure 6. Average SMAD dynamics are TGFβ dose dependent.
A Median nuc/cyto SMAD2 ratio, nuclear (nuc) and cytoplasmic (cyto) level of cells stimulated with 0, 1, 2.5, 5, 25 or 100pM TGFβ and tracked over 24h. Shaded area represent data between 25th and 75th percentiles.
B Median nuc/cyto SMAD4 ratio of cells stimulated with 0, 1, 2.5, 5, 25 or 100pM TGFβ and tracked over 24h. Shaded area represent data between 25th and 75th percentiles.
C Median SMAD2-YFP ratio of cells plated in three independent glass bottom plates stimulated with 2.5 or 100pM TGFβ at the same day and tracked over 24h (biological triplicates). Shaded area represent data between 25th and 75th percentiles.

3.1.3.1 Target genes are TGFβ dose dependent

TGFβ is known to control multiple cell fates in a TGFβ- concentration manner (Schmierer & Hill, 2007). In support of these effects, I checked the impact of different TGFβ doses, and therefor different corresponding SMAD dynamics, on target gene expression (SMAD7, PAI1 and TIEG). Cells were simultaneously stimulated with 1, 2.5, 5, 25 and 100pM TGFβ and harvested at defined time points

during 24h post stimulus. RT-PCR measurements revealed that changing the TGFβ stimulus alters the induction levels of the selected target genes in cell populations **(Figure 7)**. The first peak appeared to be strongly TGFβ concentration-dependent in a graded manner, while this correlation slightly diminished at later time points. However, target gene expression 24h after the 100pM TGFβ stimuli show clear differences in comparison to lower doses. In particular PAI-1 represents a more switch-like behavior. While expression decreased to basal levels after a maximum at 3 or 6h for concentrations of 25pM or below, stimulation with 100pM led to an about 20-fold induction at the end of the observation period. In conclusion expression of TGFβ target genes are dose-dependent like the median response in the time-lapse data.

Figure 7

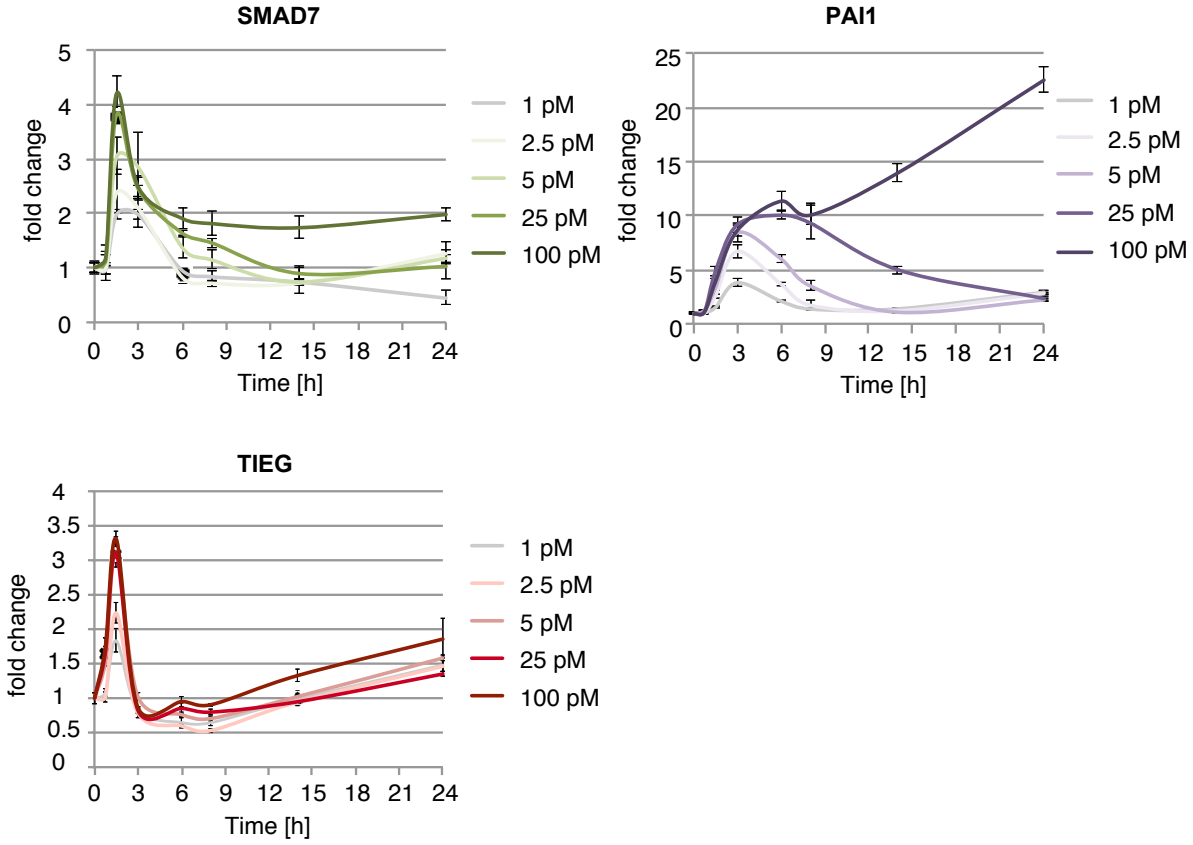

3.1.3.1 Figure 7. Target genes are TGFβ dose dependent.
Expression of SMAD target genes in MCF10A WT cells with varying concentrations of TGFβ over 24h. Expression kinetics of SMAD7, PAI-1 and TIEG were measured by RT-qPCR at indicated time points. β-Actin was used as an internal control. Error bars indicate standard deviation of technical triplicates.

3.1.3.2 Target genes are stimulation period dependent

Since target gene expression correspond to the average TGFβ dose response of SMADs, these finding further leads to the question which phases or stimulation periods are essential for the full target gene transcription and the cellular outcome. Thus, I terminated the TGFβ response after 0.25, 0.75, 1.5, 3, 4.5, 6 and 8 hours by washing out the media five times and measured subsequently by RT-PCR the

expression of target genes (PAI-1 and SnoN) 24 hours post TGFβ treatment **(Figure 8A)**. Interestingly, the full 24h TGFβ stimulation was necessary for the induction of PAI-1 and SnoN and shorter stimulation periods had no effect on the cells **(Figure 8B)**. In summary the cells reacted to the current TGFβ state and needed long-term stimulation and continued SMAD signaling to achieve full target gene transcription 24 hours post TGFβ. Consequentially I was interested in the memory of the system, mainly determined by signaling adaptation and mRNA decay. Thus, I stimulated the cells either for 1 hour or 6 hours with 100pM TGFβ and terminated the stimulation with the TGFβReceptor I Kinase inhibitor SB431542 and measured the target gene expression every 0.5- 1h post termination **(Figure 8C)**. First of all, the memory time of the mRNA response was gene dependent. In Detail SMAD7 and TIEG mRNA got back to basal level after 2 hours and PAI-1 after 4.5 hours post termination and even dipped below basal level **(Figure 8D)**. These observations confirmed that cells respond strongly to the current TGFβ state and full gene expression depends on sustained SMAD signaling including the different phases.

Figure 8

A

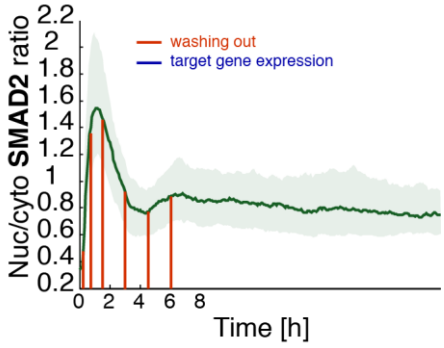

B

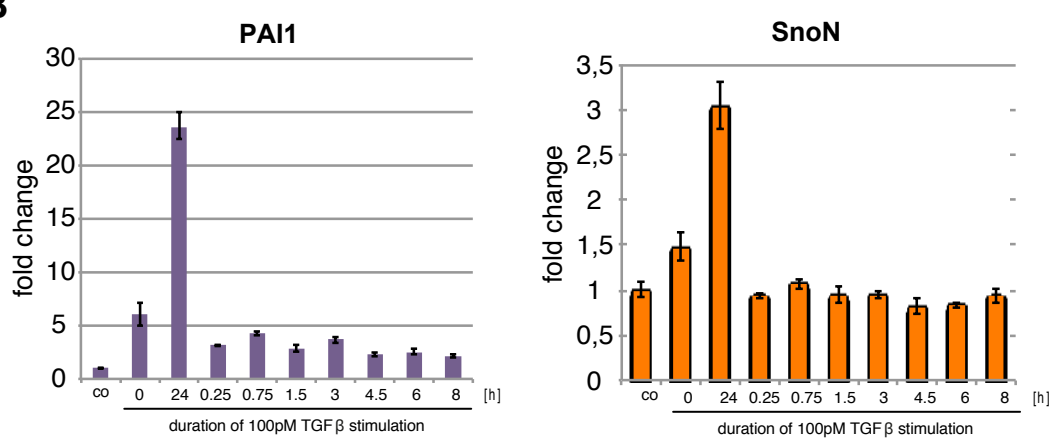

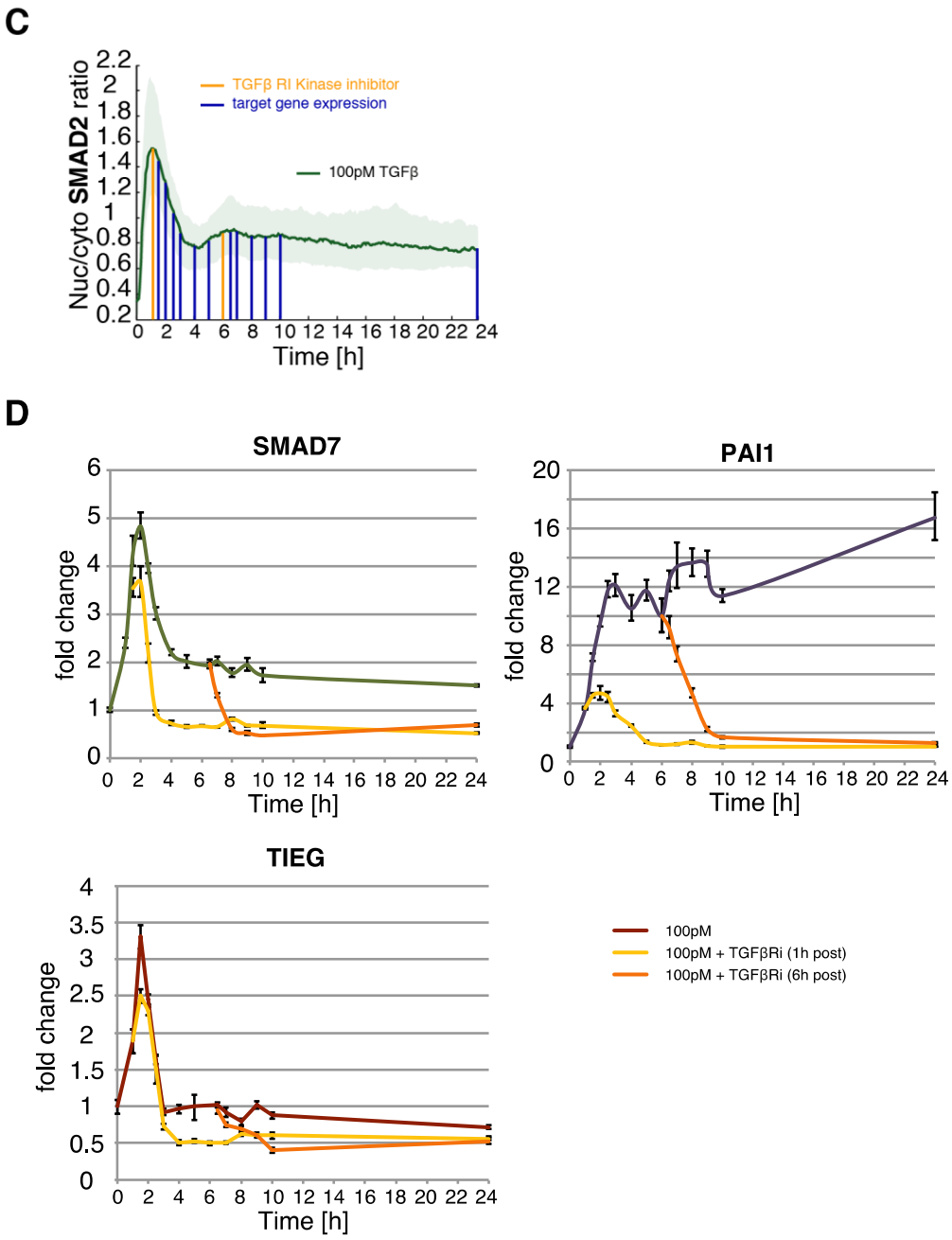

3.1.3.2 Figure 8. Target genes are stimulation period dependent.

A Scheme of experimental setup. TGFβ response was terminated after 0.25, 0.75, 1.5, 3, 4.5, 6 and 8 hours by washing out the media five times (red line) and the expression of target genes (PAI-1 and SnoN) 24h post 100pM TGFβ treatment (blue line) were measured. The median nuc / cyto SMAD2 ratio of time-lapse microscopy experiments upon 100pM TGFβ stimulation is shown for illustrative purposes.

B Expression of SMAD target genes in MCF10A WT cells with varying duration of 100pM TGFβ stimulation. Expression of PAI-1 and SnoN were measured by RT-qPCR at 24h post TGFβ stimulation with indicated stimulation periods. Control (co) was measured at time point 0 without TGFβ treatment. β-Actin was used as an internal control. Error bars indicate standard deviation of technical triplicates.

C Scheme of experimental setup. Cells were stimulated with 100pM TGFβ either for 1h or 6h and terminated with the TGFβReceptor I Kinase inhibitor SB431542 (orange line) and target gene expression every 0.5- 1h post termination was measured (blue line). The median nuc / cyto SMAD2 ratio of time-lapse microscopy experiments upon 100pM TGFβ stimulation is shown for illustrative purposes.

D Expression of SMAD target genes in MCF10A WT cells with varying duration of 100pM TGFβ stimulation. Expression kinetics of SMAD7, PAI-1 and TIEG upon 100pM TGFβ stimulation and termination at 1h or 6h with the TGFβReceptor I Kinase inhibitor SB431542 were measured by RT-qPCR at indicated time points. β-Actin was used as an internal control. Error bars indicate standard deviation of technical triplicates.

3.1.4 SMAD translocation depends on receptor activity at all time points

The next step was to verify that nuclear translocation of SMADs in the reporter systems depend on TGFβ receptor activity. From literature is known, that the TGFβR I Kinase inhibitor SB431542 immediately prevents phosphorylation and therefore nuclear accumulation of SMAD2 (Inman *et al*, 2002a). Western Blot experiments in MCF10 WT cells confirmed that phosphorylation of SMAD2 is prevented when receptor 1 is inhibited 45 min before TGFβ stimulation **(Figure 9)**. SMAD2 reporter cells treated with the specific inhibitor at the same time or 30 minutes before TGFβ stimulation showed no accumulation in the nucleus at all, while inhibitor treatment 1h after TGFβ stimulation rapidly and synchronously terminated the response and ratio values 2 hours post termination are comparable to DMSO treated control cells (3.5 hours of time-lapse imaging) **(Figure 10A, B & C)**. Interestingly, inhibitor treatment 6h after TGFβ stimulus showed that the late SMAD2 response is also fully receptor-dependent, since ratio values are comparable 1-hour post termination to control cells (7.5 hours of time-lapse imaging). The SMAD4 reporter cell line showed similar results **(Figure 10D)**. In conclusion the TGFβ response of the reporter cell lines was at all time points receptor-dependent.

Figure 9

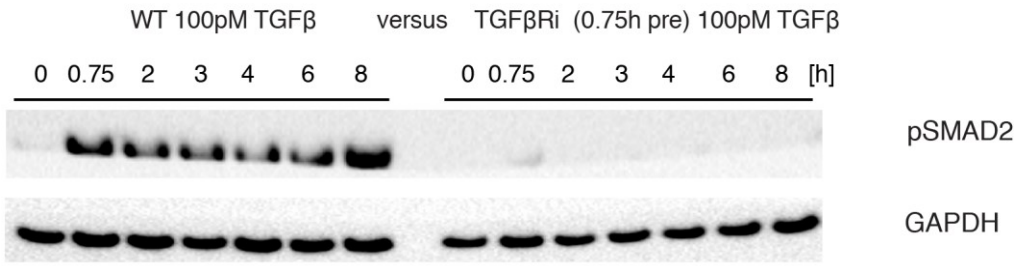

3.1.4 Figure 9. SMAD translocation depends on receptor activity at all time points shown in western blot experiment. Western blot analysis of MCF10A WT cells treated with the TGFβReceptor I Kinase inhibitor SB431542 (TGFβRi) 0.75h pre 100pM TGFβ stimulation. SMAD2 phosphorylation was analyzed at indicated time points. GAPDH was used as a loading control.

Figure 10

A

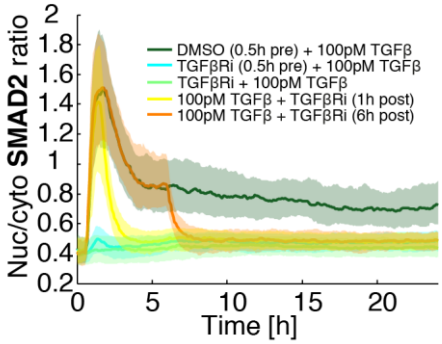

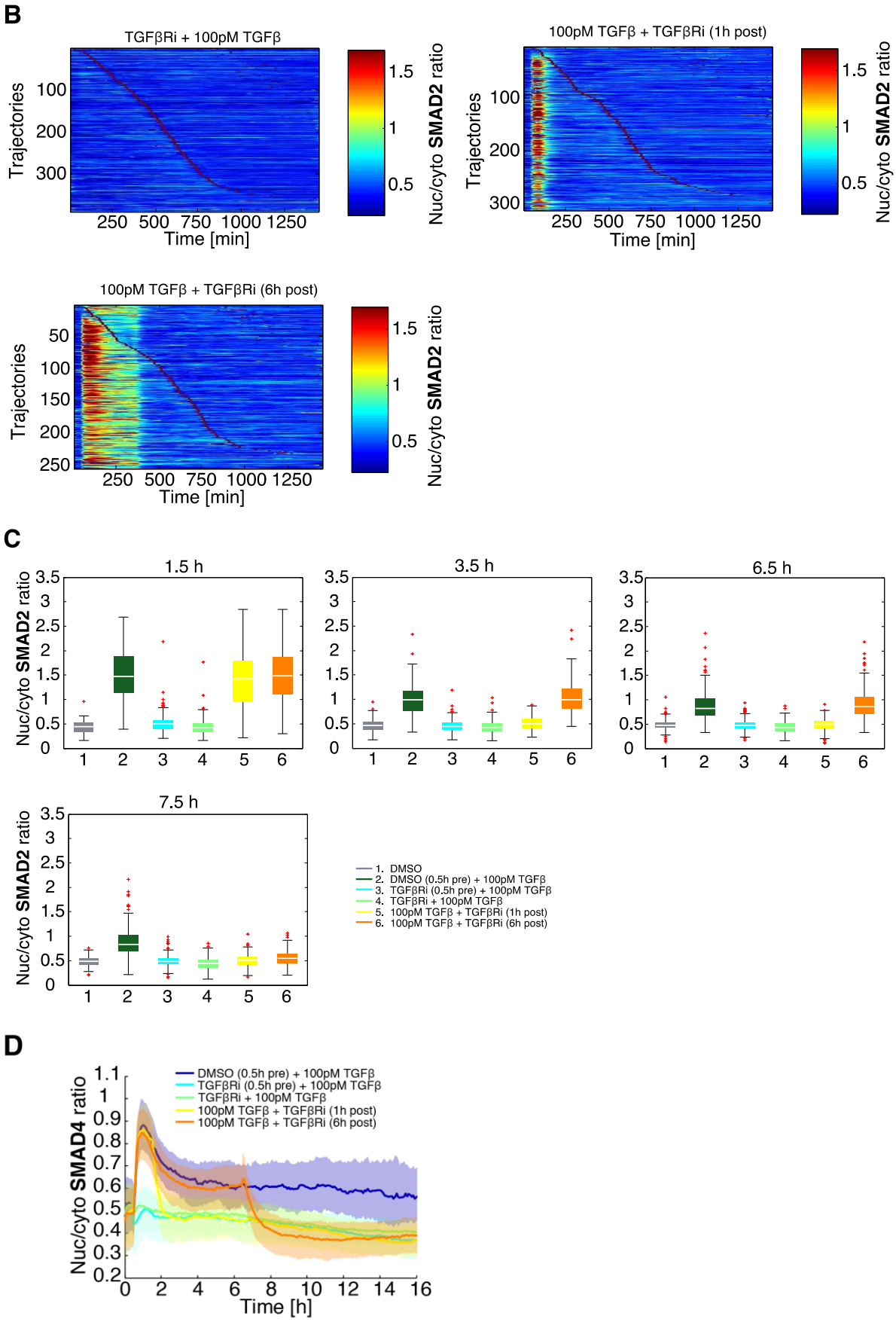
B
TGFβRi + 100pM TGFβ
100pM TGFβ + TGFβRi (1h post)
100pM TGFβ + TGFβRi (6h post)
Trajectories
Time [min]
Nuc/cyto SMAD2 ratio
C
1.5 h
3.5 h
6.5 h
7.5 h
Nuc/cyto SMAD2 ratio
1. DMSO
2. DMSO (0.5h pre) + 100pM TGFβ
3. TGFβRi (0.5h pre) + 100pM TGFβ
4. TGFβRi + 100pM TGFβ
5. 100pM TGFβ + TGFβRi (1h post)
6. 100pM TGFβ + TGFβRi (6h post)
D
Nuc/cyto SMAD4 ratio
Time [h]
DMSO (0.5h pre) + 100pM TGFβ
TGFβRi (0.5h pre) + 100pM TGFβ
TGFβRi + 100pM TGFβ
100pM TGFβ + TGFβRi (1h post)
100pM TGFβ + TGFβRi (6h post)

3.1.4 Figure 10. SMAD translocation depends on receptor activity at all time points shown in time-lapse microscopy experiments.
A Median nuc/cyto SMAD2 ratio of reporter cells stimulated with 100pM TGFβ and treated with TGFβReceptor I Kinase inhibitor SB431542 (TGFβRi) at indicated time points. DMSO was used for the control. Shaded area represent data between 25th and 75th percentiles.
B Heat maps of SMAD2 translocation in individual cells over 24h. Cells were stimulated with 100pM TGFβ and treated with TGFβReceptor I Kinase inhibitor SB431542 (TGFβRi) at indicated time points. Each horizontal line represents a single cell and the nuc/cyto ratio is shown as indicated in the legend. Cells were sorted by the time of the first division as indicated by red marks.
C Nuc/cyto SMAD2 ratio values at 1.5, 3.5, 6.5 and 7.5h for reporter cells stimulated with 100pM TGFβ and treated with TGFβReceptor I Kinase inhibitor SB431542 (TGFβRi) at indicated time points. White lines indicate median; boxes include data between the 25th and 75th percentiles; whiskers extend to maximum values within 1.5× the interquartile range; crosses represent outliers.
D Median nuc/cyto SMAD4 ratio of reporter cells stimulated with 100pM TGFβ and treated with TGFβReceptor I Kinase inhibitor SB431542 (TGFβRi) at indicated time points. DMSO was used for the control. Shaded area represent data between 25th and 75th percentiles.

3.1.5 SMAD translocation is dynamic and heterogeneous in individual cells

So far I only analyzed median dynamics across the population. However, heat maps of treated SMAD2 reporter cells with varying TGFβ doses showed a high cell-to-cell variability for all conditions **(Figure 11A)**. Focusing on one specific concentration of 100pM TGFβ, several example trajectories and the median of the population demonstrate the broad variability of dynamics, although all cells were genetically identical **(Figure 11B)**. In **Figure 11C** five reacting single cells are highlighted and compared to the median 100pM TGFβ response. While the first cell showed a very high peak amplitude, strong adaptation and moderate second signaling, the second one was marked by a lower amplitude and adaptation to a very low signaling plateau afterwards. The third and fourth cell were characterized by even two or three nuclear translocation peaks and the last one was marked by a low first amplitude and a strong late accumulation of SMAD2. These complex and heterogeneous dynamics were not limited to saturating TGFβ concentrations, as I also noticed pronounced variability when treating the cells with lower ligand concentrations **(Figure 11D).** Analysis of the SMAD4 reporter cell line also revealed, that the extent and duration of SMAD nuclear accumulation was highly variable **(Figure 11E).**

Figure 11

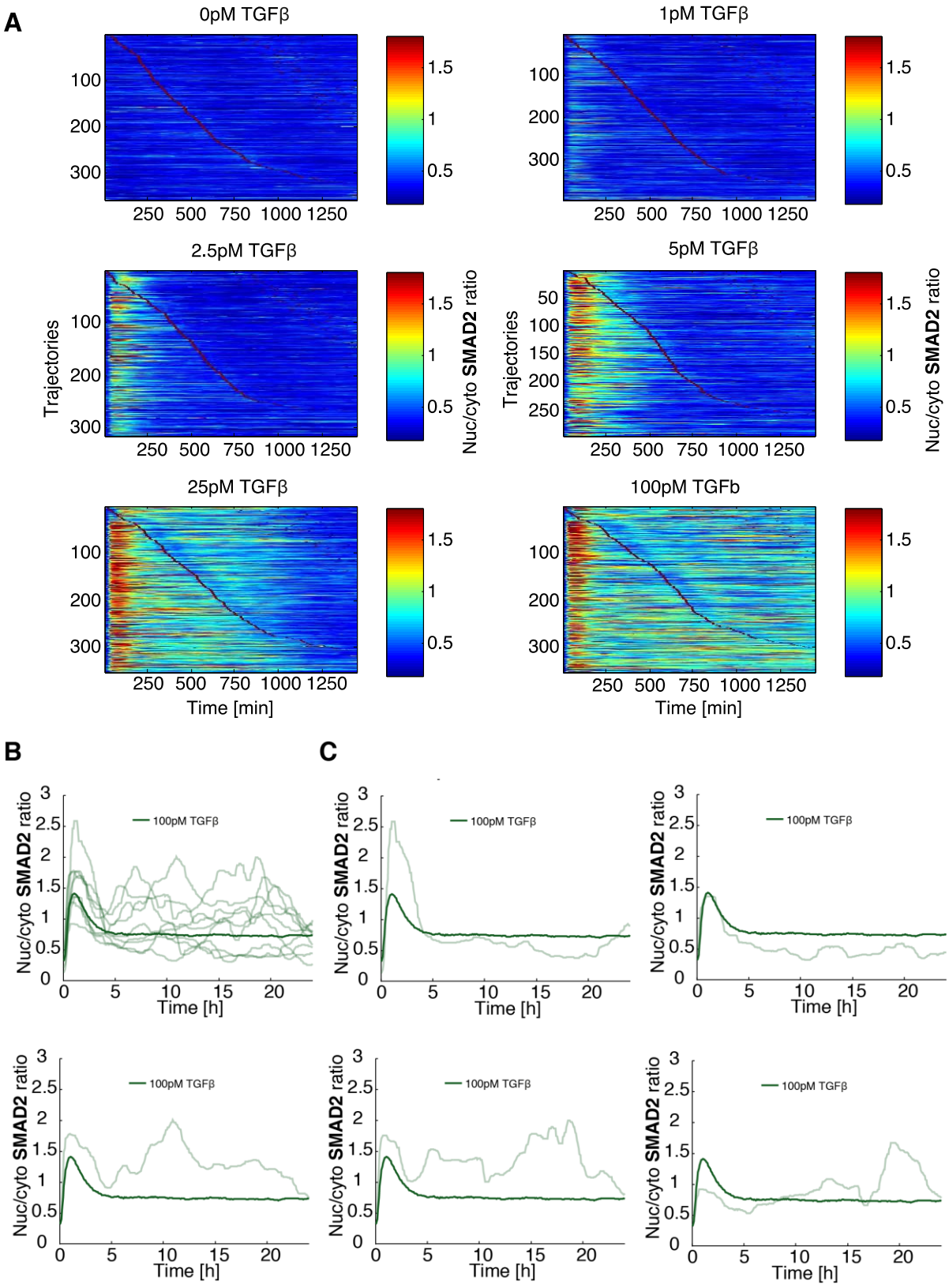
A
0pM TGFβ
1pM TGFβ
2.5pM TGFβ
5pM TGFβ
25pM TGFβ
100pM TGFb
Trajectories
Nuc/cyto SMAD2 ratio
Time [min]
B
C
100pM TGFβ
Nuc/cyto SMAD2 ratio
Time [h]

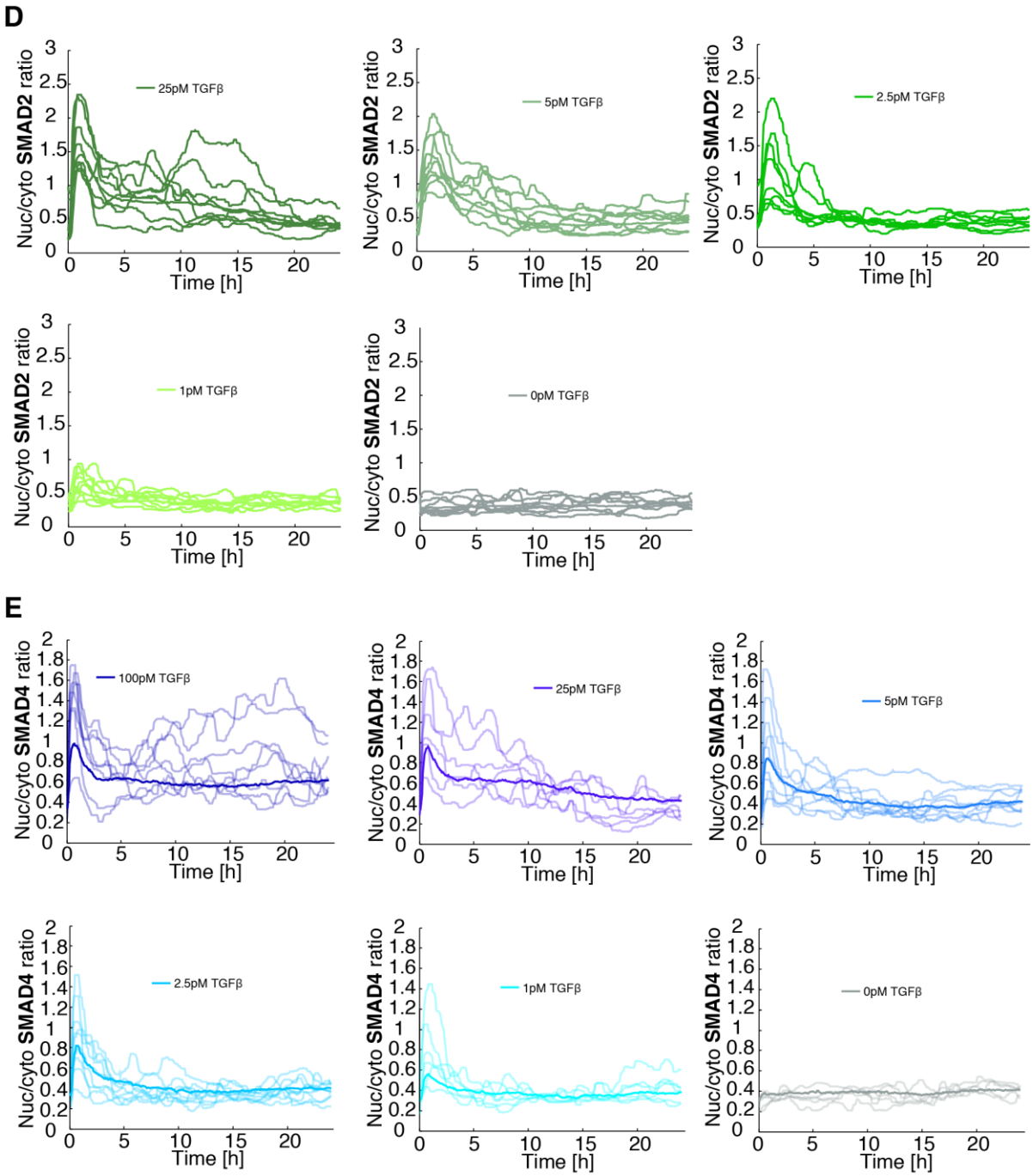

3.1.5 Figure 11. SMAD translocation is dynamic and heterogeneous in individual cells.
A Heat maps of SMAD2 translocation in individual cells over 24h. Cells were stimulated with varying concentrations of TGFβ. Each horizontal line represents a single cell and the nuc/cyto ratio is shown as indicated in the legend. Cells were sorted by the time of the first division as indicated by red marks.
B Time-resolved analysis of the SMAD2 nuclear to cytoplasmic localization for individual cells (thin lines) compared to the median nuc/cyto SMAD2 ratio of the entire population (thick line) upon stimulation with 100pM TGFβ.
C Exemplary individual cells (thin lines) compared to the median nuc/cyto SMAD2 ratio of the entire population (thick line) upon stimulation with 100pM TGFβ.
D Time-resolved analysis of the SMAD2 nuclear to cytoplasmic localization for individual cells (thin lines) compared to the median nuc/cyto SMAD2 ratio of the entire population (thick line) upon stimulation with 25, 5, 2.5, 1 and 0pM TGFβ.
E Time-resolved analysis of the SMAD4 nuclear to cytoplasmic localization for individual cells (thin lines) compared to the median nuc/cyto SMAD4 ratio of the entire population (thick line) upon stimulation with 100, 25, 5, 2.5, 1 and 0pM TGFβ.

3.1.6 Extraction of signaling features from single cell data

Next, to investigate the heterogeneous signaling more detailed, I extracted in collaboration with Marcel Jentsch single cell features in order to address the questions, which features change in a dose and time dependent manner and which of these features are robust and which are variable across individual cells. In **Figure 12A** I defined a complete response when increase and decrease are completed. Special features are schematically shown in **Figure 12B**. First, I examined the proportion of responding SMAD2 reporter cells for the varying TGFβ doses **(Figure 12C).** Almost all cells treated with 5pM - 100pM TGFβ ligand reacted to the stimulus. Furthermore, over 90% for 2.5pM, nearly 65% for 1pM and 20% of untreated cells responded above the threshold. The length of the first increase was robust over all conditions at about an hour, as well as the time of the maximum amplitude (around 2 hours) for the whole time-lapse imaging. However, the maximum amplitude increased with rising TGFβ concentrations and showed already saturation for 25pM ligand concentration. Accordingly, the first slope (A_{max} - A_{min}) is maximal increased at 25pM TGFβ stimulation. The length of the first response is for all varying TGFβ concentrations 5 hours, only for 5pM TGFβ I noticed an extension to almost 7.5 hours. In addition, this extension (about 7 hours) is also visible for the measured length of a complete response over the entire imaging period compared to 5 hours for the other ligand concentrations. Considering the integrated first response, a rise at 5pM TGFβ is apparent. Furthermore, the mean ratio value 5 hours after the first response is up to 25pM TGFβ increased and only for 100pM TGFβ was the final value after 24 hours of imaging significantly above the basal level. Moreover, feature detection of the SMAD4 reporter cell line showed similar results, although the proportion of responding cells was lower than for SMAD2 **(Figure 12D).** Over 80% for 25 and 100pM, over 70% for 5pM and 2.5pM, over 50% for 1pM and less than 30% of untreated cells responded above the threshold.

Figure 12

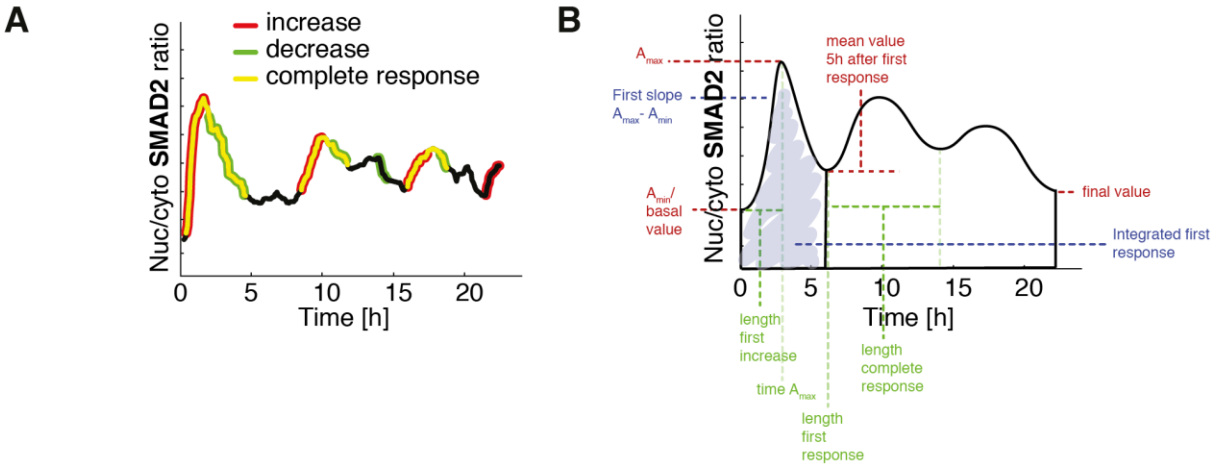

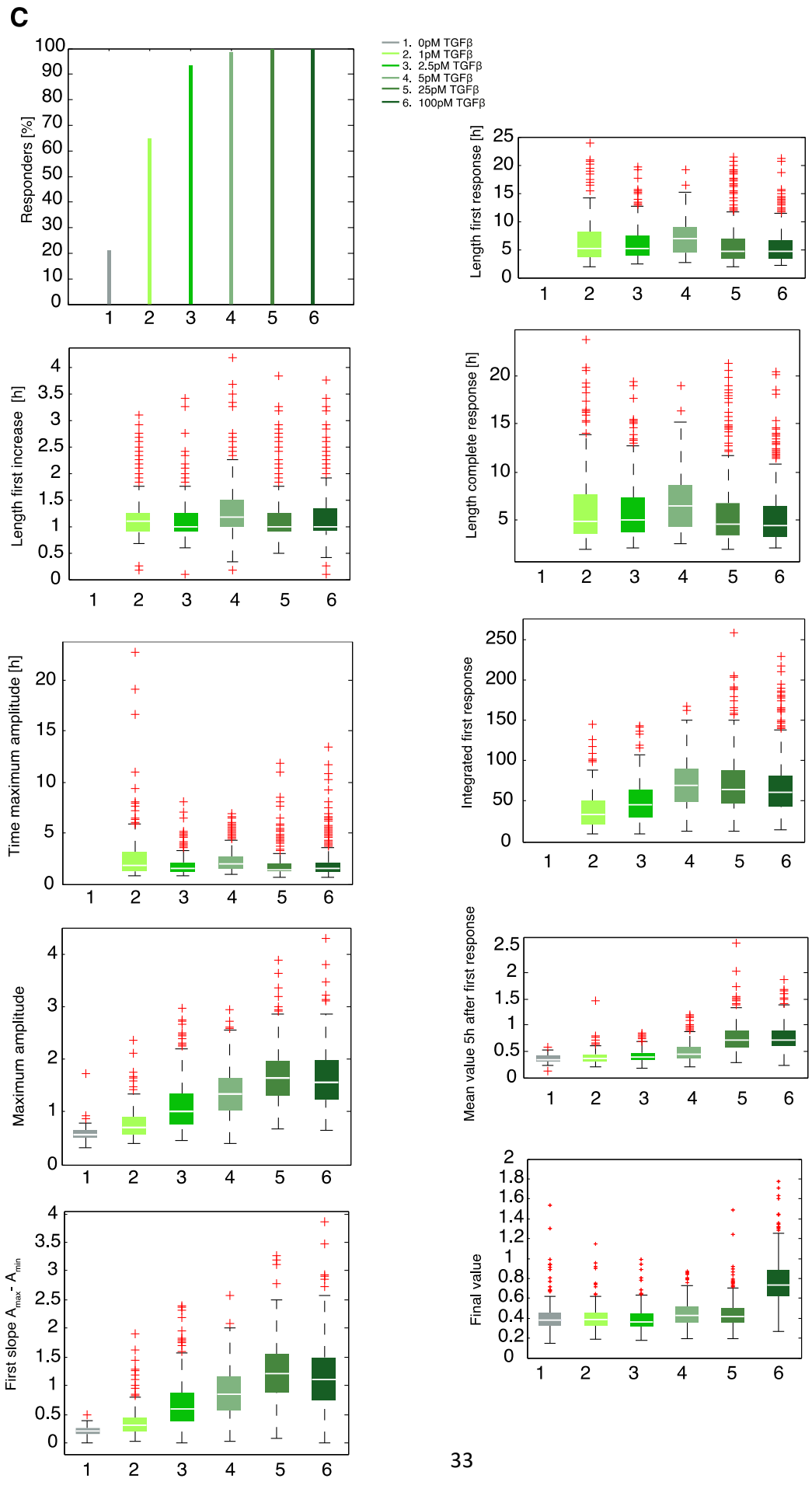
C
1. 0pM TGFβ
2. 1pM TGFβ
3. 2.5pM TGFβ
4. 5pM TGFβ
5. 25pM TGFβ
6. 100pM TGFβ
Responders [%]
Length first response [h]
Length first increase [h]
Length complete response [h]
Time maximum amplitude [h]
Integrated first response
Maximum amplitude
Mean value 5h after first response
First slope A_{max} - A_{min}
Final value

D

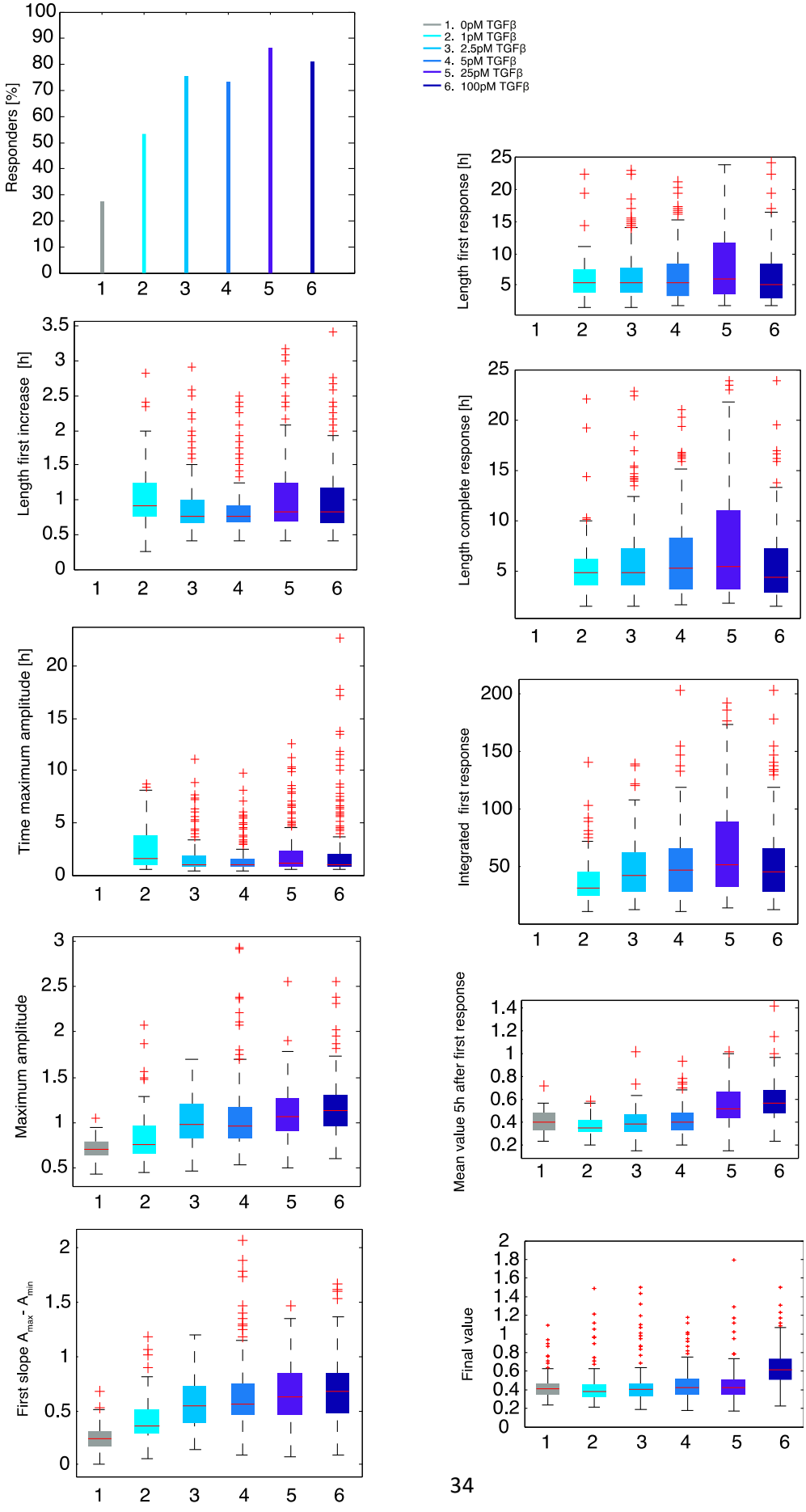
1. 0pM TGFβ
2. 1pM TGFβ
3. 2.5pM TGFβ
4. 5pM TGFβ
5. 25pM TGFβ
6. 100pM TGFβ
Responders [%]
Length first response [h]
Length first increase [h]
Length complete response [h]
Time maximum amplitude [h]
Integrated first response
Maximum amplitude
Mean value 5h after first response
First slope A_{max} - A_{min}
Final value

3.1.6 Figure 12. Extraction of signaling features from single cell data.
A Scheme for defining a complete response (in yellow) consisting of increase (red) and decrease (green) using an exemplary individual cell.
B Scheme of the individual signaling features and representation on an exemplary individual cell (Amax = maximum amplitude, time Amax = time maximum amplitude, Amin= basal level).
C Signaling features for the SMAD2 reporter cells stimulated with varying TGFβ concentrations as indicated. White lines indicate median; boxes include data between the 25th and 75th percentiles; whiskers extend to maximum values within 1.5× the interquartile range; crosses represent outliers.
D Signaling features for the SMAD4 reporter cells stimulated with varying TGFβ concentrations as indicated. White lines indicate median; boxes include data between the 25th and 75th percentiles; whiskers extend to maximum values within 1.5× the interquartile range; crosses represent outliers.

3.1.7 Individual cells are clustered according to their dynamic response

Next, I aimed to understand how phenotypic responses and cell fates of TGFβ can be specifically encoded by SMAD signaling. I hypothesized that the phenotypic effects are determined by the individual SMAD signaling pattern rather than by a specific ligand concentration applied to a population of cells. Since the separation of dynamic signaling responses according to varying TGFβ doses is not complete due to the strong cell- to- cell variability, we used a clustering approach to achieve a better separation in more homogenous groups. Marcel Jentsch established a method based on dynamic time warping (DTW) that calculates a distance matrix by pair-wise comparison of single time series and grouped cells according to this distance using hierarchical clustering. Applying all the cells from the varying TGFβ dose experiment (around 2000), cells were re-sorted in six clusters according to their dynamic behavior, irrespective of the stimulus level applied. The median response of cells in each cluster showed qualitatively distinct signaling behavior **(Figure 13A).** The identified signaling classes differ in their dynamic features, for instance in the amplitude, adaptation and late response. Cells in cluster 1 hardly respond to stimulation and can therefore be considered as non-responders. As expected this cluster shrinks with increasing TGFβ concentration **(Figure 13B).** Cells in other clusters respond either more transiently (cluster 2 and 3) or show sustained dynamics (cluster 4-6). Specifically, cells in cluster 2 and 3 show barely a second response and differ in a lower (cluster 2) and a very high amplitude with strong adaptation (cluster 3). Cluster 4 is characterized by lower amplitude, but a moderate late signaling response. While cluster 5 show a high amplitude and a strong, but shrinking second response, cluster 6 is marked by a strong and sustained second response with a moderate amplitude. Interestingly cluster 6 only exists for 100pM TGFβ. The distribution of the distinct signaling clusters changes with the stimulation dose of TGFβ. As expected, increasing ligand concentrations induce a shift from non-responders towards transient and then sustained signaling **(Figure 13B).** However, this separation is not sharp but rather gradual and obviously the clustering provides a better separation than sorting to different TGFβ concentration as shown in the silhouette plots **(Figure 13C & D).** The technique provides a graphical representation of how well each trajectory lies within its cluster. On the right side of each plot you can see trajectories that are more similar to

the own group and on the left side trajectories that are more similar to other groups. In conclusion these clusters are more homogeneous in SMAD dynamics than groups based on the TGFβ stimulation strength.

Figure 13

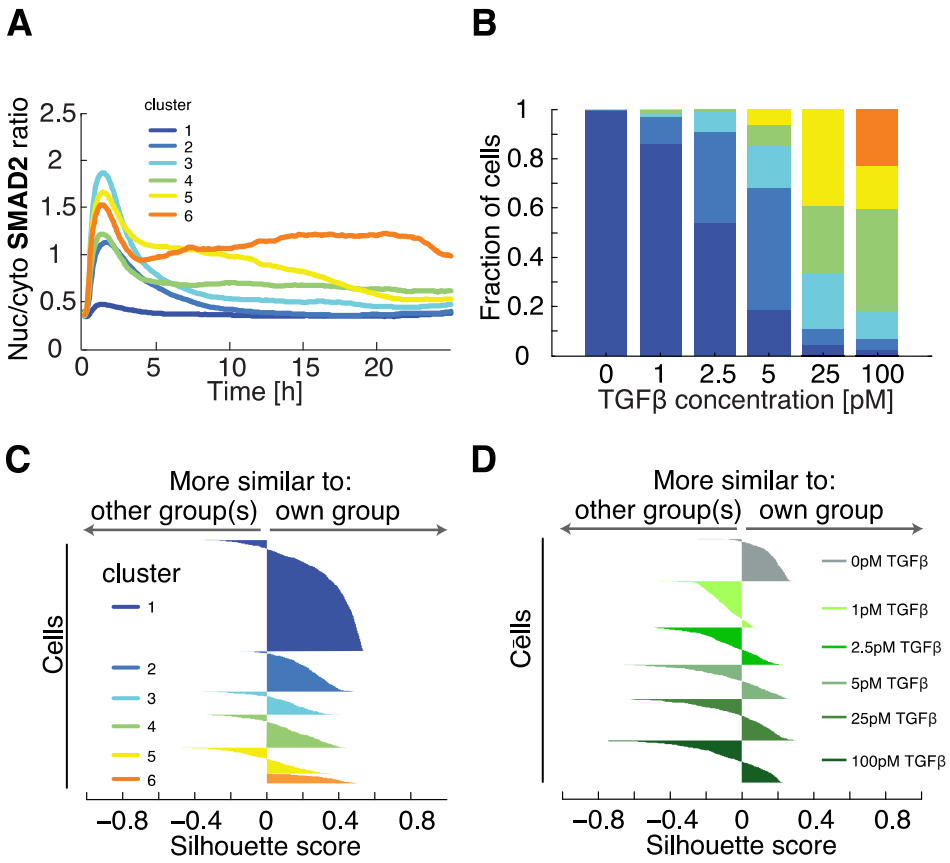

3.1.7 Figure 13. Individual cells are clustered according to their dynamic response.
A Individual cells were clustered into six signaling classes (cluster) according to their time-resolved nuc/cyto SMAD2 ratio using dynamic time warping (DTW). Each line represents the median over all cells of the indicated cluster. Cells stimulated with varying TGFβ concentrations were included in the analysis.
B Distributions of signaling classes (cluster) depending on TGFβ dose.
C Silhouette plots of cells sorted according to signaling classes (cluster). Plots provide a graphical representation of how well the nuc/cyto SMAD2 ratios of each cell correspond to trajectories of other cells in its own group according to the cDTW measure. Positive silhouette scores indicate that SMAD2 responses are more similar to the own group, while negative scores signify that the corresponding trajectory is closer to any of the other groups.
D Silhouette plots of cells sorted according to TGFβ concentration.

3.1.8 Cell fate decisions encoded in heterogeneous signaling dynamics

In order to understand information processing, I finally addressed the question whether phenotypic responses and cell fates are primarily encoded by the extracellular ligand concentration or by specific dynamics of SMAD signaling. TGFβ is known to block proliferation and to induce migration based on EMT (Katsuno *et al*, 2013). Therefore, we quantified changes in proliferation by calculating the cumulative fraction of the dividing cells over time and motility based on the movement of each cell calculated by the summed distance in pixel made over the last 4 hours of time-lapse imaging.

Considering first the varying TGFβ doses, the results in **Figure 14A** revealed that cells divide slightly less with increasing extracellular TGFβ concentration. Furthermore, 1pM and 2.5pM TGFβ stimulated cells showed the same motility around 80 pixels as untreated cells **(Figure 14B).** 5pM- 100pM TGFβ stimulated cells move faster at around 100- 120 pixels. In contrast sorting cells by the distinct signaling clusters led to a better separation of phenotypic responses. Cluster 6 was characterized by a considerably lower fraction of dividing cells, cluster 5 and 4 showed an intermediate number of cell divisions and cluster 3 and 2 proliferated with the rate as non-responders **(Figure 14C).** In addition, motility increased with the cluster number **(Figure 14D).** This data suggests that migration and proliferation may be controlled by different aspects of the dynamic SMAD signaling response. Migration tended to be affected already by a transient peak of SMAD translocation (cluster 2-5), whereas the anti-proliferative effects seemed to require sustained SMAD signaling (cluster 4-6) and a very high amplitude is not sufficient (cluster 3). It needs to be highlighted that a clear shift to migration, EMT and cell cycle arrest required a strong and sustained second signaling phase (cluster 6) rather than a high first amplitude. In conclusion, phenotypic responses and cell fate decisions are correlated with signaling classes of distinct long- term dynamic behavior.

Figure 14

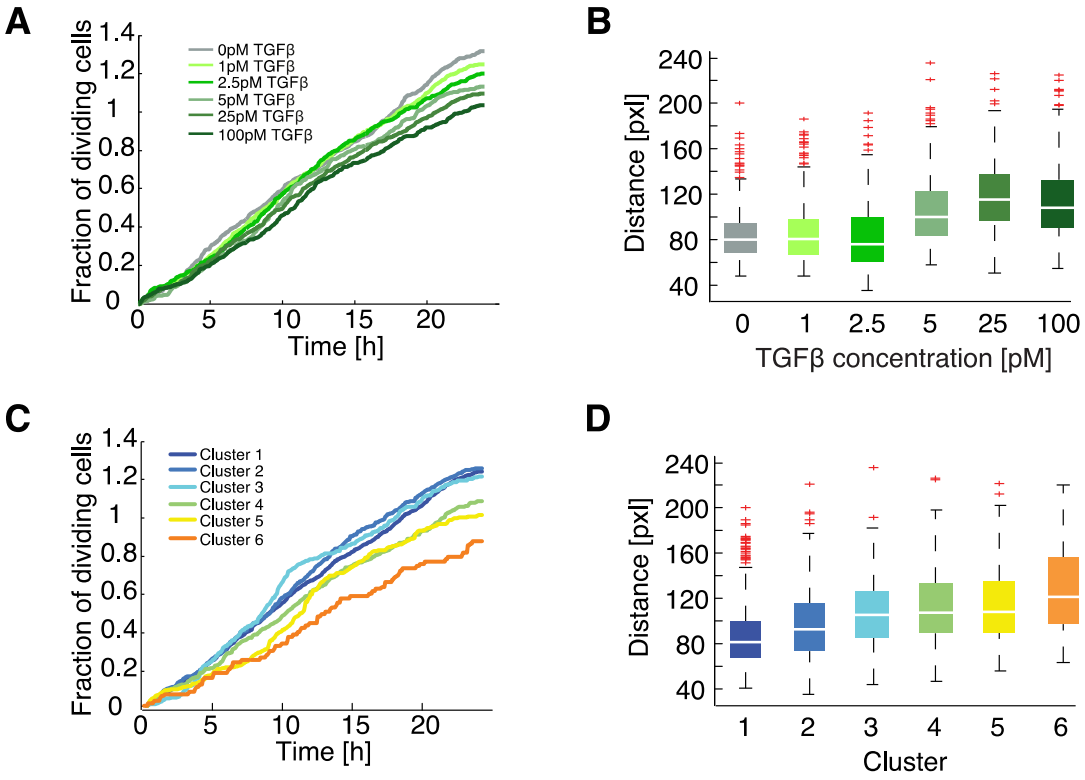

3.1.8 Figure 14. Cell fate decisions encoded in heterogeneous signaling dynamics.
A Cell proliferation of SMAD2 reporter cells shown as fraction of dividing cells 24h after a varying TGFβ stimulus. Above 1 means that cells have divided several times.
B Motility of each cell as summed distance in pixel (pxl) covered between 20 and 24h after stimulation with varying TGFβ concentrations. Cells were sorted according to TGFβ concentrations. White lines indicate median; boxes include data

between the 25th and 75th percentiles; whiskers extend to maximum values within 1.5× the interquartile range; crosses represent outliers.
C Cell proliferation of SMAD2 reporter cells shown as fraction of dividing cells within 24h for the different signaling classes (cluster). Above 1 means that cells have divided several times.
D Motility of each cell as summed distance in pixel (pxl) covered between 20 and 24h after stimulation with varying TGFβ concentrations. Cells were sorted according to signaling classes (cluster). White lines indicate median; boxes include data between the 25th and 75th percentiles; whiskers extend to maximum values within 1.5× the interquartile range; crosses represent outliers.

3.1.9 Combining smFISH of target genes with single cell trajectories

Phenotypic responses and cell fate decisions are determined by modulated target gene expression. But it is still unknown how the highly heterogeneous SMAD dynamics encode and transmit information to the level of target gene expression. In order to gain a better understanding of the decoding of SMAD dynamics on the RNA level, I correlated the single-cell target gene expression of PAI- 1 with single-cell SMAD signaling by combining 3 hours and 14 hours of live- cell imaging of the SMAD2- reporter cell line stimulated with 25pM TGFβ with subsequent single molecule fluorescent in situ hybridization (smFISH). An illustration of the approach is shown in **Figure 15A.** In brief, cells are seeded on a relocation grid for the time-lapse microscopy experiment and SMAD2 translocation was measured and clustered as described in 3.1.1, 3.1.7 and 6.12. Subsequently, cells were fixed and specific PAI-1 probes for smFISH labeled with CalFluor-610 were applied and imaged as z-stacks. The RNA amount of each cell was calculated using Star Search analysis tool and matched manually to the identical tracked single cell from the microscopy experiment. Considering the absolute RNA counts per cell before treatment, 3 hours or 14 hours post 25pM TGFβ ligand stimulation, the target gene expression also showed high cell-to- cell variability with a median of 59 RNA/cell at basal level, 444 RNA/cell (7.5 fold) at 3 hours and 242 RNA/cell (4.1 fold) at 14 hours **(Figure 15B and C)**. Interestingly, the amount of PAI-1 at basal level had a wide distribution as indicated by a coefficient of variation (CV) of almost 1.2 **(Figure 15D).** More important was indeed how 3 hours of individual SMAD signaling correlate to the PAI-1 RNA count in the respective cell at 3 hours post stimulation, which correspond to the peak of PAI-1 target gene expression. First, I grouped the trajectories of SMAD2 signaling into 6 clusters, as illustrated in the heat map, and then looked at the distribution of the RNA to the respective cluster **(Figure 15E)**. Although the clusters are characterized by distinct dynamic behavior, the RNA count per cell was around 400 for all clusters. I also grouped the RNA results into 3 clusters ranging from high to low RNA counts per cell and looked at the distribution of the respective median trajectories **(Figure 15F).** Obviously, the heterogeneous SMAD2 dynamics are not correlated with PAI-1 expression 3 hours post stimulation. However, considering 14 hours of individual SMAD signaling, I observed a correlation of long-term SMAD2 dynamics to the PAI-1 target gene expression. Similarly, I grouped the trajectories of SMAD2 signaling into 4 clusters and then looked at the distribution of the RNA to the respective cluster **(Figure 15G).** Cells in cluster 1 are marked by a low amplitude, low second signaling and a lower median count

of RNA per cell of 187. Cells of cluster 3 are characterized by a moderate amplitude, strong sustained signaling and a higher count of RNA per cell of 329. While cells of cluster 2 showed an intermediate amplitude and intermediate second response, cells of cluster 4 showed a very high amplitude, strong but decreasing late response, both clusters showed intermediate counts of RNA per cell of around 240. Obviously, the first peak amplitude of SMAD2 dynamics is not responsible for the altered RNA distribution but features of the long-term dynamics since cluster 3 with a strong sustained late signaling showed the highest amount of RNA. In addition, dividing the RNA results into 3 clusters from high to low RNA counts per cell (140, 292 and 588), showed that cluster 1 with low RNA amount correlates with the median trajectory with a lower late signaling and cluster 3 with high RNA amount correlates with the median trajectory with a higher late signaling **(Figure 15H)**. The amplitude of SMAD2 dynamics was not correlated to PAI-1 target gene expression 14 hours post stimulation. In conclusion, considering 14 hours of individual SMAD signaling, I observed a correlation of long-term SMAD2 dynamics to the PAI-1 target gene expression. Nevertheless, further experiments are needed to get conclusive results.

Figure 15

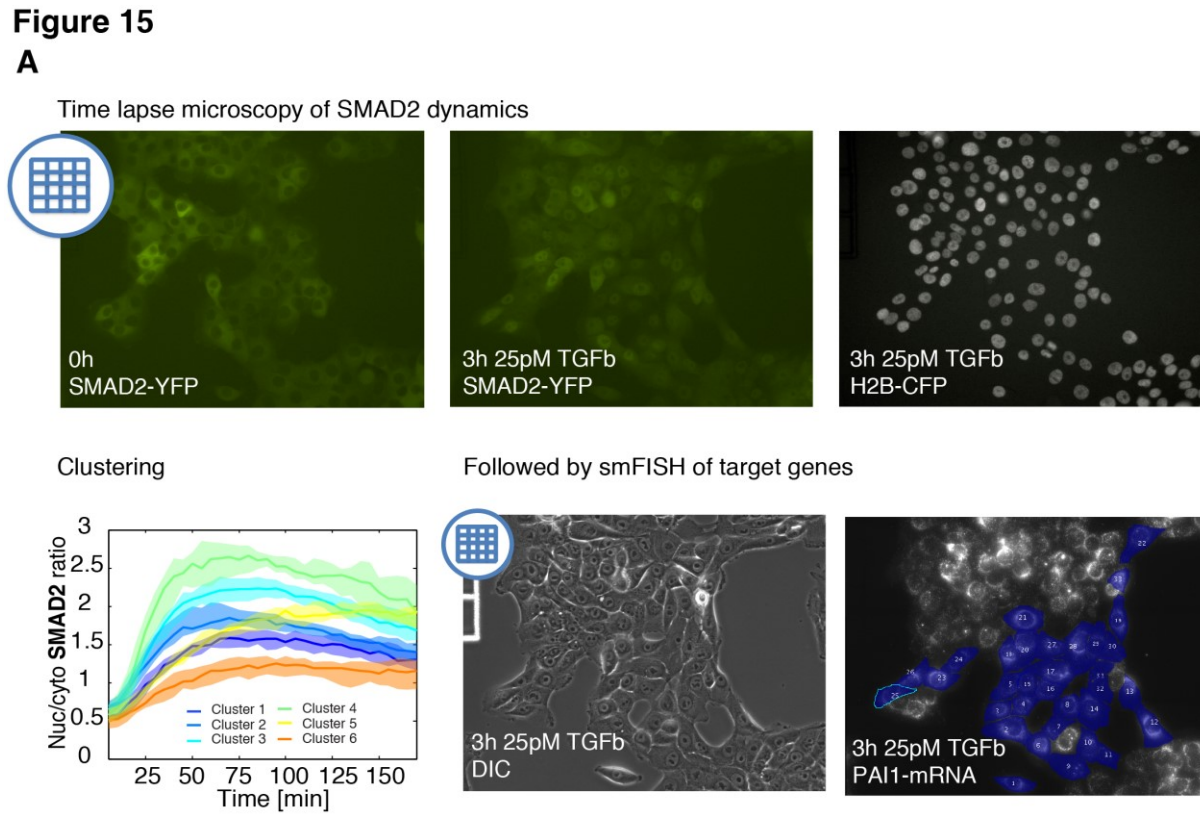

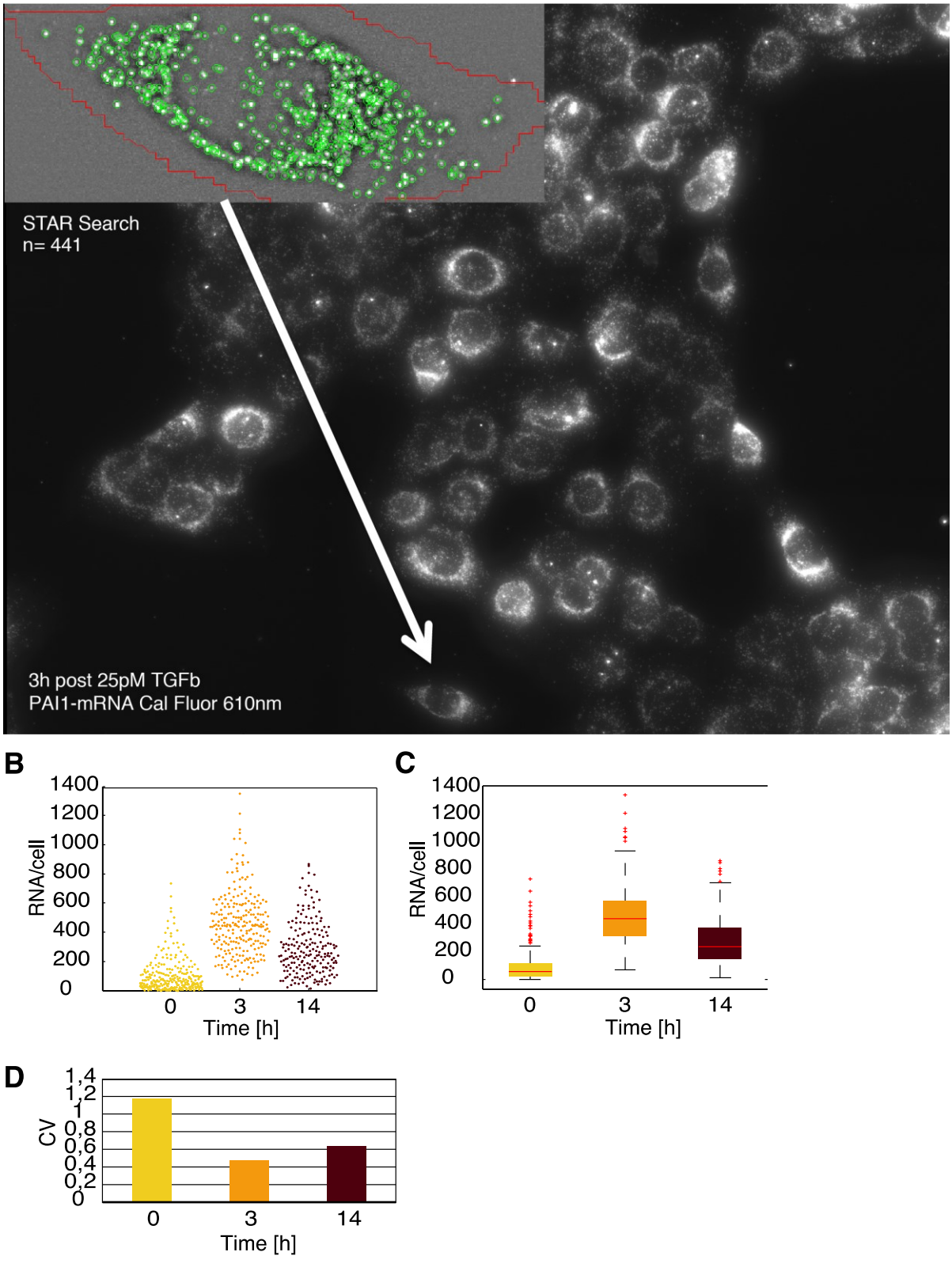
STAR Search
n= 441
3h post 25pM TGFb
PAI1-mRNA Cal Fluor 610nm
B
RNA/cell
1400
1200
1000
800
600
400
200
0
0
3
14
Time [h]
C
RNA/cell
1400
1200
1000
800
600
400
200
0
0
3
14
Time [h]
D
CV
1,4
1,2
1
0,8
0,6
0,4
0,2
0
0
3
14
Time [h]

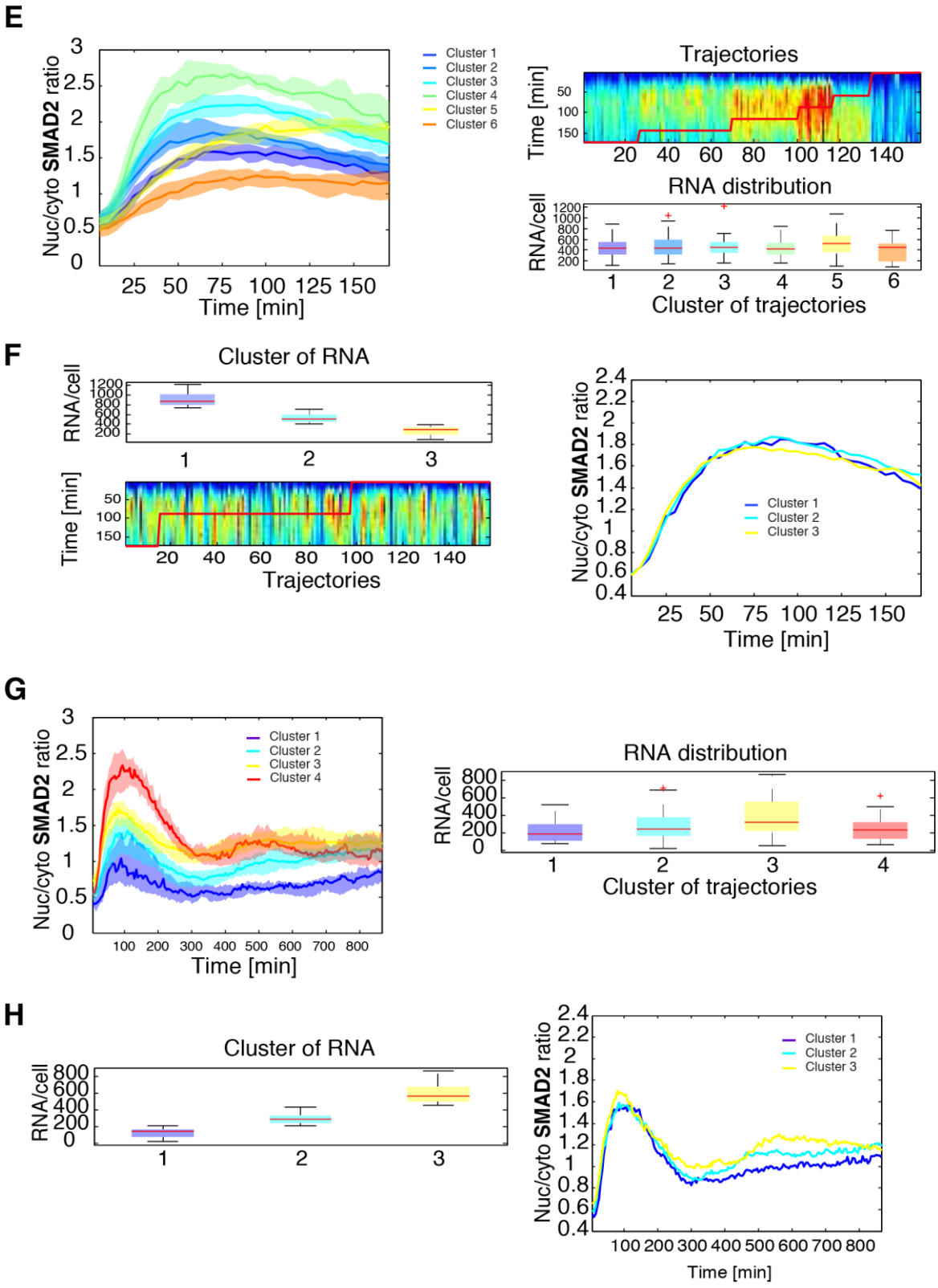

3.1.9 Figure 15. Combining smFISH of target genes with single cell trajectories.
A Individual steps of the method: combining time-lapse microscopy experiments and smFISH using the example of 3h 25pM TGFβ stimulation and subsequent PAI-1 smFISH analysis. SMAD2 reporter cells are seeded on a relocation grid for the time-lapse microscopy experiment (three upper panel) and SMAD2 translocation was measured and clustered (middle right picture). Subsequently, cells were fixed and specific PAI-1 probes for smFISH labeled CalFluor-610 were applied and imaged with z-stacks. The RNA amount of each cell was calculated using Star Search Analysis tool and matched manually to the identical tracked single cell from the microscopy experiment (remaining panels).
B Bee swarm plot of PAI-1 RNA distribution 0, 3 and 14h after 25pM TGFβ treatment.

C Box plot of PAI-1 RNA distribution 0, 3 and 14h after 25pM TGFβ treatment. Median of 59 RNA/cell at basal level, 444 RNA/cell at 3h and 242 RNA/cell at 14h post TGFβ treatment. Red lines indicate median; boxes include data between the 25th and 75th percentiles; whiskers extend to maximum values within 1.5× the interquartile range; crosses represent outliers.
D Coefficient of variation (CV) of PAI-1 RNA distribution 0, 3 and 14h after 25pM TGFβ treatment.
E Individual cells were clustered into six signaling classes (cluster) according to their time-resolved nuc/cyto SMAD2 ratio 3h after 25pM TGFβ stimulation (left panel). Each line represents the median over all cells of the indicated cluster. Shaded area represent data between 25th and 75th percentiles. Cluster are illustrated in the heat map (red line, right upper panel) and PAI-1 RNA distribution of the respective cluster is shown as a box plot (right lower panel). Red lines indicate median; boxes include data between the 25th and 75th percentiles; whiskers extend to maximum values within 1.5× the interquartile range; crosses represent outliers.
F Individual cells were clustered into three cluster according to the PAI-1 RNA amount per cell 3h after 25pM TGFβ stimulation (left upper panel). Cluster are illustrated in the heat map (red line, left lower panel) matching with the corresponding nuc/cyto SMAD2 ratio trajectories. The distribution of the respective median nuc/cyto SMAD2 ratio of the three RNA cluster are shown in the right panel.
G Individual cells were clustered into four signaling classes (cluster) according to their time-resolved nuc/cyto SMAD2 ratio 14h after 25pM TGFβ stimulation (left panel). Each line represents the median over all cells of the indicated cluster. Shaded area represent data between 25th and 75th percentiles. PAI-1 RNA distribution of the respective cluster is shown as a box plot (right panel). Red lines indicate median; boxes include data between the 25th and 75th percentiles; whiskers extend to maximum values within 1.5× the interquartile range; crosses represent outliers.
H Individual cells were clustered into three cluster according to the PAI-1 RNA amount per cell 14h after 25pM TGFβ stimulation (left panel). The distribution of the respective median nuc/cyto SMAD2 ratio of the three RNA cluster are shown in the right panel.

3.1.10 SMAD2 and SMAD4 show similar dynamics in the same individual cell

Next, I focused on the question whether SMAD2 or SMAD4 individual response pattern are crucial for the target gene expression and cell fate decisions. I observed that the average response and signaling features are similar to varying TGFβ doses (3.1.3, 3.1.6). But what happens in the same individual cell? Are SMAD2 and SMAD4 dynamics coupled and protein fluctuations co-related? To this end I generated a combined fluorescent reporter cell line (E9) by fusing SMAD4 to the yellow fluorescent protein Venus (YFP) and SMAD2 to the red fluorescent protein mCherry under the control of a constitutive promoter (UbCp), respectively **(Figure 16A)**. As an inverse variant I generated a combined cell line (A3) by fusing SMAD2 to YFP and SMAD4 to mCherry. In addition, both cell lines also stably express the nuclear marker histone H2B-CFP under the control of UbCp to enable automated image analysis. I created both variants to exclude possible influences by the distinct fluorescence proteins. First, I examined the average response of SMAD2 and SMAD4 of the SMAD2-mCherry- SMAD4-YFP (E9) cell line for the different TGFβ concentrations as shown in **Figure 16B**. The results for both transcription factors look similar. Example trajectories for the varying TGFβ doses in **Figure 16C** showed that patterns of the individual SMAD2 and SMAD4 trajectories were strongly correlated. Furthermore, the correlation coefficient for all the trajectories over time confirmed that SMAD2 and SMAD4 dynamics were highly co-regulated although the signaling peak is marked with a slightly lower correlation **(Figure 16D)**. Moreover, the inverse cell line A3 showed similar dynamics for SMAD2 and SMAD4 in the average response as well, but with lower fluorescence intensities than the previously presented YFP-tagged cell lines **(Appendix Figure A1)**. However, example trajectories and the correlation coefficient showed high accordance of SMAD2 and SMAD4 signaling in the same individual cell **(Appendix Figure A2 and**

A3). In conclusion, translocation of SMAD2 and SMAD4 into the nucleus and shuttling back to the cytoplasm were co-regulated and coupled and fluctuations were synchronized, hence they regulate target gene expression und cell fate decisions together.

Figure 16

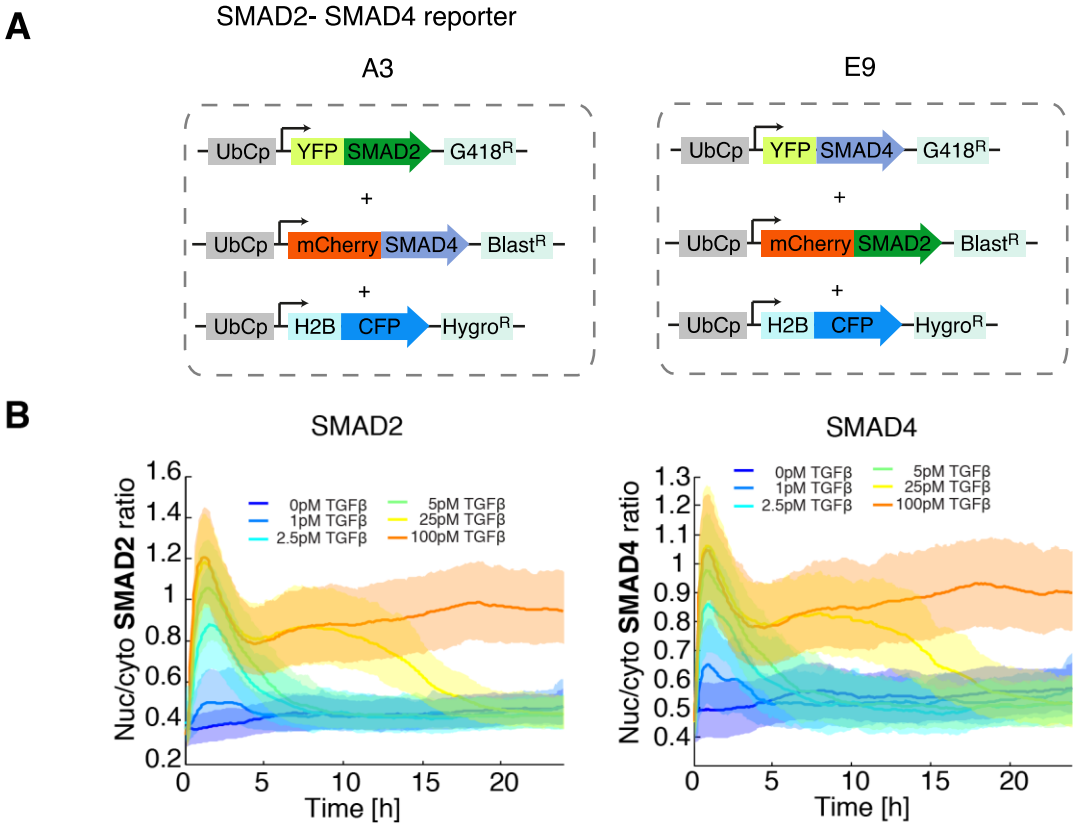

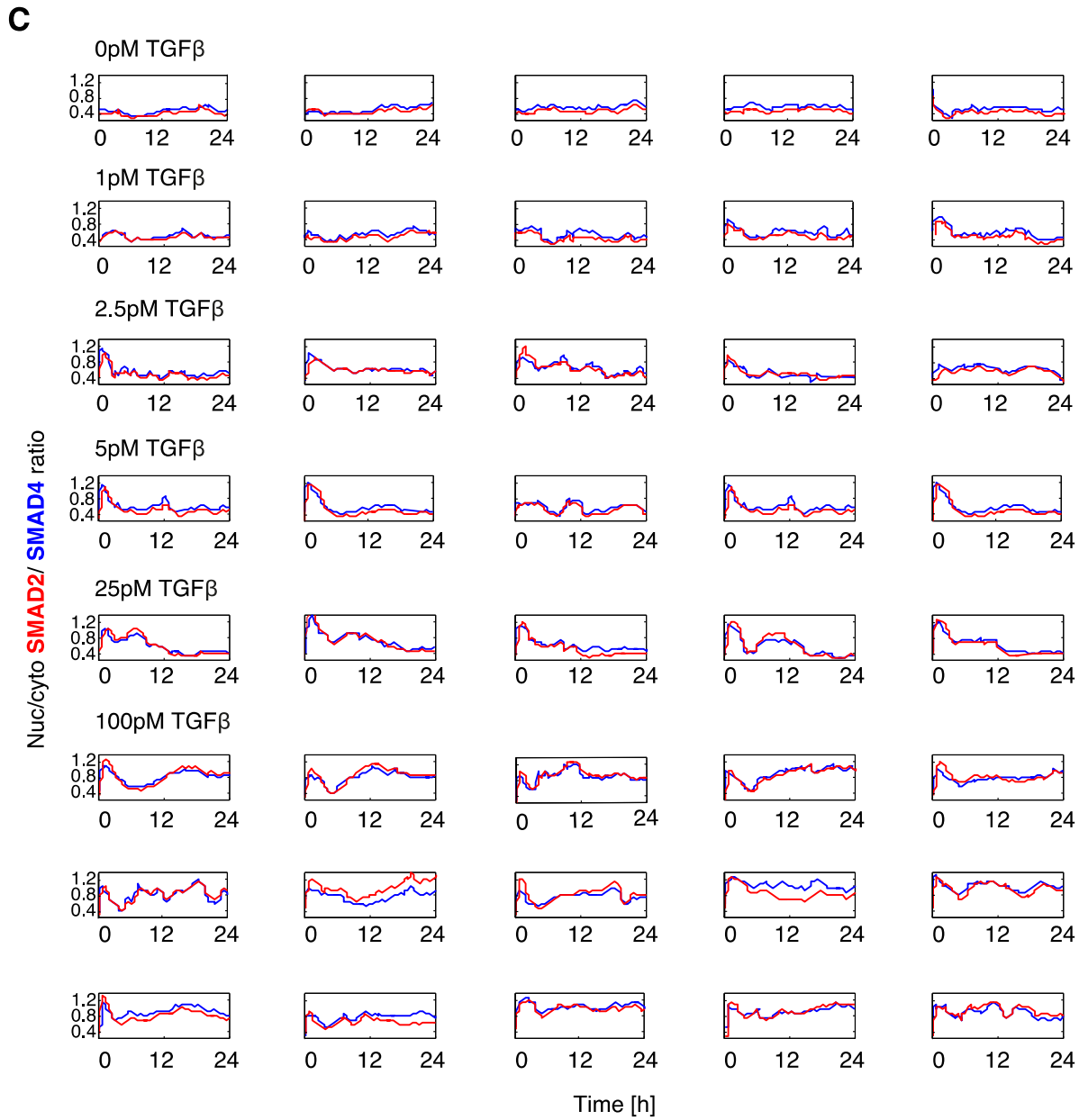
C
0pM TGFβ
1pM TGFβ
2.5pM TGFβ
5pM TGFβ
25pM TGFβ
100pM TGFβ
Nuc/cyto SMAD2/ SMAD4 ratio
Time [h]
1.2
0.8
0.4
0
12
24

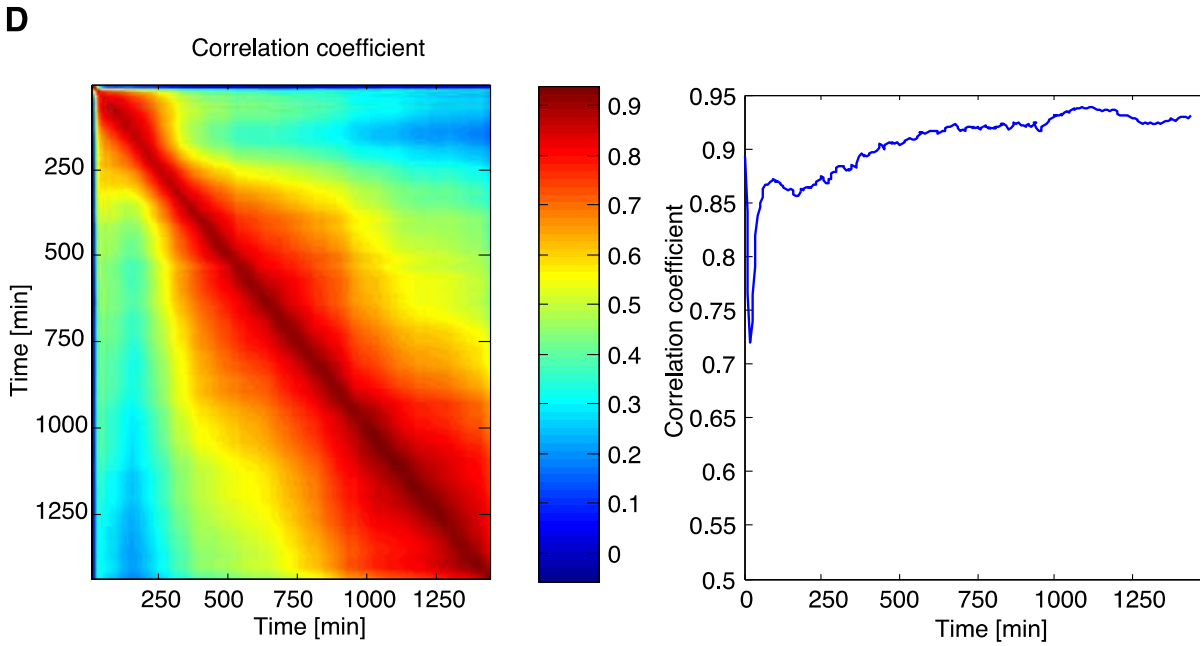

3.1.10 Figure 16. SMAD2 and SMAD4 show similar dynamics in the same individual cell.
A Schematic figure of the SMAD2-YFP- SMAD4-mCherry reporter cell line (A3) and of the SMAD4-YFP- SMAD2-mCherry reporter cell line (E9). A3: SMAD2 was fused to mVenus (YFP) under the control of UbCp with the selection marker G418 (Geneticin) and SMAD4 was fused to the red fluorescent protein mCherry under the control of UbCp with the selection marker blasticidin (Blast)
As a nuclear marker, H2B was fused to the cyan fluorescent protein mCerulean (CFP) under the control of UbCp with the selection marker hygromycin. E9: SMAD4 was fused to mVenus (YFP) under the control of UbCp with the selection marker G418 (Geneticin) and SMAD2 was fused to mCherry under the control of UbCp with the selection marker blasticidin (Blast). As a nuclear marker, H2B was fused to CFP under the control of UbCp with the selection marker hygromycin.
B Median nuc/cyto SMAD2 and SMAD4 ratio of the combined SMAD4-YFP- SMAD2-mCherry (E9) reporter cell line stimulated with 0, 1, 2.5, 5, 25 or 100pM TGFβ and tracked over 24h. Shaded area represent data between 25th and 75th percentiles.
C Time-resolved analysis of SMAD2 (red lines) and SMAD4 (blue lines) translocation in the same individual (E9) reporter cells stimulated with varying concentrations of TGFβ.
D Heat map of correlation coefficient of SMAD2 and SMAD4 translocation in (E9) reporter cells is shown as indicated in the legend (left panel) and correlation coefficient over 24h (right panel).

3.2 Regulatory and adaption mechanisms

In the next step I aimed to understand what molecular mechanisms control dynamic signal processing, especially what mechanisms underlying the decomposition into distinct signaling classes. How do different adaption mechanisms act together to control long term dynamics? Which changes in protein levels and activities determine the response of individual cells to a given stimulus? In order to address these questions systematically, I investigated several regulatory mechanisms that are known to influence the TGFβ response: ligand depletion, receptor internalization and degradation, proteasomal degradation and transcriptional feedback loops (Clarke *et al*, 2009; Chen, 2009; Zhang & Laiho, 2003; Yan, *et al*, 2009; Wegner *et al*, 2012).

3.2.1 Full ligand decay correlate with signaling termination

Studies indicate that TGFβ depletion plays a significant role in determining the duration of signaling in cells (Clarke *et al*, 2009). To gain a better understanding how complete adaptation of the signaling pathway is connected to TGFβ ligand depletion by cellular uptake and lysosomal degradation, we measured extracellular TGFβ ligand concentration by using Mink lung epithelial cells (MLEC), stably transfected with an expression construct containing a truncated PAI-1 promoter fused to the firefly luciferase reporter gene (Abe *et al*, 1994). Conditions are the same as for the microscopy experiments. Cells were stimulated with 25pM or 100pM TGFβ and supernatant was removed and analyzed at several time points in separate dishes **(Figure 17)**. I found that the estimated ligand decay of an initial TGFβ concentration of 25pM is completed within 20 hours with a half-life around 6 hours. These findings correspond with the complete adaptation of the signaling pathway to basal pre-stimulation level in the microscopy experiments. Furthermore, cells stimulated with 100pM TGFβ revealed an extracellular ligand concentration around 20pM after 24 hours, which is estimated with a half- life around 9 hours. This agrees with the non-complete adaptation to basal level for 100pM TGFβ stimulation within 24 hours. In conclusion, the half-lives differ for both concentrations and these time-lapse imaging experiments suggest that the full ligand decay mainly affects the signaling termination and as long as extracellular TGFβ is present, SMADs accumulate into the nucleus.

Figure 17

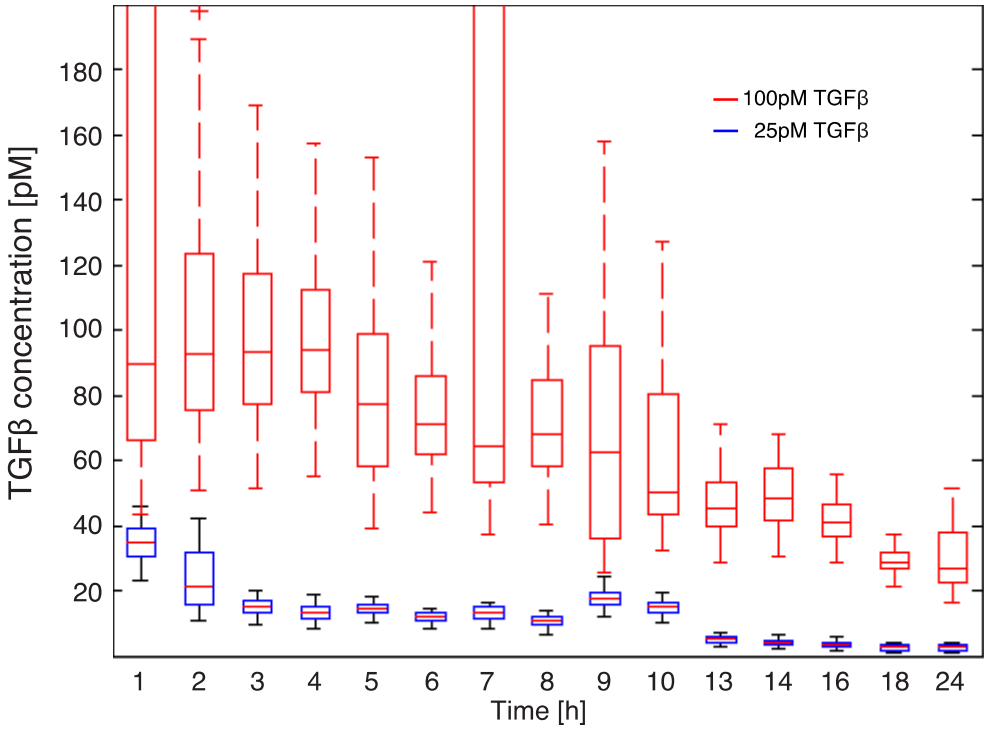

3.2.1 Figure 17. Full ligand decay correlate with signaling termination.

TGFβ concentration measurement to estimate the TGFβ decay and half-life for different initial concentrations in time-lapse microscopy experiments. MCF10A SMAD2 reporter cells were seeded two days before stimulation with 25pM or 100pM and supernatants from live-cell microscopy experiments were collected at indicated time points. Mink lung epithelial cells (MLECs) stably transfected with a reporter containing a truncated PAI-1 promoter (3TP promoter with three consecutive TPA response elements) fused to the firefly luciferase gene were used and luciferase activity was measured. The fit to a standard curve was used to convert measured relative luciferase activities into absolute TGFβ concentrations. Red lines indicate median; boxes include data between the 25th and 75th percentiles; whiskers extend to maximum values within 1.5× the interquartile range; crosses represent outliers.

3.2.2 Role of negative feedback loops

What is the role of negative feedback loops in regulating TGFβ dynamics? As mentioned before, SMAD7 as the main transcriptional feedback down-regulates TGFβ signaling by blocking receptor bindings, preventing formation and nuclear accumulation of SMAD2/SMAD3/SMAD4, repression of SMAD target genes, receptor dephosphorylation and degradation and SMAD7 competes with SMAD4 to associate with R-SMADs and recruits the E3 ubiquitin ligase NEDD4L to activated R-SMADs, leading to their polyubiquitination and proteasomal degradation (Hayashi *et al*, 1997; Kavsak *et al,* 2000; Yan *et al*, 2009; Wegner K *et al*, 2012; Yan *et al*, 2016).

3.2.2.1 SMAD7 transcription is strongly correlated to the first peak amplitude of SMAD2 signaling

In order to systematically investigate the role of feedback loops in shaping SMAD dynamics, it was first necessary to clarify how the SMAD7 transcription is coupled to TGFβ pathway activation.

So far, I could show that expression of TGFβ target genes are dose-dependent like the median response in the time-lapse data (3.1.3.1). To examine this more specifically, I combined smFISH of SMAD7 with time-lapse imaging of SMAD2 1.5h and 14h post 100pM TGFβ stimulation. Considering first the absolute RNA counts per cell at basal level (376 cells analyzed) and 1.5 hours (623 cells) or 14 hours (174 cells) post 100pM TGFβ ligand stimulation, the target gene expression also showed high cell-to-cell variability with a median of 29 RNA/cell at basal level, 57 RNA/cell (2 fold) at 1.5 hours and 39 RNA/cell (1.3 fold) at 14 hours **(Figure 18A, B and C)**. The coefficient of variation (CV) is moderate for all three conditions between 0.45- 0.65 **(Figure 18D)**. More important was how 1.5 hours of individual SMAD2 signaling correlate to the SMAD7 RNA count in the respective cell at 1.5 hours post stimulation, which correspond to the peak of SMAD7 target gene expression **(Figure 18E).** I grouped the trajectories of SMAD2 signaling into 4 clusters, which is illustrated in the heat map, and then looked at the distribution of the RNA to the respective cluster **(Figure 18F).** Cells in cluster 1 are marked by a low amplitude and little nuclear accumulation of SMAD2 and low counts of RNA per cell of 41. Cells of cluster 2-4 are characterized by an increasing amplitude and slope and coinciding higher amounts of RNA per cell of 50, 62 and 62, respectively. Obviously, the first peak amplitude of SMAD2 dynamics was correlated to the RNA distribution. To confirm this result, I divided the RNA results into 4 clusters

from high to low RNA counts per cell and looked at the distribution of the respective median trajectories **(Figure 18G).** Cluster 1 is characterized by a low RNA amount (median of 29 RNA/cell) correlated with the trajectories with a lower amplitude and cluster 3 with the highest RNA amount (median of 129 RNA/cell) correlate with the median with a higher amplitude and slope. Nonetheless, considering 14 hours of individual SMAD signaling, trajectories of SMAD2 signaling are grouped into 3 clusters with distinct dynamic behavior, but RNA counts per cell were around 40 for all clusters **(Figure 18H).** Equally, I divided the RNA results into 4 clusters from high to low RNA counts per cell, but the distribution of the respective median trajectories looked the same **(Figure 18I).** In conclusion early SMAD7 transcription reflected strongly SMAD2 signaling, but for long-term dynamics the correlation was not obvious.

Figure 18

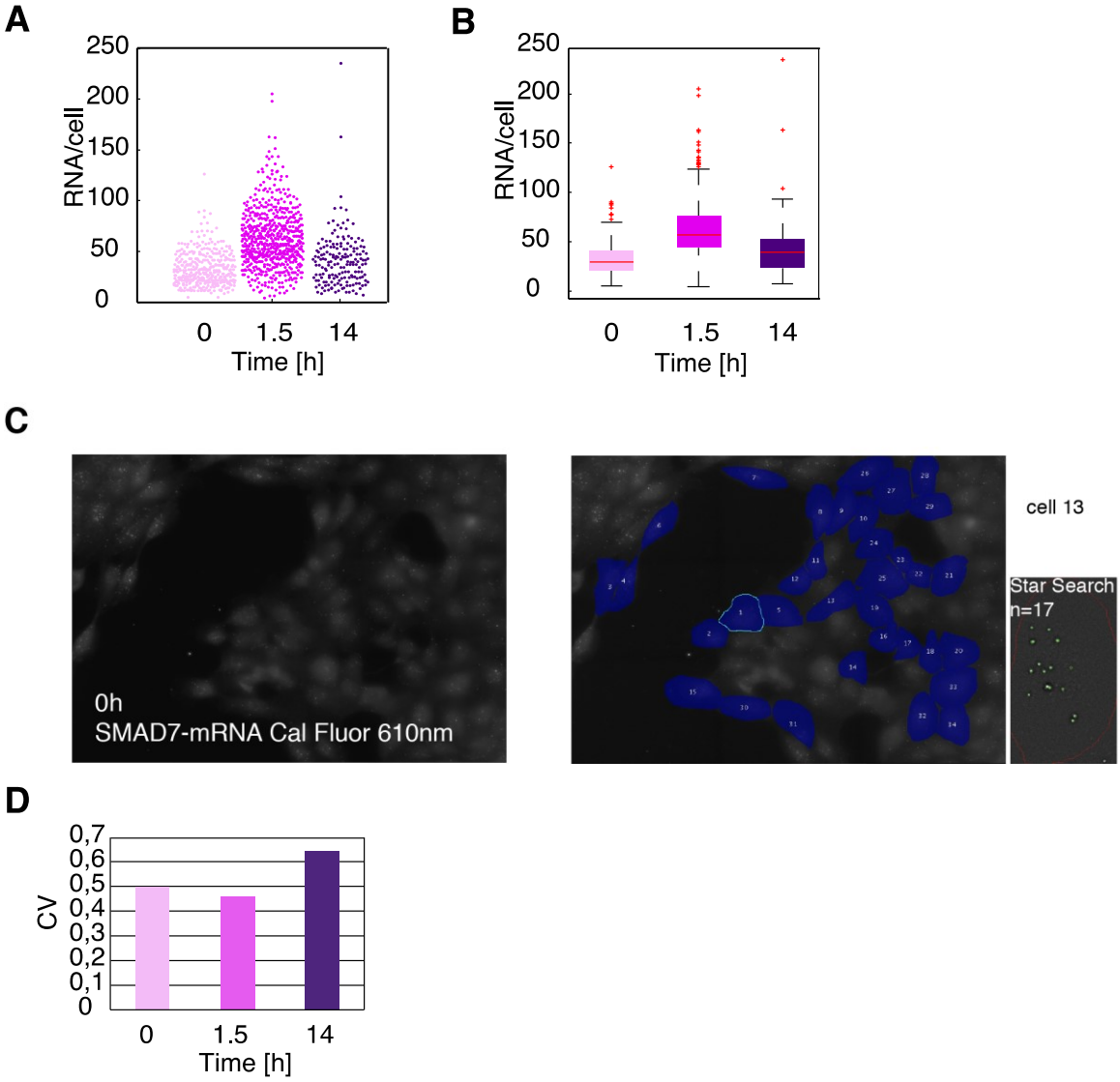

E

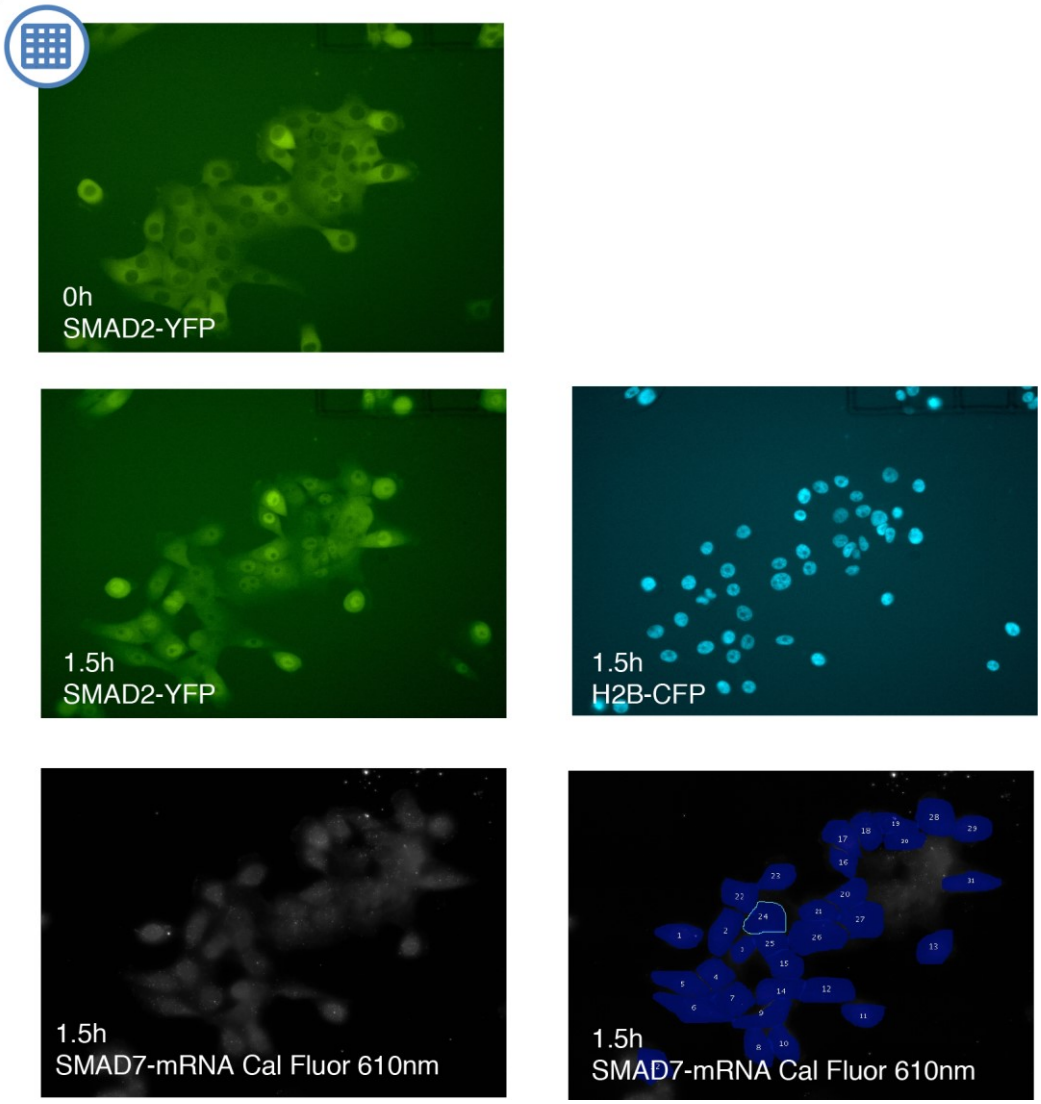
0h
SMAD2-YFP
1.5h
SMAD2-YFP
1.5h
H2B-CFP
1.5h
SMAD7-mRNA Cal Fluor 610nm
1.5h
SMAD7-mRNA Cal Fluor 610nm

F

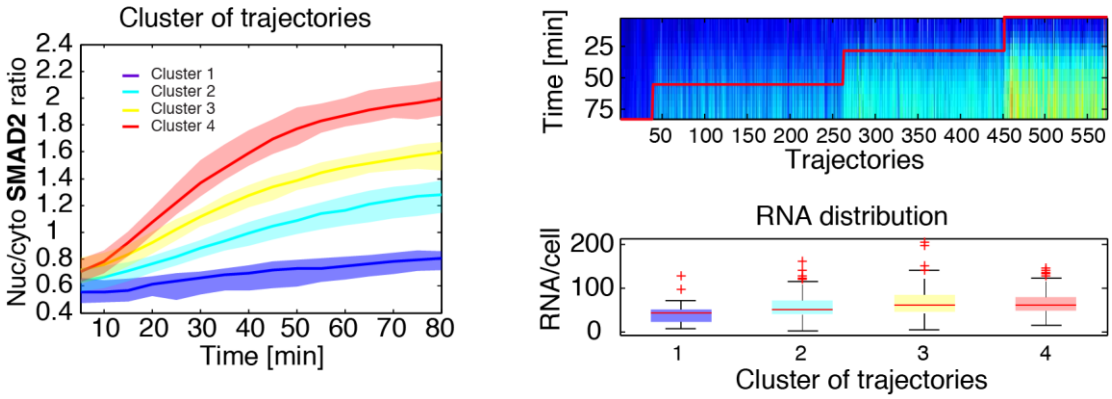
Cluster of trajectories
Nuc/cyto SMAD2 ratio
Cluster 1
Cluster 2
Cluster 3
Cluster 4
Time [min]
Time [min]
Trajectories
RNA distribution
RNA/cell
Cluster of trajectories

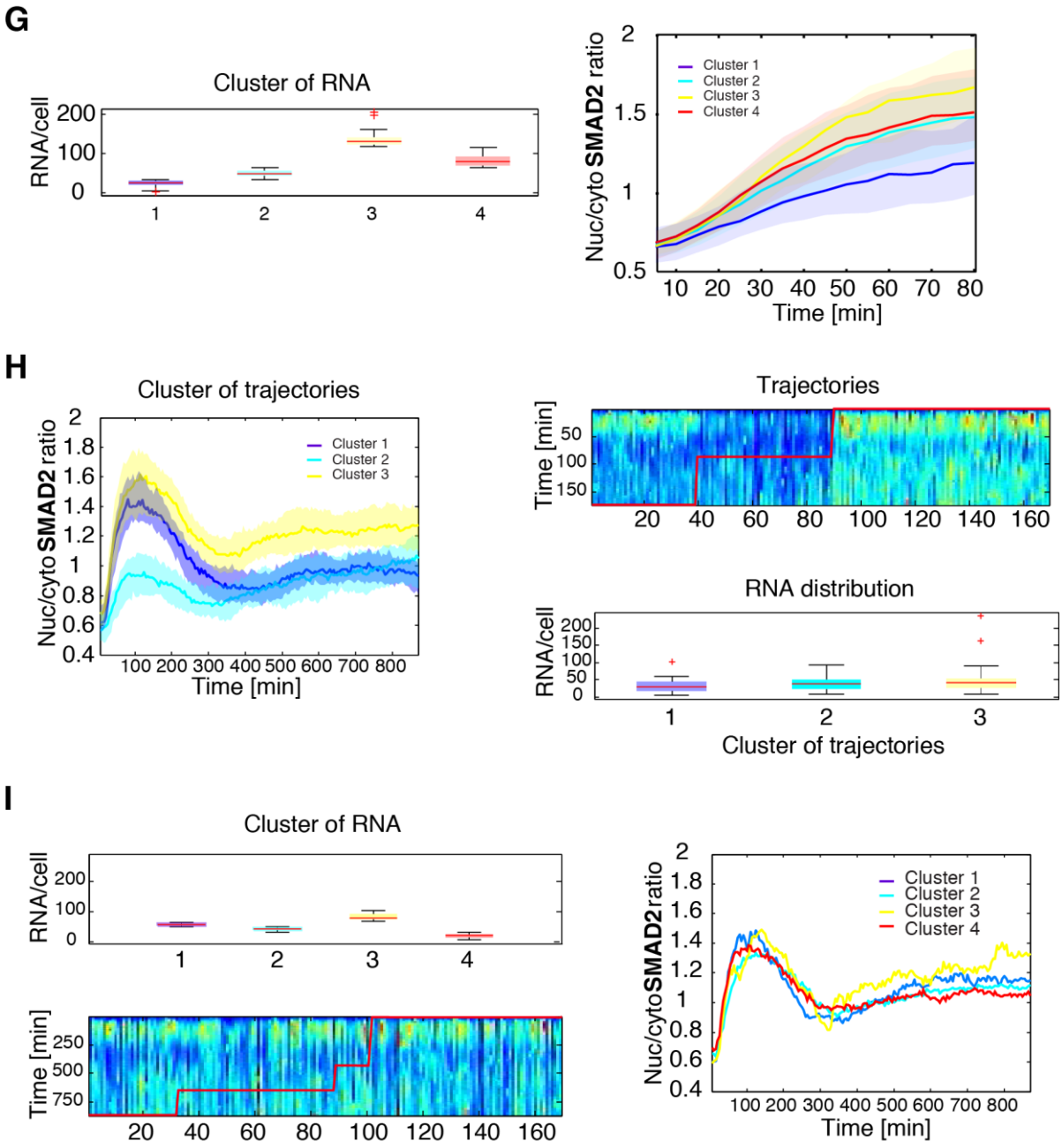

3.2.2.1 Figure 18. SMAD7 transcription is strongly correlated to the first peak amplitude of SMAD2 signaling.
A Bee swarm plot of SMAD7 RNA distribution 0, 1.5 and 14h after 100pM TGFβ treatment.
B Box plot of SMAD7 RNA distribution 0, 1.5 and 14h after 100pM TGFβ treatment. Median of 29 RNA/cell at basal level, 57 RNA/cell at 1.5h and 39 RNA/cell at 14h post TGFβ treatment. Red lines indicate median; boxes include data between the 25th and 75th percentiles; whiskers extend to maximum values within 1.5× the interquartile range; crosses represent outliers.
C Exemplary analysis of basal SMAD7 RNA distribution. SMAD7 probes for smFISH labeled CalFluor-610 were applied and RNA amount of each cell was calculated using Star Search Analysis tool.
D Coefficient of variation (CV) of SMAD7 RNA distribution 0, 1.5 and 14h after 100pM TGFβ treatment.
E Combining time-lapse microscopy experiment (100pM TGFβ stimulation 1.5h) and SMAD7 smFISH analysis. SMAD2 reporter cells are seeded on a relocation grid for the time-lapse microscopy experiment (three upper panels). Subsequently, cells were fixed and specific SMAD7 probes for smFISH labeled CalFluor-610 were applied. The RNA amount of each cell was calculated using Star Search Analysis tool.
F Individual cells were clustered into four signaling classes (cluster) according to their time-resolved nuc/cyto SMAD2 ratio 1.5h after 100pM TGFβ stimulation (left panel). Each line represents the median over all cells of the indicated cluster. Shaded area represent data between 25th and 75th percentiles. Cluster are illustrated in the heat map (red line, right upper panel) and SMAD7 RNA distribution of the respective cluster is shown as a box plot (right lower panel). Red lines

indicate median; boxes include data between the 25th and 75th percentiles; whiskers extend to maximum values within 1.5× the interquartile range; crosses represent outliers.
G Individual cells were clustered into four cluster according to the SMAD7 RNA amount per cell 1.5h after 100pM TGFβ stimulation (left panel). The distribution of the respective median nuc/cyto SMAD2 ratio of the four RNA cluster are shown in the right panel.
H Individual cells were clustered into three signaling classes (cluster) according to their time-resolved nuc/cyto SMAD2 ratio 14h after 100pM TGFβ stimulation (left panel). Each line represents the median over all cells of the indicated cluster. Shaded area represent data between 25th and 75th percentiles. Cluster are illustrated in the heat map (red line, right upper panel) and SMAD7 RNA distribution of the respective cluster is shown as a box plot (right lower panel). Red lines indicate median; boxes include data between the 25th and 75th percentiles; whiskers extend to maximum values within 1.5× the interquartile range; crosses represent outliers.
I Individual cells were clustered into four cluster according to the SMAD7 RNA amount per cell 14h after 100pM TGFβ stimulation (left upper panel). Cluster are illustrated in the heat map (red line, left lower panel) matching with the corresponding nuc/cyto SMAD2 ratio trajectories. The distribution of the respective median nuc/cyto SMAD2 ratio of the four RNA cluster are shown in the right panel.

3.2.2.2 Inhibition of transcription by DRB attenuates early adaptation

Finally, to determine whether transcriptional negative feedback loops establish signal adaptation, I blocked these feedbacks by the general transcription inhibitor DRB (5,6-dichloro-1--D-ribofuranosylbenzimidazole), which efficiently inhibits transcription at the early elongation stage by inhibiting CDK7, 8 and 9 kinases and preventing RNA polymerase II to proceed after initiation (Chodosh *et al*, 1989; Yamaguchi *et al*, 1998; Rickert *et al*, 1999). First, the efficiency of DRB on MCF10A cells was assessed by measuring *SMAD7* expression at time points 0, 1.5 and 3h post TGFβ stimulation by RT-PCR. DRB was added at different times before and after 100pM TGFβ treatment. DRB 0.25h prior TGFβ stimulus was sufficient to maintain basal level and to prevent accumulation of SMAD7 at its peak of 1.5h to 3.47-fold and keep it constant around the basal level **(Figure 19A)**. In addition, 3h value in DMSO control treated cells was 1.61-fold and with 0.25h prior DRB only 0.65-fold. Since DRB acts rather fast and transcription rates for *SMAD7* were kept around the basal level and thus cellular changes and compensatory mechanisms are minimized, I added DRB 0.25h prior 100pM TGFβ stimulation for time-lapse microscopy experiments. As shown in **Figure 19B**, DRB alone had no effect on SMAD2 signaling. However, stimulating SMAD2 reporter with DRB prior to TGFβ stimulation, the amplitude was amplified, and adaptation was attenuated, as presented in boxplots for the ratio values 1h and 3h post stimulation **(Figure 19B and E)**. The longer duration of nuclear SMAD2 accumulation was particularly evident in the heat maps **(Figure 19C)**. Since the cells started to die when adding DRB, only the first 6 hours of the response were analyzed. Furthermore, cells also showed an increased amplitude and slower adaptation when DRB was added 0.5 and 0.75h post TGFβ stimulation or slightly enhanced signaling 1.5h post stimulation **(Figure 19D)**. The same results were obtained by treating cells 0.25h prior to 25pM and 5pM TGFβ. The amplitude was increased and the TGFβ response was boosted, but nevertheless early adaptation took place **(Figure 19F, Appendix Figure A4 and A5)**. In conclusion these results indicate that transcriptional feedbacks like SMAD7 have an impact on the

early adaptation of SMAD2 signaling, but other regulatory mechanisms are apparently involved since early adaptation was attenuated and not prevented.

Figure 19

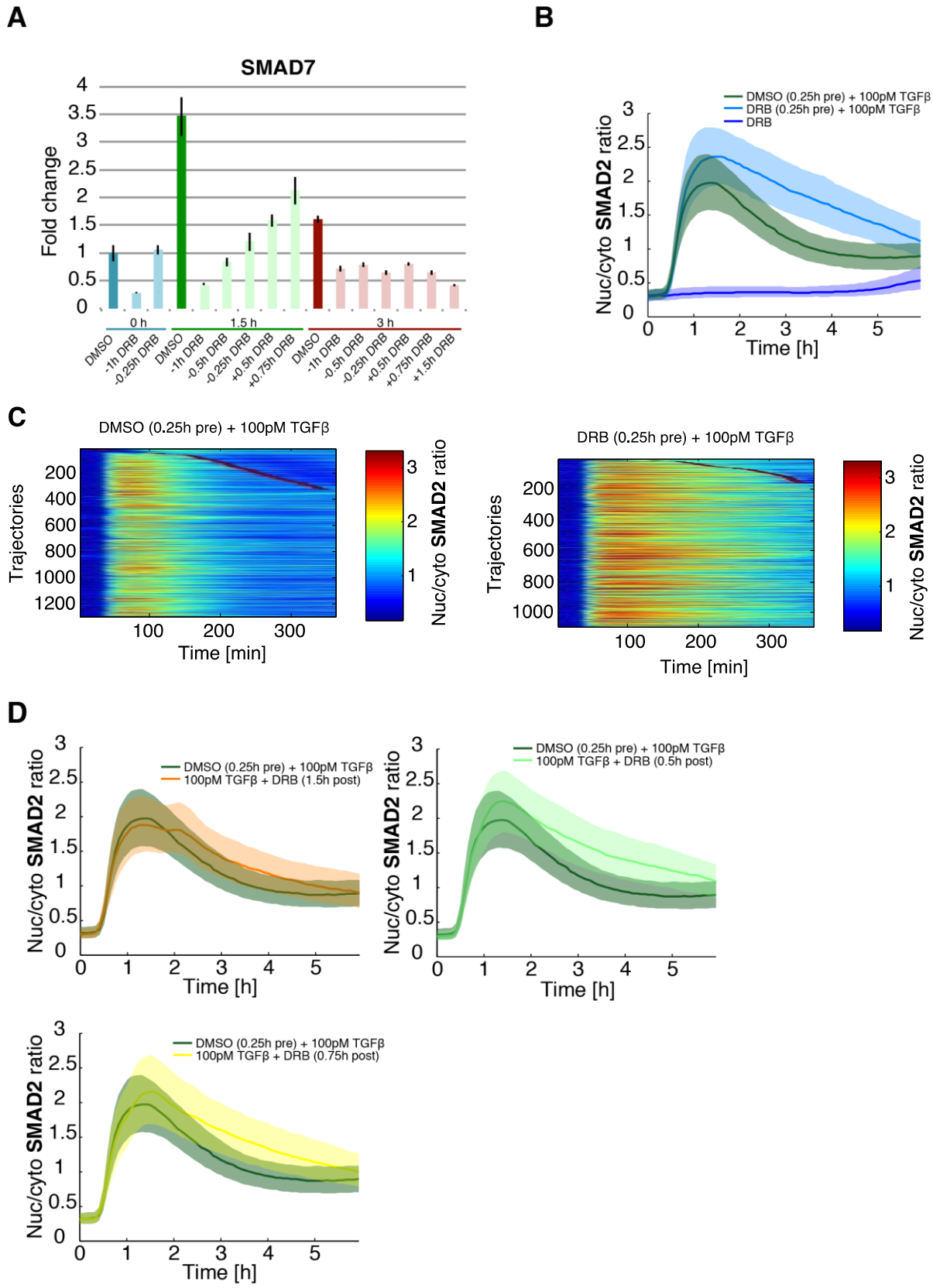

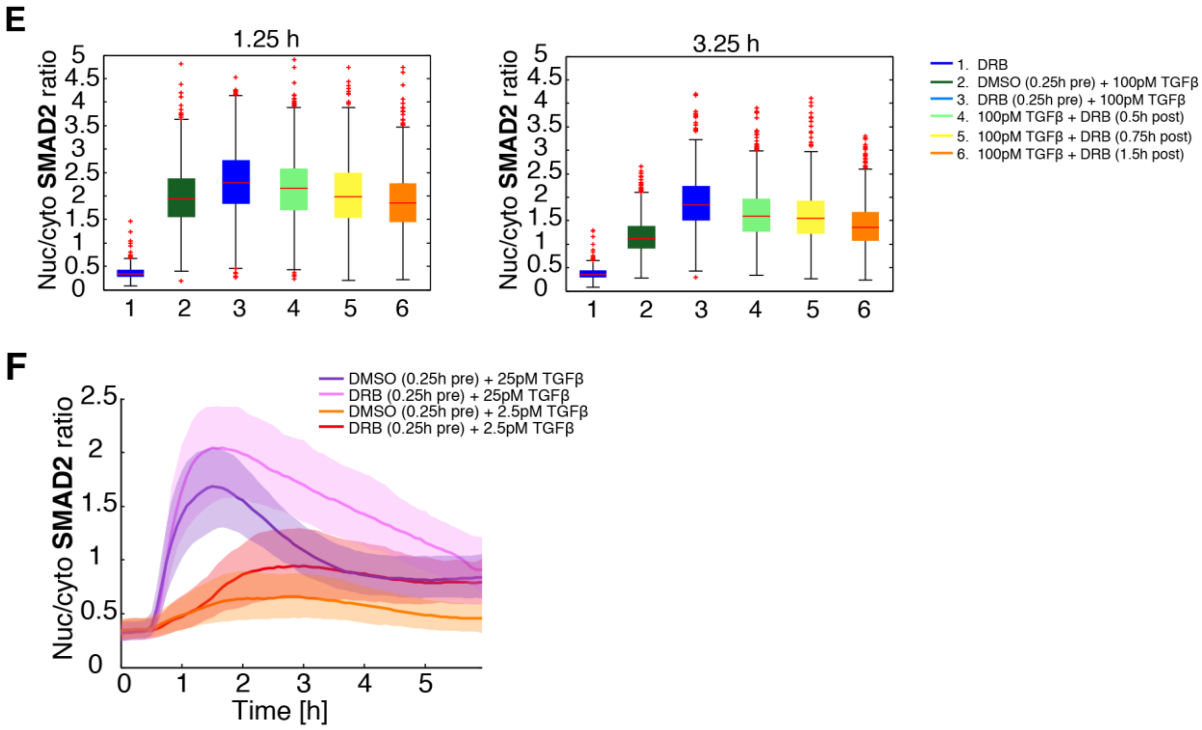

3.2.2.2 Figure 19. Inhibition of transcription by DRB attenuates early adaptation.
A Expression of SMAD7 in MCF10A WT cells stimulated with 100pM TGFβ and treated with DRB (5,6-dichloro-1-beta-D-ribobenzimidazole) at indicated time points (relative to TGFβ stimulation) were measured by RT-qPCR at indicated time points (0, 1.5h and 3h). DMSO was used for the control condition. β-Actin was used as an internal control. Error bars indicate standard deviation of technical triplicates.
B Median nuc/cyto SMAD2 ratio of reporter cells stimulated with 100pM TGFβ and treated with DRB at indicated time points. DMSO was used for the control. Shaded area represent data between 25th and 75th percentiles.
C Heat maps of SMAD2 translocation in individual cells over 24h. Cells were stimulated with 100pM TGFβ and treated with DMSO or DRB 0.25h pre TGFβ stimulus. Each horizontal line represents a single cell and the nuc/cyto ratio is shown as indicated in the legend. Cells were sorted by the time of the first division as indicated by red marks.
D Median nuc/cyto SMAD2 ratio of reporter cells stimulated with 100pM TGFβ and treated with DRB at indicated time points post TGFβ stimulus. DMSO was used for the control. Shaded area represent data between 25th and 75th percentiles.
E Signaling features for the SMAD2 reporter cells at 1.25h and 3.25h stimulated with 100pM TGFβ and treated with DRB at indicated time points. Red lines indicate median; boxes include data between the 25th and 75th percentiles; whiskers extend to maximum values within 1.5× the interquartile range; crosses represent outliers.
F Median nuc/cyto SMAD2 ratio of reporter cells stimulated with 2.5 or 25pM TGFβ and treated with DRB at indicated time points. DMSO was used for the control. Shaded area represent data between 25th and 75th percentiles.

3.2.2.3 SMAD7 knock out CRISPR Cas9 cell line

In order to investigate the role of the reported main transcriptional negative feedback regulator SMAD7 more specifically (Yan *et al*, 2009), I aimed to generate a *SMAD7* CRISPR Cas9 knockout cell line and perform live-cell imaging to determine how a complete knock out affects the dynamics of SMAD2.

3.2.2.3.1 Generating clonal cell lines and validating selected clones by determining the mutation state of the *SMAD7* gene locus

For this purpose, a clonal SMAD2-YFP Cas9 reporter cell line was generated which additionally expresses the *Cas9* gene after lentiviral infection and acts as a new control cell line. Furthermore, this cell line was transfected with an sgRNA targeting exon2 of the *SMAD7* gene to create a polyclonal

SMAD7 knock out cell line (Shalem *et al*, 2014). No functional protein will be produced due to nonsense-mediated decay when missense mutations occur.

The T7 endonuclease assay confirmed a high level of mutated genomic DNA (6.4). Therefore, 5 stable clonal cell lines (Clone 1, 6, 9, 12 and 16) were selected and the mutation state of the *SMAD7* gene locus was determined by sequencing and validated by RT-PCR and Western Blot to identify the one with the most complete knock out. Sequencing results showed that clone 9 had the wild type *SMAD7* gene and clone 1, 6 and 16 only show heterozygous deletions leading to an open reading shift and an early stop codon. Fortunately, clone 12 showed a deletion on both alleles (22 and 7 base pairs), leading to an open reading frame shift and an early stop codon and therefore to a complete *SMAD7* knock out **(Figure 20A).** In addition, RT-PCR data indicated that the basal SMAD7 mRNA level was reduced from Clon12 to 0.0095-fold compared to the SMAD2-YFP Cas9 reporter cell line. Furthermore, Western blot experiments revealed that 3h after 100pM TGFβ treatment clone 1, 6, 16 and in particular clone 12 showed more pSMAD2 and more total SMAD2 **(Figure 20B)**, which indicates a successful CRISPR CAS9 knock out of *SMAD7*.

Figure 20

A

Smad7 exon2

ccccctccttactccagatacccgatggattttctcaaacca parental

cccctccttactccagata- -c tt tggattttctcaaacca SMAD7 $^{-/+}$ allele 1 clon1
cccctccttactccagatacccgatggattttctcaaacca SMAD7 $^{-/+}$ allele 2 clon1

cccctcctt- --- - - -- -- -- - - --- -----tctcaaacca SMAD7 $^{-/+}$ allele 1 clon6
cccctccttactccagatacccgatggattttctcaaacca SMAD7 $^{-/+}$ allele 2 clon6

cccctccttactcca - --- -- -- --- - - -------- - acca SMAD7 $^{-/-}$ allele 1 clon12
cccctccttactcca - --- -- -gatggattttctcaaacca SMAD7 $^{-/-}$ allele 2 clon12

cccctccttactcca - --- -- -gatggattttctcaaacca SMAD7 $^{-/+}$ allele 1 clon16
cccctccttactccagatacccgatggattttctcaaacca SMAD7 $^{-/+}$ allele 2 clon16

B

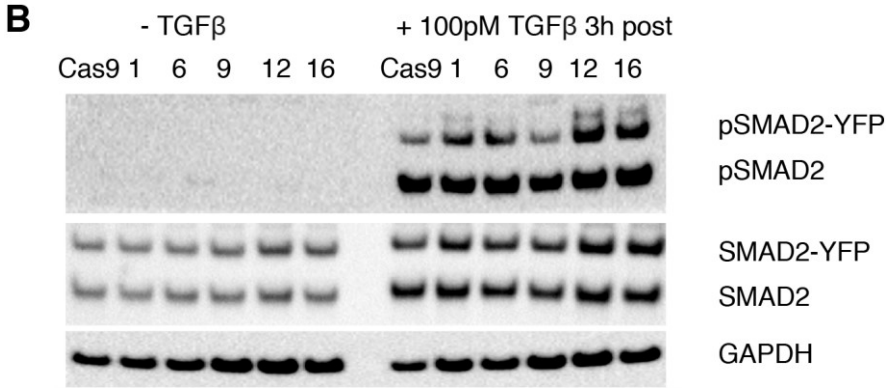

3.2.2.3.1 Figure 20. Generating clonal cell lines and validating selected clones by determining the mutation state of the SMAD7 gene locus.
A Sequencing results for SMAD7 EXON 2 of MCF10A WT (parental) and SMAD7 CRISPR Cas9 knockout cell lines clone 1, 6, 12 & 16.
B Western blot analysis of SMAD2 activation in the control clonal SMAD2-YFP Cas9 reporter cell line (Cas9) and in the SMAD7 CRISPR Cas9 knockout cell lines clone 1, 6, 9, 12 & 16. Cells were stimulated with 100pM TGFβ and SMAD2 and SMAD2 phosphorylation was analyzed 3h post stimulus. GAPDH was used as a loading control.

3.2.2.3.2 Sustained *SMAD7* knock out affects SMAD2 dynamics

Finally, the next step was to determine how *SMAD7* knock out affects the TGFβ response of SMAD2 measured by live cell imaging. For this purpose, the control cell line SMAD2-YFP Cas9, the partially *SMAD7* knock out clones 1 & 16 and the complete knock out clone 12 were stimulated with 100 pM TGFβ and monitored for 21 hours. First of all, clone 1 and 16 show a slight increase in the basal nuclear and cytoplasmic values and they are extremely elevated for clone 12 **(Figure 21A and B)**. Since the nuc/cyto ratio would be deceptive here, the focus was on the nuclear SMAD2 level **(Figure 21C)**. The amplitudes of clone 1 and 16 were significantly increased and for clone 12 even doubled compared to the SMAD2-YFP Cas9 reporter cell line. Nonetheless, the early adaptation took place to a higher plateau level for all three clones. Clustering all cells of the experiment into 4 clusters revealed that the proportion of cells from cluster 4, with the strongest SMAD2 response, was increased for clone 1 and clone 16 and is approximately 50% of the cells of clone 12 **(Figure 21D and E)**. Furthermore, the fraction of dividing cells from cluster 4 was reduced and the movement over the period of 21 hours was increased **(Figure 21F and G)**. This confirms that a strong sustained SMAD2 response shift cells to migration, EMT and cell cycle arrest and is regulated by the negative feedback regulator SMAD7. Furthermore, to address the question how the SMAD7 knock out affects the TGFβ dose-response of SMAD2, clone 12 and SMAD2- YFP Cas9 cell line were stimulated with 25pM and 5pM TGFβ **(Figure 21H and I)**. As before, the amplitudes of clone 12 were increased and the early adaptation was weakened with a higher nuclear SMAD2 plateau level afterwards, which delayed the final adaptation to basal level **(Appendix Figure A6)**. The resulting extended response of SMAD2 was particularly apparent in the heat maps **(Appendix Figure A7)**.

Figure 21

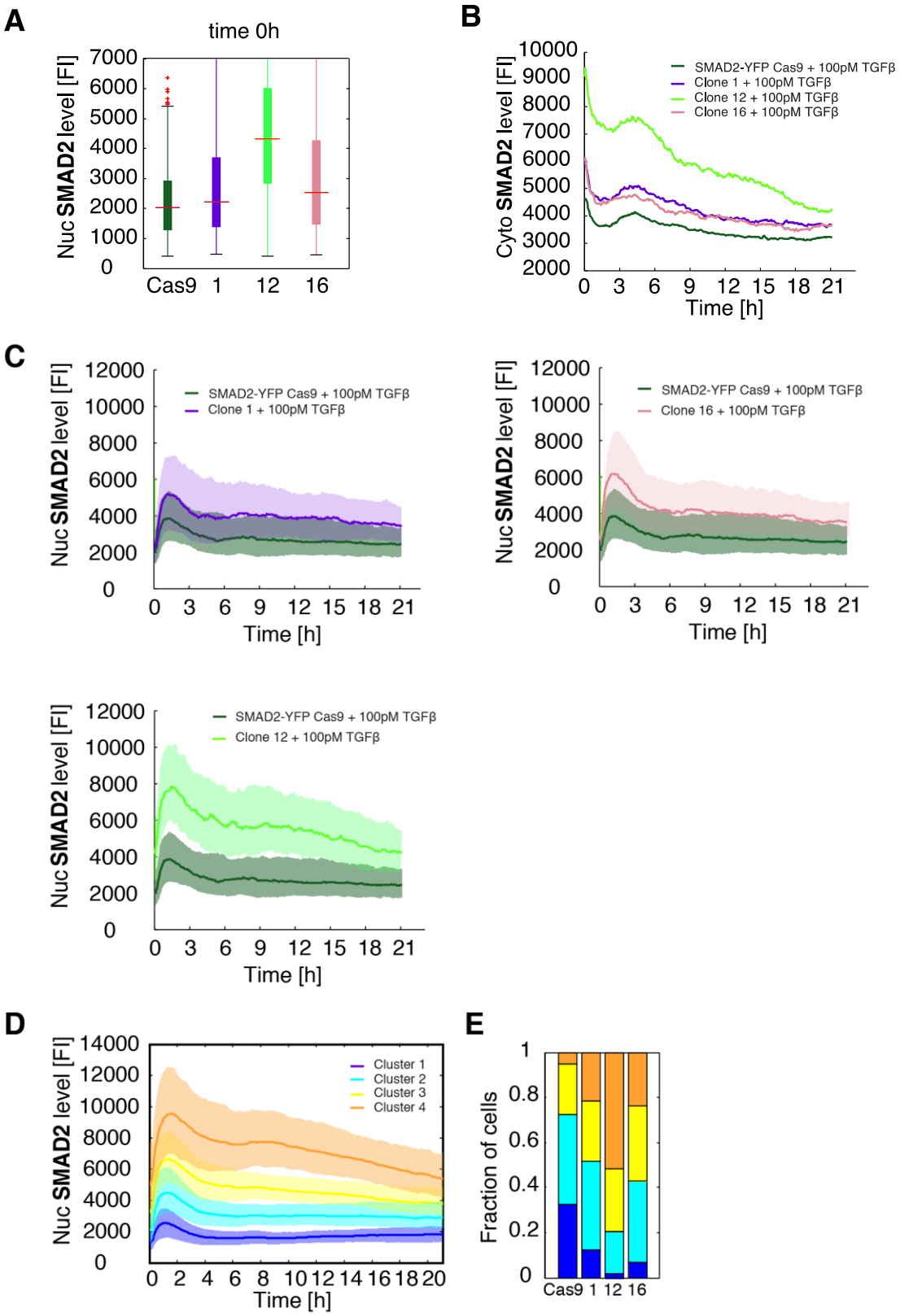
A
time 0h
Nuc SMAD2 level [FI]
Cas9
1
12
16
B
Cyto SMAD2 level [FI]
SMAD2-YFP Cas9 + 100pM TGFβ
Clone 1 + 100pM TGFβ
Clone 12 + 100pM TGFβ
Clone 16 + 100pM TGFβ
Time [h]
C
Nuc SMAD2 level [FI]
SMAD2-YFP Cas9 + 100pM TGFβ
Clone 1 + 100pM TGFβ
Clone 16 + 100pM TGFβ
Clone 12 + 100pM TGFβ
Time [h]
D
Nuc SMAD2 level [FI]
Cluster 1
Cluster 2
Cluster 3
Cluster 4
Time [h]
E
Fraction of cells
Cas9 1 12 16

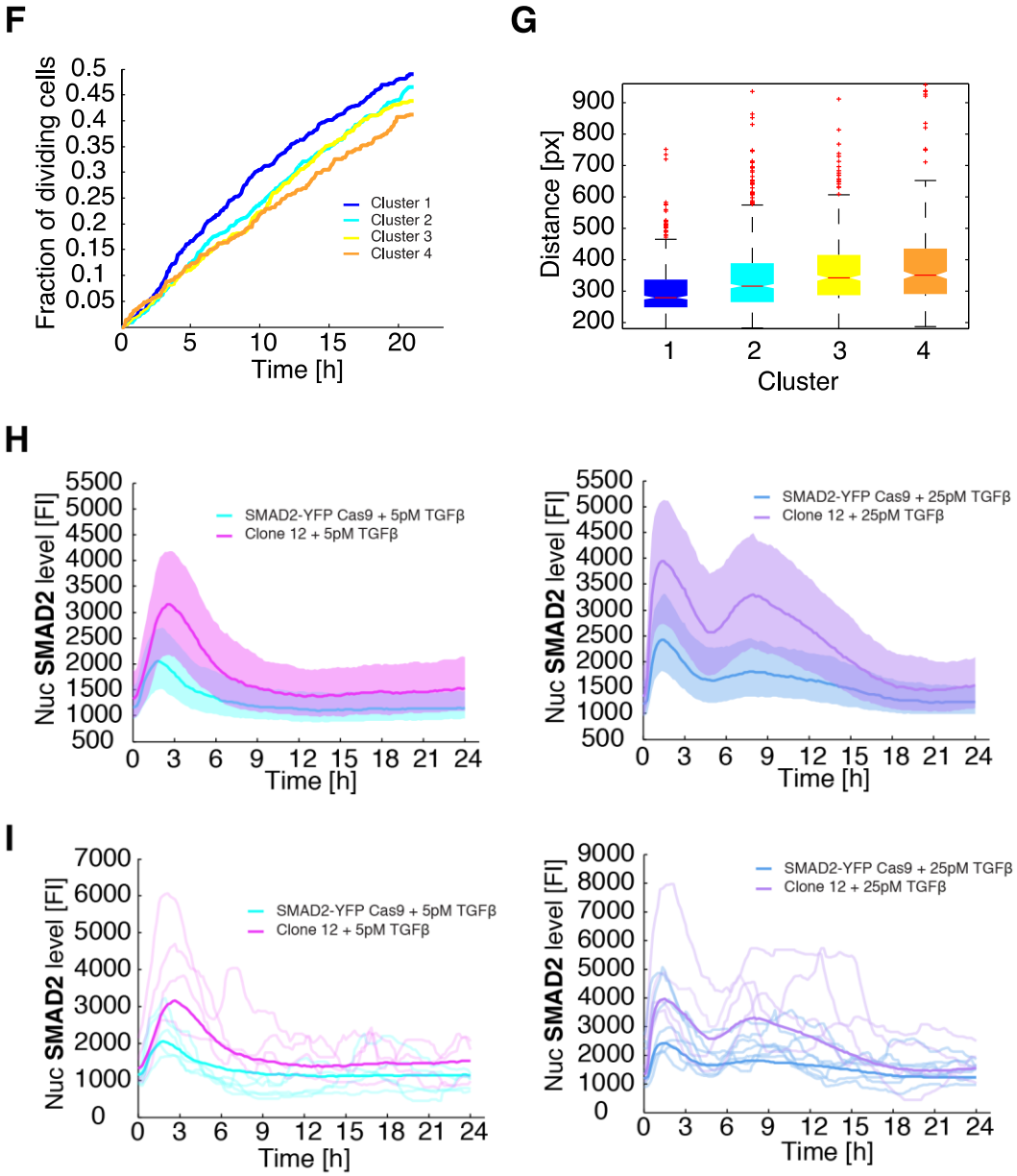

3.2.2.3.2 Figure 21. Sustained *SMAD7* knock out affects SMAD2 dynamics.

A Basal nuclear level of the control clonal SMAD2-YFP Cas9 reporter cell line (Cas9) and for the SMAD7 CRISPR Cas9 knockout cell lines clone 1, 12 & 16. Red lines indicate median; boxes include data between the 25th and 75th percentiles; whiskers extend to maximum values within 1.5× the interquartile range; crosses represent outliers.

B Median cytoplasmic SMAD2 level of the control clonal SMAD2-YFP Cas9 reporter cell line (SMAD2-YFP Cas9) and for the SMAD7 CRISPR Cas9 knockout cell lines clone 1, 12 & 16 stimulated with 100pM TGFβ.

C Median nuclear SMAD2 level of the control clonal SMAD2-YFP Cas9 reporter cell line (SMAD2-YFP Cas9) and for the SMAD7 CRISPR Cas9 knockout cell lines clone 1, 12 & 16 stimulated with 100pM TGFβ and tracked over 21h. Shaded area represent data between 25th and 75th percentiles.

D Individual cells of the control clonal SMAD2-YFP Cas9 reporter cell line (SMAD2-YFP Cas9) and for the SMAD7 CRISPR Cas9 knockout cell lines clone 1, 12 & 16 stimulated with 100pM TGFβ

were clustered into 4 signaling classes (cluster) according to their time-resolved nuclear SMAD2 level using dynamic time warping (DTW). Each line represents the median over all cells of the indicated cluster. Shaded area represent data between 25th and 75th percentiles.

E Distributions of signaling classes (cluster) on the different reporter cell lines.

F Cell proliferation of reporter cells shown as fraction of dividing cells within 21h for the different signaling classes (cluster).

G Motility of each cell as summed distance in pixel (pxl) covered 21h after stimulation with 100pM TGFβ. Cells were sorted according to signaling classes (cluster). Red lines indicate median; boxes include data between the 25th and 75th percentiles; whiskers extend to maximum values within 1.5× the interquartile range; crosses represent outliers.

H Median nuclear SMAD2 level of the control clonal SMAD2-YFP Cas9 reporter cell line (SMAD2-YFP Cas9) and for the SMAD7 CRISPR Cas9 knockout cell line clone 12 stimulated with 5 or 25pM TGFβ and tracked over 24h. Shaded area represent data between 25th and 75th percentiles.
I Individual nuclear SMAD2 trajectories for the control clonal SMAD2-YFP Cas9 reporter cell line (SMAD2-YFP Cas9) and for the SMAD7 CRISPR Cas9 knockout cell line clone 12 stimulated with 5 or 25pM TGFβ and tracked over 24h.

3.2.2.3.3 Dependency of SMAD target genes on SMAD7

In order to determine the effects of *SMAD7* knock down on changes in downstream responses and possible compensation mechanisms, for example up regulation of further feedback loops, I analyzed target genes expression in Clone 12 by RT-PCR. SMAD6, another negative feedback loop, TIEG, the repressor of *SMAD7* and SARA, a cofactor that interacts directly with SMAD2/ 3 and functions to recruit SMAD2/ 3 to the TGFβ receptor are not affected by *SMAD7* knock out after treatment with 100pM TGFβ **(Figure 22)**. In contrast, the peak of PAI1 at 3 hours was increased to nearly 20-fold compared to 13.9-fold of the SMAD2-YFP Cas9 control cell line. Also, late expression at 14 and 24 hours was slightly increased. Since at 100pM TGFβ the expression could be already saturated, the PAI1 expression was examined with 5pM TGFβ and also showed a higher induction of 14.1-fold instead of 9-fold. In conclusion, *SMAD7* knock out led not only to a stronger SMAD2 response, but also in case of PAI1 to an enhanced downstream response.

Figure 22

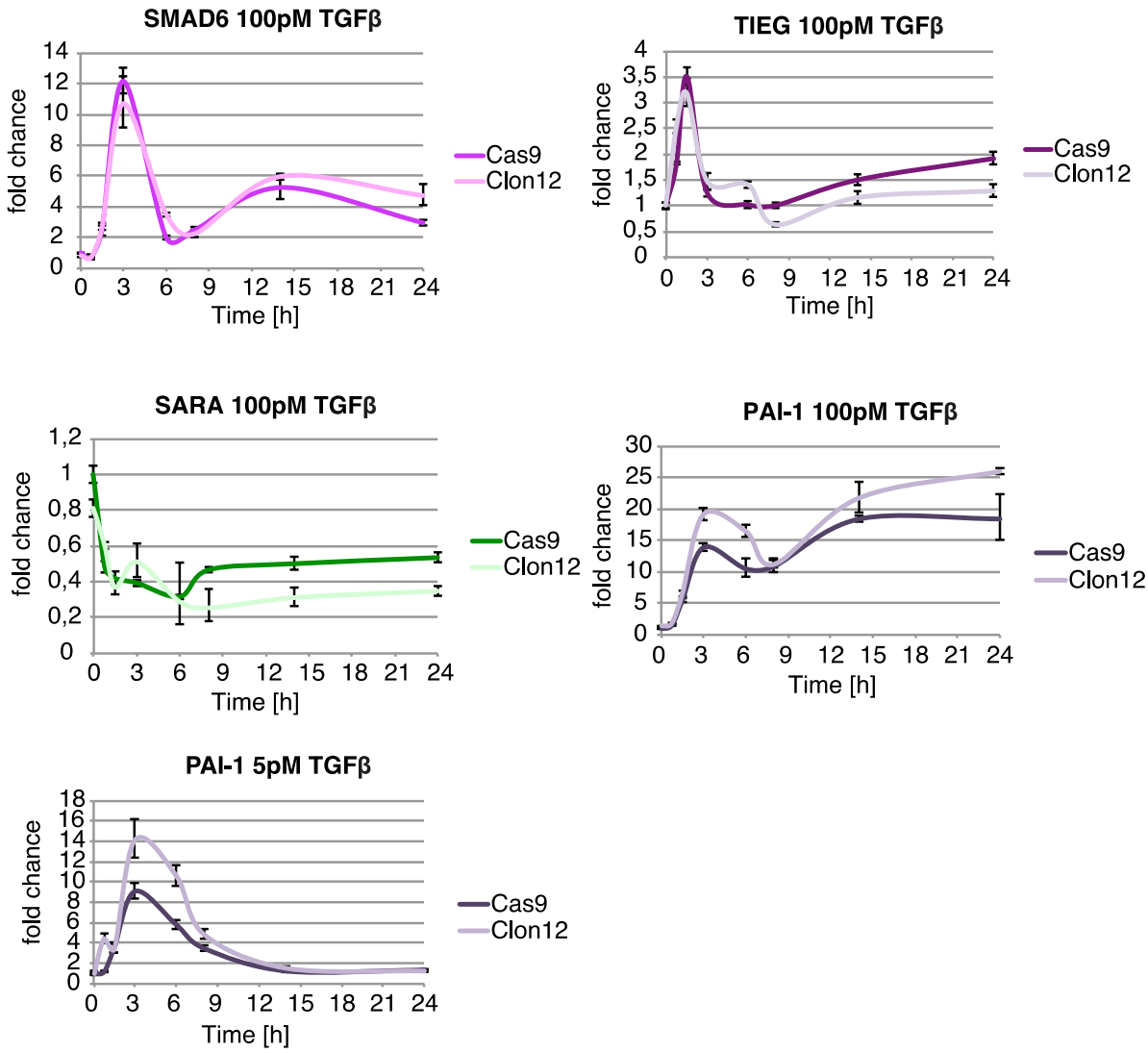

3.2.2.3.3 Figure 22. Dependency of SMAD target genes on SMAD7.
Expression of TGFβ target genes in the control clonal SMAD2-YFP Cas9 reporter cell line (Cas9) and in the SMAD7 CRISPR Cas9 knockout cell line clone 12 stimulated with 5 or 100pM TGFβ were measured by RT-qPCR at indicated time points. β-Actin was used as an internal control. Error bars indicate standard deviation of technical triplicates.

3.2.2.4 Transient SMAD7 knock out affects SMAD2 dynamics

Since the homozygous *SMAD7* CRISPR Cas9 knock out clone 12 has a sustained knock out with possible compensatory mechanisms, it was crucial to investigate how a transient *SMAD7* knock out affects SMAD2 dynamics. Thus, I used a clonal cell line (F10) with inducible shRNA expression for SMAD7 gene silencing in the background of the SMAD2-YFP cell line to investigate the role in shaping the different dynamics. The pTRIPZ lentiviral vector used provided inducible shRNA expression in the presence of doxycycline (Thermo Scientific Open Biosystems Expression Arrest TRIPZ Lentiviral shRNAmir). First, the efficiency of the TET-ON system after 48 and 72 hours of doxycycline treatment was tested by RT-PCR, whereby in the medium the horse serum was replaced by BSA for all conditions. Results showed

a knock down of SMAD7 of the F10 clonal cell line to 19% after 48 hours of doxycycline compared to the SMAD2-YFP cell line and a knock down to 22% after 72 hours **(Figure 23A)**. Therefore, an incubation time of 48 hours was used for all further experiments. First of all, it is obvious that doxycycline alone did not trigger translocation of SMAD2 in the control cell line SMAD2-YFP and in F10 **(Figure 23B)**. Furthermore, the control cell line stimulated with 100pM TGFβ and with 100pM TGFβ and doxycycline showed the same known dynamics for the nuclear and cytoplasmic SMAD2, as well as for their ratio values. In contrast, the *SMAD7* transient knock down cell line stimulated with doxycycline and 100pM TGFβ showed a lower amplitude and slightly less late signaling of SMAD2. However, the F10 cell line, as well as the *SMAD7* CRISPR Cas9 knock out clone 12, showed changes in the basal nuclear and cytoplasmic SMAD2 levels. Focusing only on the nuclear values, its apparent that the amplitude was similar but the late SMAD response was amplified. The cytoplasmic levels were in particular elevated over the period of 24 hours. Furthermore, the high variabilities in the nuclear and cytoplasmic levels of the F10 cell line are noticeable, which presumably reflects the respective effectiveness of the TET-ON system. In conclusion, the results are similar to clone 12, basal levels were increased, the amplitude of nuclear SMAD2 was not necessarily increased, but the early adaptation was weakened with a higher nuclear SMAD2 plateau level afterwards. Western results confirmed the time-lapse microscopy results. Biological triplicates showed that the transient F10 SMAD7 knockdown cell line after doxycycline treatment already exhibited more basal SMAD2 **(Figure 23C)**. Furthermore, Western results revealed more SMAD4 and more phosphorylated SMAD2 for F10 stimulated with 100pM TGFβ and doxycycline **(Figure 23D)**.

Figure 23

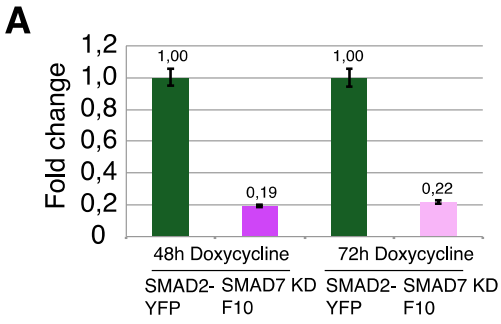

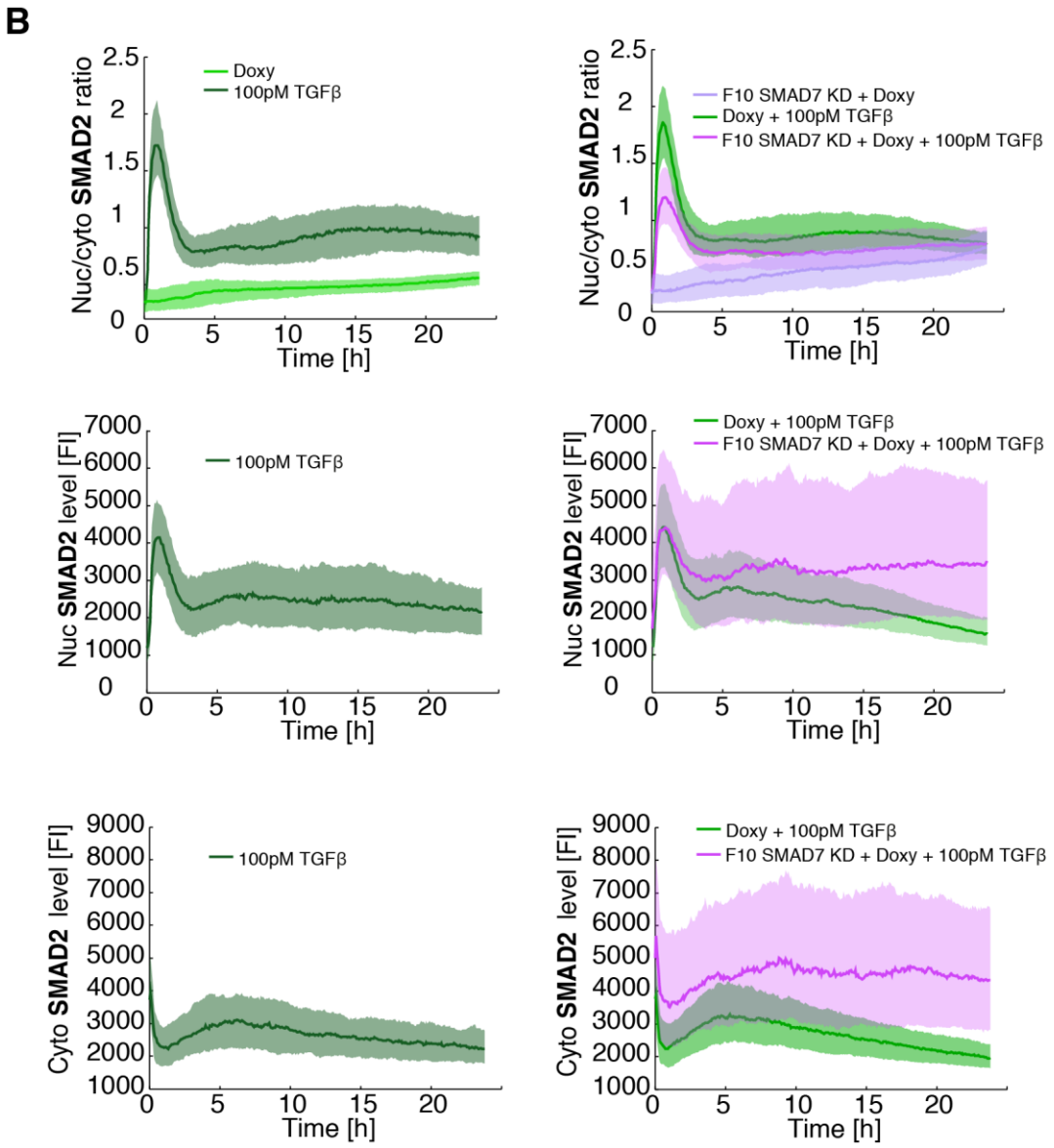
B
Nuc/cyto SMAD2 ratio
Doxy
100pM TGFβ
Time [h]
F10 SMAD7 KD + Doxy
Doxy + 100pM TGFβ
F10 SMAD7 KD + Doxy + 100pM TGFβ
Nuc SMAD2 level [FI]
Cyto SMAD2 level [FI]
C
SMAD2-YFP
SMAD2-YFP + Doxy
F10 SMAD7 KD + Doxy
SMAD2- YFP
SMAD2
GAPDH
D
SMAD2-YFP Doxy + 100pM TGFβ
F10 SMAD7 KD Doxy + 100pM TGFβ
0 0.75 2 3 4 6 8 [h]
pSMAD2
SMAD4
GAPDH

3.2.2.4 Figure 23. Transient *SMAD7* knock out affects SMAD2 dynamics.
A Expression of SMAD7 in SMAD2-YFP reporter cells and in the transient F10 SMAD7 knockdown cells (SMAD7 KD F10) after 48 or 72 hours of doxycycline at basal level. β-Actin was used as an internal control. Error bars indicate standard deviation of technical triplicates.
B Median nuc/cyto SMAD2 ratio, median nuclear and cytoplasmic SMAD2 level of the SMAD2-YFP reporter cells stimulated with 100pM TGFβ or as an control stimulated with only doxycycline (doxy, left panels). Median nuc/cyto SMAD2 ratio, median nuclear and cytoplasmic SMAD2 level of the SMAD2-YFP reporter cells and the transient F10 SMAD7 knockdown cells (F10 SMAD7 KD) stimulated with 100pM TGFβ and 48h pretreated with doxycycline (doxy) or as an control F10 SMAD7 KD cells only pretreated with doxycycline. Shaded area represent data between 25th and 75th percentiles.
C Western blot analysis of biological triplicates of phosphorylated SMAD2 and total SMAD2 at basal level in the SMAD2-YFP reporter cells 48h pretreated with or without doxycycline (doxy) and in the transient F10 SMAD7 knockdown cells (F10 SMAD7 KD) 48h pretreated with doxycycline (doxy). GAPDH was used as a loading control.
D Western blot analysis of phosphorylated SMAD2 and total SMAD4 in the SMAD2-YFP reporter cells and in the transient F10 SMAD7 knockdown cells (F10 SMAD7 KD) 48h pretreated with doxycycline (doxy) and stimulated with 100pM TGFβ. GAPDH was used as a loading control.

3.2.3 Inhibition of proteasomal degradation boost nuclear SMAD accumulation

Receptor-regulated SMADs interact with SMURF2, the E3 Ubiquitin Ligase, that targets SMAD2 and SMAD4 for ubiquitination and proteasome-mediated degradation (Lin, 2000; Kavsak, 2000). To test whether Ubiquitin-dependent degradation plays a role in shaping the dynamics of SMADs I treated the cells with the proteasome inhibitor MG132. MG132 (carbobenzoxy-Leu-Leu-leucinal), a peptide aldehyde, reduces the degradation of ubiquitin-conjugated proteins by blocking the 26S complex (Lee & Goldberg, 1998). Treating the SMAD2-YFP cell line with MG132 45 minutes before TGFβ stimulation or at the same time highly boosted SMAD2 accumulation into the nucleus **(Figure 24A and B, Appendix Figure A8)**. The maximum amplitude was increased, the time of the maximum amplitude was delayed and the length of the complete response and the mean value 5 hours after the first response were significantly increased **(Figure 24C)**. Particularly for the nuclear levels it is noticeable that hardly any adaptation took place **(Figure 24A)**. Also, treatment of MG132 0.75, 1.5 and 3 hours post TGFβ stimulation immediately enhanced SMAD2 accumulation into the nucleus **(Figure 24A and C, Appendix Figure A8)**. The SMAD4-YFP cell line behaved essentially like the SMAD2-YFP cell line and revealed an extremely amplified SMAD4 signaling through MG132 **(Appendix Figure A9 and A10)**. Here, the amplification of the amplitude, the delay of the maximum amplitude and the mean value 5 hours after the first response were even more obvious **(Appendix Figure A11)**. Surprisingly, the SMAD2-YFP cell line stimulated only with MG132, showed already SMAD2 accumulation over time in the nucleus, which was also reflected in the ratio. The cytoplasmic SMAD2 level did not increase particularly **(Figure 24D)**. In order to verify the time-lapse microscopy results I performed Western Blot experiments and treated MCF10A wild type cells 45 minutes before 100pM TGFβ stimulation with MG132. Results revealed more phosphorylated SMAD2, total SMAD2 and SMAD4 **(Figure 24E)**. In addition, I observed more TGFβ Receptor I if cells are prestimulated with MG132. Furthermore SMURF2 showed no changes and p21 is significantly enhanced. In addition, as expected enhanced SMAD2 and SMAD4 accumulation into the nucleus through MG132 led to increased target gene expression, shown in

Figure 24F for Snail, SnoN and SARA. In conclusion inhibition of proteasomal degradation led to strongly enhanced TGFβ signaling due to enhanced pSMAD2 and SMAD4 levels in the nucleus and stabilized receptors. In detail treatment with the inhibitor prevented the early adaptation and shifted the adaptation to later time points. Therefore, proteasomal degradation plays a strong role for the adaptation process.

Figure 24

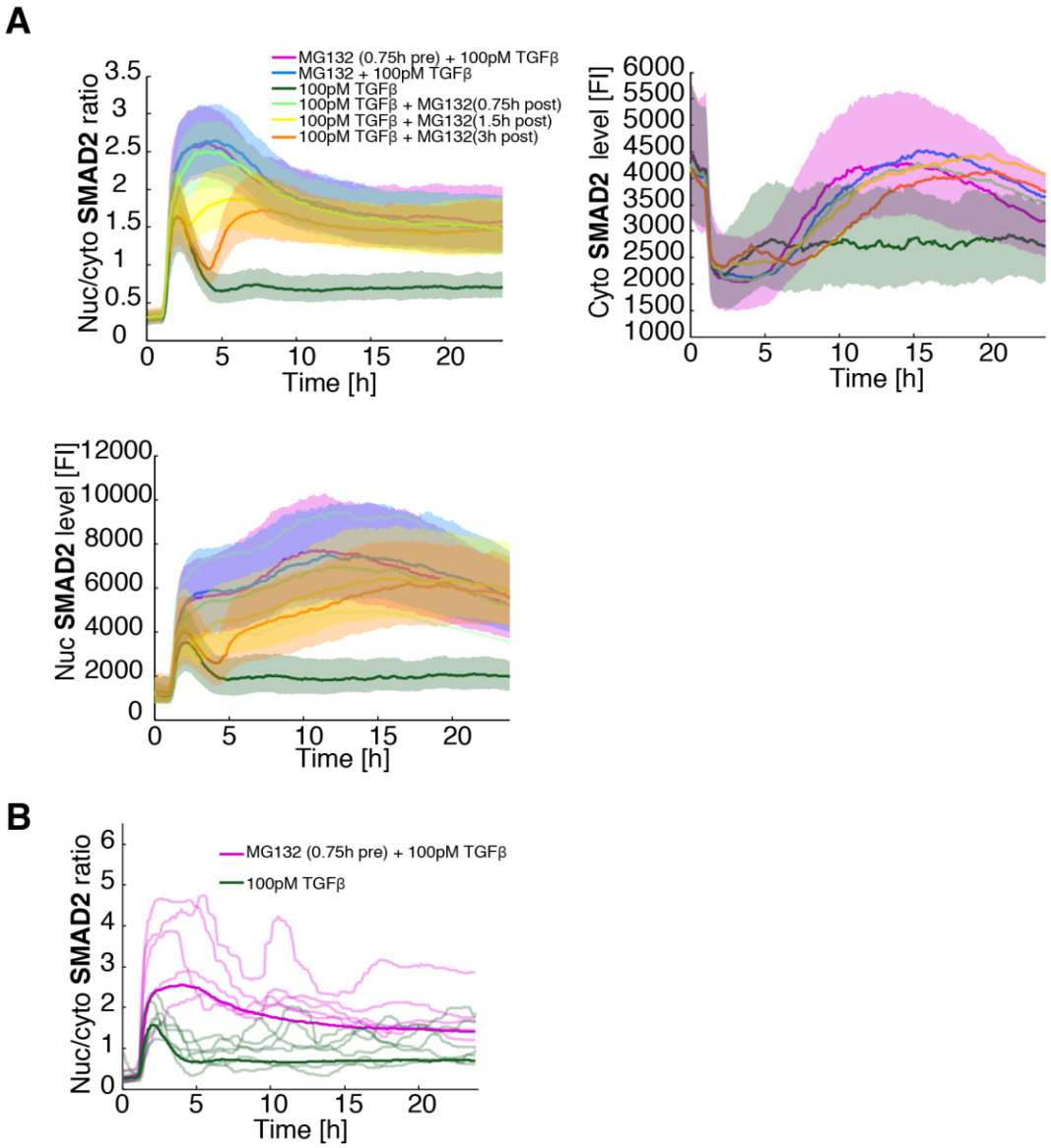

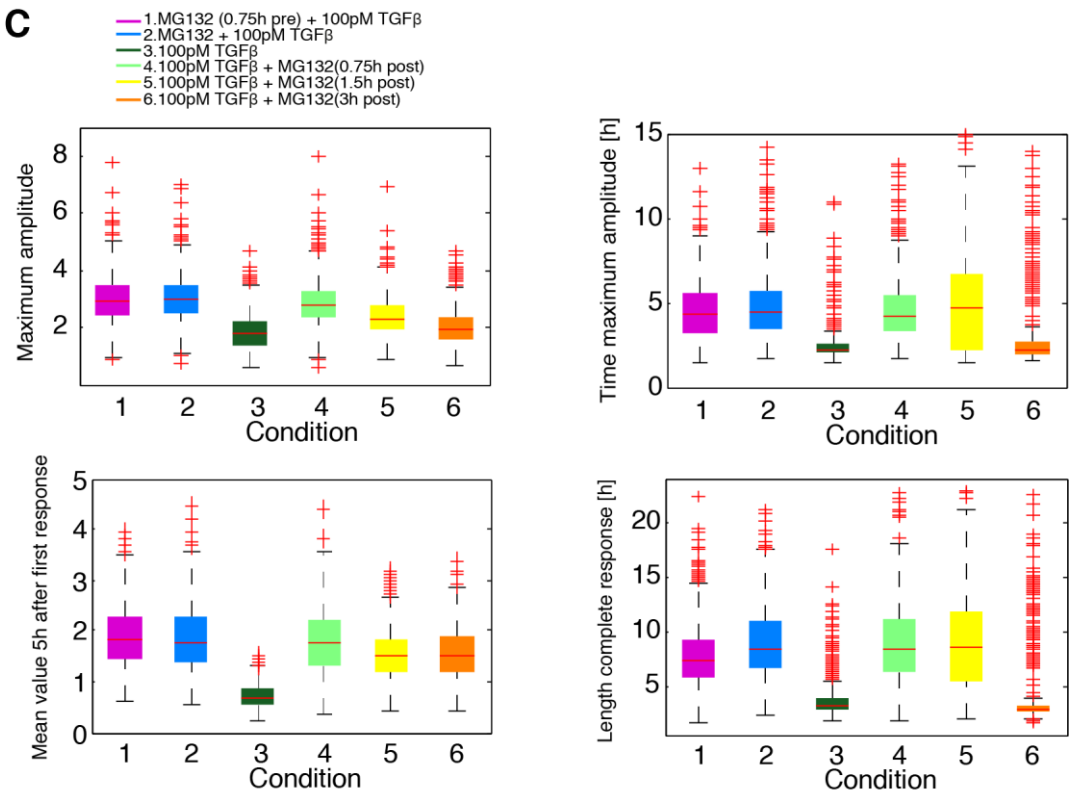
C
1.MG132 (0.75h pre) + 100pM TGFβ
2.MG132 + 100pM TGFβ
3.100pM TGFβ
4.100pM TGFβ + MG132(0.75h post)
5.100pM TGFβ + MG132(1.5h post)
6.100pM TGFβ + MG132(3h post)
Maximum amplitude
Time maximum amplitude [h]
Mean value 5h after first response
Length complete response [h]
Condition

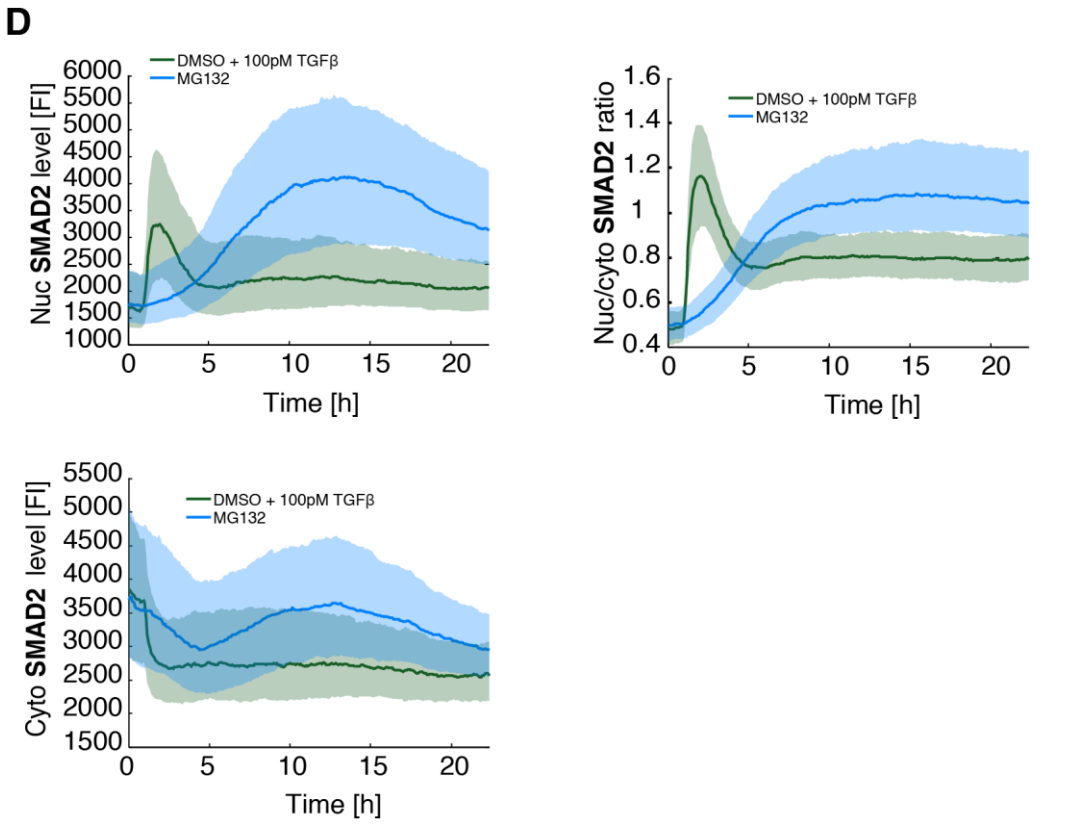
D
DMSO + 100pM TGFβ
MG132
Nuc SMAD2 level [FI]
Nuc/cyto SMAD2 ratio
Cyto SMAD2 level [FI]
Time [h]

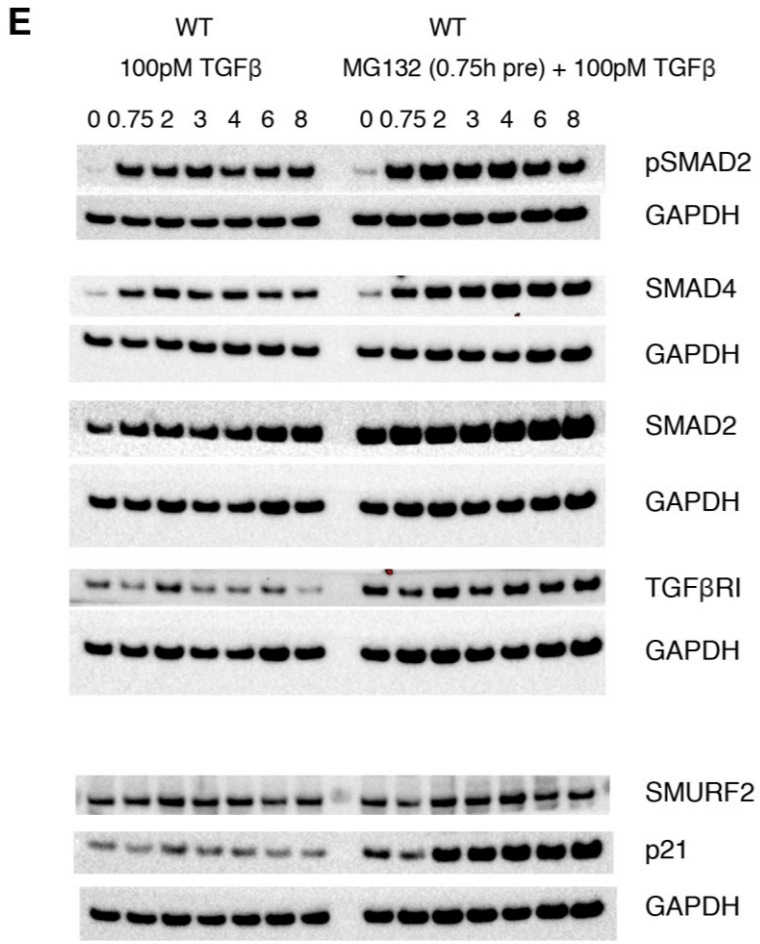
E
WT
100pM TGFβ
WT
MG132 (0.75h pre) + 100pM TGFβ
0 0.75 2 3 4 6 8
0 0.75 2 3 4 6 8
pSMAD2
GAPDH
SMAD4
GAPDH
SMAD2
GAPDH
TGFβRI
GAPDH
SMURF2
p21
GAPDH

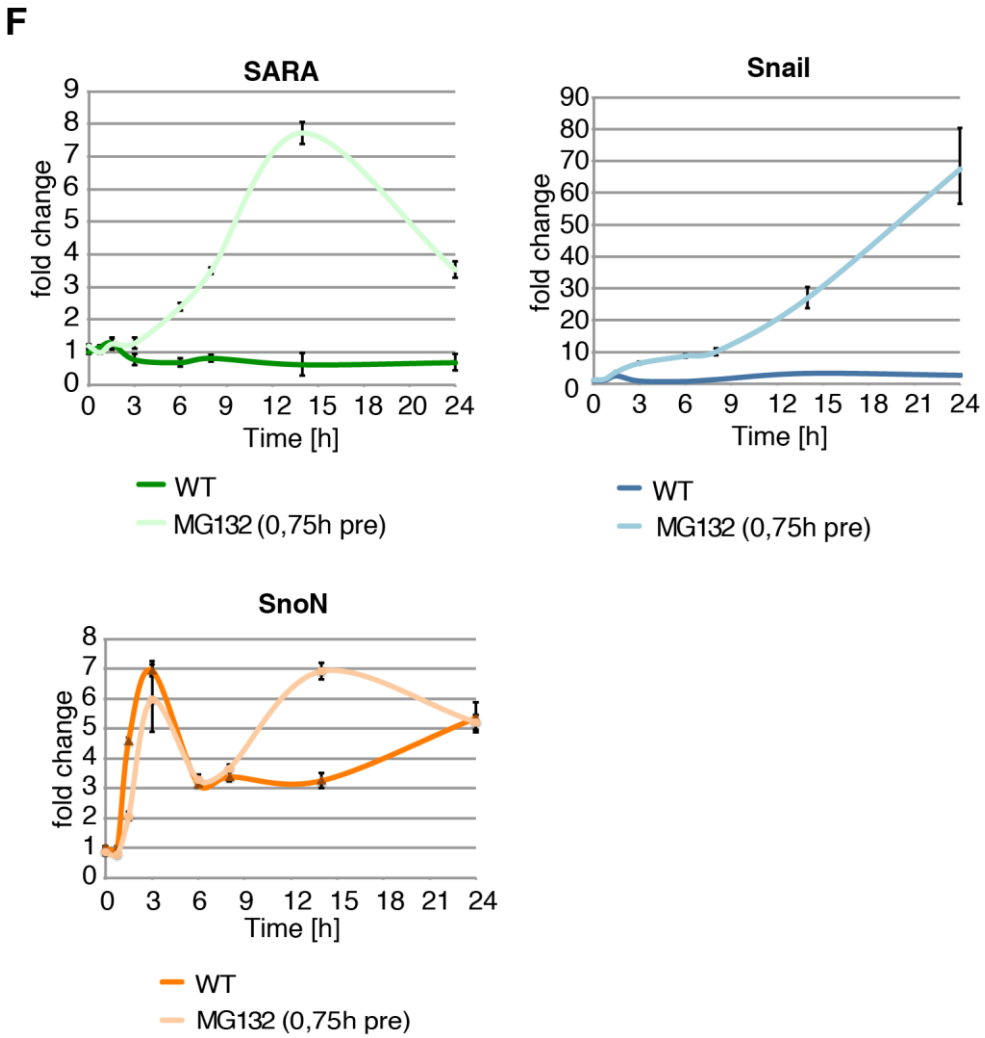

3.2.3 Figure 24. Inhibition of proteasomal degradation boost nuclear SMAD accumulation.
A Median nuc/cyto SMAD2 ratio, median cytoplasmic and nuclear SMAD2 level of the SMAD2-YFP reporter cells stimulated with 100pM TGFβ and treated with the proteasome inhibitor
MG132 at indicated time points. Shaded area represent data between 25th and 75th percentiles.
B Exemplary individual nuc/cyto SMAD2 ratio trajectories (thin lines) for the SMAD2-YFP reporter cells stimulated with 100pM TGFβ and treated with MG132 0.75h pre 100pM TGFβ compared to the median nuc/cyto SMAD2 ratio of the entire population (thick line).
C Signaling features for the nuc/cyto SMAD2 ratio in the SMAD2 reporter cells stimulated with 100pM TGFβ and treated with MG132 at indicated time points. Red lines indicate median; boxes include data between the 25th and 75th percentiles; whiskers extend to maximum values within 1.5× the interquartile range; crosses represent outliers.
D Median nuclear SMAD2 level, median nuc/cyto SMAD2 ratio and cytoplasmic level of the SMAD2-YFP reporter cells stimulated with DMSO and 100pM TGFβ or with the proteasome inhibitor
MG132 only. Shaded area represent data between 25th and 75th percentiles.
E Western blot analysis of phosphorylated SMAD2, total SMAD4 and SMAD2, TGFβRI, SMURF2 and p21 in MCF10A WT cells stimulated with 100pM TGFβ and 0.75h pretreated with MG132. GAPDH was used as a loading control.
F Expression of TGFβ target genes in MCF10A WT cells stimulated with 100pM TGFβ and 0.75h pretreated with MG132. β-Actin was used as an internal control. Error bars indicate standard deviation of technical triplicates.

3.2.4 Receptor internalization and degradation: Endocytotic pathways

Endocytosis of cell surface receptors is a major regulatory event in signal transduction (Baass *et al*, 1995; Di Fiore & De Camilli, 2001; McPherson *et al*, 2001). TGFβ receptor signaling and turnover are regulated by distinct endocytic compartments to finally regulate SMAD2 activation (Di Guglielmo *et al*, 2003). Clathrin-mediated endocytosis targets receptor proteins to the early endosome antigen-1

(EEA1)- positive endosome, where the SMAD2 anchor SARA is enriched, and promotes TGFβ signaling through recycling or receptors enter the late endosome-lysosome for degradation (Di Guglielmo *et al,* 2003; Hayes *et al,* 2002; Itoh *et al*, 2002; Panopoulou *et al,* 2002). The lipid raft- caveolar internalization pathway contains the SMAD7-SMURF2 bound receptor and is required for rapid receptor turnover and degradation. Hereby SMAD7 interacts with TGFβRI and recruits the E3 ligases SMURF1 and SMURF2, which direct ubiquitin-dependent degradation of the TGFβ receptor- SMAD7-complex. (Di Guglielmo *et al,* 2003; Ebisawa *et al*, 2001; Kavsak *et al,* 2000). Immunofluorescence experiments showed that TGFβ receptor II is stabilized in MCF10A WT cells 0.75h post 100pM TGFβ stimulation und subsequently degraded to less than the basal level **(Figure 25A and B)**. To address the question how the distinct receptor internalization and degradation processes affect SMAD2 dynamics I inhibited the endocytic pathways with dynasore or nystatin respectively and performed time-lapse microscopy experiments. Dynasore is a newly identified cell- permeable inhibitor of dynamin GTPase activity, that facilitates the formation of coated pits in the process of clathrin-dependent endocytosis. Thus, dynasore is a potent enhancer of TGFβ signaling (Macia *et al*, 2006; Nankoe and Sever, 2006; Chen *et al*, 2009). Treatment with nystatin disrupts the lipid raft- caveolar endocytic pathway and shifts receptors into the non-raft compartment EEA1. Therefore, the inhibitor stabilizes the receptors and slightly enhances signaling and SMAD2 activation (Di Guglielmo *et al*, 2003). Monitoring living single cells treated with nystatin 0.75h before 100pM TGFβ stimulation revealed an unchanged SMAD2 ratio **(Figure 25C)**. However, the nuclear and cytosolic SMAD2 values were greatly increased **(Figure 25C and Appendix Figure A12)**. Here, the time of the maximum amplitude, increase and the end time of the first response was unchanged, but inhibiting the caveolar endocytic pathway enhanced the maximum amplitude and the mean intensity within 5h after the first response **(Appendix Figure A13)**. Therefore, SMAD2 accumulated strongly into the nucleus, but with a clearly early adaptation and an extenuated late adaptation, so that SMAD2 remained at a high nuclear level. Interestingly, the increased nuclear SMAD2 values led to an increased mobility of the cells **(Figure 25D)**. Inhibiting the clathrin-dependent endocytosis with dynasore 0.75h before 100pM TGFβ stimulation led to increased nuclear and cytosolic SMAD2 values, while the ratio was almost unchanged **(Figure 25E and F)**. The maximum amplitude and the mean intensity within 5h after response were slightly increased, so that SMAD2 accumulated slightly more into the nucleus, whereas the time of the maximum amplitude, increase and the end time of the first response remained unchanged **(Appendix Figure A14)**. However, the mobility of the cells was not changed **(Figure 25G)**. Taken together these results suggest that TGFβ receptor signaling and turnover play a huge role for the adaptation process of SMAD2 dynamics, especially for the late adaptation. Since early adaptation was attenuated and not prevented, other regulatory mechanisms are apparently involved.

Figure 25

A

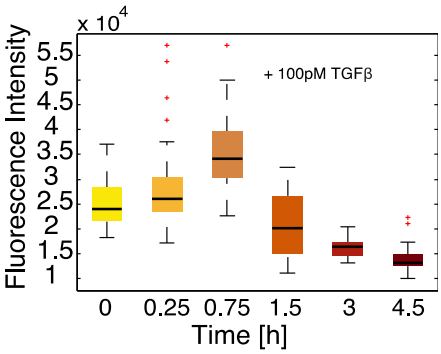
x 10^4
Fluorescence Intensity
5.5
5
4.5
4
3.5
3
2.5
2
1.5
1
+ 100pM TGFβ
0
0.25
0.75
1.5
3
4.5
Time [h]

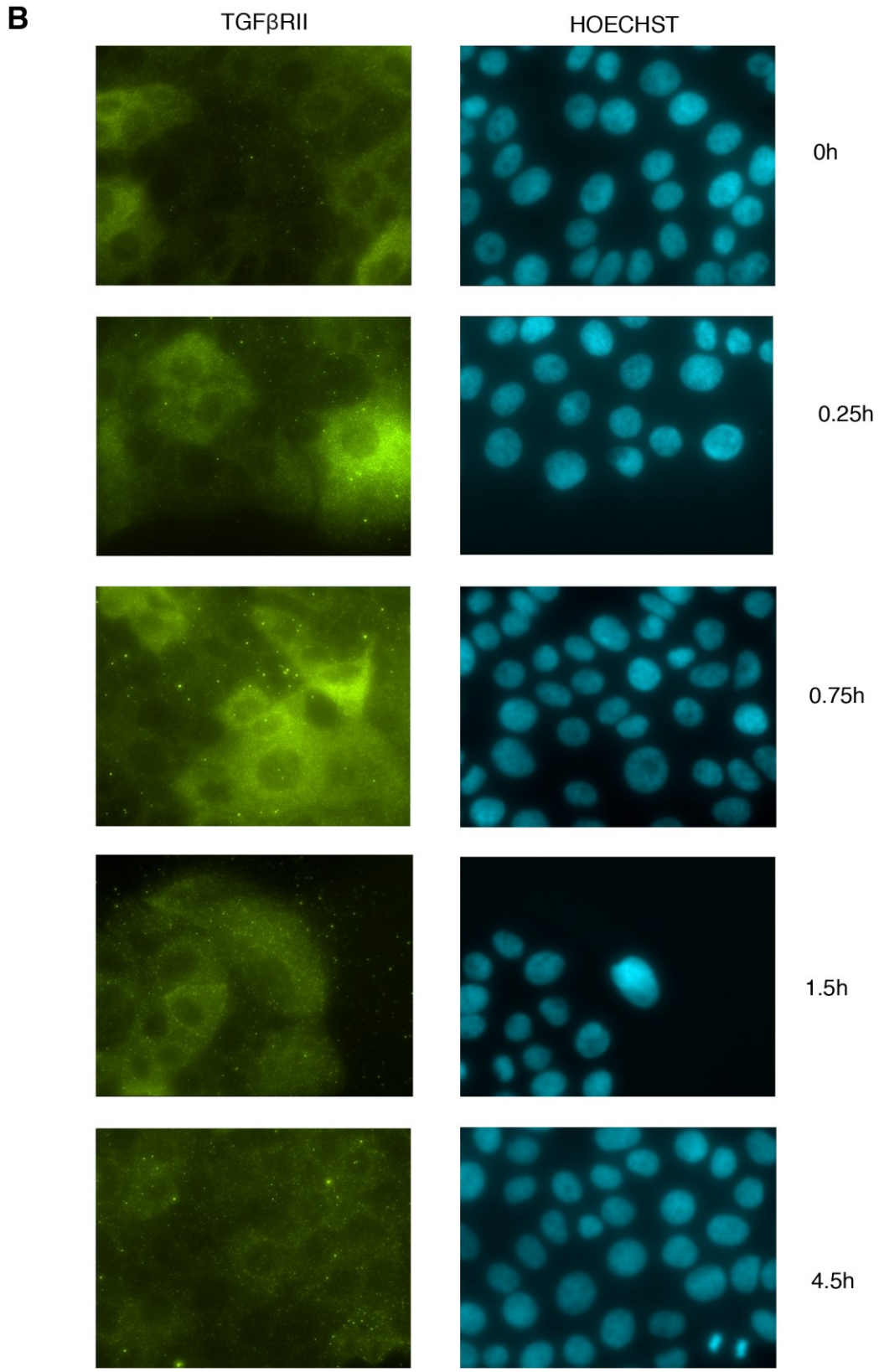
B
TGFβRII
HOECHST
0h
0.25h
0.75h
1.5h
4.5h

C

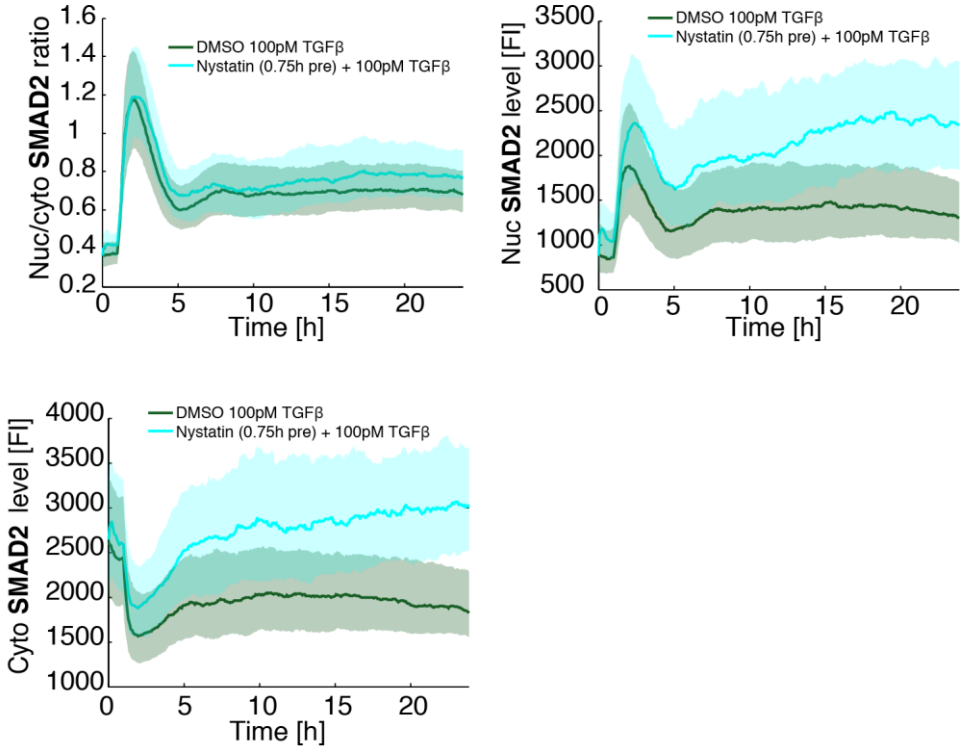
Nuc/cyto SMAD2 ratio
DMSO 100pM TGFβ
Nystatin (0.75h pre) + 100pM TGFβ
Time [h]
Nuc SMAD2 level [FI]
Cyto SMAD2 level [FI]

D

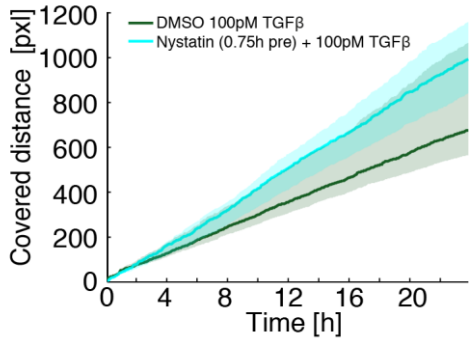
Covered distance [pxl]
DMSO 100pM TGFβ
Nystatin (0.75h pre) + 100pM TGFβ
Time [h]

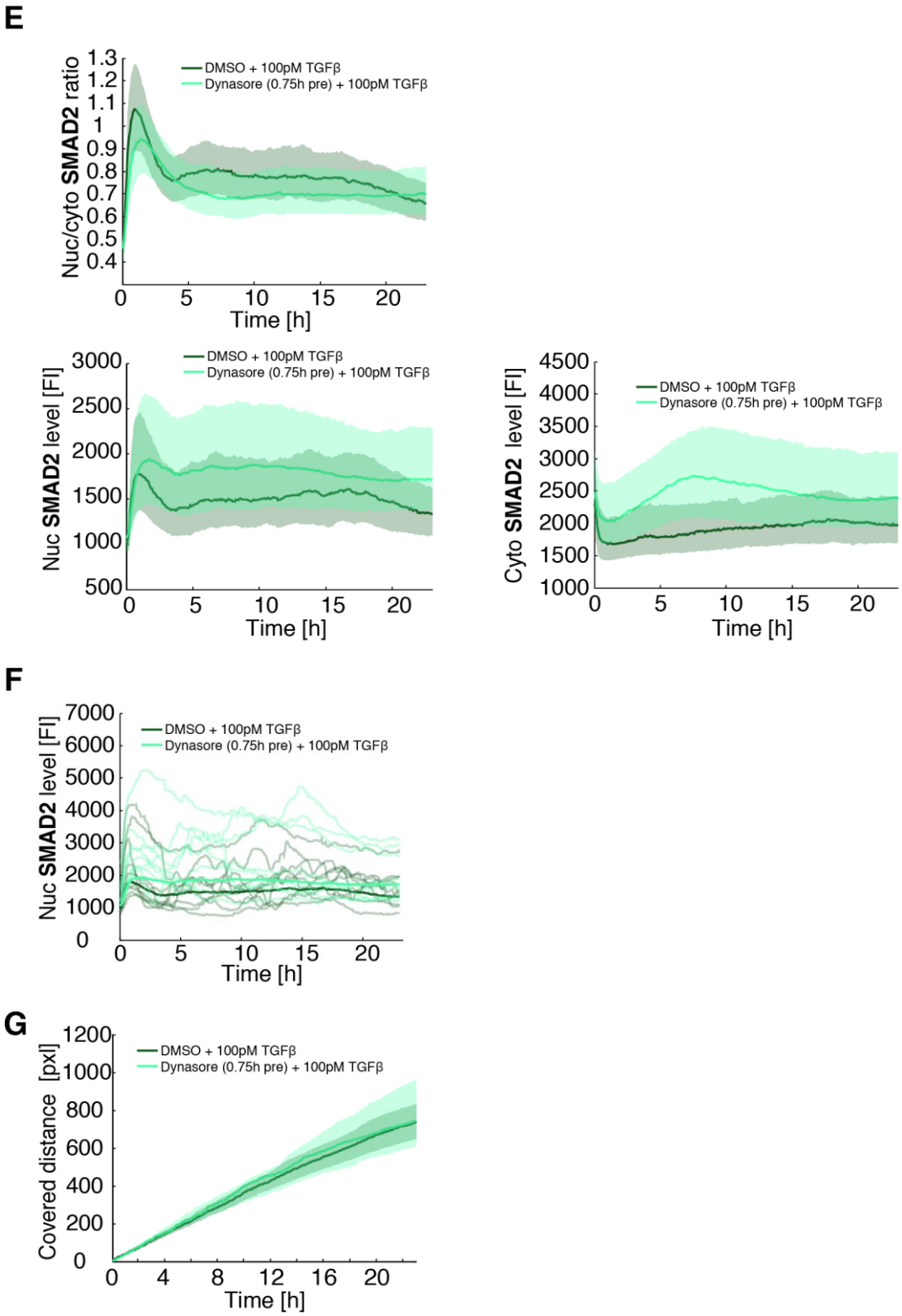

3.2.4 Figure 25. Receptor internalization and degradation: Endocytotic pathways.

A Fluorescence intensity of TGFβRII was measured in MCF10A WT cells stimulated with 100pM TGFβ by immunofluorescence. Black lines indicate median; boxes include data between the 25th and 75th percentiles; whiskers extend to maximum values within 1.5× the interquartile range; crosses represent outliers.

B Exemplary pictures of fluorescence intensities of TGFβRII in MCF10A WT cells stimulated with 100pM TGFβ by immunofluorescence at indicated time points. Nuclear staining was carried out with Hoechst 33342.

C Median nuc/cyto SMAD2 ratio, nuclear and cytoplasmic level of the SMAD2-YFP reporter cells stimulated with 100pM TGFβ and 0.75h pretreated with Nystatin. DMSO was used as a control. Shaded area represent data between 25th and 75th percentiles.

D Motility of each cell as summed distance in pixel (pxl) covered 24h after stimulation with 100pM TGFβ and 0.75h pretreated with Nystatin. Median indicated as a thick line and shaded area represent data between 25th and 75th percentiles.
E Median nuc/cyto SMAD2 ratio, nuclear and cytoplasmic level of the SMAD2-YFP reporter cells stimulated with 100pM TGFβ and 0.75h pretreated with Dynasore. DMSO was used as a control. Shaded area represent data between 25th and 75th percentiles.
F Exemplary individual nuclear SMAD2 trajectories (thin lines) for the SMAD2-YFP reporter cells stimulated with 100pM TGFβ and 0.75h pretreated with Dynasore compared to the median nuclear SMAD2 level of the entire population (thick line).
G Motility of each cell as summed distance in pixel (pxl) covered 24h after stimulation with 100pM TGFβ and 0.75h pretreated with Dynasore. Median indicated as a thick line and shaded area represent data between 25th and 75th percentiles.

3.2.5 TGFβ signaling shows a refractory period depending on signaling state due to adaptation mechanisms

The refractory period is the recovery time of the signaling system to be ready for a second stimulus. In order to examine the refractory time and to understand which mechanism restricts reactivation of the pathway and constitute the refractory period, I performed time-lapse microscopy experiments of SMAD2 reporter cells stimulated repeatedly with different TGFβ concentrations at various time points. First, I measured SMAD2 dynamics upon 100pM re-stimulation after 3 and 6 hours, respectively, and at 3 and 6 hours by replacing the medium completely after 3 washing steps. As shown in **Figure 26A and B** within the monitored 24 hours the system was incapable of responding again to stimulation. To prove as a control experiment that cells can be stimulated at later times under our conditions, individual trajectories stimulated with 100pM TGFβ only at 3 or 6 hours are shown in the heat map **(Figure 26B)**. In the next experiment, the reporter cells were stimulated with 5pM TGFβ and re-stimulated at 3 hours after 3 washing steps and medium change. As shown in **Figure 26C and Appendix Figure A15** the SMAD2 ratio (nuclear dynamics are similar) was hardly changed and only a slight amplification of SMAD2 signaling can be observed. This is particularly evident by the similar SMAD2 ratio values at 4 hours, 1 hour after re-stimulation **(Appendix Figure A16)**. Interestingly, the cells re-stimulated at 6 hours revealed a new peak at 7 hours but remained clearly below the first peak **(Figure 26C, Appendix Figure A15 and A16)**. Re-stimulation at 8 hours leads to a strong second response at 9h. The amplitude remained slightly below the first response but is approximately equal with the response of the cells stimulated just once at 8 hours with 5pM TGFβ. Reasons for this could be the TGFβ molecules per cell, which decrease with increasing cell number, or the decreased TGFβ concentration of the stock solution, which was stored on ice during the experiment. Until now, it seems that cells can only be completely restimulated after the terminal adaptation has been completed. To determine if SMAD7 feedback contributes to the refractory period after stimulation I inhibited transcriptional feedback loops with DRB 0.25h pre TGFβ stimulation and repeated the stimulation experiments with 5pM TGFβ after 3 hours. SMAD7 expression is about 3-fold 3 hours post 5pM stimulation (3.1.3.1). The cells treated with DRB and re-stimulated with 5pM TGFβ showed a stronger

signaling with increased first amplitude but without significant re-stimulation in the ratio data **(Figure 26D)**. However, the nuclear levels show a clear re-stimulation with a new peak at 7.5h on almost initial peak level **(Figure 26D, E and Appendix Figure A17)** In a control experiment, the cells were treated with DRB and stimulated only after 3 hours with 5pM TGFβ **(Figure 26F)**. The response was similar to the re-stimulation peak. In conclusion complete re-stimulation was only possible when SMAD2 shuttling into the nucleus is terminated and transcriptional negative feedback loops contribute to the refractory period of the system, at least for small concentrations.

Figure 26

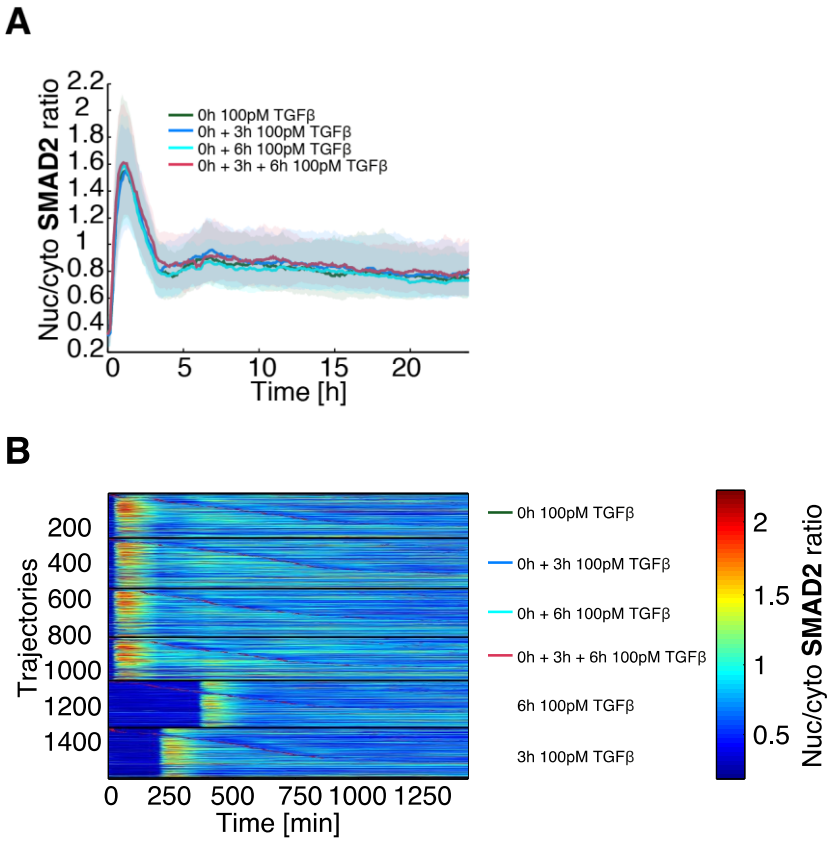

3.2.5 TGFβ signaling shows a refractory period depending on signaling state due to adaptation mechanisms

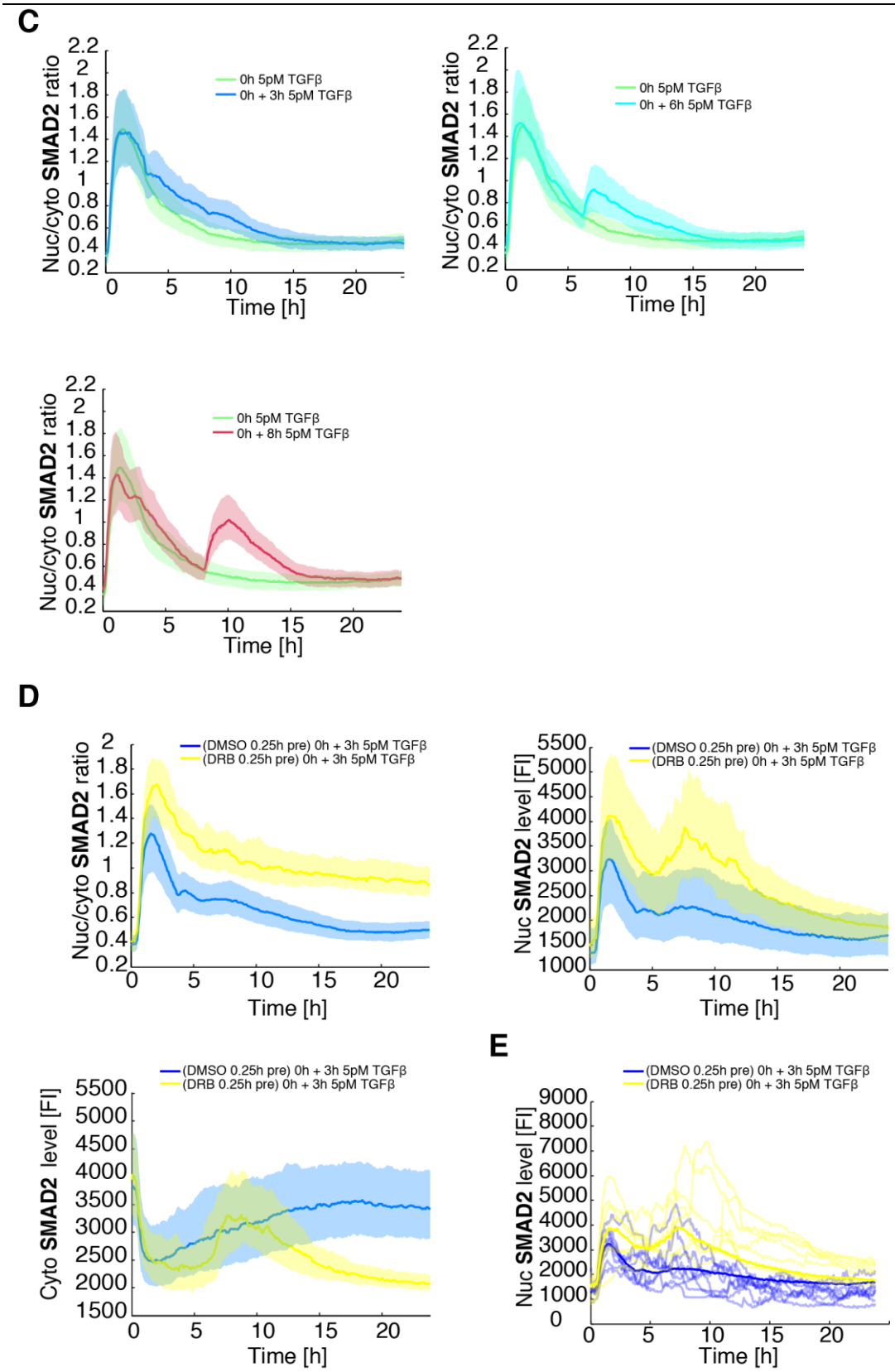

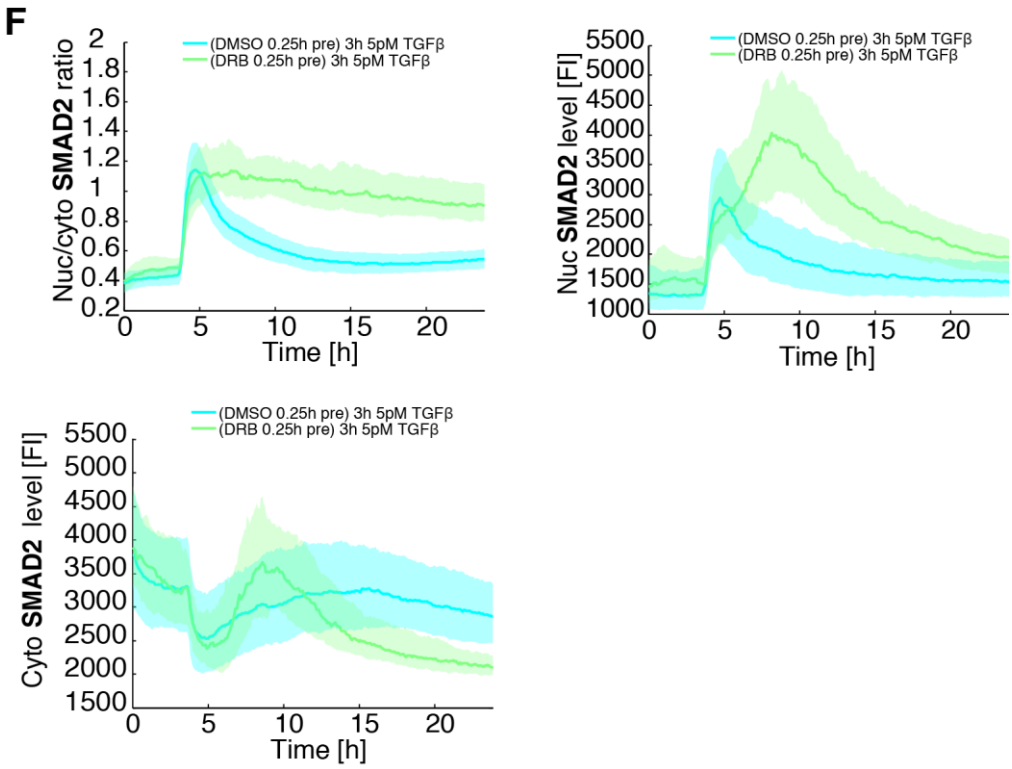

3.2.5 Figure 26. TGFβ signaling shows a refractory period.
A Median nuc/cyto SMAD2 ratio of the SMAD2-YFP reporter cells stimulated with 100pM TGFβ and restimulated with 100pM TGFβ at indicated time points. Shaded area represent data between 25th and 75th percentiles.
B Heat maps of SMAD2 translocation in individual cells over 24h. Cells were stimulated with 100pM TGFβ and restimulated with 100pM TGFβ at indicated time points. Cells were sorted by the time of the first division as indicated by red marks.
C Median nuc/cyto SMAD2 ratio of the SMAD2-YFP reporter cells stimulated with 5pM TGFβ and restimulated with 5pM TGFβ at indicated time points. Shaded area represent data between 25th and 75th percentiles.
D Median nuc/cyto SMAD2 ratio, nuclear and cytoplasmic level of the SMAD2-YFP reporter cells stimulated with 5pM TGFβ and restimulated 3h post with 5pM TGFβ and 0.25h pretreated with DRB. DMSO was used as a control. Shaded area represent data between 25th and 75th percentiles.
E Exemplary individual nuclear SMAD2 trajectories (thin lines) for the SMAD2-YFP reporter cells stimulated with 5pM TGFβ and restimulated 3h post with 5pM TGFβ and 0.25h pretreated with DRB compared to the median nuclear SMAD2 level of the entire population (thick line).
F Median nuc/cyto SMAD2 ratio, nuclear and cytoplasmic level of the SMAD2-YFP reporter cells stimulated with 5pM TGFβ and 0.25h pretreated with DRB. DMSO was used as a control. Shaded area represent data between 25th and 75th percentiles.

3.3 Source of variability

Since the cellular state of the cell, like the refractory time, is crucial for the TGFβ response, the question generally came up which factors influence the enormous heterogeneity of the SMAD response. Why do individual and genetically identical cells react differently to a given TGFβ stimulus? To this end, I examined how the cell cycle state, cell density or cell location contribute to the observed heterogeneity in single cell responses, since these factors are suggested in previous studies to have impact on cell-to-cell variability (Loewer & Lahav, 2011; Snijder & Pelkmans, 2011).

3.3.1 Cell cycle state is not the main cause of heterogeneity

In order to investigate if the variability in the signaling response is correlated to a specific cell cycle phase at stimulation, I imaged the SMAD2-YFP reporter cells 24 hours before stimulation with varying TGFβ concentrations **(Figure 27A)**. When sorting cells according to the time of the last division before TGFβ stimulation or by the amplitude of the response, no obvious correlation between cell cycle phase and TGFβ response was observed for all different TGFβ concentrations. The heat map in **Figure 27B** indicates exemplary the results for 100pM TGFβ stimulation of more than 400 cells. To compare the distributions of cell divisions with the heterogeneous TGFβ response in detail, Marcel Jentsch mapped the SMAD signaling responses for each individual cell to the previously defined signaling classes **(Figure 27C)**. As shown in **Figure 27D**, there are no significant differences in the distributions of the cell divisions of the respective signaling classes. Furthermore, the influence of specific cell cycle phases was investigated by using specific inhibitors for the G2 (RO3306) and G0 / G1 arrest (Gefitinib). To prove the efficiency of the inhibitors, a *f*luorescent, *u*biquitination-based *c*ell *c*ycle *i*ndicator (Fucci)-based MCF10A cell line was generated by Gitta Blendinger to monitor the proportion of arrested cells (Sakaue-Sawano *et al*, 2008). The authors harnessed the regulation of cell cycle-dependent ubiquitination in order to generate two antiphase oscillating indicators for cell-cycle progression. These fluorescent probes effectively label individual G1 phase nuclei red and those in S / G2 / M phases green **(Figure 27E)**. Then by using the inhibitor RO3306, that inhibits effectively and reversible CDK1 (Vassilev, 2006), the majority of the cells are arrested after 8 hours at G2 phase of the cell cycle **(Figure 27F)**. Therefore, I used RO3306 4 hours, where cells partially arrested, and 8 hours prior TGFβ stimulation, but cells arrested in G2 showed the same median response to 100pM TGFβ stimulation as freely cycling cells **(Figure 27G)**. Moreover, using Gefitinib, an inhibitor that induces G0/ G1 arrest (Zhou, 2009), showed for the Fucci cell line a maximum of cells in G1 arrest at 19 hours of incubation with the inhibitor **(Figure 27H)**. SMAD2-YFP reporter cells pretreated with Gefitinib 20,5 hours prior to 100pM TGFβ stimulation showed only weak accumulation of SMAD2 into the nucleus **(Figure 27I)**. Especially the heat maps showed clearly that there is hardly any pathway activity **(Figure 27J)**. Since G1 arrest is also a known cell fate of TGFβ treatment (Hocevar & Howe, 1998), this could be a reason that cells in G1 are almost not reacting to TGFβ.

In conclusion, cell cycle state is not the main cause of heterogeneity. Furthermore, synchronized cells in G2 with a CDK1 inhibitor showed no impact on the TGFβ response. An exception is already arrested cells in G0 / G1, which showed almost no SMAD2 response after 100pM TGFβ stimulation.

Figure 27

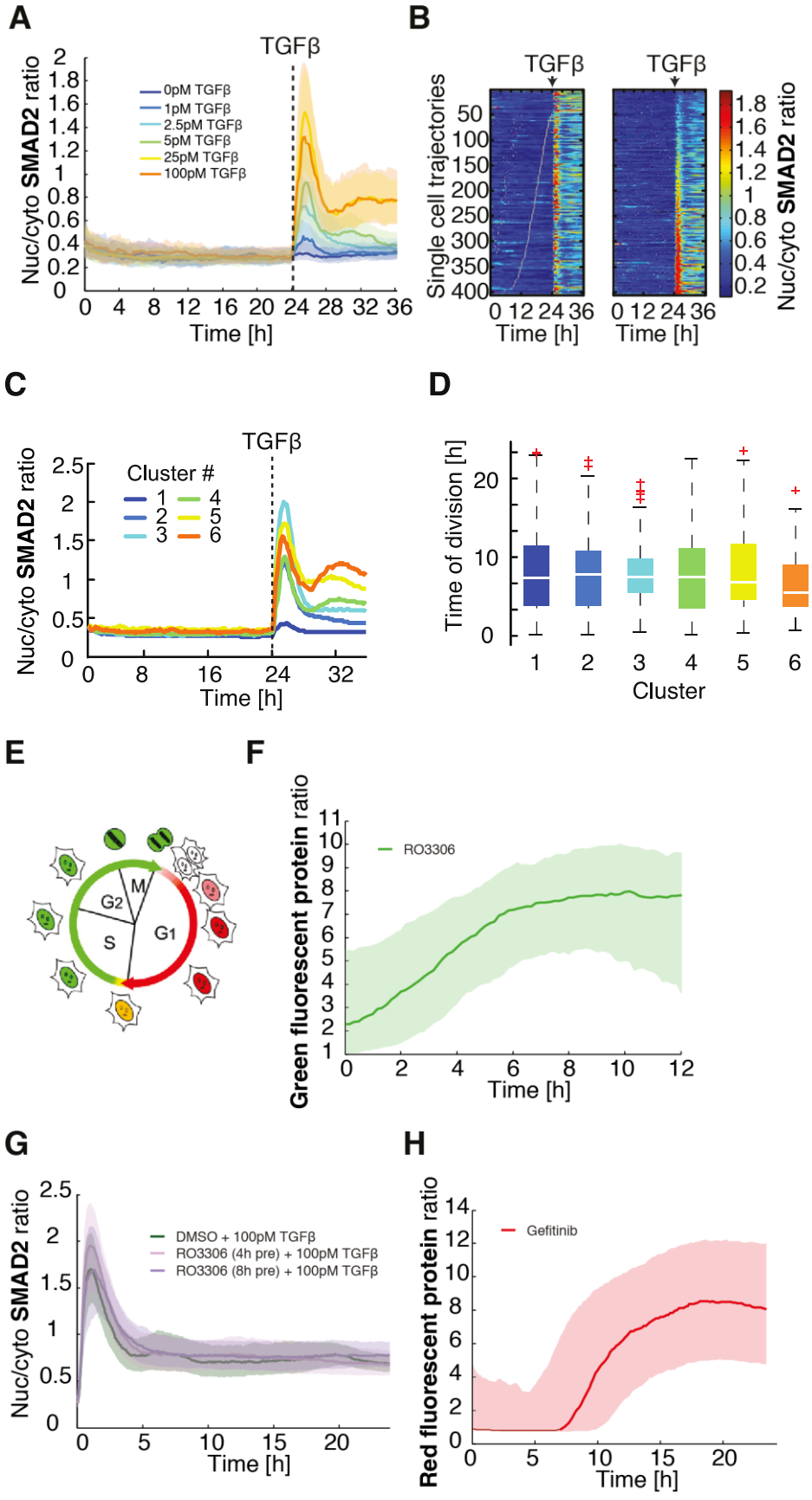
A
TGFβ
Nuc/cyto SMAD2 ratio
0pM TGFβ
1pM TGFβ
2.5pM TGFβ
5pM TGFβ
25pM TGFβ
100pM TGFβ
Time [h]
B
TGFβ
TGFβ
Single cell trajectories
Nuc/cyto SMAD2 ratio
Time [h]
C
TGFβ
Cluster #
Nuc/cyto SMAD2 ratio
Time [h]
D
Time of division [h]
Cluster
E
G2
M
S
G1
F
Green fluorescent protein ratio
RO3306
Time [h]
G
Nuc/cyto SMAD2 ratio
DMSO + 100pM TGFβ
RO3306 (4h pre) + 100pM TGFβ
RO3306 (8h pre) + 100pM TGFβ
Time [h]
H
Red fluorescent protein ratio
Gefitinib
Time [h]

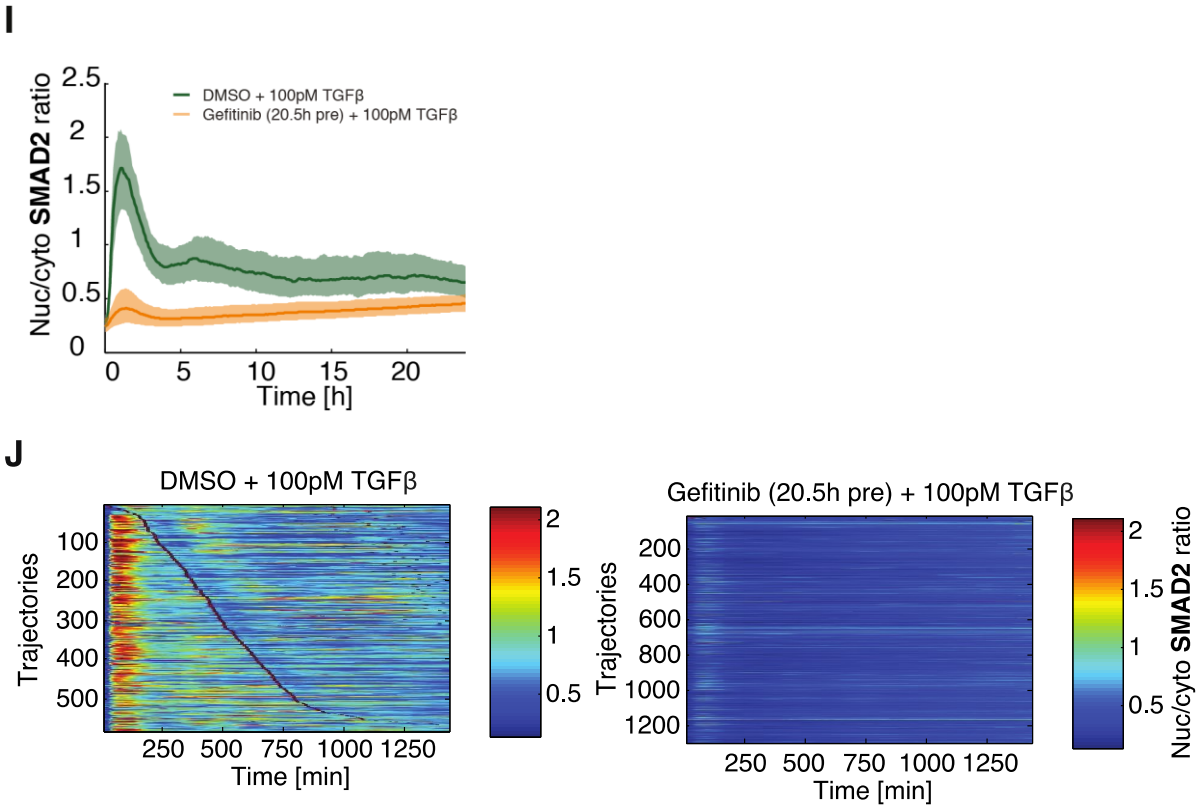

3.3.1 Figure 27. Cell cycle state is not the main cause of heterogeneity.
A Median nuc/cyto SMAD2 ratio of the SMAD2-YFP reporter cells stimulated with varying TGFβ concentrations. Cells were imaged for 24 h before stimulation with TGFβ. Shaded area represent data between 25th and 75th percentiles.
B Heat map of SMAD2 translocation in individual cells over time. Cells were imaged for 24 h before stimulation with 100pM TGFβ. The nuc/cyto SMAD2 ratio is shown as indicated in the legend. Time of cell division is indicated by white marks. Cells were sorted either by the time of the last division
before stimulation (left panel) or by the amplitude of their response (right panel).
C Mapping of SMAD2 translocation dynamics in individual cells to six signaling classes (cluster). Median nuc/cyto SMAD2 ratios for resulting cluster are shown.
D Time of last cell division before stimulus for each cluster. White lines indicate median; boxes include data between the 25th and 75th percentiles; whiskers extend to maximum values within 1.5× the interquartile range; crosses represent outliers.
E A fluorescent, ubiquitination-based cell cycle indicator (Fucci)- based MCF10A cell line
(Sakaue-Sawano *et al*, 2008). The authors generated two antiphase oscillating indicators for cell-cycle progression. These fluorescent probes effectively label individual G1 phase nuclei red and those in S / G2 / M phases green.
F Green fluorescent protein nuc/cyto ratio of the Fucci- based MCF10A cell line treated with RO-3306. Shaded area represent data between 25th and 75th percentiles.
G Median nuc/cyto SMAD2 ratio of the SMAD2-YFP reporter cells stimulated with 100pM TGFβ and pretreated with RO-3306 at indicated time points. Shaded area represent data between 25th and 75th percentiles.
H Red fluorescent protein nuc/cyto ratio of the Fucci- based MCF10A cell line treated with Gefitinib. Shaded area represent data between 25th and 75th percentiles.
I Median nuc/cyto SMAD2 ratio of the SMAD2-YFP reporter cells stimulated with 100pM TGFβ and 20.5h pretreated with Gefitinib. Shaded area represent data between 25th and 75th percentiles.
J Heat maps of SMAD2 translocation in individual cells over 24h. Cells were stimulated with 100pM TGFβ and 20.5h pretreated with Gefitinib. Cells were sorted by the time of the first division as indicated by red marks.

3.3.2 Local cell density is not sufficient to explain signaling heterogeneity

Since the cell cycle status had no particular influence on the SMAD translocation, I next examined the cell density and the specific cell location with the neighboring cells. To investigate how the TGFβ response depends on cell density, I seeded a different number of cells 48 hours prior to 100pM TGFβ

stimulation (0.25, 0.5, 0.75, 1.5, 3, and 6 x 10^5 cells). For comparison, all other experiments were performed with a 2.5 x 10^5 cell seeding. As shown in **Figure 28A**, the SMAD2 ratio response looked quite similar. The basal ratio values were relatively constant and decreased only slightly with increasing cell number **(Figure 28B)**, whereby the ratio amplitude increased only slightly with increasing cell number **(Figure 28C)**. The exception here was the maximum seeded cell number of 6 × 10^5 with a lower amplitude and a stronger adaptation **(Figure28A & C)**. However, the nuclear SMAD2 response was highly dependent on cell density **(Figure 28D)**. Even the basal nuclear values depended on the cell density, the lower the cell number, the higher the nuclear level, with the exception of the maximum cell number of 6 × 10^5 cells **(Figure 28E)**. Accordingly, the amplitude also decreased extremely with increasing cell density **(Figure 28F)**. The late signaling also showed these differences, which becomes particularly clear in **Figure 28G** for the example trajectories for 0.25 and 6 x 10^5 seeded cells. Furthermore, the cytoplasmic levels decreased with increasing cell density, in particular the basal values **(Figure 28H & I)**. These results can also be transferred to SMAD4, as shown for the nuclear SMAD4 values in **Figure 28J**. In summary, the ratio TGFβ response was largely independent of cell density, but the amount of SMADs in the nucleus increased with lower cell density. This applied to the basal level, amplitude and the late SMAD response. Cell contacts, cell volume, available number of receptors and most likely TGFβ molecules per cell could play a role. Since the cell density in this experimental setup is determined by too many factors, in another experiment I considered the influence of the local cell density with the neighboring cells on the TGFβ response. From the number and distance of neighboring cells, Marcel Jentsch calculated a density score for each individual cell, based on the weighted distance of cells in a 640 µm radius. The basis for this is the experiment of **Figure 27C**, where the cells were stimulated after 24 hours with 100 pM TGFβ and then sorted into six signaling classes. However, as shown in **Figure 28K**, the distributions for all signaling classes are overlapping and local cell density are not sufficient to explain signaling heterogeneity.

Figure 28

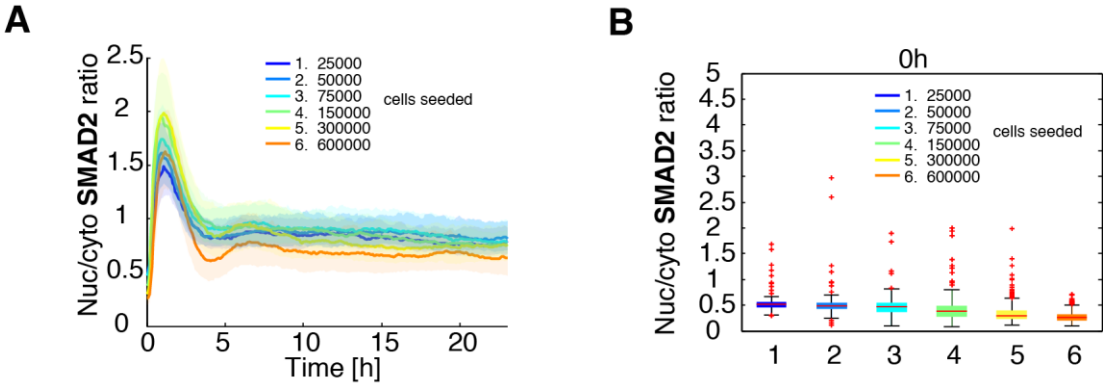

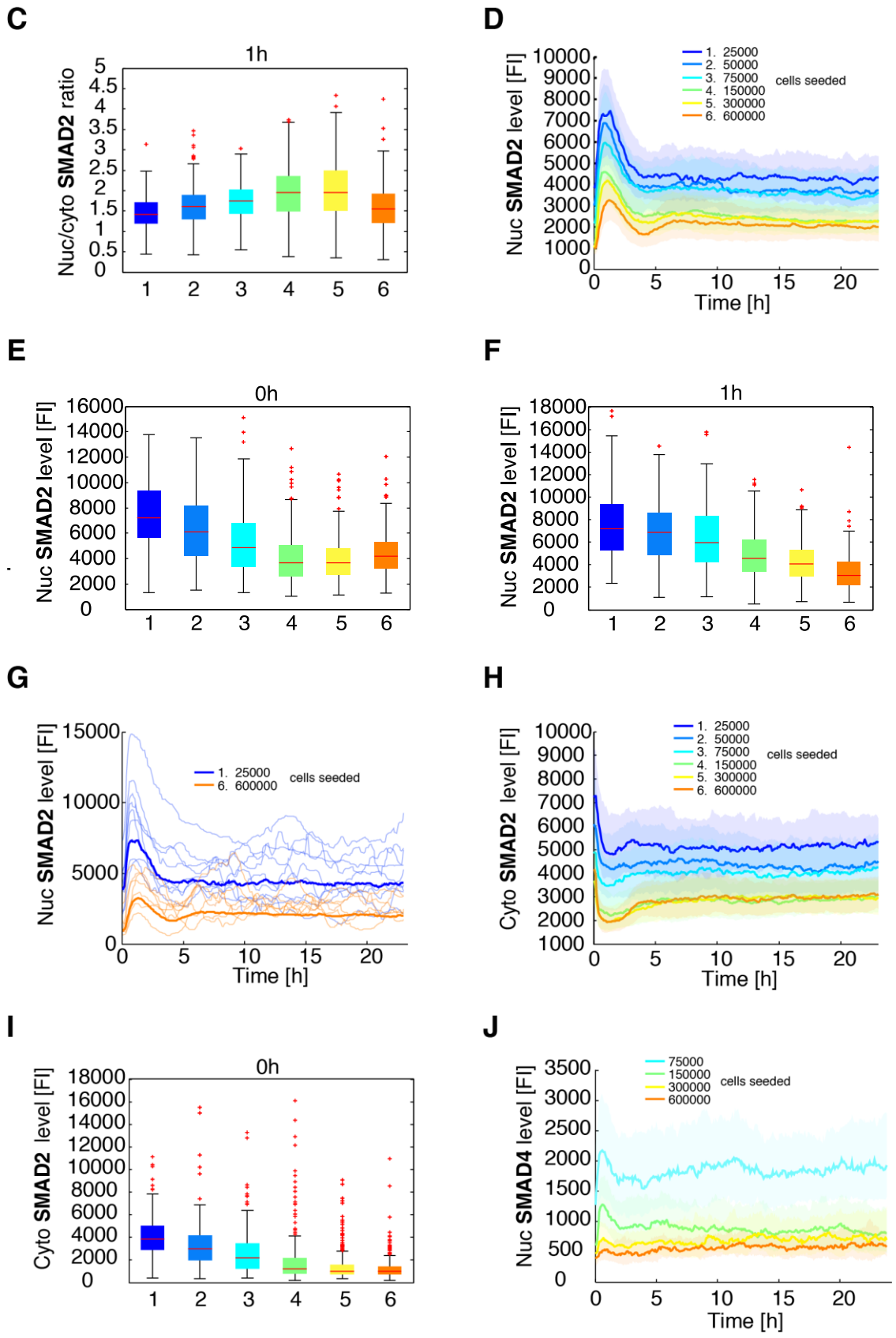
C
1h
Nuc/cyto SMAD2 ratio
D
Nuc SMAD2 level [FI]
1. 25000
2. 50000
3. 75000
4. 150000
5. 300000
6. 600000
cells seeded
Time [h]
E
0h
Nuc SMAD2 level [FI]
F
1h
Nuc SMAD2 level [FI]
G
Nuc SMAD2 level [FI]
1. 25000
6. 600000
cells seeded
Time [h]
H
Cyto SMAD2 level [FI]
1. 25000
2. 50000
3. 75000
4. 150000
5. 300000
6. 600000
cells seeded
Time [h]
I
0h
Cyto SMAD2 level [FI]
J
Nuc SMAD4 level [FI]
75000
150000
300000
600000
cells seeded
Time [h]

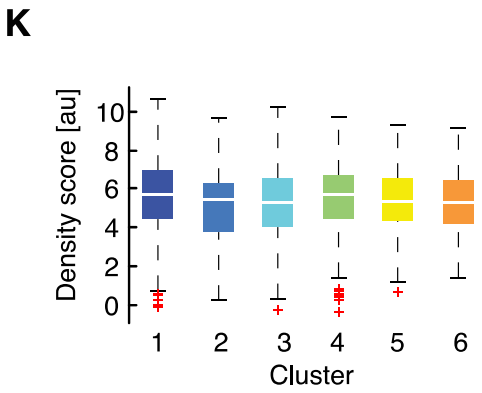

3.3.2 Figure 28. Local cell density is not sufficient to explain signaling heterogeneity.
A Median nuc/cyto SMAD2 ratio of the SMAD2-YFP reporter cells seeded with a different number of cells 48 hours prior to 100pM TGFβ stimulation. For comparison, all other experiments were performed with a 2.5 x 105 cell seeding. Shaded area represent data between 25th and 75th percentiles.
B Basal nuc/cyto SMAD2 ratio of the SMAD2 reporter cells seeded with a different number of cells 48 hours prior. Red lines indicate median; boxes include data between the 25th and 75th percentiles; whiskers extend to maximum values within 1.5× the interquartile range; crosses represent outliers.
C Nuc/cyto SMAD2 ratio of the SMAD2 reporter cells seeded with a different number of cells 48 hours prior to 100pM TGFβ stimulation at 1h time point. Red lines indicate median; boxes include data between the 25th and 75th percentiles; whiskers extend to maximum values within 1.5× the interquartile range; crosses represent outliers.
D Median nuclear SMAD2 level of the SMAD2-YFP reporter cells seeded with a different number of cells 48 hours prior to 100pM TGFβ stimulation. Shaded area represent data between 25th and 75th percentiles.
E Basal nuclear SMAD2 level of the SMAD2 reporter cells seeded with a different number of cells 48 hours prior. Red lines indicate median; boxes include data between the 25th and 75th percentiles; whiskers extend to maximum values within 1.5× the interquartile range; crosses represent outliers.
F Nuclear SMAD2 level of the SMAD2 reporter cells seeded with a different number of cells 48 hours prior to 100pM TGFβ stimulation at 1h time point. Red lines indicate median; boxes include data between the 25th and 75th percentiles; whiskers extend to maximum values within 1.5× the interquartile range; crosses represent outliers.
G Exemplary individual nuclear SMAD2 trajectories (thin lines) for the SMAD2-YFP reporter cells seeded with the indicated number of cells 48 hours prior to 100pM TGFβ stimulation compared to the median nuclear SMAD2 level of the entire population (thick line).
H Median cytoplasmic SMAD2 level of the SMAD2-YFP reporter cells seeded with a different number of cells 48 hours prior to 100pM TGFβ stimulation. Shaded area represent data between 25th and 75th percentiles.
I Basal cytoplasmic SMAD2 level of the SMAD2 reporter cells seeded with a different number of cells 48 hours prior. Red lines indicate median; boxes include data between the 25th and 75th percentiles; whiskers extend to maximum values within 1.5× the interquartile range; crosses represent outliers.
J Median nuclear SMAD4 level of the SMAD4-YFP reporter cells seeded with a different number of cells 48 hours prior to 100pM TGFβ stimulation.
K Cell density for the experiment of Figure 27C, where the cells were stimulated after 24 hours with 100pM TGFβ and then sorted into six signaling classes. Density scores before stimulus for each signaling class represent a weighted sum of all neighboring cells within 640 µm radius.

3.4 The activity of MAP kinases determines long-term dynamics of SMAD signaling

I hypothesized that the dynamic response of SMADs may be influenced by crosstalk of non-canonical TGFβ signaling and other signaling networks. Crosstalk describes how signal integration from multiple inputs within a response network affects a common biological output (Vert & Chory, 2011). Cross-signaling mechanisms between SMADs and MAPK (mitogen-activated protein kinase) pathways have been described recently, but how they influence the SMAD dynamics remains unexplained (Javelaud & Mauviel, 2005; Kolosova, 2011; Yumoto *et al*, 2013).

3.4.1 Inhibiting non- canonical activation of JNK has no influence on SMAD signaling

The crosstalk between the JNK1 (c-Jun N-terminal kinase 1) and SMAD3 pathways in RPMCs (rat peritoneal mast cells) has been explored and they found that JNK1 was critical for the TGF-β1-induced SMAD3 phosphorylation and nuclear translocation in RPMCs (Liu, 2012). Nevertheless, the influence of the JNK on SMAD2 and SMAD4 dynamics is unclear. Therefore, I inhibited JNK1, 2 and 3 with different concentrations of the JNK inhibitor VIII (CAS 894804-07-0) and monitored SMAD2 and SMAD4 translocation by time-lapse microscopy. Neither the nuclear nor cytoplasmic levels of SMAD2 and SMAD4 changed over the measured period in MCF10A cells (**Figure 29A & B**).

Figure 29

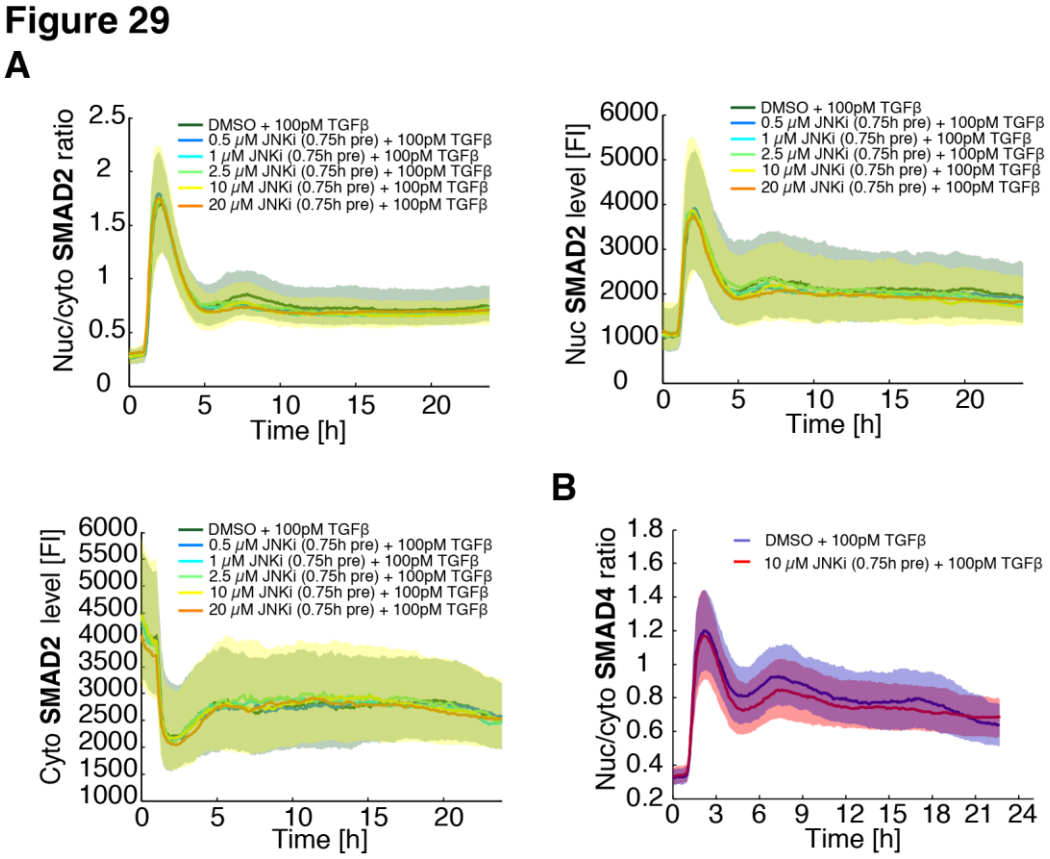

3.4.1 Figure 29. Inhibiting non- canonical activation of JNK has no influence on SMAD signaling.
A Median nuc/cyto SMAD2 ratio, nuclear and cytoplasmic level of the SMAD2-YFP reporter cells stimulated with 100pM TGFβ and treated with JNK Inhibitor VIII at indicated concentrations. DMSO was used for the control. Shaded area represent data between 25th and 75th percentiles.
B Median nuc/cyto SMAD4 ratio of the SMAD4-YFP reporter cells stimulated with 100pM TGFβ and treated with 10μM JNK Inhibitor VIII. DMSO was used for the control. Shaded area represent data between 25th and 75th percentiles.

3.4.2 Inhibiting non- canonical activation of p38 alters long-term SMAD dynamics

To further analyze the influence of non-canonical TGFβ signaling on dynamic response of SMADs I focused on the p38 pathway. TGFβ receptors activate MAP3Ks (Mitogen-activated protein kinase kinase kinases or MEKKs) like TAK1 (Transforming growth factor beta-activated kinase 1 or MAP3K7), which in turn activates MKKs (Mitogen-activated protein kinase kinases) like 3, 4, 6 and finally

phosphorylate p38 (**Figure 1B**, Zhang, 2009). P38 signaling pathways are activated by stress stimuli and are involved in inflammation, cell cycle, cell death, development, cell differentiation, senescence and tumorigenesis in specific cell types (Zarubin & Han, 2005). I used p38 kinase inhibitors and investigated how dynamics of SMAD2 and SMAD4 change over time.

3.4.2.1 Inhibition of p38 modulates the dynamics and localization of SMADs

To increase p38 inhibition efficiency I combined two different inhibitors SB202190 und BIRB 796. SB202190 is widely used to inhibit p38α and p38β Isoforms. Pyridinyl imidazole inhibitors, including this compound, directly bind p38 MAP kinases in the ATP binding pocket (Davies *et al*, 2000; Frantz *et al*, 1998; Fox *et al*, 1998). BIRB 796 is an inhibitor of all isoforms of p38. Its binding induces a slow conformational change that locks the protein into an inactive conformation (Pargellis *et al*, 2002; Kuma *et al*, 2005). Indeed, I observed that inhibition of p38 activity with both inhibitors 0.75 hours pre 100pM TGFβ stimulation modulated the dynamics and localization of SMAD2 by slightly lowering the amplitude of the first peak (1.75h post experiment start) and preventing nuclear accumulation of SMAD2 at all later time points **(Figure 30A)**. Thus, the ratio values at 5h showed a stronger adaptation of the p38 inhibitor pretreated and 100pM TGFβ stimulated cells and no further activation of the pathway took place, illustrated by the 15h value **(Figure 30C)**. Cells treated only with the p38 inhibitors showed no change in basal SMAD2 activation **(Figure 30A & C)**. That the p38 inhibitors prevented the late TGFβ response in almost all cells is particularly apparent in the heat maps **(Appendix Figure A18)**. In **Figure 30D**, four example trajectories are presented for cells pretreated with the p38 inhibitors following 100pM TGFβ stimulation compared to the trajectories of non-inhibited but TGFβ stimulated cells. And in fact, most of the trajectories with the p38 inhibitors only showed the first peak compared to the variability of trajectories without inhibitors. Also, for lower TGFβ concentrations, such as 1, 2.5, 5 and 25pM TGFβ, was the amplitude diminished and no late response was recognizable **(Figure 30B, C and E)**. In order to show next that this is not a side effect of the combination of two inhibitors, I used both inhibitors individually with different concentrations **(Figure 30F)**. With increasing concentrations of SB202190 and BIRB 796, the p38 effect increased on the late SMAD2 response respectively. For all further experiments the combination of both inhibitors in moderate concentrations were used. Moreover, to validate the time-lapse microscopy results, I performed immunofluorescence experiments and inhibited p38 kinase activity in MCF10A WT cells and stimulated the cells with 100pM TGFβ. An analysis of nuclear and cytoplasmic total SMAD2 levels of hundreds of cells also resulted in a stronger adaptation and a non-existent late response **(Figure 30G)**. Representative cells for 1h and 8h post TGFβ stimulation of inhibited and non-inhibited cells are shown in **Figure 30H**. In addition, time-lapse microscopy experiments of the SMAD4 reporter cell line also showed a reduced amplitude and

SMAD4 almost completely shuttled out of the nucleus at 5h with no further late response activation at 100pM TGFβ stimulation and p38 kinase inhibition **(Appendix Figure A19, A20 and A22)**. Furthermore, p38 inhibitors alone did not show any change in SMAD4 activation **(Appendix Figure A19 and A22)**. Also, the ratio values of the SMAD4 reporter cell line stimulated with 2.5pM TGFβ confirmed the SMAD2 experiments **(Appendix Figure A21 and A22)**.

Figure 30

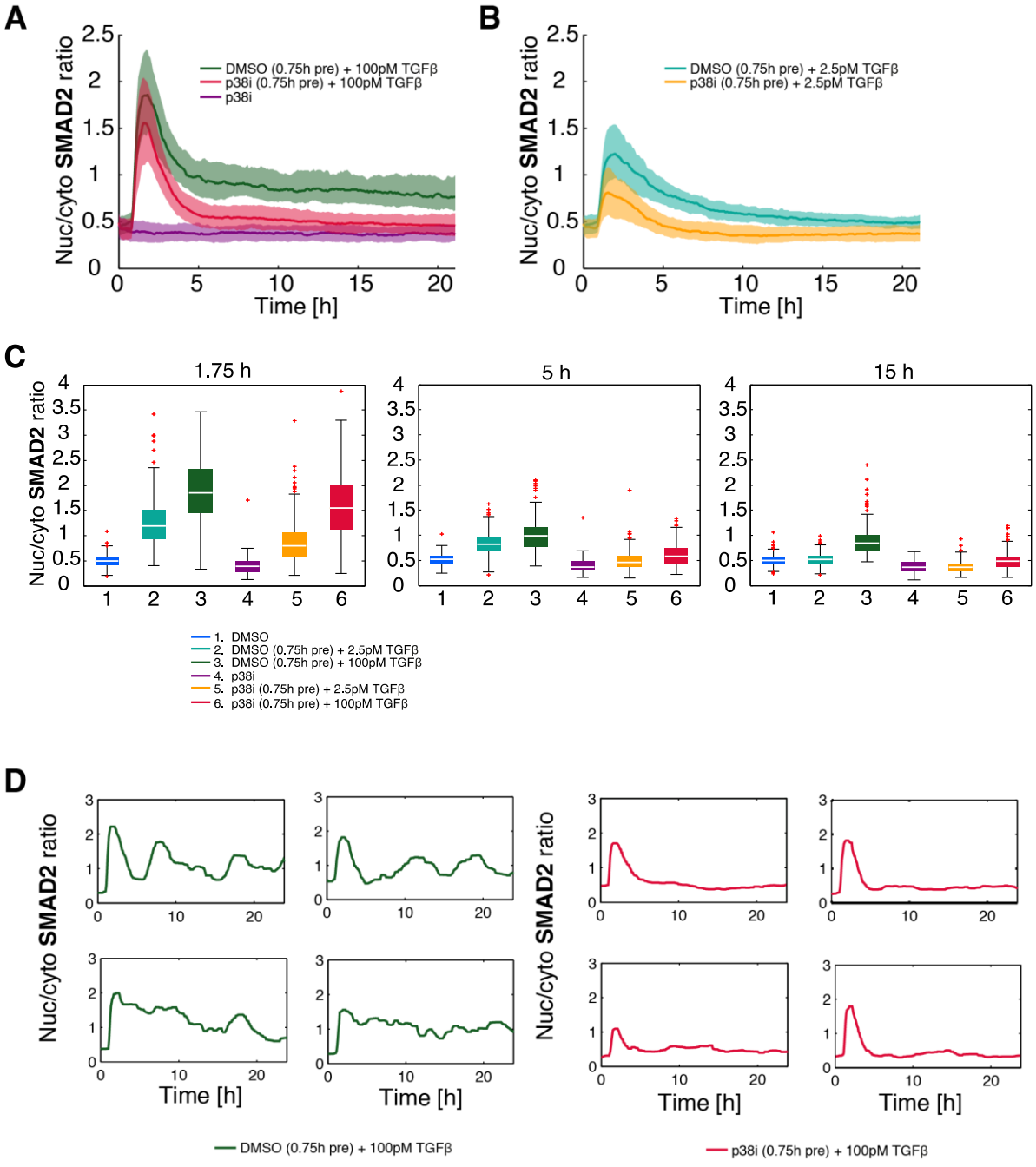

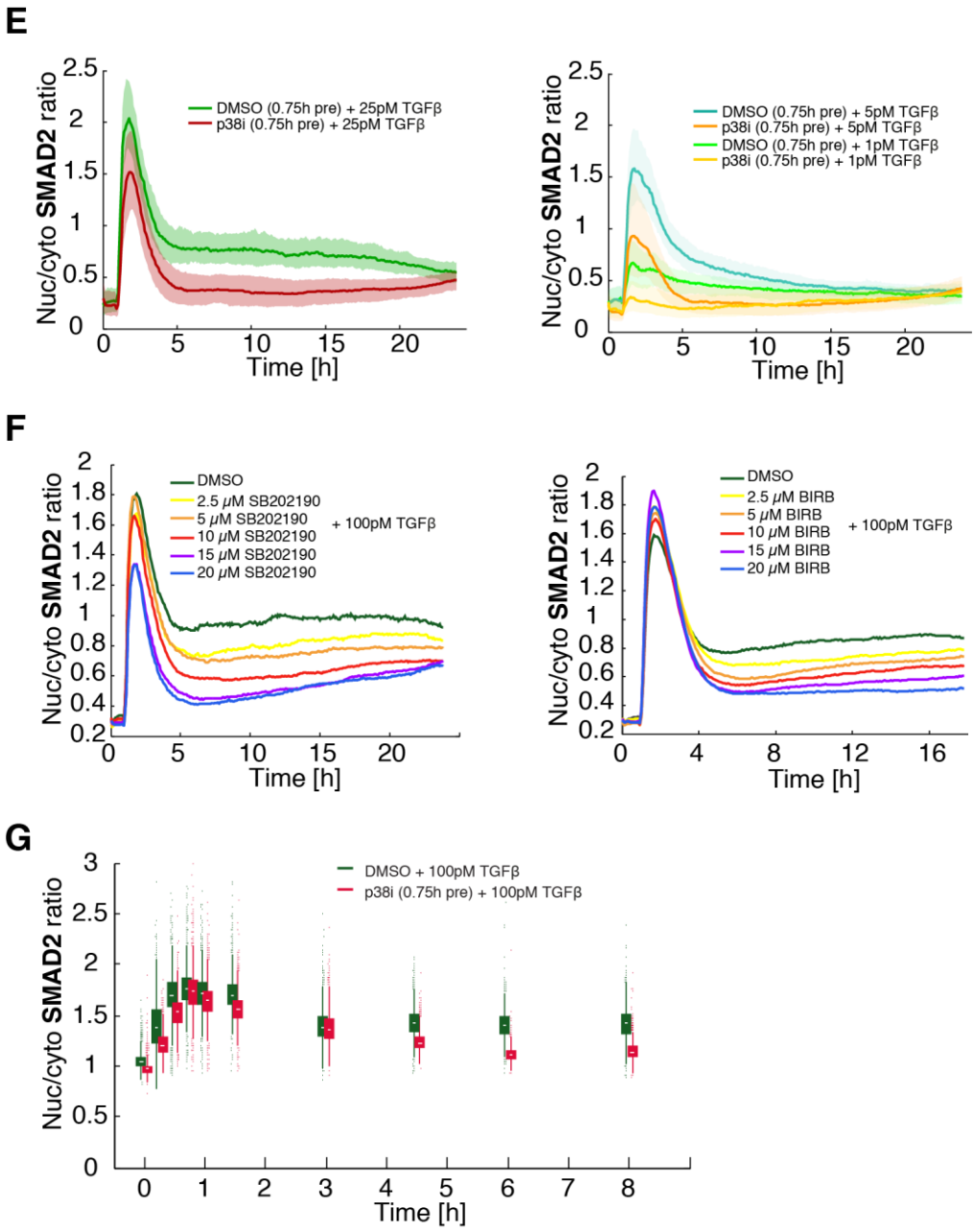
E
Nuc/cyto SMAD2 ratio
Time [h]
DMSO (0.75h pre) + 25pM TGFβ
p38i (0.75h pre) + 25pM TGFβ
DMSO (0.75h pre) + 5pM TGFβ
p38i (0.75h pre) + 5pM TGFβ
DMSO (0.75h pre) + 1pM TGFβ
p38i (0.75h pre) + 1pM TGFβ
F
DMSO
2.5 μM SB202190
5 μM SB202190
10 μM SB202190
15 μM SB202190
20 μM SB202190
+ 100pM TGFβ
DMSO
2.5 μM BIRB
5 μM BIRB
10 μM BIRB
15 μM BIRB
20 μM BIRB
+ 100pM TGFβ
G
DMSO + 100pM TGFβ
p38i (0.75h pre) + 100pM TGFβ

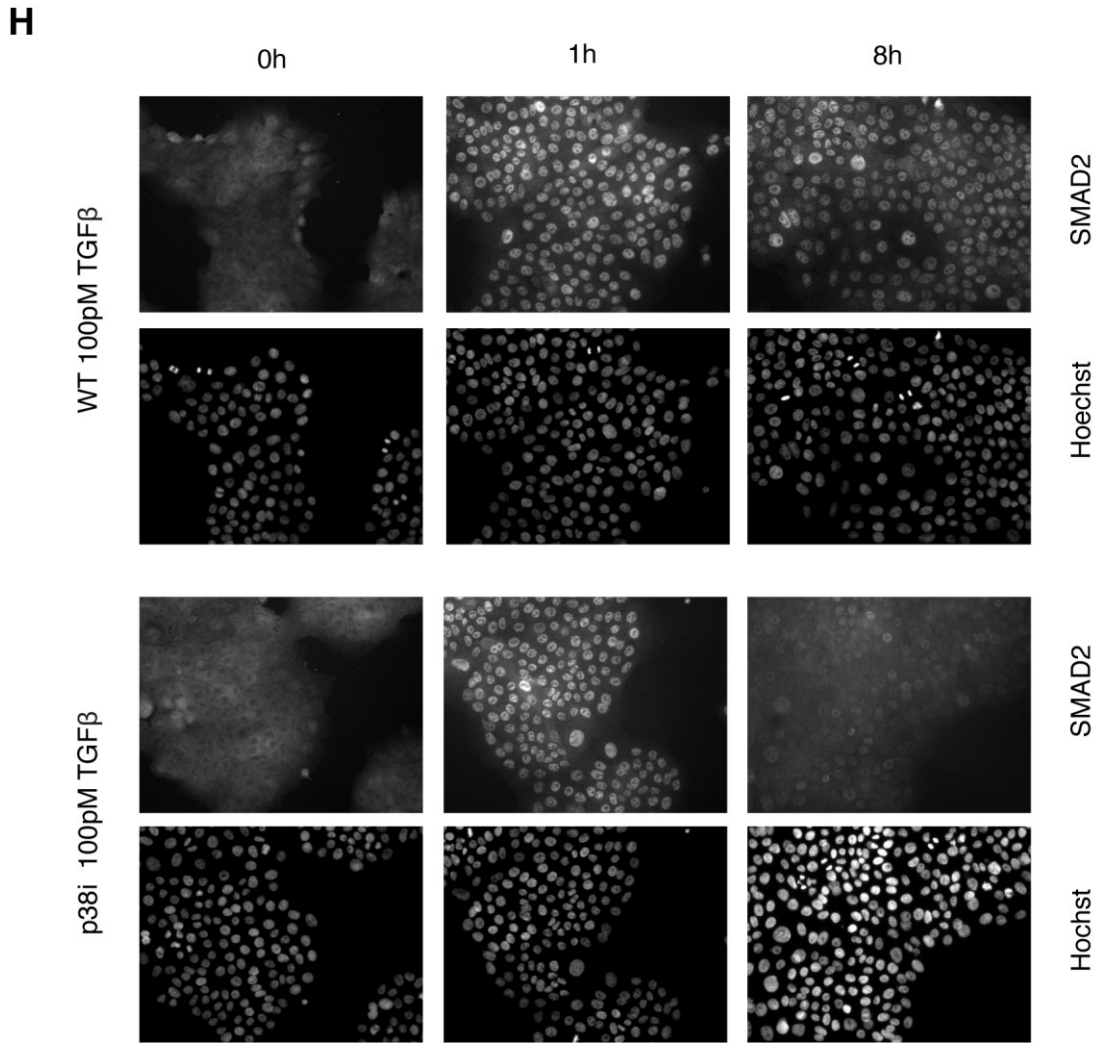

3.4.2.1 Figure 30. Inhibition of p38 modulates the dynamics and localization of SMADs.
A Median nuc/cyto SMAD2 ratio of the SMAD2-YFP reporter cells stimulated with 100pM TGFβ and 0.75h pretreated with p38 inhibitors (SB202190 & BIRB796). DMSO and only p38 inhibitors were used as controls. Shaded area represent data between 25th and 75th percentiles.
B Median nuc/cyto SMAD2 ratio of the SMAD2-YFP reporter cells stimulated with 2.5pM TGFβ and 0.75h pretreated with p38 inhibitors. Shaded area represent data between 25th and 75th percentiles.
C Nuc/cyto SMAD2 ratio of the SMAD2 reporter cells stimulated with 2.5 or 100pM TGFβ and 0.75h pretreated with p38 inhibitors at time points 1.75, 5 and 15h. White lines indicate median; boxes include data between the 25th and 75th percentiles; whiskers extend to maximum values within 1.5× the interquartile range; crosses represent outliers.
D Exemplary individual nuc/cyto SMAD2 trajectories for the SMAD2-YFP reporter cells stimulated with 100pM TGFβ (green lines) and additionally 0.75h pretreated with p38 inhibitors (red lines).
E Median nuc/cyto SMAD2 ratio of the SMAD2-YFP reporter cells stimulated with 1, 5 or 25pM TGFβ and 0.75h pretreated with p38 inhibitors. Shaded area represent data between 25th and 75th percentiles.
F Median nuc/cyto SMAD2 ratio of the SMAD2-YFP reporter cells stimulated with 100pM TGFβ and treated with SB202190 or BIRB796 at indicated concentrations. DMSO was used for the control.
G Nuc/cyto SMAD2 ratio was measured in MCF10A WT cells stimulated with 100pM TGFβ and 0.75h pretreated with p38 inhibitors by immunofluorescence at indicated time points. White lines indicate median; boxes include data between the 25th and 75th percentiles; whiskers extend to maximum values within 1.5× the interquartile range; crosses represent outliers.
H Exemplary pictures of SMAD2 fluorescence intensities in MCF10A WT cells stimulated with 100pM TGFβ and 0.75h pretreated with p38 inhibitors by immunofluorescence at 1 and 8h. Nuclear staining was carried out with Hoechst 33342.

3.4.2.2 p38 inhibition causes specific termination of the late response

In order to investigate whether the late response is specifically suppressed by the p38 inhibitors or whether the effect of the inhibitors is just delayed, I added them either 45min before, at the same time or one-hour post TGFβ stimulation. As expected, the late response was gone. More interesting adding the inhibitors 6 hours after TGFβ treatment terminated further activation fast **(Figure 31A)**. Therefore, the late response is p38 kinase activity dependent. In order to examine the signaling termination more precisely, TGFβ receptors were inhibited in parallel in a further experiment. Obviously, termination with p38 inhibitors was slightly slower and not as strong as with TGFβ receptor inhibitors, as illustrated by the ratio values for 7, 8 and 15 hours **(Figure 31B and C)**. Furthermore, I was able to observe the same effect for SMAD4 when I added the p38 inhibitors and the TGFβ receptor inhibitor 6 hours after 100pM TGFβ stimulation **(Figure 31D and E)**.

Figure 31

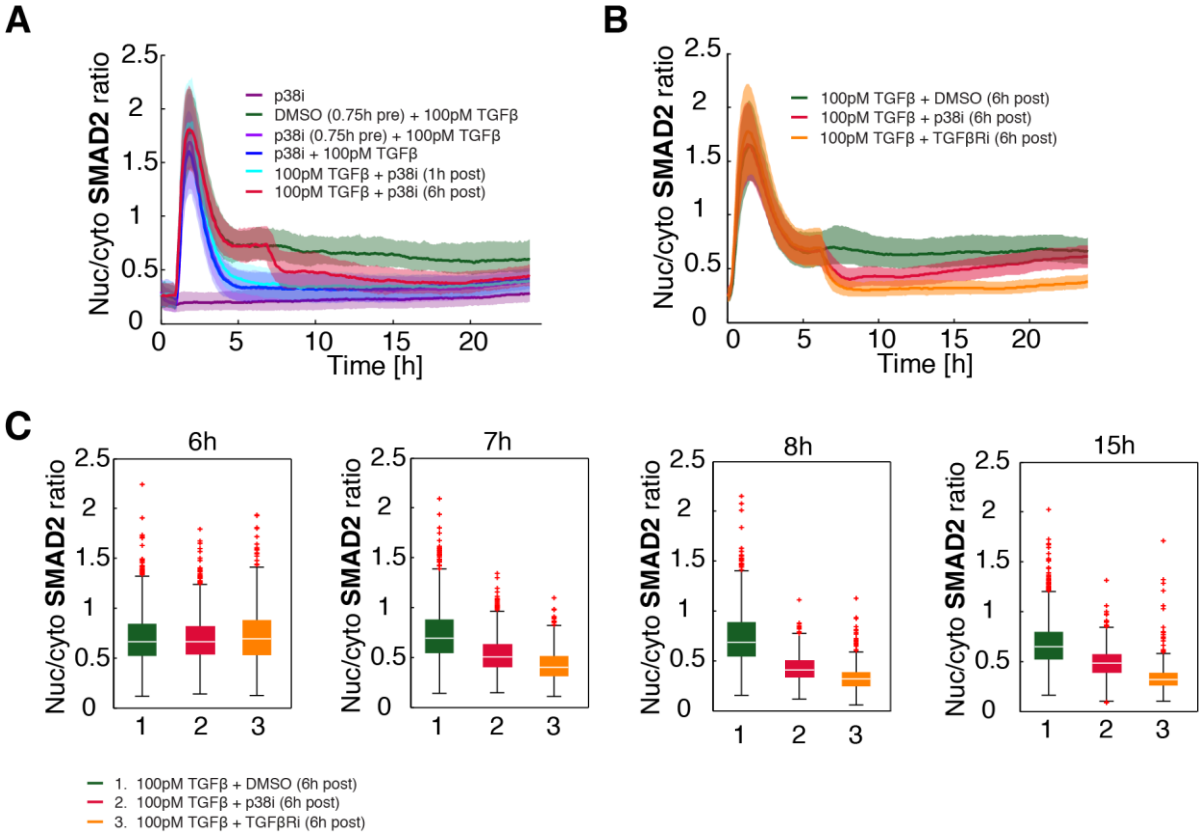

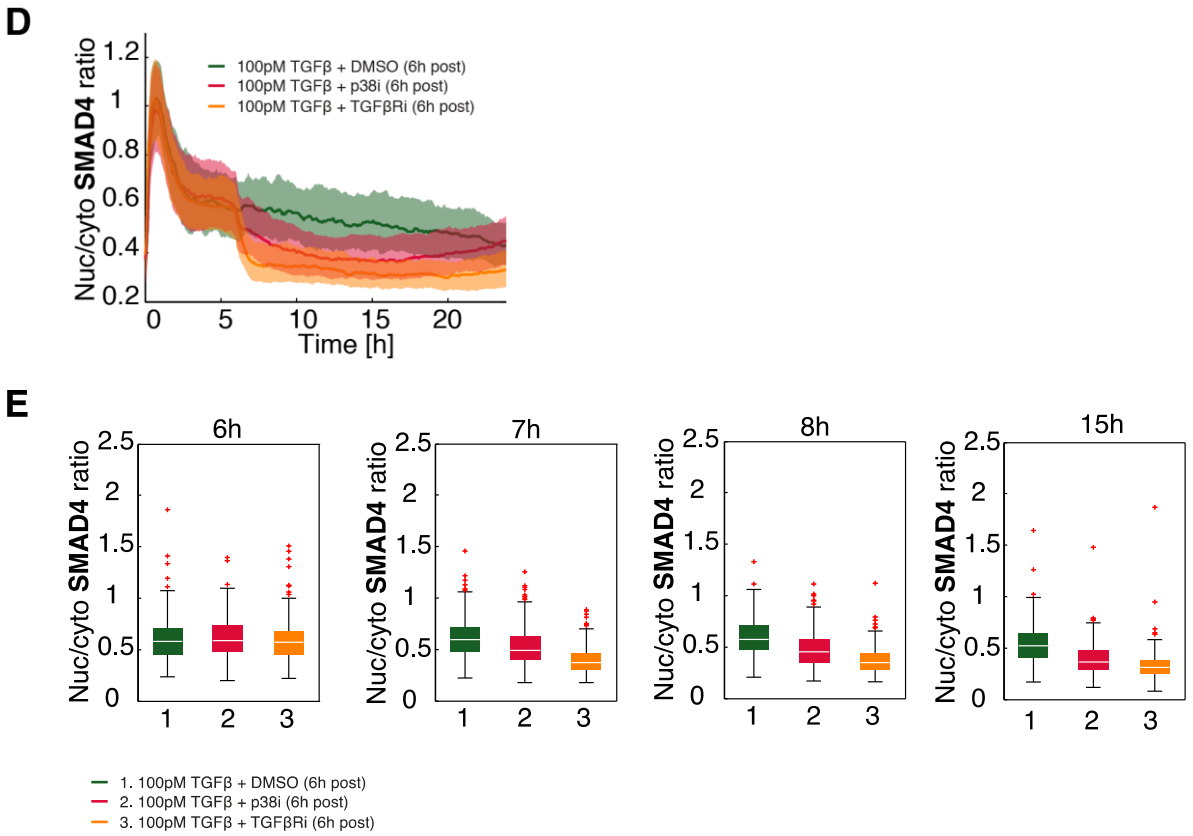

3.4.2.2 Figure 31. p38 inhibition causes specific termination of the late response.
A Median nuc/cyto SMAD2 ratio of the SMAD2-YFP reporter cells stimulated with 100pM TGFβ and p38 inhibitors (SB202190 & BIRB796) at indicated time points. Shaded area represent data between 25th and 75th percentiles.
B Median nuc/cyto SMAD2 ratio of the SMAD2-YFP reporter cells stimulated with 100pM TGFβ and 6h post p38 inhibitors or TGF-β RI Kinase inhibitor VI SB431542 (TGFβRi). Shaded area represent data between 25th and 75th percentiles.
C Nuc/cyto SMAD2 ratio of the SMAD2 reporter cells stimulated with 100pM TGFβ and 6h post p38 inhibitors or TGF-β RI Kinase inhibitor VI SB431542 (TGFβRi) at time points 6, 7, 8 and 15h. White lines indicate median; boxes include data between the 25th and 75th percentiles; whiskers extend to maximum values within 1.5× the interquartile range; crosses represent outliers.
D Median nuc/cyto SMAD4 ratio of the SMAD4-YFP reporter cells stimulated with 100pM TGFβ and 6h post p38 inhibitors or TGF-β RI Kinase inhibitor VI SB431542 (TGFβRi). Shaded area represent data between 25th and 75th percentiles.
E Nuc/cyto SMAD4 ratio of the SMAD4 reporter cells stimulated with 100pM TGFβ and 6h post p38 inhibitors or TGF-β RI Kinase inhibitor VI SB431542 (TGFβRi) at time points 6, 7, 8 and 15h. White lines indicate median; boxes include data between the 25th and 75th percentiles; whiskers extend to maximum values within 1.5× the interquartile range; crosses represent outliers.

3.4.2.3 p38 inhibition results in less phosphorylation of SMAD2 and SMAD3

As a next step to decrypt the underlying mechanisms, I have done Western experiments. First, I tested the p38 inhibitors for their effectiveness by determining the phosphorylation status of HSP27, a target gene of p38 (Freshney *et al,* 1994; Cuenda *et al,* 1995). Inhibition of kinase activity 6 hours after TGFβ stimulation resulted in a strong reduction of phosphorylation of HSP27 0.5h post and hardly detectable amounts of pHSP27 one hour after inhibition, which indicated that inhibition was successful **(Figure 32)**. Furthermore, after inhibition SMAD2 was less phosphorylated while total SMAD2 level remained unchanged. Interestingly, SMAD3 was also less phosphorylated, whereas total SMAD3 was unchanged.

Figure 32

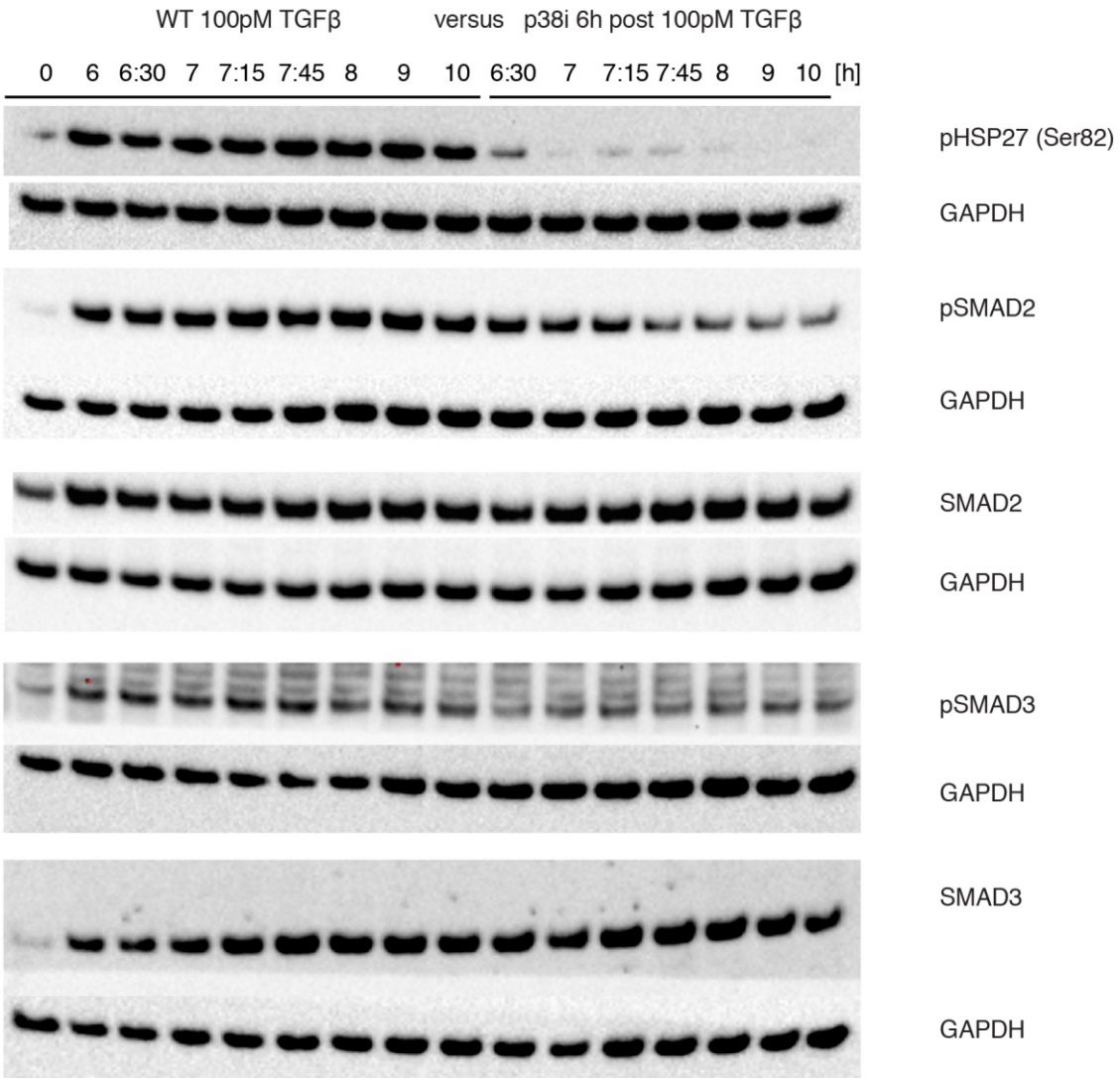

3.4.2.3 Figure 32. p38 inhibition results in less phosphorylation of SMAD2 and SMAD3.
Western blot analysis of phosphorylated HSP27 (Ser82), phosphorylated SMAD2, total SMAD2, phosphorylated SMAD3 and total SMAD3 in MCF10A WT cells stimulated with 100pM TGFβ and 6h post p38 inhibitors (SB202190 & BIRB796). GAPDH was used as loading controls.

3.4.2.4 Dependency of SMAD target genes and cell fate on p38 kinase activity

Consequentially I was interested in the impact of this dynamic remodeling on gene expression and cell fate. Therefore, I performed some RT-PCRs after inhibiting the kinase activity of p38 **(Figure 33A)**. First, the SMAD2 expression remained more or less constant and unchanged by the inhibition. The negative feedback loops SnoN and SMAD7 were somewhat less expressed, while TIEG (TGF-beta inducible early gene) and SARA (SMAD anchor for receptor activation) remained unchanged. In addition, p21, which plays a role in proliferation and cell cycle arrest, was unaltered by p38 inhibition. But very exciting, Snail, a key regulator of TGF-β-induced epithelial-mesenchymal transition (EMT) (Naber *et al*, 2013), was clearly less expressed at later time points. Based on these observations, I measured the movement

of cells over 20 hours as covered distance in pixels. Cells treated with the inhibitors 0.75h before 100pM TGFβ stimulation moved significantly slower and thus probably EMT was decreased **(Figure 33B)**. Therefore, p38 kinase activity is responsible for the second response of SMAD2 and SMAD4 and necessary probably for EMT.

Figure 33

A

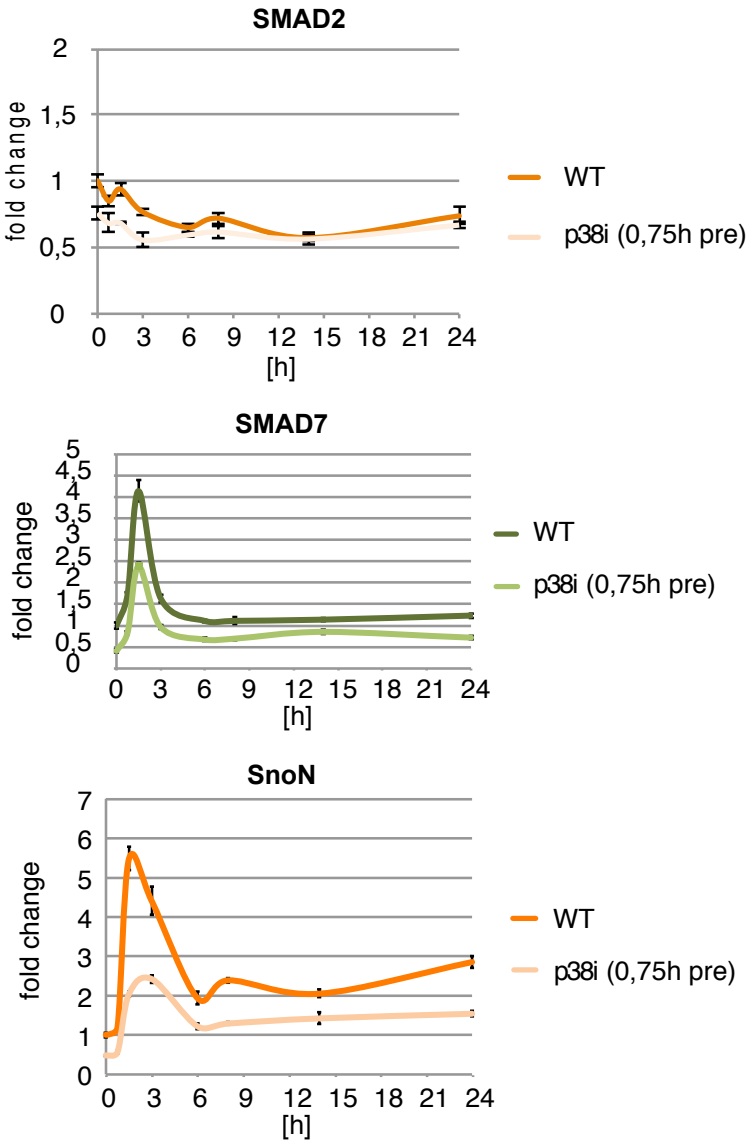

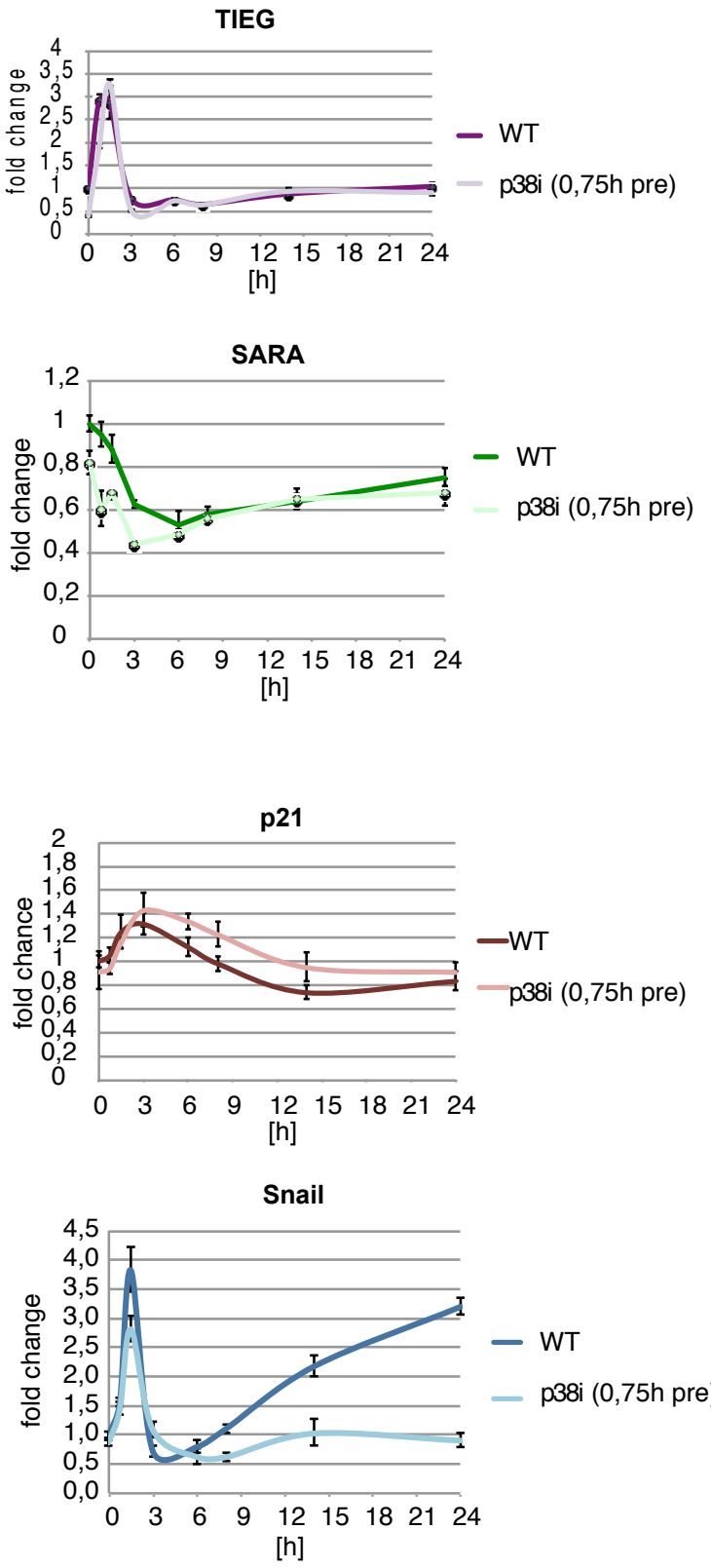
TIEG
fold change
4
3,5
3
2,5
2
1,5
1
0,5
0
0 3 6 9 12 15 18 21 24
[h]
WT
p38i (0,75h pre)
SARA
fold change
1,2
1
0,8
0,6
0,4
0,2
0
0 3 6 9 12 15 18 21 24
[h]
WT
p38i (0,75h pre)
p21
fold chance
2
1,8
1,6
1,4
1,2
1
0,8
0,6
0,4
0,2
0
0 3 6 9 12 15 18 21 24
[h]
WT
p38i (0,75h pre)
Snail
fold change
4,5
4,0
3,5
3,0
2,5
2,0
1,5
1,0
0,5
0,0
0 3 6 9 12 15 18 21 24
[h]
WT
p38i (0,75h pre)

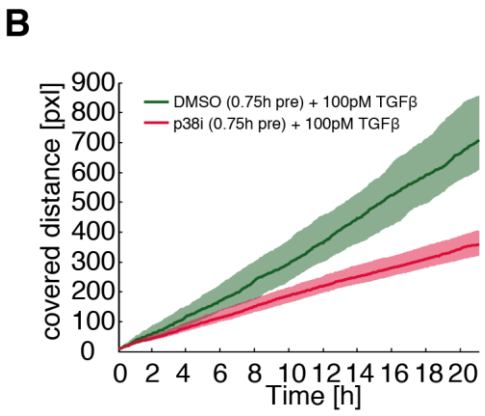

3.4.2.4 Figure 33. Dependency of SMAD target genes and cell fate on p38 kinase activity.
A Expression of TGFβ target genes in MCF10A WT cells stimulated with 100pM TGFβ and 0.75h pretreated with p38 inhibitors (SB202190 & BIRB796). β-Actin was used as an internal control. Error bars indicate standard deviation of technical triplicates.
B Motility of each cell as summed distance in pixel (pxl) covered 21h after stimulation with 100pM TGFβ and 0.75h pretreated with p38 inhibitors. Median indicated as a thick line and shaded area represent data between 25th and 75th percentiles.

3.4.2.5 SMAD2 and SMAD4 dynamics are differentially affected by TAK1 inhibition

Next, I was interested in the upstream components of p38 that influence the dynamics and localization of SMADs. As mentioned above, TGFβ receptors activate TAK1 (Transforming growth factor-β activated kinase-1), which in turn activates MKKs and p38. Therefore, I used the inhibitor (5Z)-7-Oxozeaenol, that inhibits both the kinase and the ATPase activity of TAK1 (Wu *et al*, 2013) and investigated how dynamics of SMAD2 and SMAD4 change.

3.4.2.5.1 TAK1 Inhibition modulates the dynamics and localization of SMADs

First, I investigated how SMAD2 dynamics depend on different inhibitor concentrations in time-lapse microscopy experiments. With increasing (5Z)-7-Oxozeaenol concentration 0.75h before 100pM TGFβ stimulation, I observed decreased SMAD2 translocation **(Figure 34A).** Especially the ratio values at 1.75h compared to the control amplitude were reduced **(Figure 34B).** At later time points there was low SMAD2 activation probably due to degradation of the TAK1 inhibitor. At 4 µM TAK1 inhibitor concentration almost no SMAD2 translocation was observed, which can be seen particularly in the heat maps **(Appendix Figure A23)**. For all further experiments 2 µM TAK1 inhibitor was used, in accordance with concentrations used in the literature. In the next experiment, it's obvious that (5Z)-7-Oxozeaenol alone led to no translocation of SMAD2 **(Figure 34C).** That the first response disappeared with TAK1 inhibition and 100pM TGFβ stimulation was also reflected in the nuclear and cytoplasmic values **(Figure 34C and D)**. This also applied to cells, which have been inhibited and stimulated with smaller TGFβ concentrations as shown in **Figure 34D and E** for 2.5pM TGFβ. In order to validate the time-lapse experiments, immunofluorescence experiments were carried out by inhibiting TAK1 in wild type cells 0.75h pre 100pM TGFβ stimulation with (5Z)-7-Oxozeaenol. Measurement of the total

SMAD2 nuc/ cyto ratio confirmed the results of time-lapse microscopy, as seen in **Figure 34F**. The first response of SMAD2 activation disappeared, as shown for one hour and 3 hours post 100pM TGFβ stimulation for TAK1 inhibited compared to non-inhibited cells **(Appendix Figure A24)**. The blockade of SMAD2 activation decreased at later time points, since presumably the effectiveness of the inhibitor decreased. Therefor as a conclusion TAK1 activity seems essential for SMAD2 signaling.

Interestingly, it was quite different for SMAD4 when investigating the dynamics in time-lapse experiments with different (5Z) -7-Oxozeaenol concentrations 0.75h pre 100pM TGFβ. In comparison to the control, DMSO and 100pM TGFβ, SMAD4 accumulated strongly from the cytoplasm into the nucleus with increasing TAK1 inhibitor concentration **(Figure 34G)**. However, after the increased amplitude an adaptation took place and SMAD4 signaling was normal at later time points, since presumably the inhibitor concentration was no longer sufficient. The fact that the SMAD4 response has been enormously increased is particularly evident in the heat maps **(Appendix Figure A25)**. However, dynamics for low TAK1 inhibitor concentrations, 0.1 and 0.25 µM, did not show this effect and are presumably below a threshold. As for SMAD2, 2 µM TAK inhibitor was used for all further experiments. In **Figure 34H**, single cell trajectories are shown, in which one can recognize as well as in the median that at approx. 8 hours there was another peak of SMAD4 translocation. This was coupled to the slight SMAD2 activity at this time point. Unexpectedly, (5Z)-7-Oxozeaenol alone (without TGFβ) led to a strong translocation of SMAD4, as shown in comparison to the control (DMSO and 100pM TGFβ) and for single cell trajectories **(Figure 34I and M).** The enhanced SMAD4 response can also be observed in cells which have been inhibited and treated with smaller TGFβ concentrations, as shown in **Appendix Figure A26** for 2.5pM TGFβ. And surprisingly adding (5Z) -7-Oxozeaenol 6 hours post 100pM TGFβ stimulation resulted in an immediate import of SMAD4 with a larger amplitude (around 11 hours) than the first TGFβ response **(Figure 34K, Appendix Figure A27 and A28).** The increased SMAD4 response was almost adapted to normal value after 15 hours **(Appendix Figure A28)**. In conclusion TAK1 inhibition enhances SMAD4 signaling independent of SMAD2 and TGFβ.

Figure 34

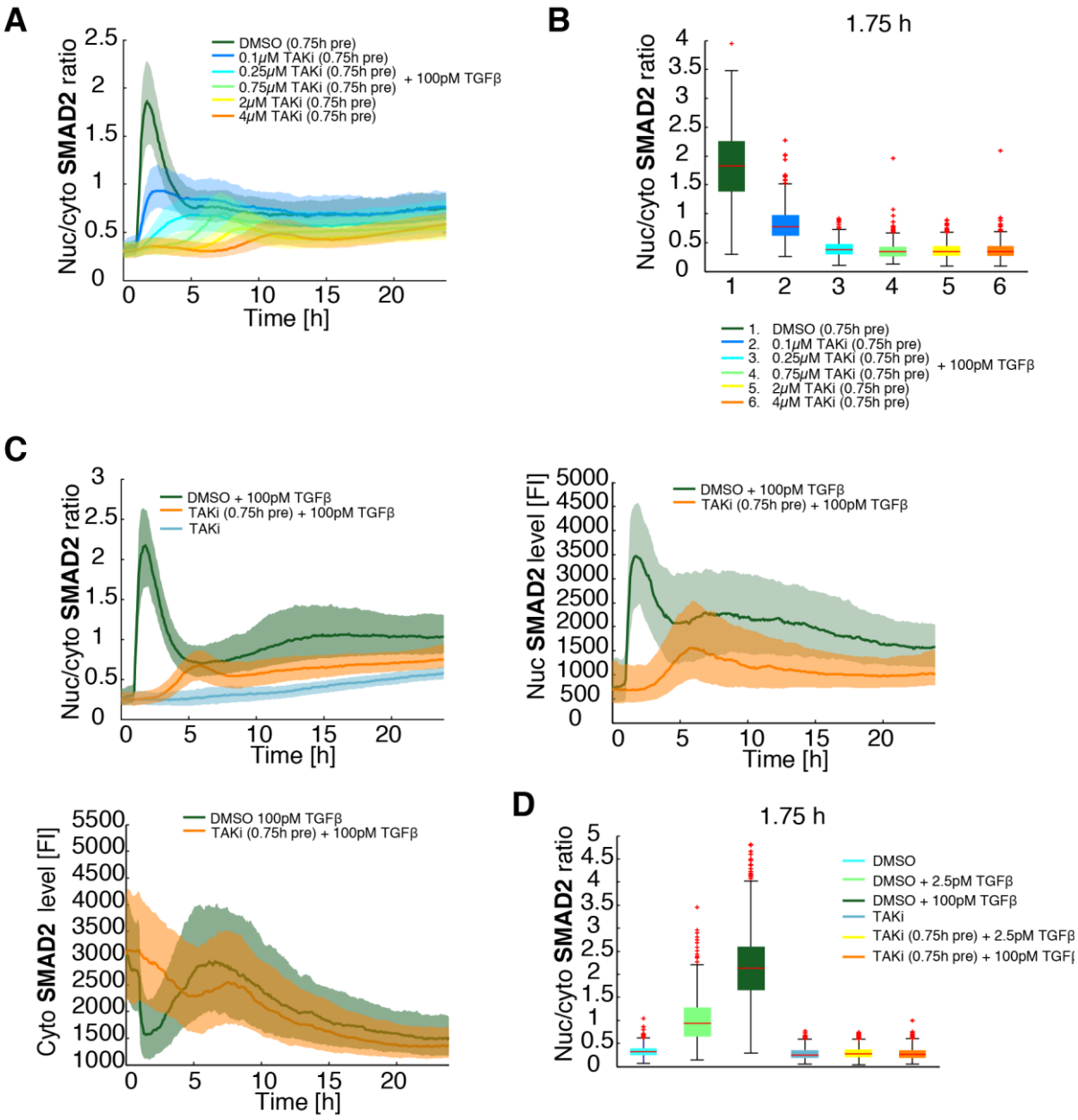
A
Nuc/cyto SMAD2 ratio
DMSO (0.75h pre)
0.1μM TAKi (0.75h pre)
0.25μM TAKi (0.75h pre)
0.75μM TAKi (0.75h pre)
2μM TAKi (0.75h pre)
4μM TAKi (0.75h pre)
+ 100pM TGFβ
Time [h]
B
1.75 h
Nuc/cyto SMAD2 ratio
1. DMSO (0.75h pre)
2. 0.1μM TAKi (0.75h pre)
3. 0.25μM TAKi (0.75h pre)
4. 0.75μM TAKi (0.75h pre)
5. 2μM TAKi (0.75h pre)
6. 4μM TAKi (0.75h pre)
+ 100pM TGFβ
C
Nuc/cyto SMAD2 ratio
DMSO + 100pM TGFβ
TAKi (0.75h pre) + 100pM TGFβ
TAKi
Time [h]
Nuc SMAD2 level [FI]
DMSO + 100pM TGFβ
TAKi (0.75h pre) + 100pM TGFβ
Time [h]
Cyto SMAD2 level [FI]
DMSO 100pM TGFβ
TAKi (0.75h pre) + 100pM TGFβ
Time [h]
D
1.75 h
Nuc/cyto SMAD2 ratio
DMSO
DMSO + 2.5pM TGFβ
DMSO + 100pM TGFβ
TAKi
TAKi (0.75h pre) + 2.5pM TGFβ
TAKi (0.75h pre) + 100pM TGF

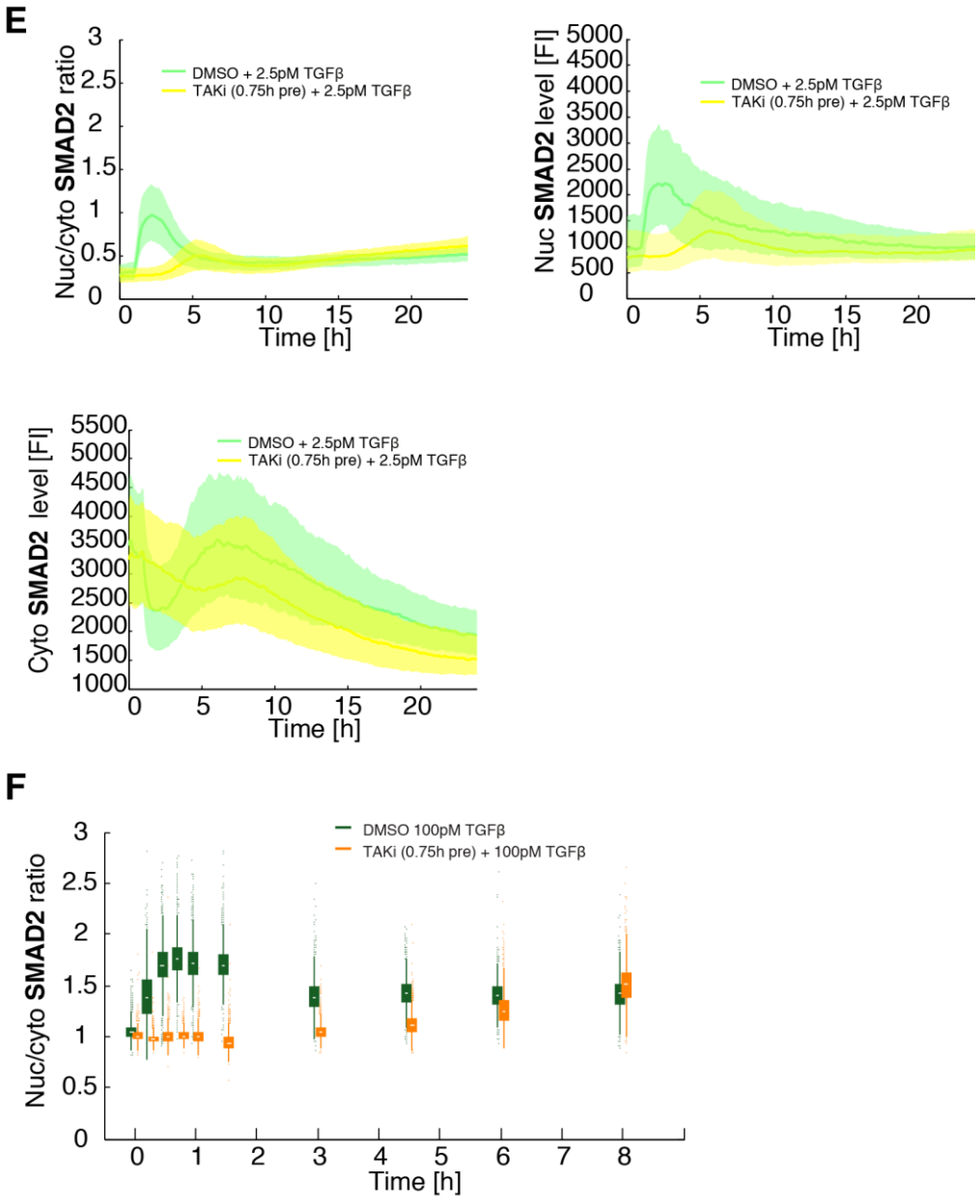
E
Nuc/cyto SMAD2 ratio
DMSO + 2.5pM TGFβ
TAKi (0.75h pre) + 2.5pM TGFβ
Time [h]
Nuc SMAD2 level [FI]
Cyto SMAD2 level [FI]
F
DMSO 100pM TGFβ
TAKi (0.75h pre) + 100pM TGFβ

G

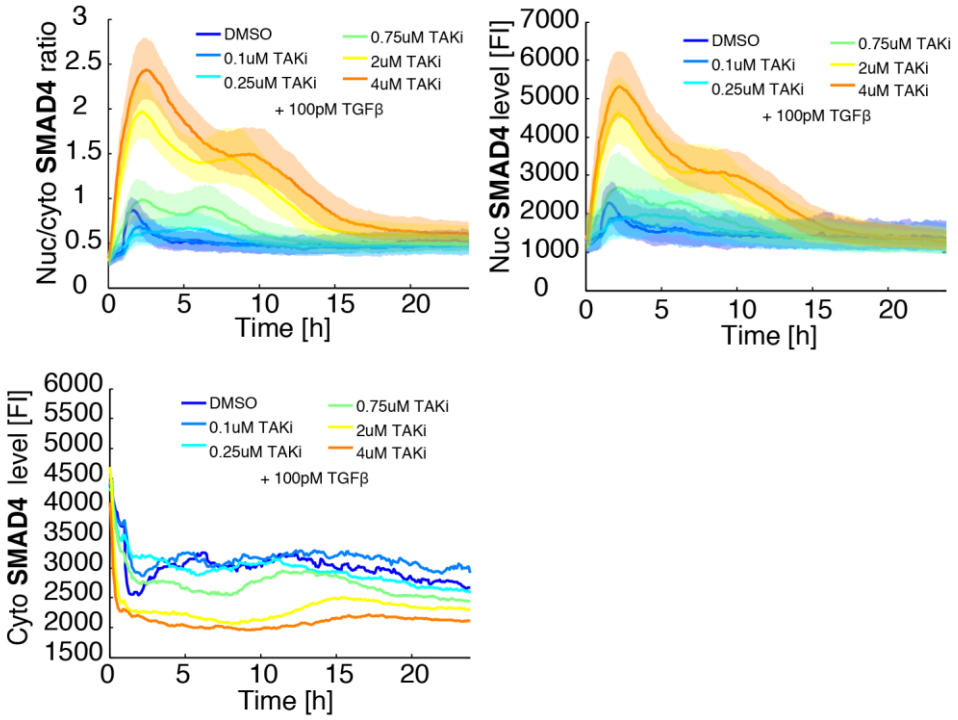
Nuc/cyto SMAD4 ratio
Time [h]
DMSO
0.1uM TAKi
0.25uM TAKi
0.75uM TAKi
2uM TAKi
4uM TAKi
+ 100pM TGFβ
Nuc SMAD4 level [FI]
Time [h]
DMSO
0.1uM TAKi
0.25uM TAKi
0.75uM TAKi
2uM TAKi
4uM TAKi
+ 100pM TGFβ
Cyto SMAD4 level [FI]
Time [h]
DMSO
0.1uM TAKi
0.25uM TAKi
0.75uM TAKi
2uM TAKi
4uM TAKi
+ 100pM TGFβ

H

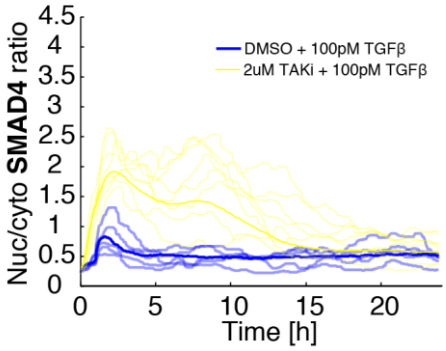
Nuc/cyto SMAD4 ratio
Time [h]
DMSO + 100pM TGFβ
2uM TAKi + 100pM TGFβ

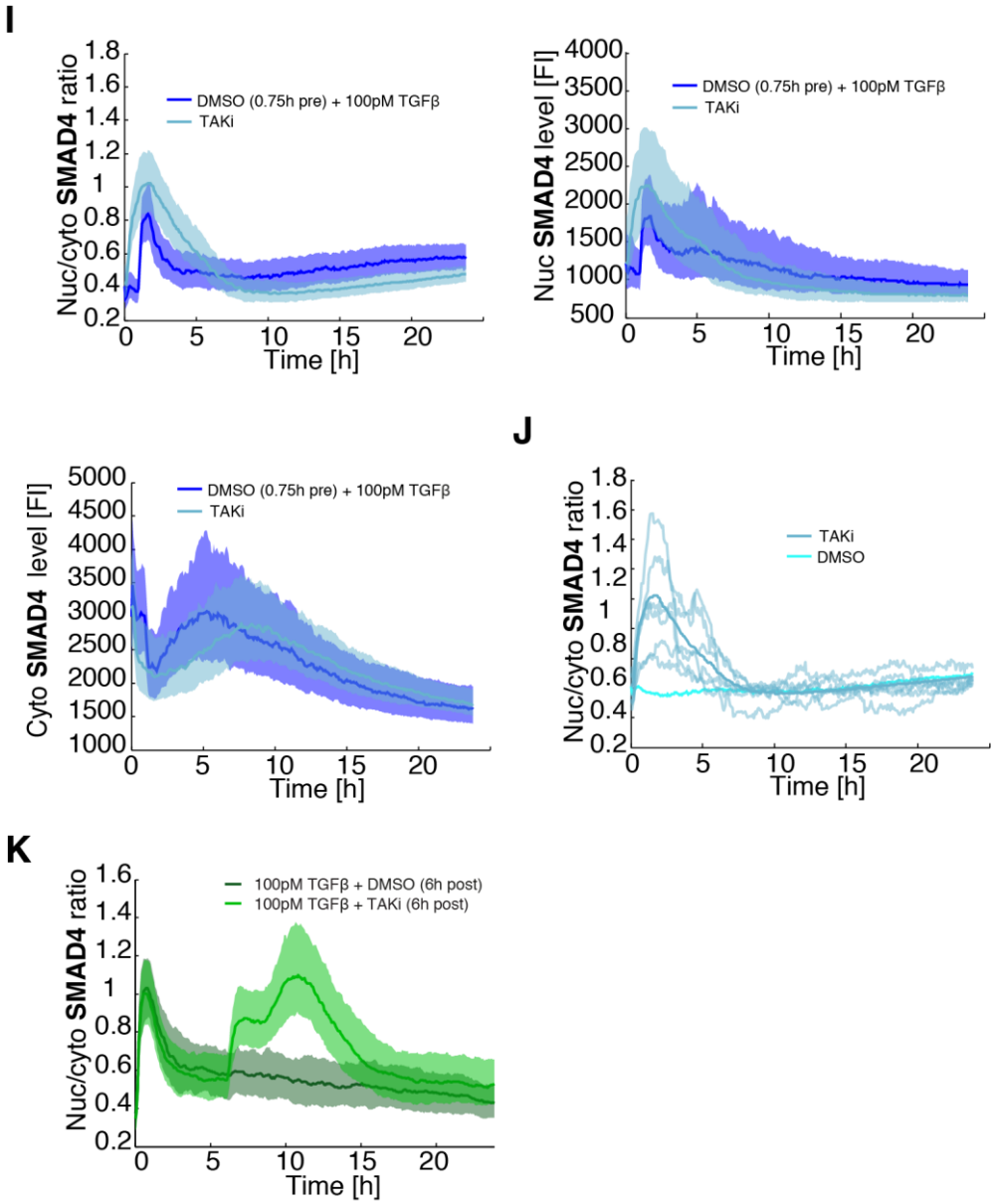

3.4.2.5.1 Figure 34. TAK1 Inhibition modulates the dynamics and localization of SMADs.
A Median nuc/cyto SMAD2 ratio of the SMAD2-YFP reporter cells stimulated with 100pM TGFβ and 0.75h pretreated with 5Z-7-Oxozeaenol
(TAKi) at indicated concentrations. Shaded area represent data between 25th and 75th percentiles.
B Nuc/cyto SMAD2 ratio of the SMAD2-YFP reporter cells stimulated with 100pM TGFβ and 0.75h pretreated with 5Z-7-Oxozeaenol
(TAKi) at indicated concentrations at time point 1.75h. Red lines indicate median; boxes include data between the 25th and 75th percentiles; whiskers extend to maximum values within 1.5× the interquartile range; crosses represent outliers.
C Median nuc/cyto SMAD2 ratio, nuclear and cytoplasmic level of the SMAD2-YFP reporter cells stimulated with 100pM TGFβ and 0.75h pretreated with 5Z-7-Oxozeaenol (TAKi). DMSO and only TAKi were used as controls. Shaded area represent data between 25th and 75th percentiles.
D Nuc/cyto SMAD2 ratio of the SMAD2 reporter cells stimulated with 2.5 or 100pM TGFβ and 0.75h pretreated with 5Z-7-Oxozeaenol (TAKi) at time point 1.75h. Red lines indicate median; boxes include data between the 25th and 75th percentiles; whiskers extend to maximum values within 1.5× the interquartile range; crosses represent outliers.
E Median nuc/cyto SMAD2 ratio, nuclear and cytoplasmic level of the SMAD2-YFP reporter cells stimulated with 2.5pM TGFβ and 0.75h pretreated with 5Z-7-Oxozeaenol (TAKi). Shaded area represent data between 25th and 75th percentiles.
F Nuc/cyto SMAD2 ratio was measured in MCF10A WT cells stimulated with 100pM TGFβ and 0.75h pretreated with 5Z-7-Oxozeaenol (TAKi) by immunofluorescence at indicated time points. White lines indicate median; boxes include data between the 25th and 75th percentiles; whiskers extend to maximum values within 1.5× the interquartile range; crosses represent outliers.

G Median nuc/cyto SMAD4 ratio, nuclear and cytoplasmic level of the SMAD4-YFP reporter cells stimulated with 100pM TGFβ and 0.75h pretreated with 5Z-7-Oxozeaenol (TAKi) at indicated concentrations. Shaded area represent data between 25th and 75th percentiles.
H Exemplary individual nuc/cyto SMAD4 ratio trajectories (thin lines) for the SMAD4-YFP reporter cells stimulated with 100pM TGFβ and 0.75h pretreated with TAKi compared to the median nuc/cyto SMAD4 ratio of the entire population (thick line).
I Median nuc/cyto SMAD4 ratio, nuclear and cytoplasmic level of the SMAD4-YFP reporter cells stimulated with 100pM TGFβ and only 5Z-7-Oxozeaenol (TAKi). Shaded area represent data between 25th and 75th percentiles.
J Exemplary individual nuc/cyto SMAD4 ratio trajectories (thin lines) of the SMAD4-YFP reporter cells treated only with 5Z-7-Oxozeaenol (TAKi) compared to the median nuc/cyto SMAD4 ratio of the entire population (thick line). DMSO was used as a control.
K Median nuc/cyto SMAD4 ratio of the SMAD4-YFP reporter cells stimulated with 100pM TGFβ and 6h post TAKi. Shaded area represent data between 25th and 75th percentiles.

3.4.2.5.2 Underlying mechanisms of TAK1 inhibition

To further confirm the microscopy results and detect underlying mechanisms, I performed western blot analysis. As shown in **Figure 35A** the first response of SMAD2 phosphorylation disappeared when TAK1 is inhibited 0.75h pre 100pM TGFβ stimulation. Later time points showed an increase in phosphorylation of SMAD2, since presumably the effectiveness of the inhibitor decreased. Furthermore, TAK1 inhibition enhanced early accumulation of SMAD4, which is especially apparent at time point 0 without TGFβ stimulation. Since TAK1 inhibition enhanced SMAD4 signaling independent of pSMAD2 and TGFβ, it was exciting to investigate how pSMAD3 behaves. In comparison to pSMAD2 the effect was not so strong, however less SMAD3 was phosphorylated by TAK1 inhibition. Thus, the accumulation of SMAD4 is also independent of pSMAD3. To show that TAK1 acts upstream of p38, I investigated the phosphorylation status of the p38 target gene HSP27. As can be seen in **Figure 35A**, HSP27 was less phosphorylated and therefore p38 inhibition successful. Furthermore, TAK1 inhibition stabilized TGFβ receptors 1 suggesting a remodeling of the receptors so that pSMAD2 may not bind and phosphorylation is prevented.

This assumption is supported by another time-lapse movie where cells are inhibited at 6 hours post 100pM TGFβ stimulation with the TAKi inhibitor (5Z)-7-Oxozeaenol or TGFβR1 inhibitor. Inhibition of TAK1 and TGFβR1 showed the same signaling termination rates for SMAD2 translocation into the nucleus **(Figure35B)**. The same ratio values are shown for 6, 7 and 10 hours in **Figure 35C**, while the (5Z)-7-Oxozeaenol efficiency probably decreased at 15 hours.

Since SMAD4 translocated decoupled from pSMAD2, pSMAD3 and TGFβ into the nucleus, I investigated whether the BMP (Bone morphogenetic proteins) signaling pathway is involved. SMAD4 acts as a shared partner for both TGFβ- specific and BMP- specific SMADs (Zhang *et al*, 1997). Three different inhibitors were used to inhibit BMP signaling: Noggin, LDN193189 and Dorsomorphin. Dorsomorphin inhibits selectively BMP type I receptor ALK2, ALK3 and ALK6, and thus blocks BMP-mediated SMAD1, 5 and 8 phosphorylation. LDN193189 inhibits the activity of the BMP type I receptors ALK2 and ALK3 and therefor activation of SMAD1, 5 and 8 (Yu *et al*, 2008a&b). Noggin has

been shown to be a high-affinity binding protein to BMP and antagonizes BMP bio-activities (Groppe *et al*, 2002; Groppe *et al*, 2003). As shown in **Figure 35D** TAK1 inhibition enhanced SMAD4 signaling independent of BMP signaling since all three inhibitors have almost no effect on the accumulation of SMAD4 after TAK1 inhibition. In addition, inhibition of the receptors also showed no effect on the SMAD4 response after TAK1 inhibition, but the second small peak due to SMAD2 activation was prevented **(Figure35E)**.

In summary TAK1 inhibition prevents phosphorylation of SMAD2 and enhances early accumulation of SMAD4 independent of pSMAD2, pSMAD3, TGFβ and BMP signaling.

Figure 35

A

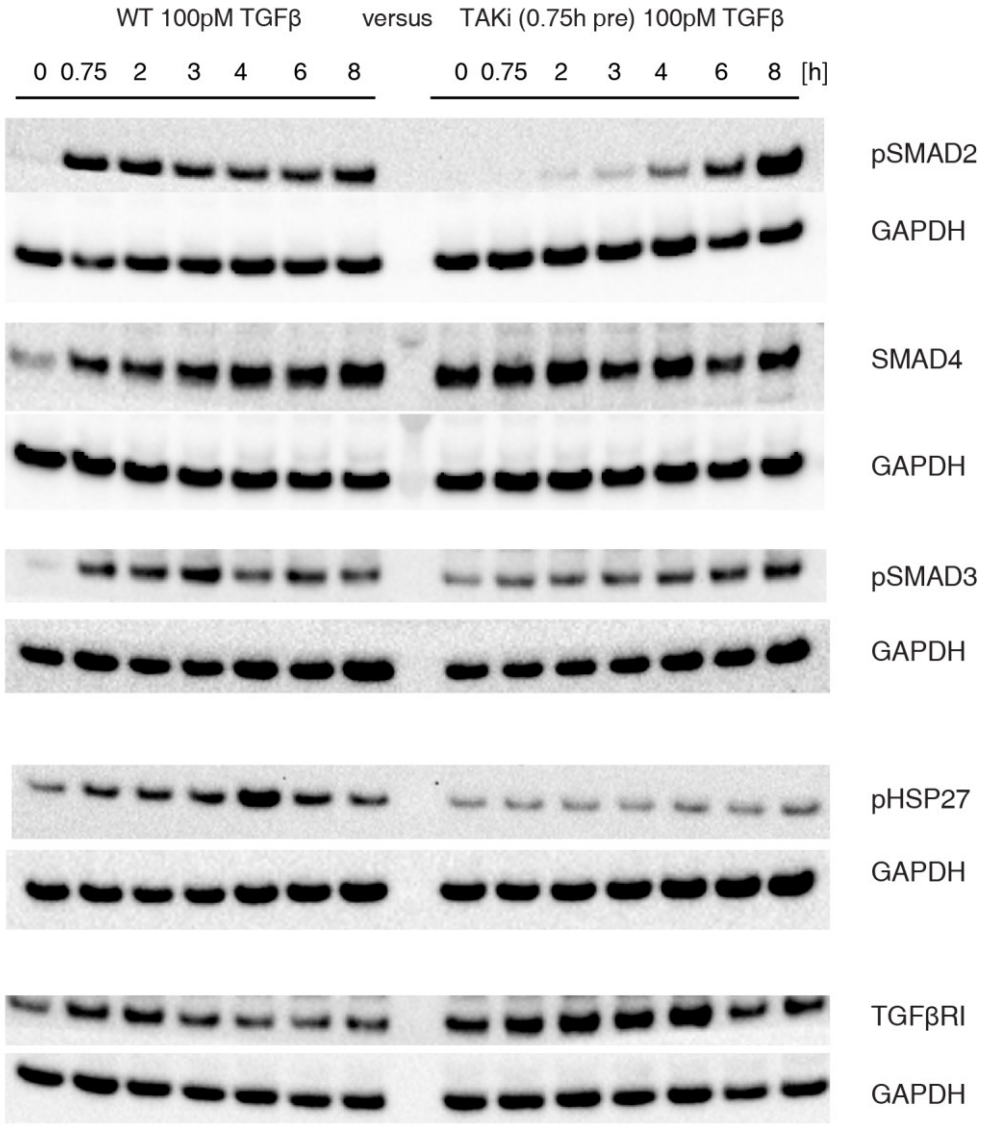

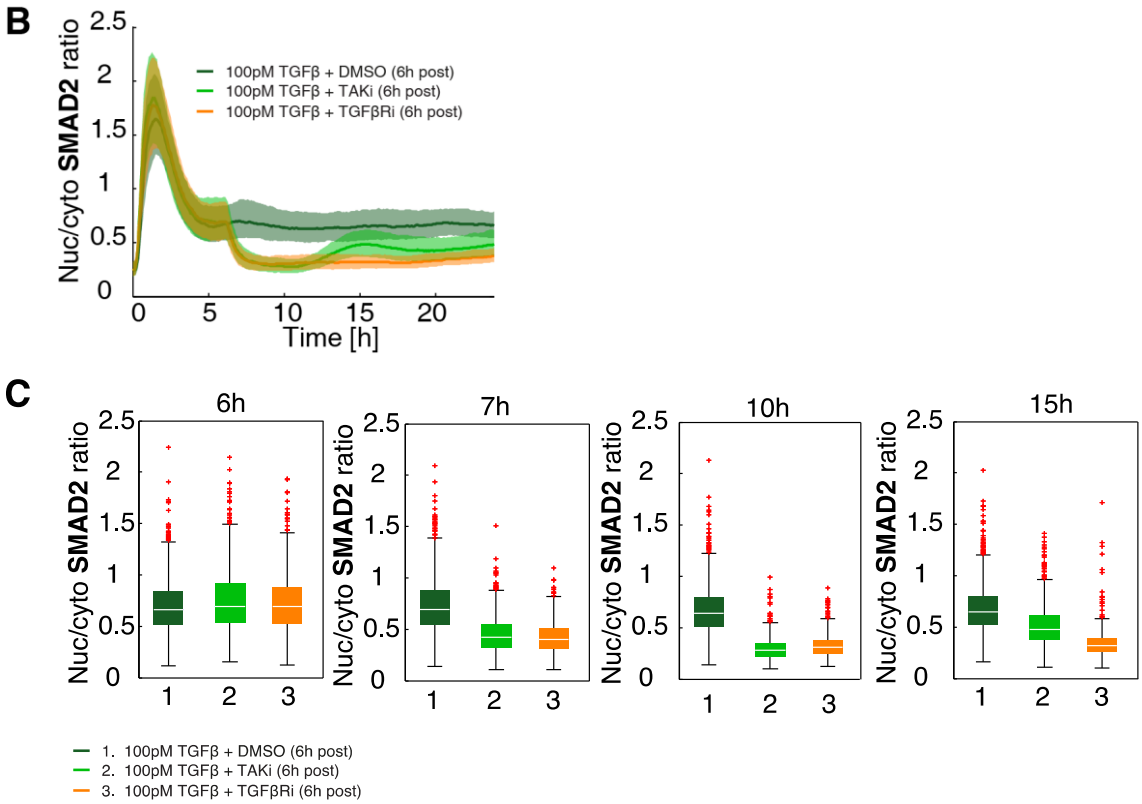
B
Nuc/cyto SMAD2 ratio
100pM TGFβ + DMSO (6h post)
100pM TGFβ + TAKi (6h post)
100pM TGFβ + TGFβRi (6h post)
Time [h]
C
6h
7h
10h
15h
Nuc/cyto SMAD2 ratio
1. 100pM TGFβ + DMSO (6h post)
2. 100pM TGFβ + TAKi (6h post)
3. 100pM TGFβ + TGFβRi (6h post)
D
DMSO 100pM TGFβ
TAKi (0.75h pre) + 100pM TGFβ
TAKi + Noggin (0.75h pre) + 100pM TGFβ
TAKi + LDN (0.75h pre) + 100pM TGFβ
TAKi + Dorsomorphin (0.75h pre) + 100pM TGFβ
Nuc/cyto SMAD2 ratio
Time [h]

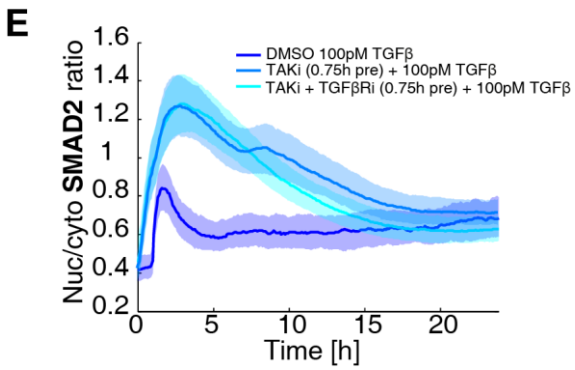

3.4.2.5.2 Figure 35. Underlying mechanisms of TAK1 inhibition.
A Western blot analysis of phosphorylated SMAD2, total SMAD4, phosphorylated SMAD3, phosphorylated HSP27 and TGFβRI in MCF10A WT cells stimulated with 100pM TGFβ and 0.75h pretreated with 5Z-7-Oxozeaenol (TAKi). GAPDH was used as loading controls.
B Median nuc/cyto SMAD2 ratio of the SMAD2-YFP reporter cells stimulated with 100pM TGFβ and 6h post TAKi or TGF-β RI Kinase inhibitor VI SB431542 (TGFβRi). Shaded area represent data between 25th and 75th percentiles.
C Nuc/cyto SMAD2 ratio of the SMAD2 reporter cells stimulated with 100pM TGFβ and 6h post TAKi or TGF-β RI Kinase inhibitor VI SB431542 (TGFβRi) at indicated time points. White lines indicate median; boxes include data between the 25th and 75th percentiles; whiskers extend to maximum values within 1.5× the interquartile range; crosses represent outliers.
D Median nuc/cyto SMAD2 ratio of the SMAD2-YFP reporter cells stimulated with 100pM TGFβ and 0.75h pretreated with BMP signaling inhibitors: Noggin, LDN193189 and Dorsomorphin. Shaded area represent data between 25th and 75th percentiles.
E Median nuc/cyto SMAD2 ratio of the SMAD2-YFP reporter cells stimulated with 100pM TGFβ and 0.75h pretreated with 5Z-7-Oxozeaenol (TAKi) and TGF-β RI Kinase inhibitor VI SB431542 (TGFβRi). Shaded area represent data between 25th and 75th percentiles.

3.4.2.5.3 Dependency of SMAD target genes on TAK1 activity

Furthermore, I was interested in the impact of this dynamic remodeling on gene expression and cell fate. Therefore, I performed RT-PCRs after inhibiting TAK1 activity and 100pM TGFβ stimulation **(Figure 36)**. First, the SMAD2 and SMAD4 expression remained more or less constant and unchanged by the inhibition. However, the strong first response of the negative feedback loops SnoN and SMAD7 were gone and at later time points there was only a slight increase. Also, TIEG showed the same behavior. Nevertheless, SARA remained unchanged. Furthermore, even for Snail and PAI1 the extreme peaks were missing, and both were less expressed at later time points. This confirms that TAK1 activity is probably needed for EMT and although the SMAD4 response is enhanced, SMAD2 accumulation is essential for the TGFβ target genes.

Figure 36

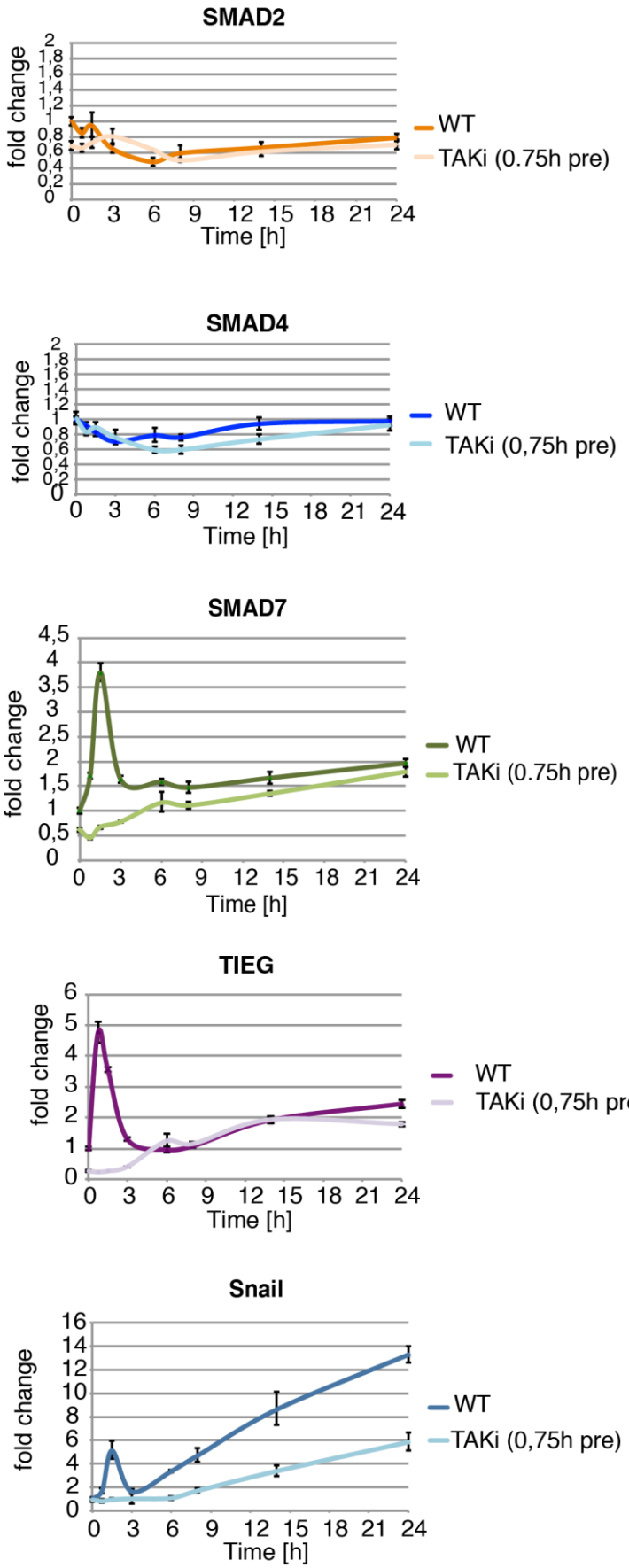
SMAD2
fold change
Time [h]
WT
TAKi (0.75h pre)
SMAD4
fold change
Time [h]
WT
TAKi (0,75h pre)
SMAD7
fold change
Time [h]
WT
TAKi (0.75h pre)
TIEG
fold change
Time [h]
WT
TAKi (0,75h pre)
Snail
fold change
Time [h]
WT
TAKi (0,75h pre)

3.4.2.5.3 Figure 36. Dependency of SMAD target genes on TAK1 activity.
Expression of TGFβ target genes in MCF10A WT cells stimulated with 100pM TGFβ and 0.75h pretreated with 5Z-7-Oxozeaenol (TAKi). β-Actin was used as an internal control. Error bars indicate standard deviation of technical triplicates.

3.4.2.6 Underlying mechanisms of p38 and SMAD cross-talk

Since TAK1-p38 pathway has an enormous impact on the dynamic remodeling of SMAD2 and SMAD4 and affects TGFβ cell fate decisions, I was curious about the underlying mechanisms of this cross-talk. I focused on the downstream effect of p38 kinase activity inhibition. There are two possible mechanisms how inhibition of p38 effects SMAD signaling. First, less SMAD2 gets phosphorylated or second more pSMAD2 gets dephosphorylated.

3.4.2.6.1 Knock down of SMAD7 does not alter the p38 effect on SMAD2

A central role of regulating SMAD2 activity plays the negative regulator SMAD7. SMAD7 interacts with p38 and it has been reported that SMAD7 is important for TGFβ-induced activation of p38 and other upstream kinases (Edlund *et al*, 2003), suggesting a potential interface between p38 and SMAD2. To determine if p38 interact with SMAD7 to regulate long-term dynamics of SMAD2, I perturbed the signaling network using p38 inhibitors in the absence or presence of SMAD7. For this purpose, I used the *SMAD7* CRISPR Cas9 knock out clone 12 (3.2.2.3) and the SMAD2-YFP Cas9 reporter cell line as a control cell line. As shown in **Figure 37A**, the effect of p38 inhibition was obvious in the SMAD2 ratio of the control cell line and in clone 12, although the response was stronger in the *SMAD7* knock down cell line as expected. Furthermore, the p38 effect was also evident at the nuclear and cellular level and hence the late response disappeared **(Figure 37B)**. In conclusion SMAD7 knock down had no Influence on the effect of p38 inhibition and therefore SMAD7 plays no or only a minor role in the mechanism.

Figure 37

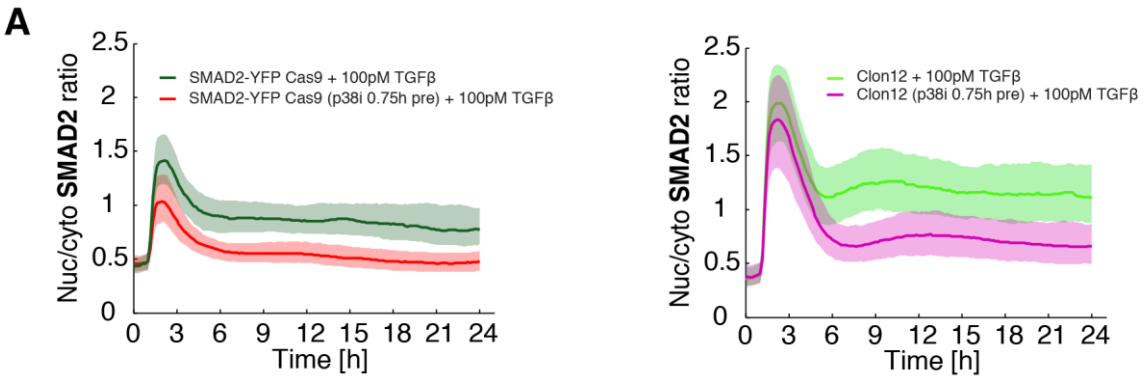

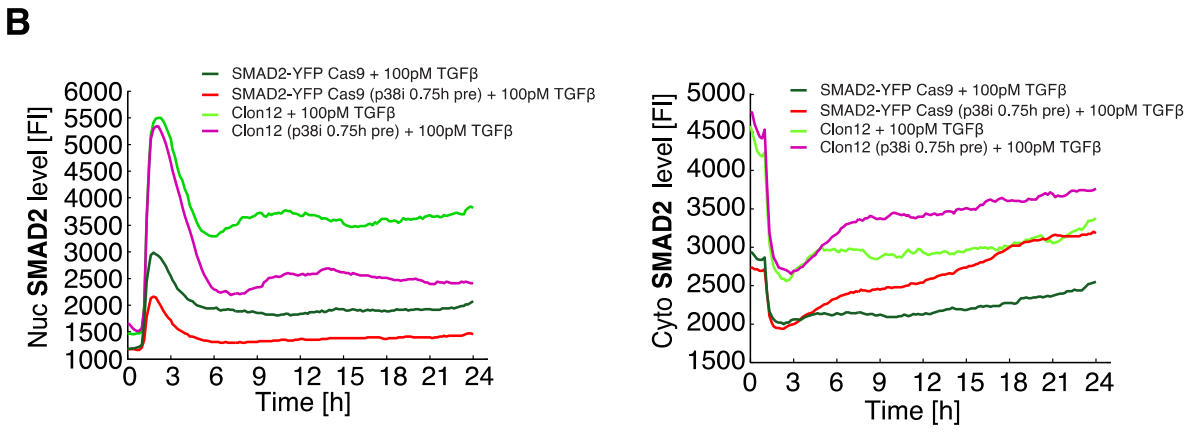

3.4.2.6.1 Figure 37. Knock down of SMAD7 does not alter the p38 effect on SMAD2.
A Median nuc/cyto SMAD2 ratio of the control SMAD2-YFP Cas9 reporter cell line and the SMAD7 CRISPR Cas9 knock out clone 12 stimulated with 100pM TGFβ and 0.75h pretreated with p38 inhibitorjls (SB202190 & BIRB796). Shaded area represent data between 25th and 75th percentiles.
B Nuclear and cytoplasmic SMAD2 level of the control SMAD2-YFP Cas9 reporter cell line and the SMAD7 CRISPR Cas9 knock out clone 12 stimulated with 100pM TGFβ and 0.75h pretreated with p38 inhibitors.

3.4.2.6.2 Inhibition of p38 does not shift receptors to degradation

As a further approach I considered that SMAD2 is less phosphorylated due to modified receptor trafficking. Receptors are either internalized into early endosomes and recycled or internalized into Caveolin-positive vesicles and subsequently degraded (3.2.4). In order to test the hypothesis that inhibition of p38 kinase activity shifts the receptor trafficking more to degradation and thus, p38 activity promotes recycling or prevent degradation, I used Nystatin. Nystatin causes disruption of the lipid raft- caveolar endocytic pathway and therefor inhibits the degradation pathway and stabilizes the receptors (Di Guglielmo *et al*, 2003). As shown in **Figure 38A** pretreatment with Nystatin and 100pM TGFβ stimulation resulted in stronger SMAD2 accumulation into the nucleus, although it was not so clearly indicated in the ratio, since more SMAD2 was also present in the cytoplasm. However, p38 inhibition and Nystatin also showed the p38 effect, which is particularly evident in the heat maps **(Figure 38A and B)**. The maximum amplitude was only marginally lower by p38 inhibition, the time of the maximum amplitude and the end time of the first response were the same, while the late response was lower, as can be seen in the mean intensity 5 hours after the first response and the final feature value **(Figure 38C)**. In conclusion preventing lipid-raft mediated receptor degradation did not prevent the reduction of SMAD translocation by p38 inhibition.

Figure 38

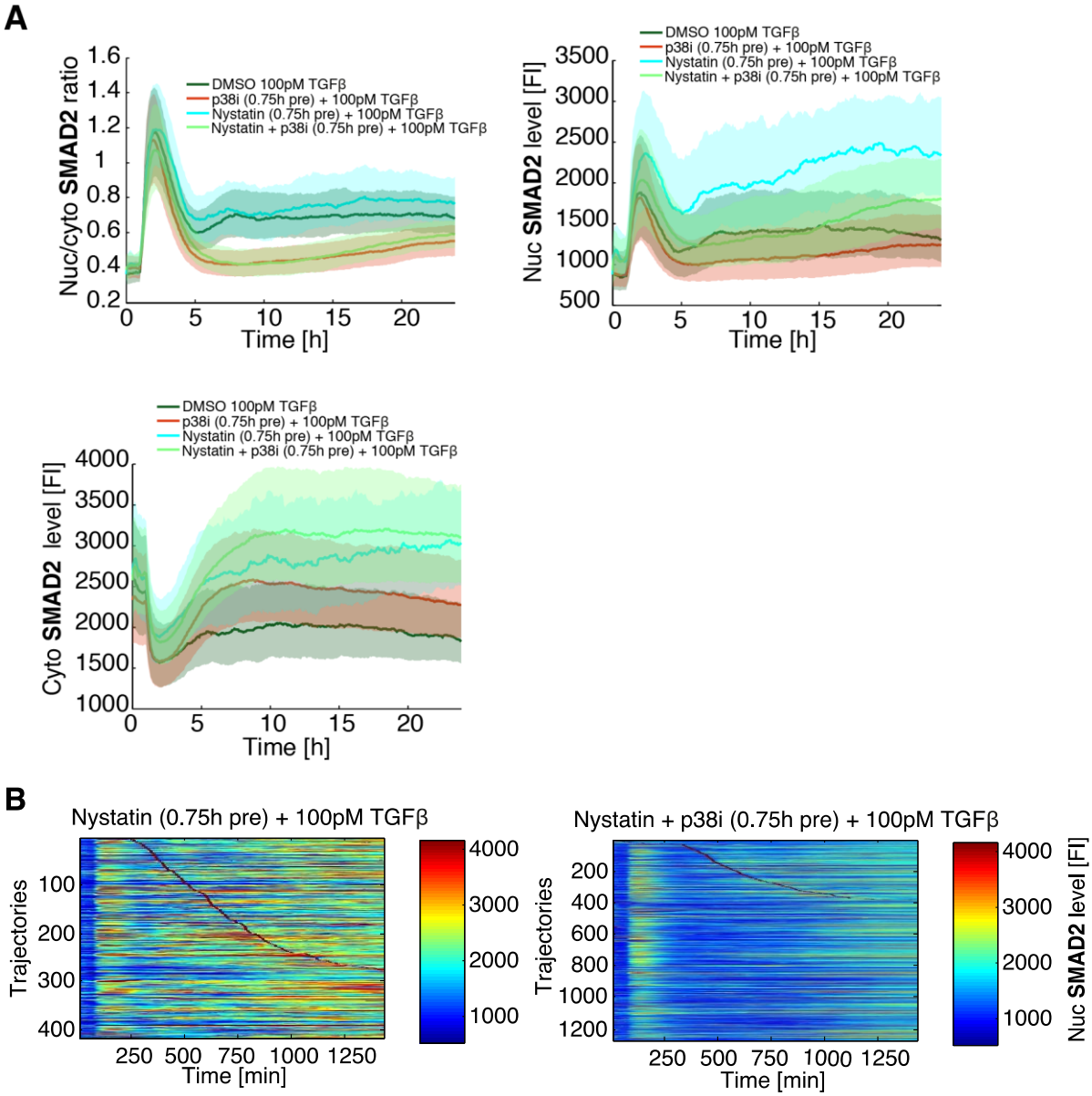
A
DMSO 100pM TGFβ
p38i (0.75h pre) + 100pM TGFβ
Nystatin (0.75h pre) + 100pM TGFβ
Nystatin + p38i (0.75h pre) + 100pM TGFβ
Nuc/cyto SMAD2 ratio
Time [h]
Nuc SMAD2 level [FI]
Cyto SMAD2 level [FI]
B
Nystatin (0.75h pre) + 100pM TGFβ
Nystatin + p38i (0.75h pre) + 100pM TGFβ
Trajectories
Time [min]
Nuc SMAD2 level [FI]

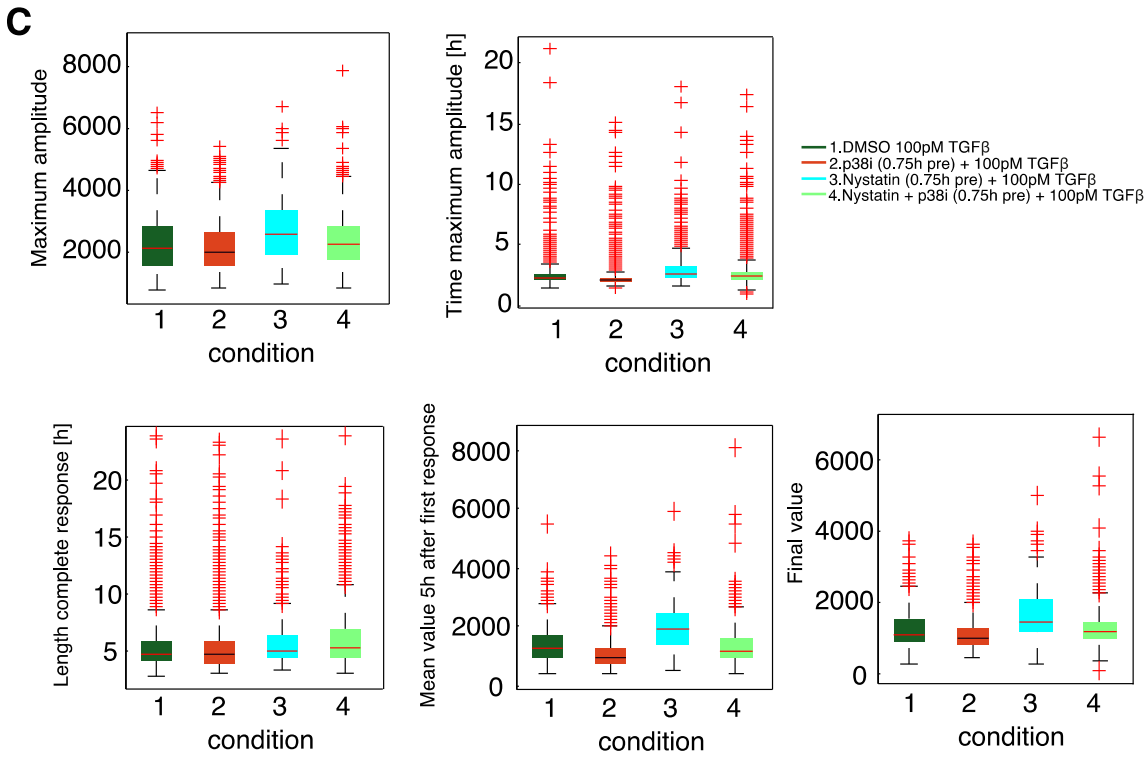

3.4.2.6.2 Figure 38. Inhibition of p38 does not shift receptors to degradation.
A Median nuc/cyto SMAD2 ratio, nuclear and cytoplasmic level of the SMAD2-YFP reporter cells stimulated with 100pM TGFβ and 0.75h pretreated with p38 inhibitors and/or Nystatin. Shaded area represent data between 25th and 75th percentiles.
B Heat maps of nuclear SMAD2 translocation in individual cells over 24h. Cells were stimulated with 100pM TGFβ and 0.75h pretreated with p38 inhibitors and/or Nystatin. Cells were sorted by the time of the first division as indicated by red marks.
C Signaling features for nuclear SMAD2 level in the SMAD2 reporter cells stimulated with 100pM TGFβ and 0.75h pretreated with p38 inhibitors and/or Nystatin. Red lines indicate median; boxes include data between the 25th and 75th percentiles; whiskers extend to maximum values within 1.5× the interquartile range; crosses represent outliers.

3.4.2.6.3 p38 effect is not mediated by alteration of the ubiquitin-dependent degradation

Next, I investigated whether the p38 effect is due to ubiquitin-dependent degradation mediated by the proteasome. Inhibition of proteasome activity causes accumulation of key TGFβ signaling components and therefore modulates SMAD dynamics (3.2.3). In this process, SMURF2 acts as an ubiquitin E3 ligase mediating proteasome-dependent degradation of SMAD2 (Lin *et al*, 2000). Since SMAD7 binds to SMURF2 to form complexes that target the receptors and other TGFβ components for degradation (Kavsak *et al*, 2000), I hypothesized that the p38 kinase interferes with this complex and thus has an impact on the dynamic remodeling of SMAD2. As shown in **Figure 39A** pretreatment with the proteasome inhibitor MG132 and 100pM TGFβ stimulation resulted in a strong SMAD2 accumulation into the nucleus. However, pretreatment with the p38 inhibitor and MG132 and TGFβ stimulation also showed the p38 effect, which is not only recognizable in the ratio, but also especially in the nuclear level **(Figure 39A)**. Compared to treatment with MG132 and TGFβ, the amplitude was slightly reduced and the mean intensity within 5 hours after response was lower **(Figure 39B)**.

Interestingly, the p38 effect was also evident when the cells were treated with the MG132 and the p38 inhibitor compared to treatment with only MG132, hence independent of TGFβ stimulation. In conclusion the p38 effect is not mediated by alteration of the ubiquitin-dependent degradation **(Figure 39C)**.

Figure 39

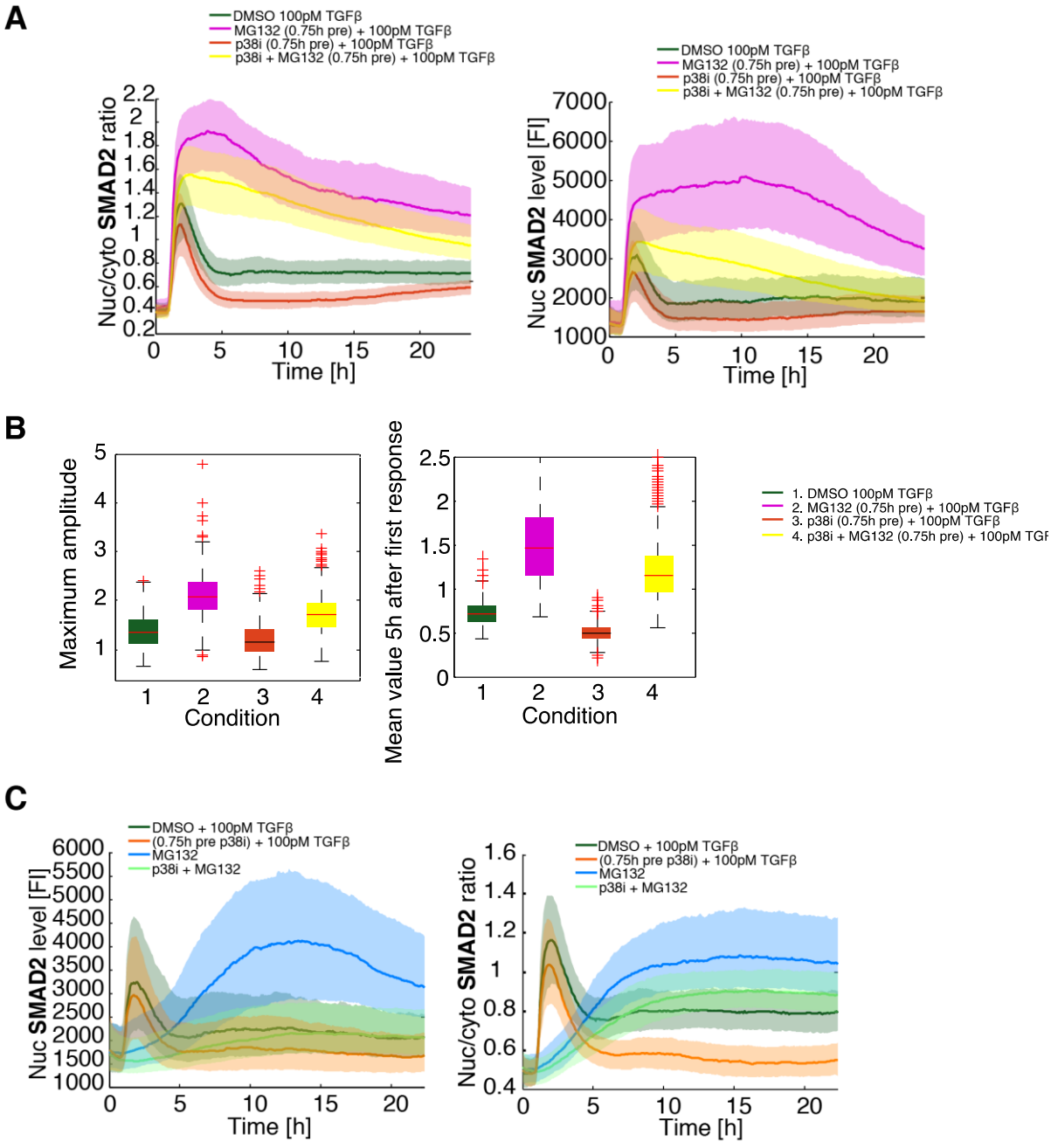

3.4.2.6.3 Figure 39. p38 effect is not mediated by alteration of the ubiquitin-dependent degradation.
A Median nuc/cyto SMAD2 ratio, nuclear and cytoplasmic level of the SMAD2-YFP reporter cells stimulated with 100pM TGFβ and 0.75h pretreated with p38 inhibitors and/or MG132. Shaded area represent data between 25th and 75th percentiles.
B Signaling features for nuc/cyto SMAD2 ratio of the SMAD2 reporter cells stimulated with 100pM TGFβ and 0.75h pretreated with p38 inhibitors and/or MG132. Red lines indicate median; boxes include data between the 25th and 75th percentiles; whiskers extend to maximum values within 1.5× the interquartile range; crosses represent outliers.

C Median nuclear SMAD2 level, nuc/cyto SMAD2 ratio and cytoplasmic level of the SMAD2-YFP reporter cells treated with only p38 inhibitors or MG132.

3.4.2.6.4 Inhibition of PP1 and PP2A does not alter the p38 effect on SMAD2

Since p38 inhibition abrogates the MG132 effect independent of TGFβ, I hypothesized that the p38 effect occurs independently of the receptors and the SMAD2 phosphorylation but could affect dephosphorylation. Thus, to understand the mechanism how the p38 kinase influences the long-term dynamics of SMADs, I focused on phosphatases. Phosphatases are grouped into three main classes based on sequence, structure and catalytic function. The largest class of phosphatases is the phosphoprotein phosphatase (PPP) family comprised of PP1, PP2A, PP2B, PP4, PP5, PP6 and PP7, and the protein phosphatase Mg^{2+}- or Mn^{2+}- dependent (PPM) family, comprised primarily of PP2C. The protein Tyr phosphatase (PTP) super-family forms the second group and the aspartate-based protein phosphatase the third (Moorhead *et al*, 2007). PP1 and PP2A are the major cellular phosphatases, which together account for more than 90% of protein phosphatase activity in eukaryotes (Virshup & Shenolikar, 2009). Therefore, I used first Okadaic acid, a phosphatase inhibitor particularly of type 1 (PP1) and 2A (PP2A) (Bialojan & Takai, 1988), but also other types including 4, 5, and 2B (PP4, PP5, PP2B) (Louzao *et al*, 2005). The hypothesis is that p38 inhibition activates phosphatases and hence activated p38 inhibits directly or indirectly phosphatases. Since MCF10A cells died 6 hours after treatment of okadaic acid, I analyzed only the first 6 hours. As shown in **Figure 40A** pretreatment with the p38 inhibitors and 100pM TGFβ stimulation resulted in less SMAD2 accumulation into the nucleus. However, p38 inhibition and Okadaic acid 0.75 hours pre 100pM TGFβ stimulation, 1.5 hours post (data not shown) and 3 hours post TGFβ still revealed the observed p38 effect, which is particularly noticeable at 5 hours **(Figure 40B)**. In conclusion using Okadaic acid I observed that inhibition of PP1 and PP2A phosphatases did not influence the p38-mediated SMAD2 response.

Figure 40

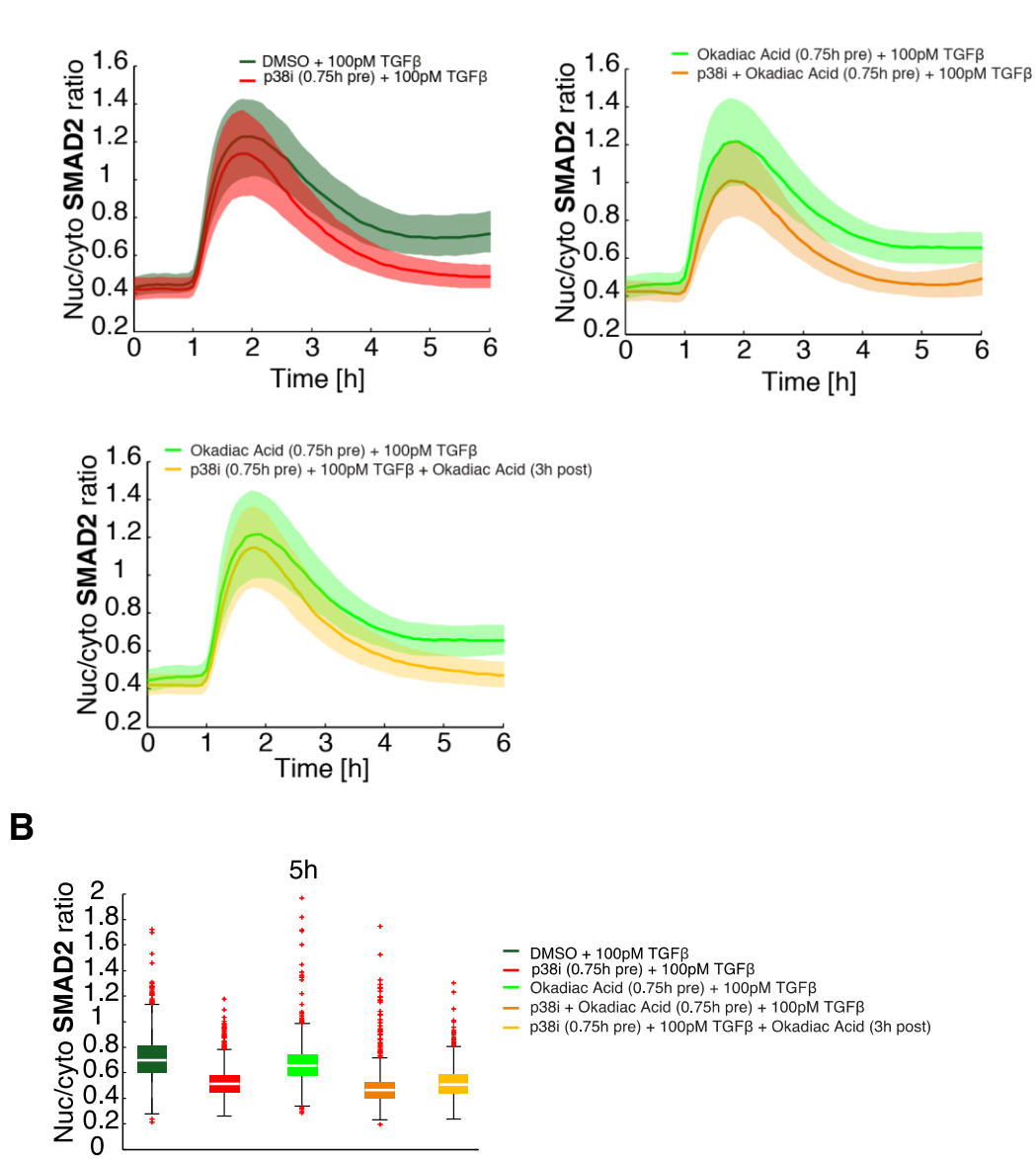

3.4.2.6.4 Figure 40. Inhibition of PP1 and PP2A does not alter the p38 effect on SMAD2.
A Median nuc/cyto SMAD2 ratio of the SMAD2-YFP reporter cells stimulated with 100pM TGFβ and 0.75h pretreated with p38 inhibitors and Okadaic acid at indicated time points. Shaded area represent data between 25th and 75th percentiles.
B Median nuc/cyto SMAD2 ratio of the SMAD2-YFP reporter cells stimulated with 100pM TGFβ and 0.75h pretreated with p38 inhibitors and Okadaic acid at indicated time points.

3.4.2.6.5 Inhibition of PP2C abrogates the p38 effect on SMADs

To further investigate the hypothesis that phosphatases mediate the p38 effect, I specifically inhibited another phosphatase group PP2C with Sanguinarine chloride. Sanguinarine is a plant alkaloid, that shows selectivity for PP2C as compared with PP1, PP2A, and PP2B in vitro (Aburai *et al*, 2010). First, I treated MCF10A cells with different concentrations of Sanguinarine chloride and 100pM TGFβ. In accordance with the literature, I chose for all further experiments the final concentration of 1 µM, as at higher concentrations cells start to die and lower concentrations have little effect on the SMAD2

response **(Figure 41A)**. As shown in **Figure 41B** cells pretreated with 1µM inhibitor and TGFβ showed a stronger accumulation of SMAD2 into the nucleus with similar amplitude and a prevented adaptation, as can be seen by the 5-hour value **(Figure 41C)**. And surprisingly p38 and Sanguinarine chloride inhibitors and TGFβ abrogated the p38 effect **(Figure 41B and C)**. In **Figure 41D** random cells for Sanguinarine pretreated and TGFβ stimulated cells with and without p38 inhibitors are plotted. The p38 effect disappeared and all cells showed a strong SMAD2 response, independent of p38 kinase inhibition. Also adding Sanguinarine 3 hours post stimulation in p38 pretreated cells immediately enhanced SMAD2 accumulation in the nucleus **(Figure 41B and C)**. Furthermore, the p38 effect was also prevented for SMAD4, measured in the combined cell line E9 when the cells were treated with Sanguinarine chloride and p38 inhibitors **(Figure 41E)**. In addition, the question arises whether inhibition with Sanguinarine chloride affected the inhibition of p38 and thus was the effect gone, since the PP2C family also acts on the p38 pathway. The phosphatase inhibition could also result in more pp38 and the p38 inhibitors could no longer function completely. To ensure that the kinase activity of p38 was still inhibited, I increased the concentrations of the inhibitors to 15µM SB202190 and 20µM BIRB. However, as can be seen in **Figure 41F,** the p38 effect disappeared with Sanguinarine chloride even at high p38 inhibitor concentrations. In conclusion inhibition of PP2C abrogated the p38-mediated SMAD response and therefore a PP2C family member was involved in the p38- SMAD-crosstalk, but the link between activated p38 and the phosphatase remain unclear.

Figure 41

A

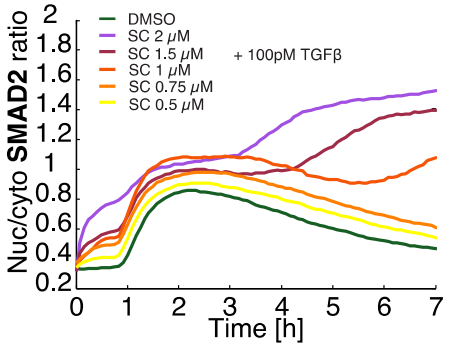

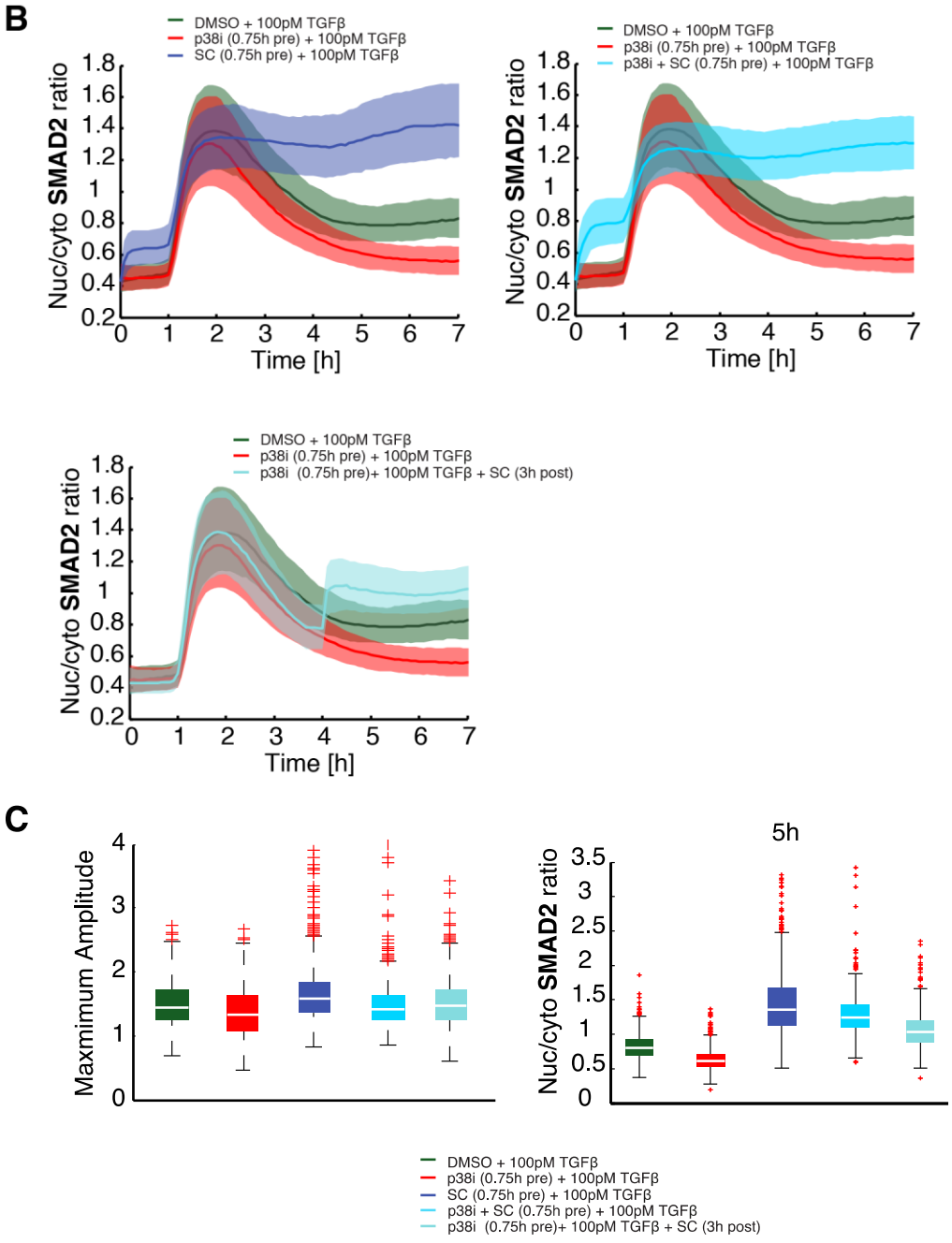
B
DMSO + 100pM TGFβ
p38i (0.75h pre) + 100pM TGFβ
SC (0.75h pre) + 100pM TGFβ
p38i + SC (0.75h pre) + 100pM TGFβ
p38i (0.75h pre)+ 100pM TGFβ + SC (3h post)
Nuc/cyto SMAD2 ratio
Time [h]
C
Maxmimum Amplitude
5h
Nuc/cyto SMAD2 ratio
D

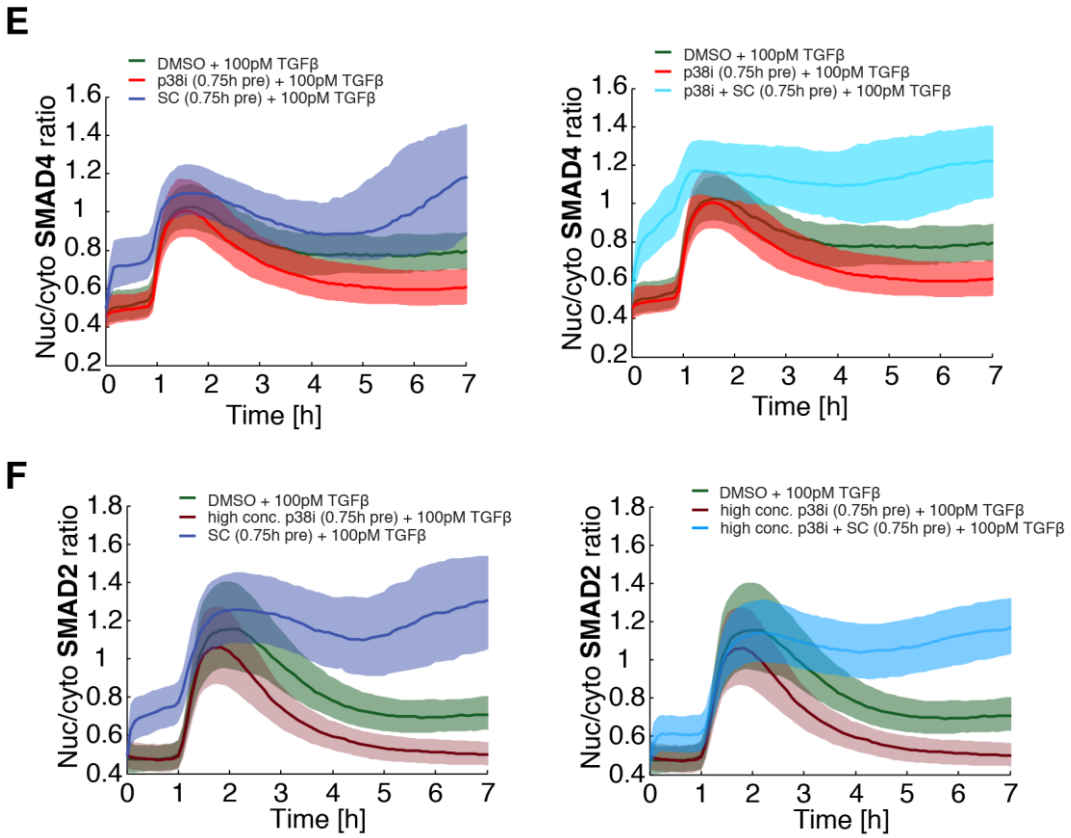

3.4.2.6.5 Figure 41. Inhibition of PP2C abrogates the p38 effect on SMADs.
A Median nuc/cyto SMAD2 ratio of the SMAD2-YFP reporter cells stimulated with 100pM TGFβ and 0.75h pretreated with Sanguinarine chloride (SC) at indicated concentrations.
B Median nuc/cyto SMAD2 ratio of the SMAD2-YFP reporter cells stimulated with 100pM TGFβ and p38 inhibitors and Sanguinarine chloride (SC) at indicated time points. Shaded area represent data between 25th and 75th percentiles.
C Signaling features for nuc/cyto SMAD2 ratio of the SMAD2 reporter cells stimulated with 100pM TGFβ and p38 inhibitors and Sanguinarine chloride (SC) at indicated time points. White lines indicate median; boxes include data between the 25th and 75th percentiles; whiskers extend to maximum values within 1.5× the interquartile range; crosses represent outliers.
D Exemplary individual nuc/cyto SMAD2 ratio trajectories (thin lines) for the SMAD2-YFP reporter cells stimulated with 100pM TGFβ and 0.75h pretreated with p38 inhibitors and/ or Sanguinarine chloride (SC) compared to the median nuc/cyto SMAD2 ratio of the entire population (thick line).
E Median nuc/cyto SMAD4 ratio of the SMAD4-YFP reporter cells stimulated with 100pM TGFβ and 0.75h pretreated with p38 inhibitors and/ or Sanguinarine chloride (SC). Shaded area represent data between 25th and 75th percentiles.
F Median nuc/cyto SMAD2 ratio of the SMAD2-YFP reporter cells stimulated with 100pM TGFβ and 0.75h pretreated with a high concentration of p38 inhibitors (15µM SB202190 and 20µM BIRB796) and/ or Sanguinarine chloride (SC). Shaded area represent data between 25th and 75th percentiles.

3.4.2.6.6 PPM1A is probably not involved in the p38-mediated TGFβ response

As mentioned, PP2C family member belong to the Mn^{2+}/Mg^{2+}-dependent PPM family, where metal ions play a catalytic and central role through the activation of a water molecule for the dephosphorylation reaction (Shi, 2009). The PP2C family represents a large group of highly conserved protein phosphatases, with 16 distinct PP2C genes in the human genome that give rise to at least 22 different isoforms (Lammers & Lavi, 2007). The different isoforms have distinct sequences and domain organizations. These PP2C isoforms also exhibit distinct functions, expression patterns, and subcellular localization. The primary function of PP2C appears to be the regulation of stress signaling, although it also plays a role in cell differentiation, growth, survival, apoptosis, and metabolism (Lu & Wang, 2008).

Some PP2C members, such as PP2Cα (PPM1A) and PP2Cβ are candidate tumor suppressor proteins, whereas others, such as PP2Cδ (Wip1), may contribute to oncogenic transformation (Shi, 2009). How these PP2C members are regulated during signaling remains largely unknown. Moreover, the PP2C family member that is involved in the p38- SMAD-crosstalk still needs to be clarified. Since PP2Cα (PPM1A) plays a critical role in terminating TGFβ signaling through direct dephosphorylation of SMAD2/SMAD3 (Lin *et al*, 2006), this phosphatase would be a good candidate. PPM1A promotes nuclear export of TGFβ-activated SMAD2/3. Ectopic expression of PPM1A abolishes TGFβ-induced antiproliferative and transcriptional responses, whereas depletion of PPM1A enhances TGFβ signaling in mammalian cells (Lin *et al*, 2006). Furthermore, PPM1A inhibited the activation of the p38 cascade (Takekawa *et al*, 1998). Thus, to understand the mechanism how the p38 kinase is linked to a PP2C family member to influence the long-term dynamics of SMADs, I knocked down PPM1A in time-lapse microscopy experiments. First, I did a knock down test 24, 48 and 72h after transfection of MCF10A WT cells with PPM1A siRNA. As seen in **Figure 42A**, PPM1A was down to 16% after 48h and even to 10% after 72h. The control was carried out with scrambled RNA. To achieve the best knock down efficiency, I transfected the SMAD2 reporter cell line 48h prior to TGFβ treatment with PPM1A siRNA. Due to the prolonged growth period, the control response is somewhat reduced after 100 pM TGFβ stimulation **(Figure 42B)**. Nonetheless, knockdown of PPM1A enhanced nuclear SMAD2 translocation. Already the first answer showed more SMAD2 in the nucleus, which can be seen especially in the heat maps **(Figure 42C)**. As there was also more SMAD2 present in the cytoplasm, the ratio concealed the effects of the knockdown of PPM1A **(Figure 42D and E).** Furthermore, fewer cells divided due to enhanced SMAD2 activation **(Figure 42F)**. The p38 effect in the nuclear control after treatment with the p38 inhibitors was also weaker, as shown in **Figure 42G**. However, the effect was clearly visible in the ratio and SMAD2 translocated after the first response from the nucleus back to the cytoplasm **(Figure 42I and K).** Nevertheless, even after PPM1A siRNA transfection and p38 inhibition, the p38 effect was recognizable **(Figure 42H, J and L).** Therefore, PPM1A was probably not involved in the p38-mediated TGFβ response. However, compensation mechanisms and incomplete knock down could conceal the function of PPM1A.

Figure 42

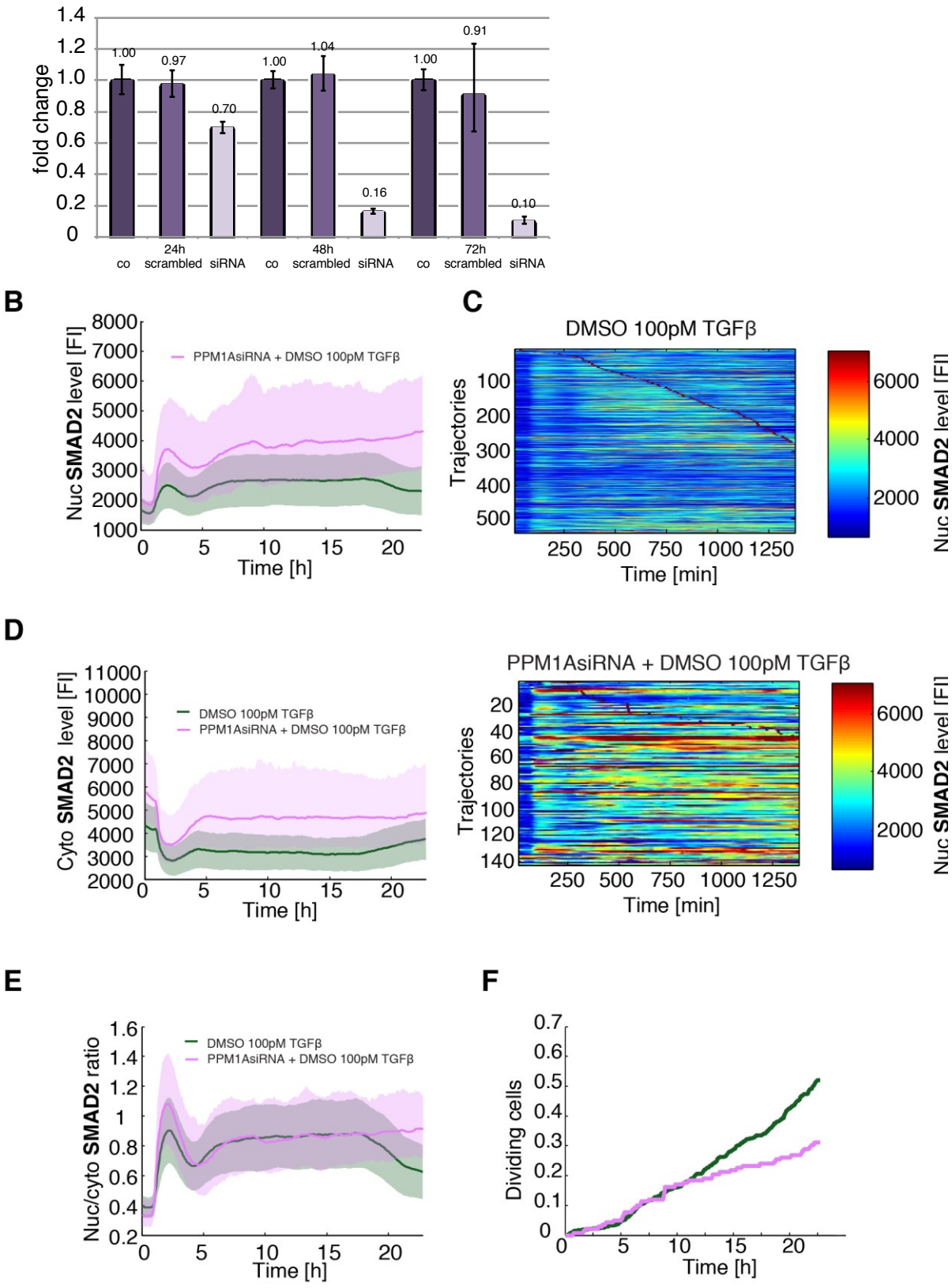
A
fold change
1.00
0.97
0.70
1.00
1.04
0.16
1.00
0.91
0.10
co
24h scrambled
siRNA
co
48h scrambled
siRNA
co
72h scrambled
siRNA
B
Nuc SMAD2 level [FI]
PPM1AsiRNA + DMSO 100pM TGFβ
Time [h]
C
DMSO 100pM TGFβ
Trajectories
Time [min]
Nuc SMAD2 level [FI]
D
Cyto SMAD2 level [FI]
DMSO 100pM TGFβ
PPM1AsiRNA + DMSO 100pM TGFβ
Time [h]
PPM1AsiRNA + DMSO 100pM TGFβ
Trajectories
Time [min]
Nuc SMAD2 level [FI]
E
Nuc/cyto SMAD2 ratio
DMSO 100pM TGFβ
PPM1AsiRNA + DMSO 100pM TGFβ
Time [h]
F
Dividing cells
Time [h]

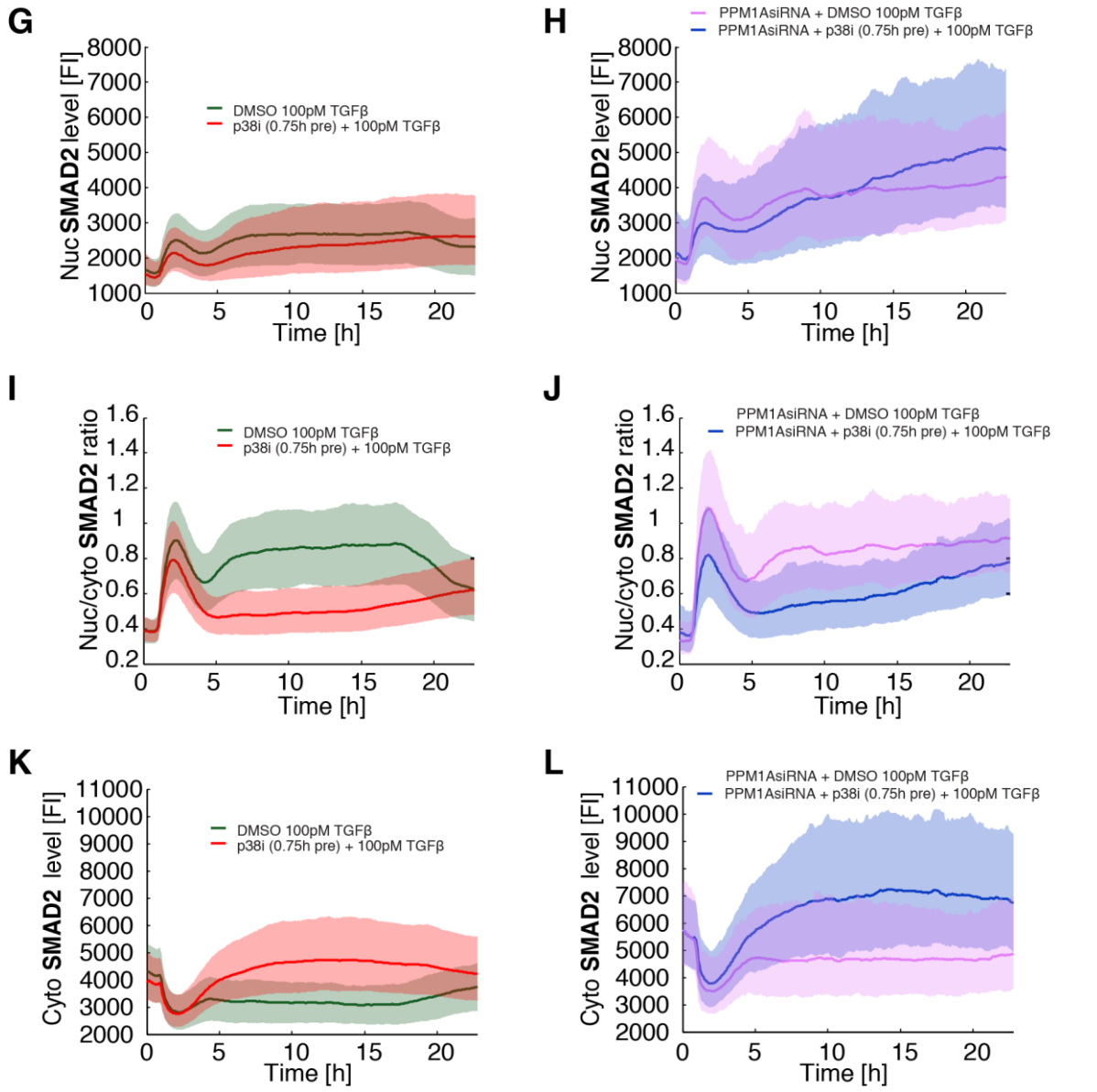

3.4.2.6.6 Figure 42. PPM1A is probably not involved in the p38-mediated TGFβ response.

A Expression of PPM1A 24, 48 and 72h after transfection of MCF10A WT cells with PPM1A siRNA. The controls were carried out without transfection or scrambled RNA. β-Actin was used as an internal control. Error bars indicate standard deviation of technical triplicates.

B Median nuclear SMAD2 level of the SMAD2-YFP reporter cells seeded 3 days prior and transfected 48h prior to 100pM TGFβ treatment with PPM1A siRNA. Shaded area represent data between 25th and 75th percentiles.

C Heat maps of nuclear SMAD2 translocation in individual cells over 24h. Cells were transfected 48h prior to 100pM TGFβ treatment with PPM1A siRNA. Cells were sorted by the time of the first division as indicated by red marks.

D Median cytoplasmic SMAD2 level of the SMAD2-YFP reporter cells transfected 48h prior to 100pM TGFβ treatment with PPM1A siRNA. Shaded area represent data between 25th and 75th percentiles.

E Median nuc/cyto SMAD2 ratio of the SMAD2-YFP reporter cells transfected 48h prior to 100pM TGFβ treatment with PPM1A siRNA. Shaded area represent data between 25th and 75th percentiles.

F Cell proliferation of SMAD2 reporter cells shown as fraction of dividing cells within 24h.

G Median nuclear SMAD2 level of the SMAD2-YFP reporter cells seeded 3 days prior to 100pM TGFβ stimulation and 0.75h pretreated with p38 inhibitors. Shaded area represent data between 25th and 75th percentiles.

H Median nuclear SMAD2 level of the SMAD2-YFP reporter cells seeded 3 days prior and transfected 48h prior to 100pM TGFβ treatment with PPM1A siRNA and 0.75h pretreated with p38 inhibitors. Shaded area represent data between 25th and 75th percentiles.

I Median cytoplasmic SMAD2 level of the SMAD2-YFP reporter cells seeded 3 days prior to 100pM TGFβ stimulation and 0.75h pretreated with p38 inhibitors.

J Median nuc/cyto SMAD2 ratio of the SMAD2-YFP reporter cells transfected 48h prior to 100pM TGFβ treatment with PPM1A siRNA and 0.75h pretreated with p38 inhibitors.

K Median nuc/cyto SMAD2 ratio of the SMAD2-YFP reporter cells seeded 3 days prior to 100pM TGFβ stimulation and 0.75h pretreated with p38 inhibitors.
L Median cytoplasmic SMAD2 level of the SMAD2-YFP reporter cells transfected 48h prior to 100pM TGFβ treatment with PPM1A siRNA and 0.75h pretreated with p38 inhibitors.

3.4.3 Inhibition of ERK signaling alters long-term SMAD dynamics

Inhibition of the p38 MAP kinase pathway results in modified other MAPK pathways like the extracellular-signal-regulated kinase (ERK) pathway (Hall & Davis, 2002). ERK is also another non-canonical MAP Kinase pathway of TGFβ activation. TGFβ- can induce phosphorylation of the receptors I and II and on Shc, which leads to recruiting of Grb2/Sos to activate Erk 1/2 (pp44/pp42) through Ras, Raf, and MEK1 (Mitogen-activated protein kinase kinase 1) and 2 (**Figure 1C,** Zhang *et al*, 2009). Interestingly, inhibition of the kinase activity of p38 and stimulation with 100pM TGFβ led in MCF10A WT cells to enhanced ERK signaling measured by phosphorylated p42 (ERK2), as the target protein, in western blot analysis **(Figure 43A)**. Since inhibition of p38 amplified ERK signaling, the question came up whether the effect of p38 was just a matter of proliferative and anti-proliferative triggers. Therefore, I initially inhibited MEK1 and 2 with AZD6244, a potent, selective, and ATP-uncompetitive inhibitor, and performed with and without p38 inhibitors in TGFβ-stimulated SMAD2 reporter cells time-lapse microscopy experiments (Davies *et al*, 2007). As can be seen in **Figure 43B**, the p38 effect at 2.5pM and 100pM TGFβ with MEK and p38 inhibitors was slightly lower but clearly recognizable. Inhibition with p38 inhibitors and Gefitinib, a tyrosine kinase inhibitor of the epidermal growth factor receptor (EGFR) (Tamura & Fukuoka, 2005), led to the same result **(Figure 43C and Appendix Figure A29)**.

In conclusion, inhibition of ERK signaling cannot abrogate the p38 effect. Nevertheless, I was interested in the impact of ERK signaling on SMAD dynamics. It is known that ERK signaling regulates target gene transcription through cofactors in conjunction with SMADs to control for instance EMT (Xie *et al*, 2004; Javelaud & Mauviel, 2005; Harish *et al*, 2015).

Figure 43

A

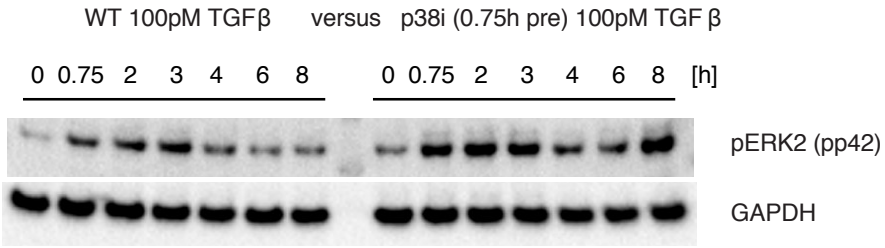

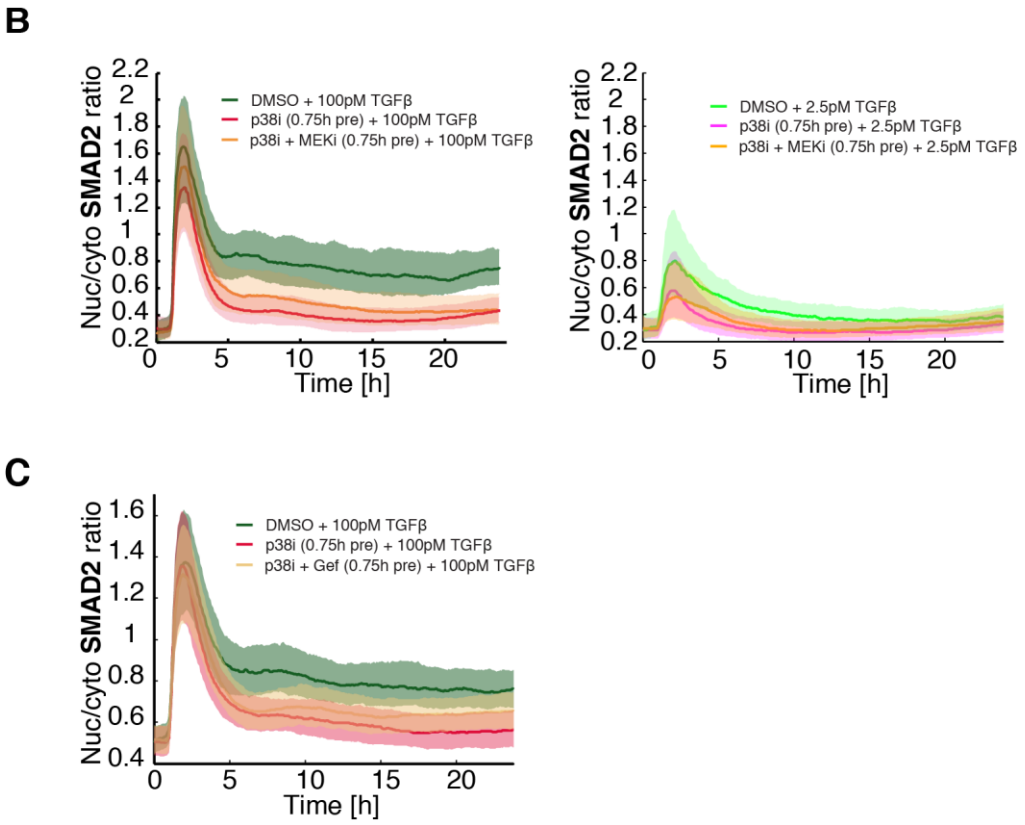

3.4.3 Figure 43. Inhibition of ERK signaling alters long-term SMAD dynamics.
A Western blot analysis of phosphorylated ERK2 (pp42) in MCF10A WT cells stimulated with 100pM TGFβ and 0.75h pretreated with p38 inhibitors (SB202190 & BIRB796). GAPDH was used as a loading control.
B Median nuc/cyto SMAD2 ratio of the SMAD2-YFP reporter cells stimulated with 2.5 or 100pM TGFβ and 0.75h pretreated with p38 inhibitors and/ or AZD6244 (MEKi). Shaded area represent data between 25th and 75th percentiles.
C Median nuc/cyto SMAD2 ratio of the SMAD2-YFP reporter cells stimulated with 100pM TGFβ and 0.75h pretreated with p38 inhibitors and/ or Gefitinib (Gef). Shaded area represent data between 25th and 75th percentiles.

3.4.3.1 TGFβ response depends on EGF concentration

In order to discover the impact of ERK signaling on the TGFβ response, I used different epidermal growth factor (EGF) concentrations in the media to vary the intensity of the signaling pathway. Normally 20 ng/ml EGF and horse serum, as well as insulin, cholera toxin and hydrocortisone were used in the medium (Debnath *et al*, 2003). To control the exact EGF concentrations in the media, I used 0.3% BSA instead of horse serum, and insulin was omitted to not interfere with ERK signaling. I kept the cells overnight (approximately 14 hours) in these conditions and changed the media before the experiments. Considering the nuclear values, it became clear that cells without EGF in the media before stimulating with 100pM TGFβ showed extremely low SMAD2 activation **(Figure 44A)**. This was reflected in a very low maximum amplitude and an absent second response, which was particularly evident in the heat maps and the final nuclear value **(Appendix Figure A30 and A31)**. With increasing EGF concentrations the amplitude and the second response rose and reached saturation for SMAD2 translocation into the nucleus at 10 ng/ml EGF **(Figure 44A, Appendix Figure A30 and A31)**. Interestingly, already the basal nuclear and cytoplasmic SMAD2 levels increased with increasing EGF

concentrations **(Appendix Figure A30)** and therefore the EGF dependencies were somewhat less marked in the ratio than in the nuclear and cytoplasmic values **(Figure 44B and C).** Interestingly, without EGF only about 50% of the cells reacted to TGFβ at all, while about 90-95% reacted to TGFβ at 1-20 ng/ml EGF concentration. Thus, the increasing TGFβ response by rising EGF concentrations was not due to a changed proportion of responders **(Figure 44D)**. Moreover, the SMAD4 reporter cell line also showed comparable results and SMAD4 translocation and activation depends on ERK signaling **(Appendix Figure A32)**. With rising EGF concentrations, the maximum amplitude and the long-term dynamics of SMAD4 increased **(Appendix Figure A33)**. The basal nuclear and cytoplasmic SMAD4 levels were also increasing with rising EGF concentrations. Since more than 90% of the cells reacted at a concentration of 1-20 ng/ml EGF in the media to 100pM TGFβ, thus the strength of the TGFβ response depended on the EGF concentration **(Appendix Figure A34)**.

Western blot analysis with MCF10A WT cells also confirmed, that the TGFβ response depended on EGF signaling. If there was no EGF in the medium (0.3% BSA instead of horse serum and no insulin), only a very weak phosphorylation of SMAD2 and SMAD3 took place upon 100pM TGFβ stimulation compared to pSMAD2 and pSMAD3 with the normal medium of 20 ng/ml EGF **(Figure 44E)**.

Furthermore, I investigated whether the cell fate changes due to a modified crosstalk of TGFβ and ERK signaling. As shown in **Figure 44F**, cells without EGF almost never divided. But the different EGF concentrations had no influence on the proportion of dividing cells. **Figure 44G** shows the covered distance of the cells at varying EGF concentrations and 100pM TGFβ, and it is evident that cells were moving more with increasing EGF concentrations and therefore both ERK and TGFβ signaling may are important for EMT.

Figure 44

A

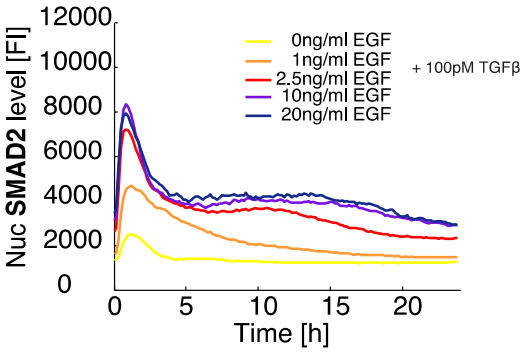

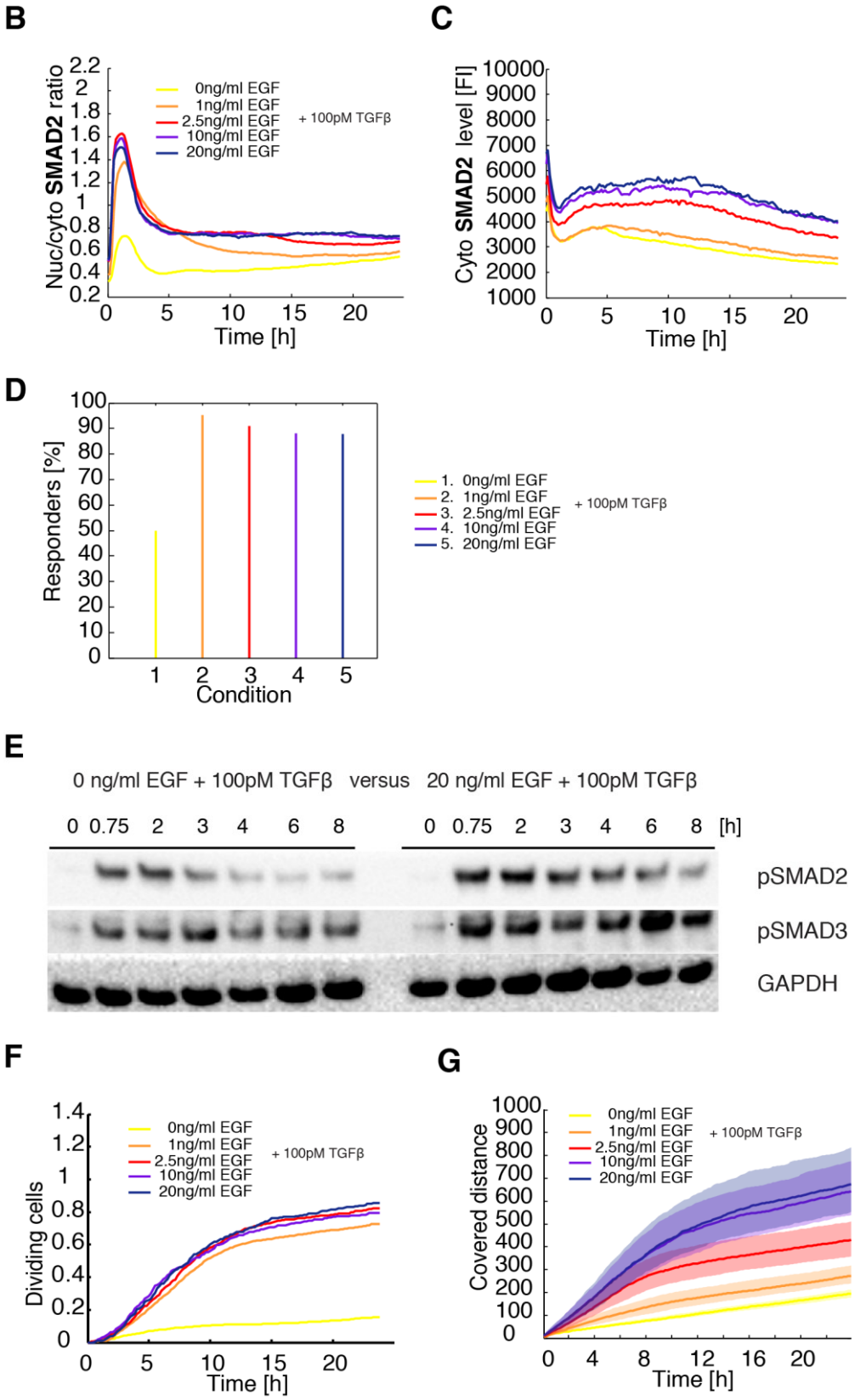

3.4.3.1 Figure 44. TGFβ response depends on EGF concentration.

A Median nuclear SMAD2 level of the SMAD2-YFP reporter cells stimulated with 100pM TGFβ at varying EGF (epidermal growth factor) concentrations.

B Median nuc/cyto SMAD2 ratio of the SMAD2-YFP reporter cells stimulated with 100pM TGFβ at varying EGF concentrations.

C Median cytoplasmic SMAD2 level of the SMAD2-YFP reporter cells stimulated with 100pM TGFβ at varying EGF concentrations.
D Responders in % of the SMAD2-YFP reporter cells stimulated with 100pM TGFβ at varying EGF concentrations.
E Western blot analysis of phosphorylated SMAD2 and SMAD3 in MCF10A WT cells stimulated with 100pM TGFβ at 0 or 20ng/ml EGF. GAPDH was used as a loading control.
F Cell proliferation of reporter cells shown as fraction of dividing cells stimulated with 100pM TGFβ at varying EGF concentrations.
G Motility of each cell as summed distance in pixel (pxl) covered 24h after stimulation with 100pM TGFβ at varying EGF concentrations.

3.4.3.2 Inhibition of the ERK cascade leads to a diminished late SMAD response

To underline that SMAD signaling depends on the ERK signaling, I inhibited the ERK cascade at different points. First Gefitinib, the tyrosine kinase inhibitor of the epidermal growth factor receptor (EGFR) (Tamura & Fukuoka, 2005), was used 0.75 hours before 100 pM TGFβ stimulation in time-lapse microscopy experiments. As shown in **Figure 45A and C**, inhibition of the EGF receptors led to reduced nuclear SMAD2 accumulation at later time points through an enhanced adaptation, while the amplitude of the initial response remained unchanged. In **Figure 45B** trajectories of random individual cells are shown. To exclude the possibility that Gefitinib would require a longer effective duration, cells were treated 2 hours before TGFβ stimulation with the inhibitor. But still the initial response remained unaffected and only the second response was modified **(Figure 45A and C).** Western blot analysis with MCF10A WT cells also confirmed the results. While total SMAD2 and total SMAD3 remain unchanged by treatment with gefitinib, the late phosphorylation of SMAD2 and SMAD3 was diminished **(Figure 45D)**. Even if the cascade was inhibited downstream of the receptors, such as the Raf kinase with the small molecular inhibitor Sorafenib (Wilhelm *et al*, 2004; Adnane *et al*, 2006) and MEK1 and 2 with AZD6244 (Davies *et al*, 2007), it confirmed the results with Gefitinib. ERK signaling was essential for late SMAD2 activation **(Figure 45E and F)**. The results were also valid for SMAD4 and treatment with Gefitinib, AZD6244 and UO126, another dual MEK1 and MEK2 inhibitor (Favata *et al*, 1998), led to a diminished late response due to a stronger adaptation **(Figure 45G)**.

In conclusion, TGFβ response depends on ERK signaling.

Figure 45

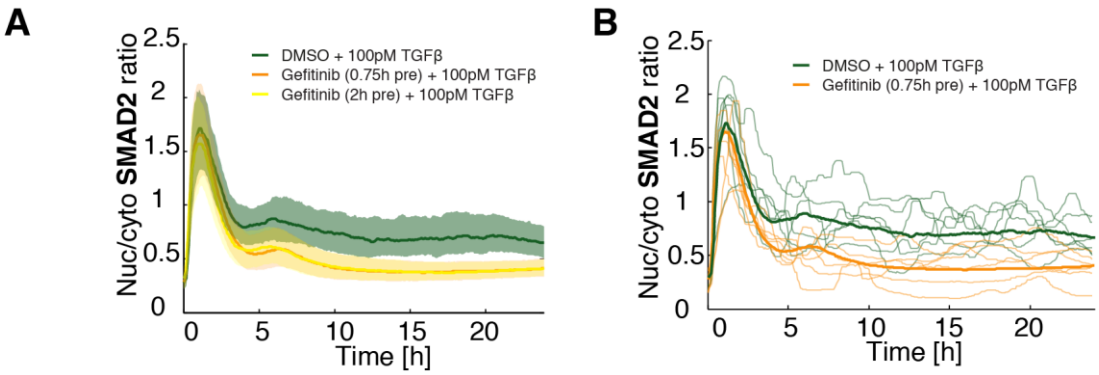

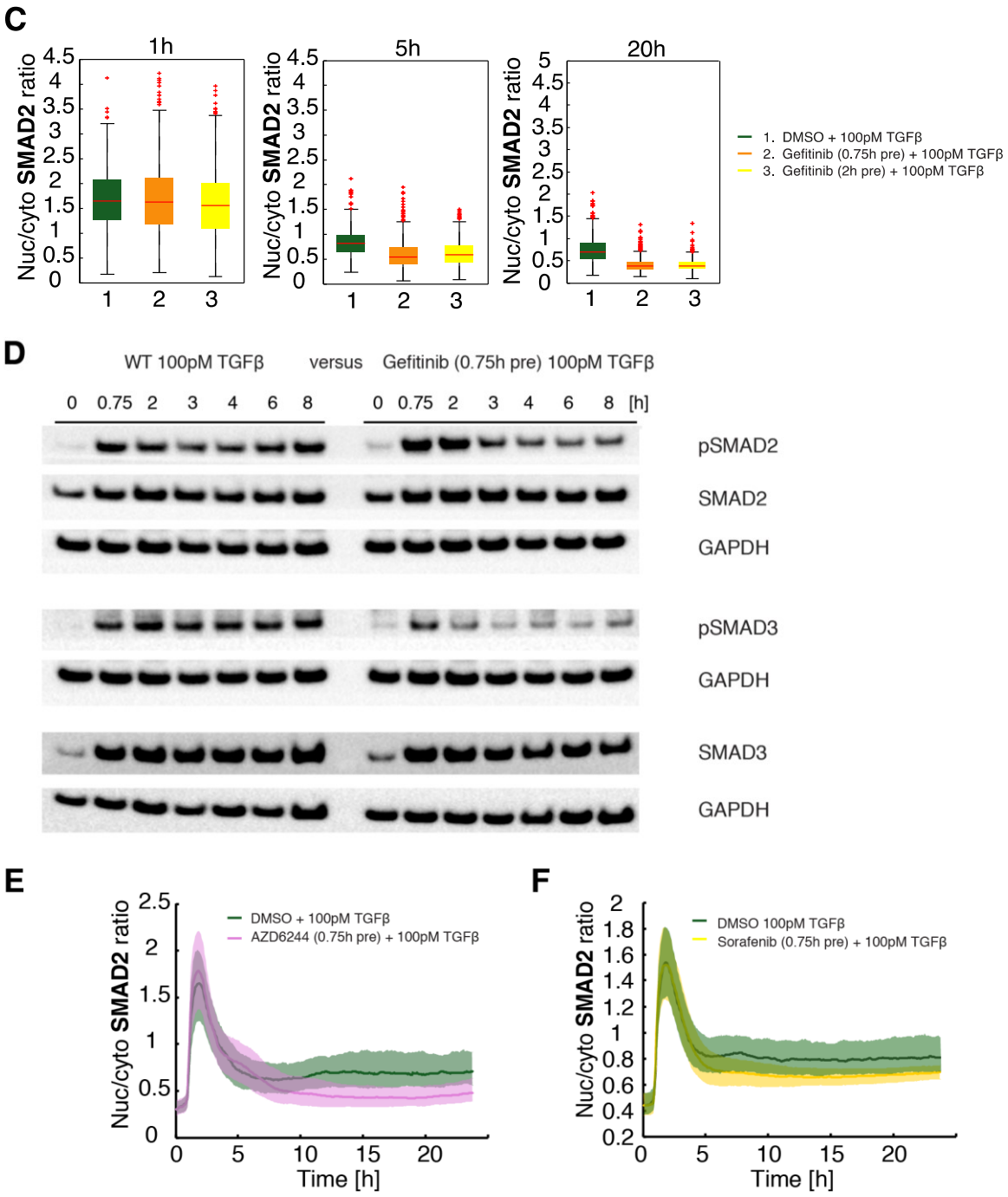
C
1h
5h
20h
Nuc/cyto SMAD2 ratio
1. DMSO + 100pM TGFβ
2. Gefitinib (0.75h pre) + 100pM TGFβ
3. Gefitinib (2h pre) + 100pM TGFβ
D
WT 100pM TGFβ
versus
Gefitinib (0.75h pre) 100pM TGFβ
0 0.75 2 3 4 6 8 [h]
pSMAD2
SMAD2
GAPDH
pSMAD3
GAPDH
SMAD3
GAPDH
E
DMSO + 100pM TGFβ
AZD6244 (0.75h pre) + 100pM TGFβ
Nuc/cyto SMAD2 ratio
Time [h]
F
DMSO 100pM TGFβ
Sorafenib (0.75h pre) + 100pM TGFβ
Nuc/cyto SMAD2 ratio
Time [h]

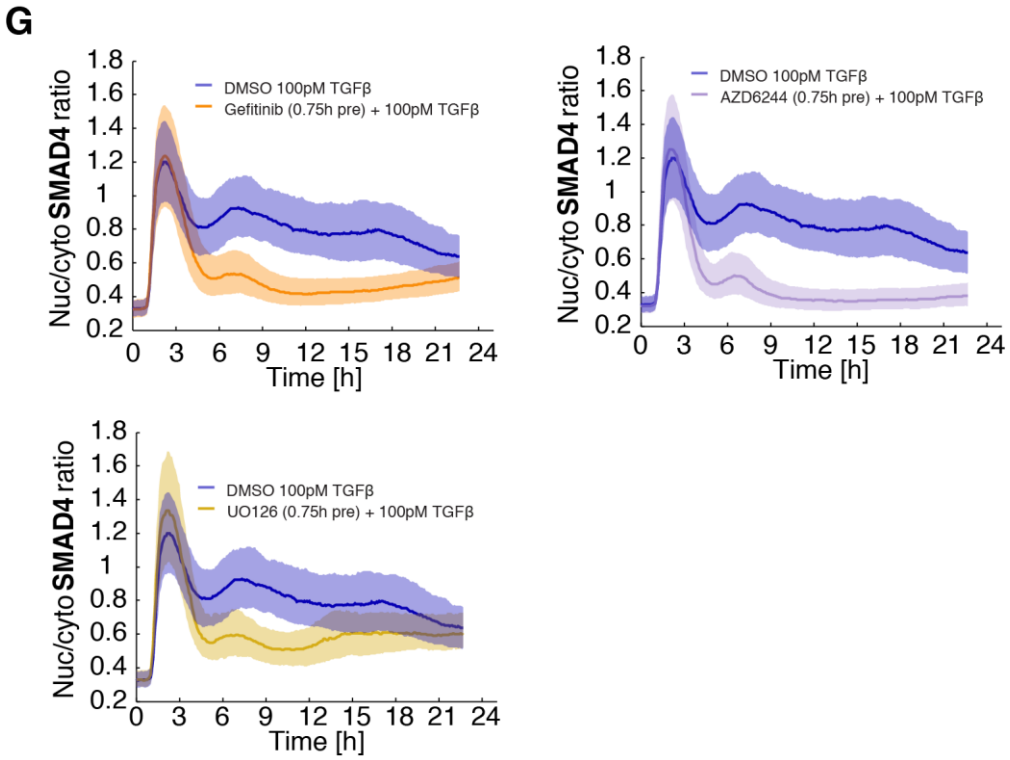

3.4.3.2 Figure 45. Inhibition of the ERK cascade leads to a diminished late SMAD response.
A Median nuc/cyto SMAD2 ratio of the SMAD2-YFP reporter cells stimulated with 100pM TGFβ pretreated with Gefitinib at indicated time points. Shaded area represent data between 25th and 75th percentiles.
B Exemplary individual nuc/cyto SMAD2 ratio trajectories (thin lines) for the SMAD2-YFP reporter cells stimulated with 100pM TGFβ and 0.75h pretreated with Gefitinib compared to the median nuc/cyto SMAD2 ratio of the entire population (thick line).
C Signaling features for nuc/cyto SMAD2 ratio of the SMAD2 reporter cells stimulated with 100pM TGFβ pretreated with Gefitinib at indicated time points. Red lines indicate median; boxes include data between the 25th and 75th percentiles; whiskers extend to maximum values within 1.5× the interquartile range; crosses represent outliers.
D Western blot analysis of phosphorylated SMAD2, SMAD2, phosphorylated SMAD3 and SMAD3 in MCF10A WT cells stimulated with 100pM TGFβ and 0.75h pretreated with Gefitinib. GAPDH was used as loading controls.
E Median nuc/cyto SMAD2 ratio of the SMAD2-YFP reporter cells stimulated with 100pM TGFβ and 0.75h pretreated with AZD6244. Shaded area represent data between 25th and 75th percentiles.
F Median nuc/cyto SMAD2 ratio of the SMAD2-YFP reporter cells stimulated with 100pM TGFβ and 0.75h pretreated with Sorafenib. Shaded area represent data between 25th and 75th percentiles.
G Median nuc/cyto SMAD4 ratio of the SMAD2-YFP reporter cells stimulated with 100pM TGFβ and 0.75h pretreated with Gefitinib, AZD6244 or UO126. Shaded area represent data between 25th and 75th percentiles.

3.4.3.3 Dependency of SMAD target genes on ERK signaling

I was also interested in the impact of this dynamic remodeling on gene expression and cell fate. Therefore, I performed RT-PCRs after Gefitinib treatment and 100pM TGFβ stimulation **(Figure 46)**. While the gene expression of SMAD7 and SnoN were hardly changed, Gefitinib prevented the late activation of Snail from 6 hours on post TGFβ stimulation. This supports the hypothesis that the long-term dynamics of SMAD2 are responsible for EMT and the balance between SMAD activation and ERK signaling defines cellular responses to TGFβ.

Figure 46

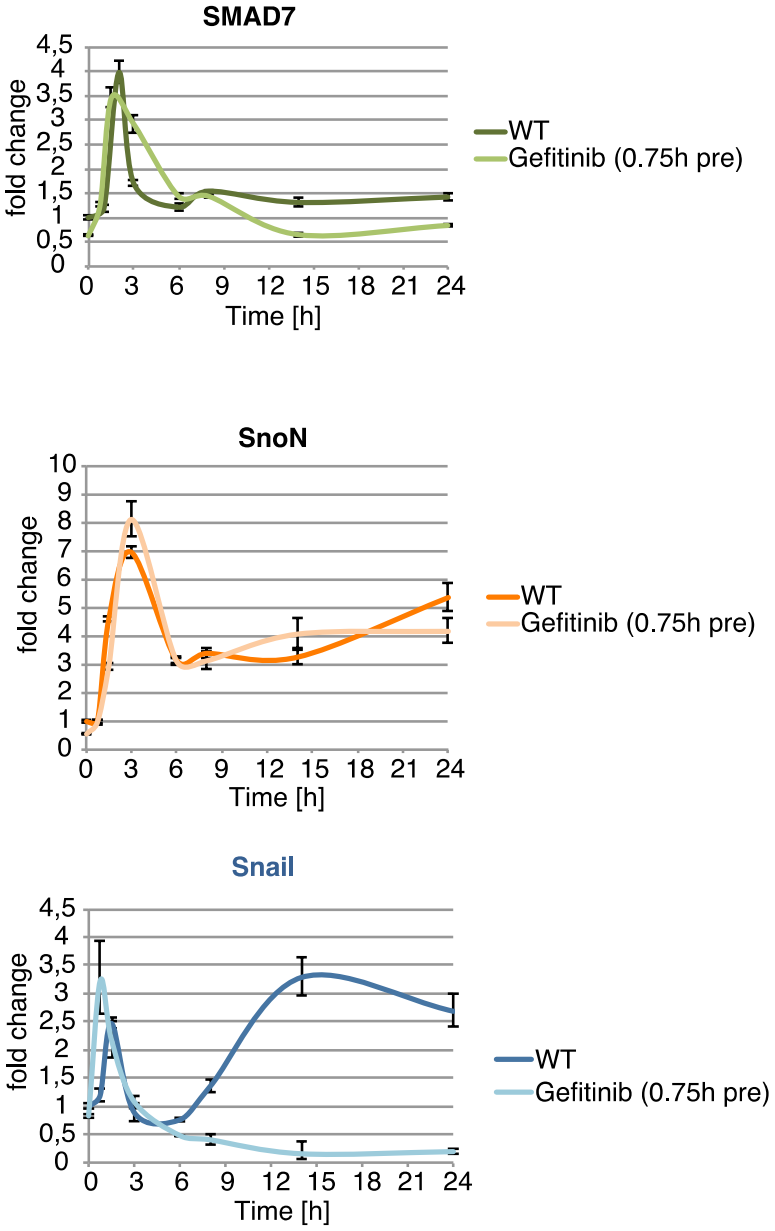

3.4.3.3 Figure 46. Dependency of SMAD target genes on ERK signaling.
Expression of TGFβ target genes of MCF10A WT cells stimulated with 100pM TGFβ and 0.75h pretreated with Gefitinib. β-Actin was used as an internal control. Error bars indicate standard deviation of technical triplicates.

3.4.3.4 Mechanism of ERK inhibition

Since ERK signaling had an enormous impact on the long-term dynamics of SMAD2 and SMAD4 and affected TGFβ cell fate decisions, I was curious about the underlying mechanisms of this cross-talk.

3.4.3.4.1 Knock down of SMAD7 does not alter the Gefitinib effect on SMAD2

To determine if ERK signaling interacts with SMAD7 to modulate the dynamics of SMAD2, I perturbed the signaling network using Gefitinib and TGFβ in the absence or presence of SMAD7. For this purpose,

I used the *SMAD7* CRISPR Cas9 knock out clone 12 (3.2.2.3) and the SMAD2-YFP Cas9 reporter cell line as a control cell line. However, considering the ratio values, the gefitinib effect was recognizable in the control cell line and for clone 12 **(Figure 47A)**. Also, the nuclear and cytoplasmic levels showed that the second response disappeared through gefitinib independent of SMAD7 **(Figure 47B and C)**. Therefore, SMAD7 played no role in the mechanism.

Figure 47

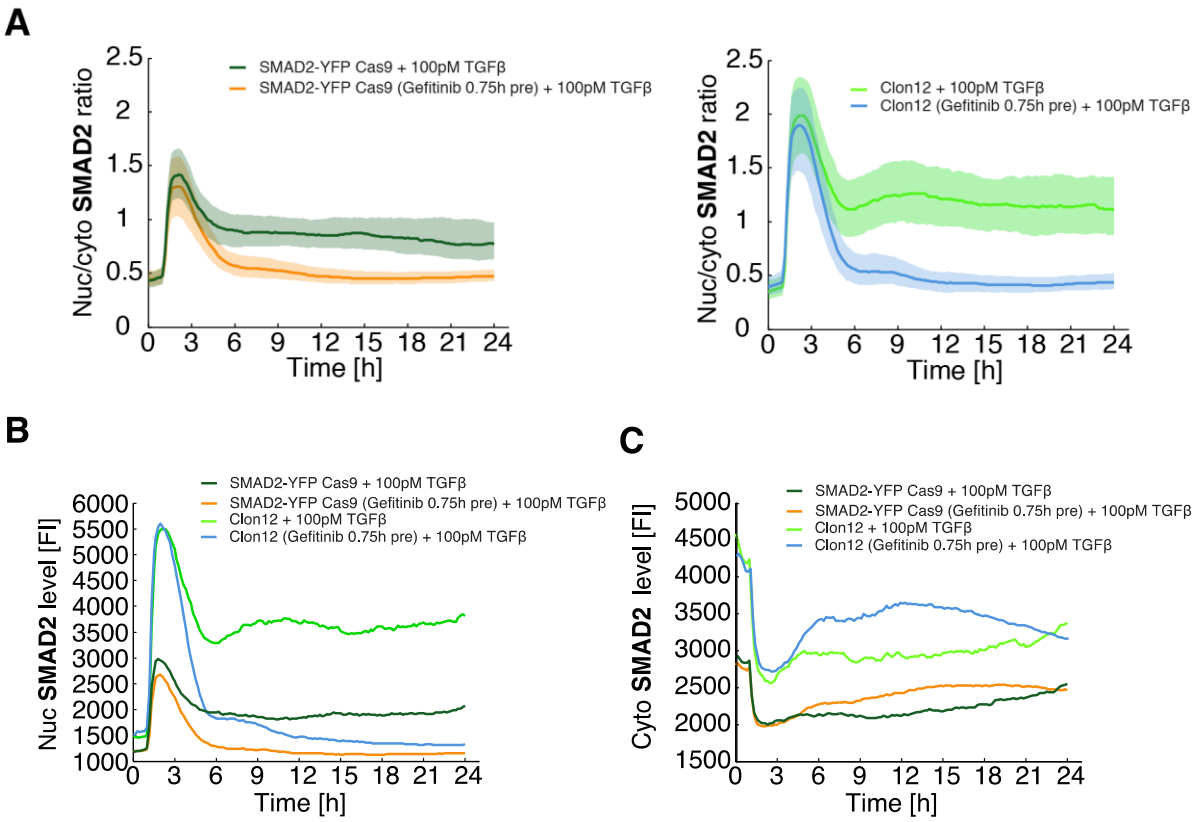

3.4.3.4.1 Figure 47. Knock down of SMAD7 does not alter the Gefitinib effect on SMAD2.
A Median nuc/cyto SMAD2 ratio of the control SMAD2-YFP Cas9 reporter cell line and the SMAD7 CRISPR Cas9 knock out clone 12 stimulated with 100pM TGFβ and 0.75h pretreated with Gefitinib. Shaded area represent data between 25th and 75th percentiles.
B Median nuclear SMAD2 level of the control SMAD2-YFP Cas9 reporter cell line and the SMAD7 CRISPR Cas9 knock out clone 12 stimulated with 100pM TGFβ and 0.75h pretreated with Gefitinib.
C Median cytoplasmic SMAD2 level of the control SMAD2-YFP Cas9 reporter cell line and the SMAD7 CRISPR Cas9 knock out clone 12 stimulated with 100pM TGFβ and 0.75h pretreated with Gefitinib.

3.4.3.4.2 Inhibition of PP1 and PP2A does not alter the ERK effect on SMAD2

Furthermore, I tested the hypothesis that ERK signaling leads finally to activated phosphatases and hence influences the long-term dynamics of SMADs. Therefore, I used Okadaic acid, a phosphatase inhibitor of the major cellular phosphatases PP1 and PP2A. As mentioned in 3.4.2.6.4 MCF10A cells were dying from 6 hours on, so I analyzed the first 7 hours after stimulation with Okadaic acid. As shown in **Figure 48A** pretreatment with Gefitinib and 100pM TGFβ stimulation resulted in less SMAD2 accumulation into the nucleus, especially seen from 5 hours on. However, Gefitinib and Okadaic acid

0.75 hours pre 100pM TGFβ stimulation still revealed the known Gefitinib effect, which is particularly noticeable at 5 hours **(Figure 48B)**. In conclusion, using Okadaic acid I observed that inhibition of PP1 and PP2A phosphatases did not abrogate the modulated SMAD2 response due to inhibition of ERK signaling.

Figure 48

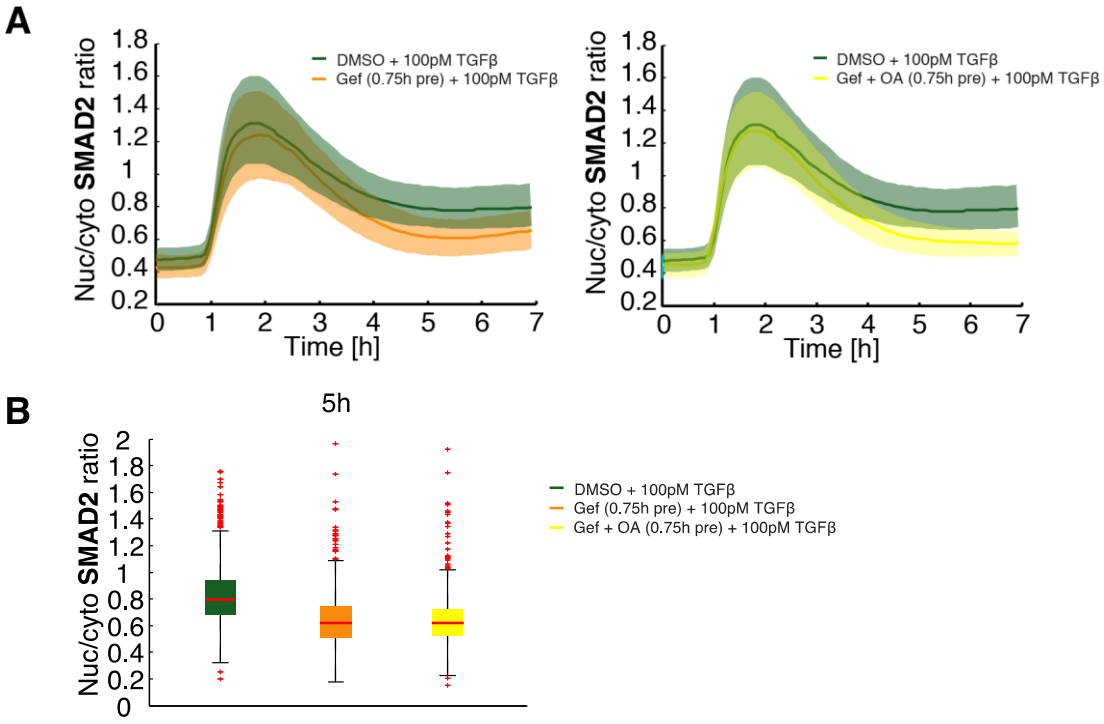

3.4.3.4.2 Figure 48. Inhibition of PP1 and PP2A does not alter the ERK effect on SMAD2.
A Median nuc/cyto SMAD2 ratio of the SMAD2-YFP reporter cells stimulated with 100pM TGFβ and 0.75h pretreated with Gefitinib and Okadaic acid (OA). Shaded area represent data between 25th and 75th percentiles.
B Nuc/cyto SMAD2 ratio of the SMAD2-YFP reporter cells stimulated with 100pM TGFβ and 0.75h pretreated with Gefitinib and Okadaic acid (OA) at 5h. Red lines indicate median; boxes include data between the 25th and 75th percentiles; whiskers extend to maximum values within 1.5× the interquartile range; crosses represent outliers.

3.4.3.4.3 Inhibition of PP2C abrogates the ERK effect on SMADs

Finally, I also investigated whether the phosphatase group PP2C interferes with ERK signaling to modulate the long-term dynamics of SMADs. Therefore, I pretreated the cells with 1µM Sanguinarine chloride and stimulated subsequently with 100pM TGFβ. As shown in **Figure 49A,** SMAD2 accumulated stronger into the nucleus with similar amplitude and less adaptation, as can be seen by the 5-hour value **(Figure 49C)**. And surprisingly treatment with Gefitinib and Sanguinarine chloride inhibitors and TGFβ abrogated the effect of inhibition of the ERK cascade on SMAD2 **(Figure 49B and C)**. In **Figure 49D** random Sanguinarine pretreated and TGFβ stimulated cells with and without Gefitinib are plotted. The effect of Gefitinib disappeared and all cells showed a strong SMAD2 response, independent of inhibition of ERK signaling. Also adding Sanguinarine 3 hours post to Gefitinib pretreated cells immediately enhanced the SMAD2 accumulation into the nucleus **(Figure 49E)**. Moreover, this also

applied to SMAD4, measured in the combined cell line E9, when the cells were treated with Sanguinarine chloride and Gefitinib **(Figure 49F)**. In addition, the question arose whether inhibition with Sanguinarine chloride affected the efficiency of gefitinib and therefore was the effect gone, since the PP2C family also acts on ERK signaling. To ensure that the inhibitor worked efficiently, I examined the phosphorylation status of the target protein ERK2 (pp42) by Western blot analysis. As shown in **Figure 49G**, I proved that the ERK cascade was also interrupted when treated with Sanguinarine and Gefitinib and ERKs remained unphosphorylated. Furthermore, the Western results confirmed that the Gefitinib effect disappeared and that SMAD2 was just as phosphorylated when treated with Sanguinarine and Gefitinib compared to just Sanguinarine treatment. In conclusion inhibition of PP2C abrogated the effect of inhibition of the ERK cascade on SMAD response and therefore a PP2C family member is involved in the ERK- SMAD-crosstalk, but the link between ERK signaling and the phosphatase remain unclear.

Figure 49

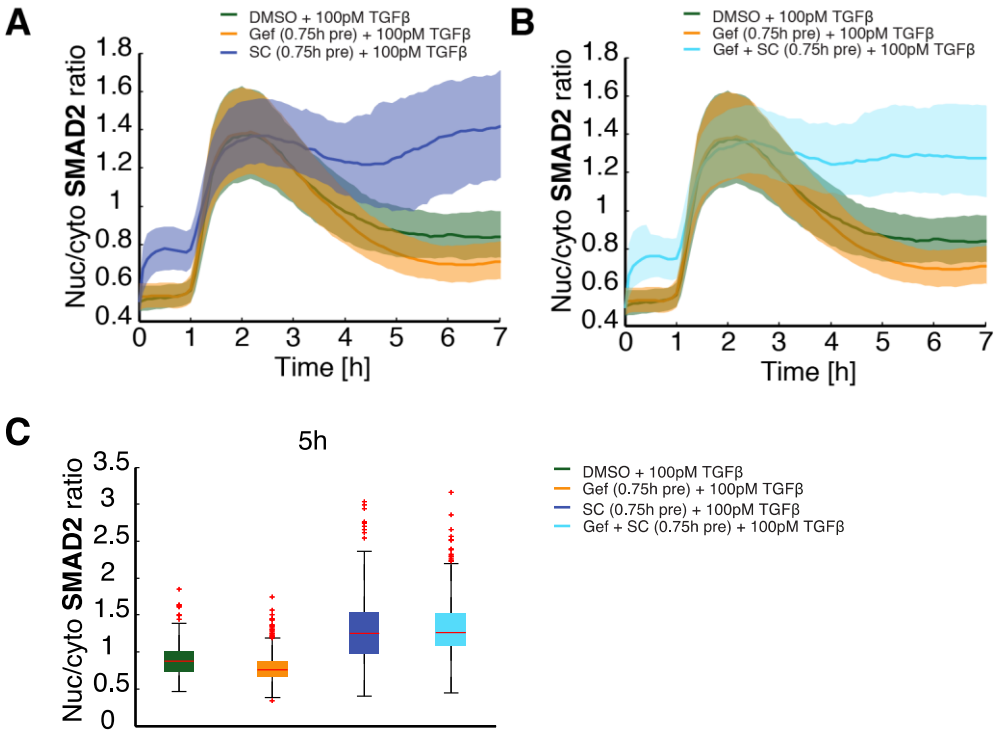

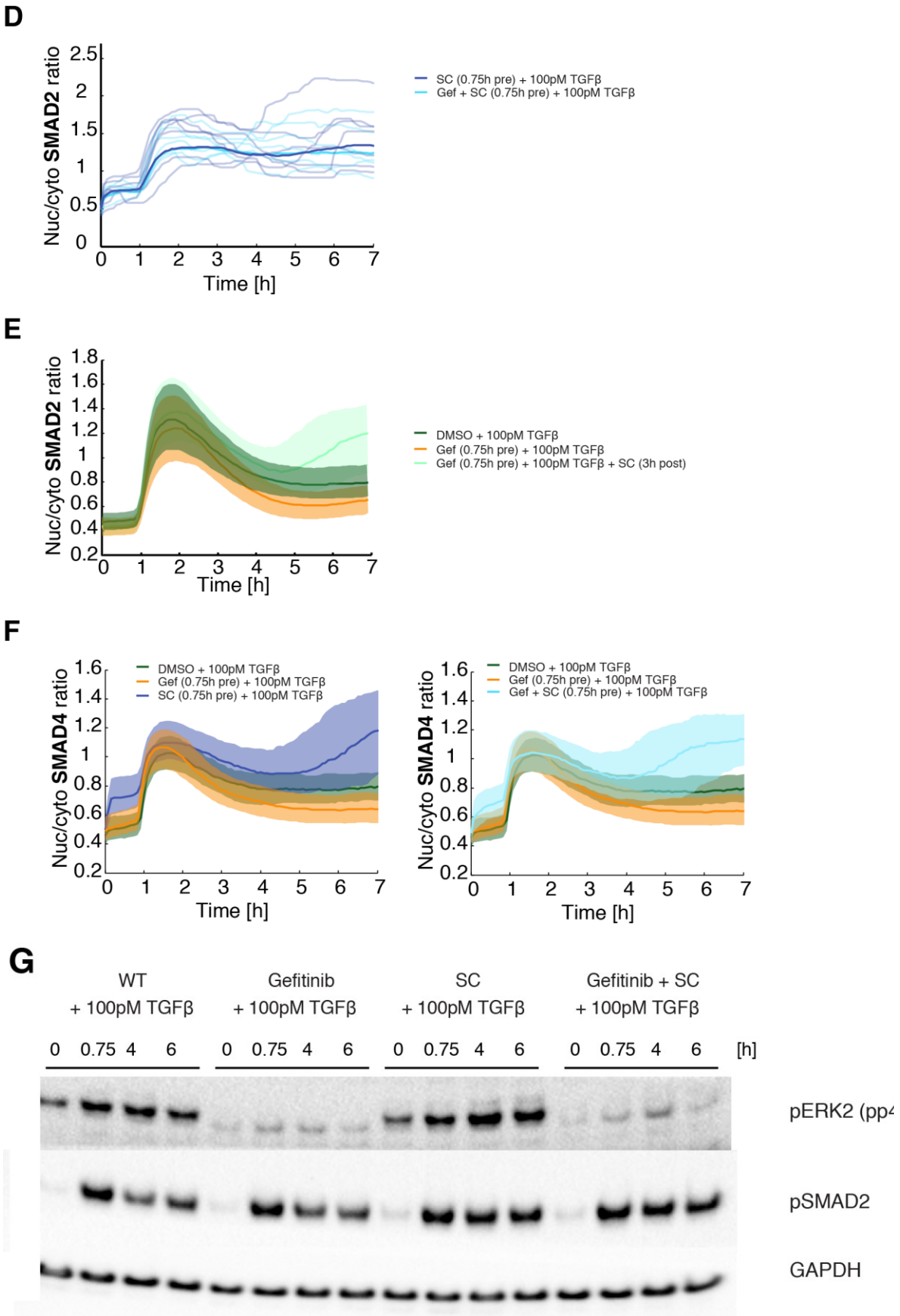

3.4.3.4.3 Figure 49. Inhibition of PP2C abrogates the ERK effect on SMADs.
A Median nuc/cyto SMAD2 ratio of the SMAD2-YFP reporter cells stimulated with 100pM TGFβ and 0.75h pretreated with Gefitinib or Sanguinarine chloride (SC). Shaded area represent data between 25th and 75th percentiles.

B Median nuc/cyto SMAD2 ratio of the SMAD2-YFP reporter cells stimulated with 100pM TGFβ and 0.75h pretreated with Gefitinib and Sanguinarine chloride (SC). Shaded area represent data between 25th and 75th percentiles.
C Nuc/cyto SMAD2 ratio of the SMAD2-YFP reporter cells stimulated with 100pM TGFβ and 0.75h pretreated with Gefitinib and/or Sanguinarine chloride (SC). Red lines indicate median; boxes include data between the 25th and 75th percentiles; whiskers extend to maximum values within 1.5× the interquartile range; crosses represent outliers.
D Exemplary individual nuc/cyto SMAD2 ratio trajectories (thin lines) for the SMAD2-YFP reporter cells stimulated with 100pM TGFβ and 0.75h pretreated with Gefitinib and/or Sanguinarine chloride (SC) compared to the median nuc/cyto SMAD2 ratio of the entire population (thick line).
E Median nuc/cyto SMAD2 ratio of the SMAD2-YFP reporter cells stimulated with 100pM TGFβ and 0.75h pretreated with Gefitinib and 3h post with Sanguinarine chloride (SC). Shaded area represent data between 25th and 75th percentiles.
F Median nuc/cyto SMAD4 ratio of the SMAD4-YFP reporter cells stimulated with 100pM TGFβ and 0.75h pretreated with Gefitinib and/or Sanguinarine chloride (SC). Shaded area represent data between 25th and 75th percentiles.
G Western blot analysis of phosphorylated ERK2 and phosphorylated SMAD2 in MCF10A WT cells stimulated with 100pM TGFβ and 0.75h pretreated with Gefitinib and/or Sanguinarine chloride (SC). GAPDH was used as a loading control.

3.4.3.4.4 PPM1A is probably involved in the ERK-mediated TGFβ response

As explained in 3.4.2.6.6, PPM1A (PP2Cα) is a PP2C family member and plays a critical role in terminating TGFβ signaling through direct dephosphorylation of SMAD2/SMAD3 (Lin *et al*, 2006). Furthermore, PPM1A negatively regulates ERK through direct dephosphorylation of pThr202 (Li *et al*, 2013). Thus, to understand the mechanism of how ERK signaling is possibly linked to PPM1A influencing the long-term dynamics of SMADs, I knocked down PPM1A in time-lapse microscopy experiments as I did for the p38 inhibitor experiments (3.4.2.6.6). Therefore, I also transfected the SMAD2 reporter cell line 48h prior to TGFβ treatment with PPM1A siRNA. The Gefitinib effect was clearly visible in the control conditions and SMAD2 translocated from the nucleus back to the cytoplasm after the first response due to gefitinib inhibition **(Figure 50A, B and C).** Interestingly, after PPM1A siRNA transfection and gefitinib inhibition, the gefitinib effect was barely recognizable at the nuclear level and in the ratio and vanished for the cytoplasmic levels **(Figure 50D, E and F).** To gather evidence that PPM1A was involved in the ERK-mediated TGFβ response, I clustered on the first 45 minutes of the cytoplasmic response to separate cells with a very good PPM1A knock down from those with worse or none knock down **(Figure 50G)**. Subsequently, I considered only the cells of cluster 1, that represented a weak knock down, and cells of cluster 5 and 6, which represented a very good PPM1A knock down **(Figure 50H and Appendix Figure A35)**. Presenting the nuclear levels of all cells from cluster 1, the gefitinib effect was recognizable in the control cells and in the PPM1A siRNA-treated cells **(Figure 50I & J)**. Interestingly, the Gefitinib effect was recognizable only in the control cells from clusters 5 and 6, and PPM1AsiRNA and Gefitinib-treated cells showed the same or even stronger response after TGFβ addition **(Figure 50K & L).** This means that without PPM1A the Gefitinib effect disappeared and thus late SMAD2 nuclear translocation was PPM1A-dependent. Therefore, I continued to study the expression of PPM1A in RT-PCR experiments after Gefitinib and 100pM TGFβ treatment in WT cells. Gefitinib slightly increased the expression of PPM1A **(Figure 50M)**. However, this was only slightly reflected in Western experiments, and the PPM1A level was only mildly elevated

by Gefitinib **(Figure 50N)**. Therefore, modifications of PPM1A must be investigated in further experiments.

Figure 50

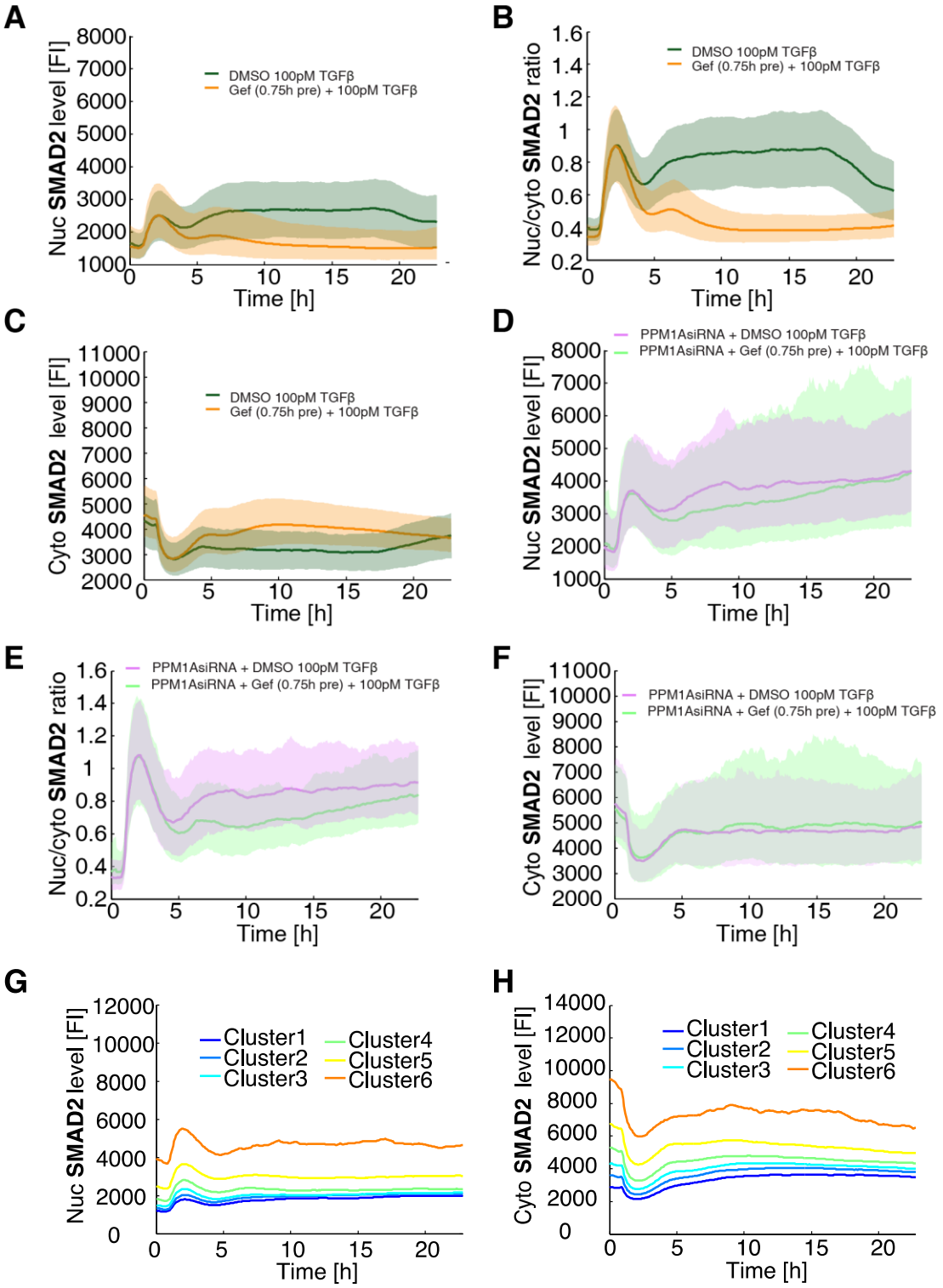

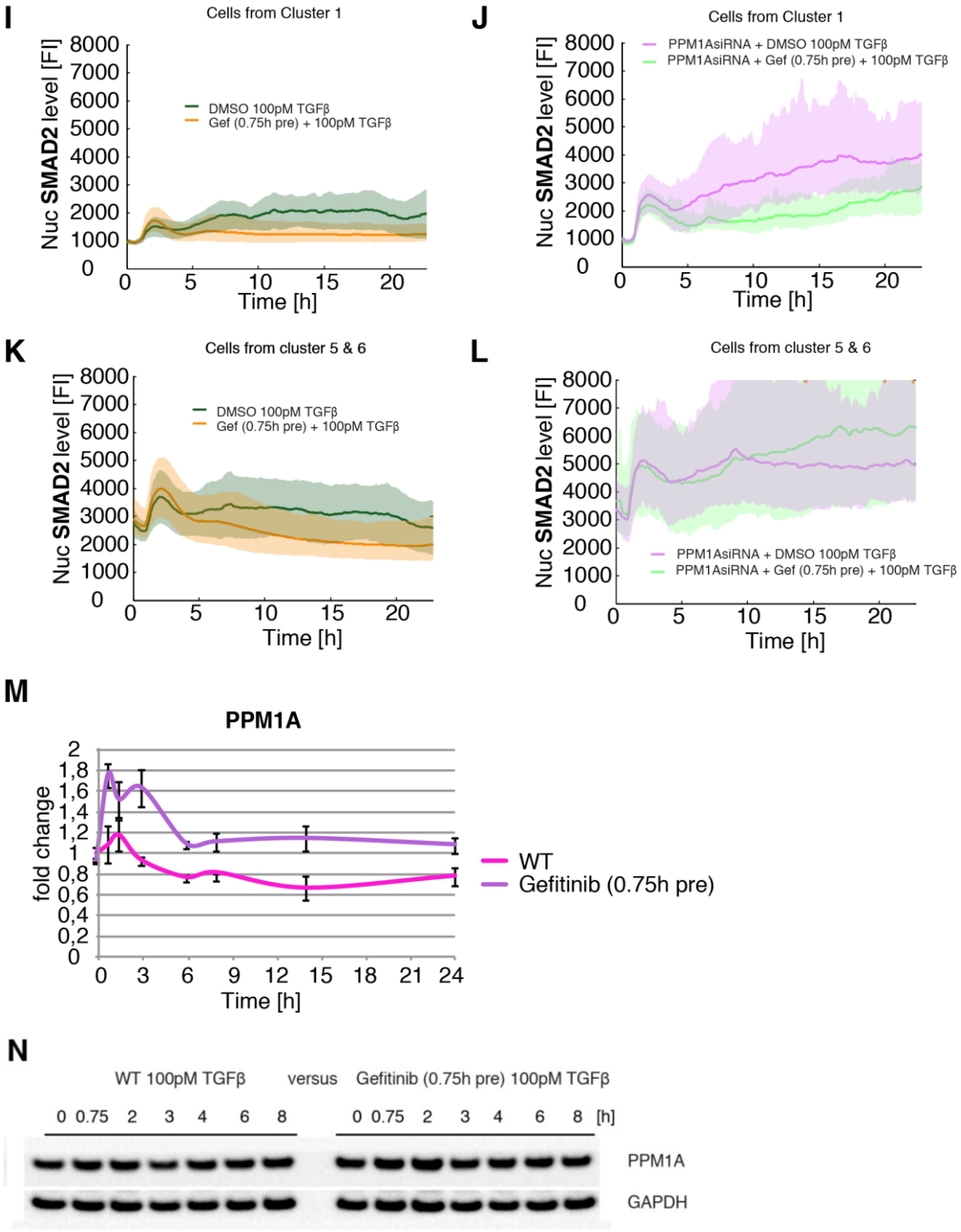

3.4.3.4.4 Figure 50. PPM1A is probably involved in the ERK-mediated TGFβ response.
A Median nuclear SMAD2 level of the SMAD2-YFP reporter cells seeded 3 days prior to 100pM TGFβ stimulation and 0.75h pretreated with Gefitinib. Shaded area represent data between 25th and 75th percentiles.
B Median nuc/cyto SMAD2 ratio of the SMAD2-YFP reporter cells seeded 3 days prior to 100pM TGFβ stimulation and 0.75h pretreated with Gefitinib. Shaded area represent data between 25th and 75th percentiles.
C Median cytoplasmic SMAD2 level of the SMAD2-YFP reporter cells seeded 3 days prior to 100pM TGFβ stimulation and 0.75h pretreated with Gefitinib. Shaded area represent data between 25th and 75th percentiles.
D Median nuclear SMAD2 level of the SMAD2-YFP reporter cells seeded 3 days prior and transfected 48h prior to 100pM TGFβ treatment with PPM1A siRNA and 0.75h pretreated with Gefitinib. Shaded area represent data between 25th and 75th percentiles.

E Median nuc/cyto SMAD2 ratio of the SMAD2-YFP reporter cells seeded 3 days prior and transfected 48h prior to 100pM TGFβ treatment with PPM1A siRNA and 0.75h pretreated with Gefitinib. Shaded area represent data between 25th and 75th percentiles.
F Median cytoplasmic SMAD2 level of the SMAD2-YFP reporter cells seeded 3 days prior and transfected 48h prior to 100pM TGFβ treatment with PPM1A siRNA and 0.75h pretreated with Gefitinib. Shaded area represent data between 25th and 75th percentiles.
G Clustering on the first 45 minutes of the cytoplasmic SMAD2 level of the SMAD2-YFP reporter cells seeded 3 days prior and transfected 48h prior to 100pM TGFβ treatment with PPM1A siRNA and 0.75h pretreated with Gefitinib to separate cells with a very good PPM1A knock down from those with worse or none knock down. Individual cells were clustered into six cluster and the corresponding median nuclear SMAD2 level over 24h is shown.
H Individual cells were clustered into six cluster (Figure 50 G) and the corresponding median cytoplasmic SMAD2 level over 24h is shown.
I Median nuclear SMAD2 level of cells from Cluster 1 seeded 3 days prior 100pM TGFβ treatment and 0.75h pretreated with Gefitinib.
J Median nuclear SMAD2 level of cells from Cluster 1 seeded 3 days prior and transfected 48h prior to 100pM TGFβ treatment with PPM1A siRNA and 0.75h pretreated with Gefitinib.
K Median nuclear SMAD2 level of cells from Cluster 5 and 6 seeded 3 days prior 100pM TGFβ treatment and 0.75h pretreated with Gefitinib.
L Median nuclear SMAD2 level of cells from Cluster 5 and 6 seeded 3 days prior and transfected 48h prior to 100pM TGFβ treatment with PPM1A siRNA and 0.75h pretreated with Gefitinib.
M Expression of PPM1A at indicated time points of MCF10A WT cells transfected 48h prior to 100pM TGFβ treatment with PPM1A siRNA and 0.75h pretreated with Gefitinib. β-Actin was used as an internal control. Error bars indicate standard deviation of technical triplicates.
N Western blot analysis of PPM1A in MCF10A WT cells stimulated with 100pM TGFβ and 0.75h pretreated with Gefitinib. GAPDH was used as a loading control.

4 DISCUSSION

4.1 Dynamics and variability of SMAD signaling in single cells

The TGFβ pathway is a multi-functional signaling system regulating many fundamental cellular and developmental processes, including cell cycle arrest, differentiation, morphogenesis and apoptosis, as well as cancer progression (Massagué, 1998; Whitman, 1998, Piek *et al*, 1999, Siegel & Massagué, 2003). The underlying mechanisms of these wide range of physiological effects to TGFβ have not been elucidated in detail. Since there has been growing evidence that the temporal dynamics of SMAD proteins are important for their functioning (Schmierer *et al*, 2008, Warmflash *et al,* 2012), I focused specifically on how the strength of the extracellular input is encoded in temporal patterns of SMADs. Moreover, I explored how signaling dynamics influence cellular outcomes and how specific dynamical patterns are both shaped and interpreted by the structure of molecular networks. In this context, I emphasized regulatory and adaptive mechanisms as well as cross-talk with non-canonical signaling pathways.

In this thesis, I provided a quantitative understanding of how cells encode and decode information about the identity and quantity of a TGFβ stimulus. I investigated SMAD2 and SMAD4 dynamics and followed pathway activation at the single-cell level by monitoring the translocation of SMADs from the cytoplasm to the nucleus with high temporal and spatial resolution, by combining fluorescent reporter cell lines with live-cell microscopy and automated image analysis. Specifically, I established stable clonal reporter cell lines for SMAD2 and SMAD4. Initially SMADs were predominantly located in the cytoplasm, followed by strong accumulation into the nucleus after TGFβ treatment until the regulatory and adaptation mechanisms stopped the pathway activation and SMADs shuttled back to the cytoplasm.

Clarke *et al* reported that cells respond to the absolute number of bioavailable TGFβ molecules in their environment. They developed a bioassay that enables them to count precisely the number of bioactive TGFβ molecules present in the medium (Clarke *et al*, 2009). Ligand molecules per cell is the input variable to which the cells respond, and ligand number per cell is the best predictor of signaling responses (Zi and Klipp, 2007a; Clarke *et al*, 2009). Like the majority of published studies we did the experiments with concentrations, but left other conditions like growth area, cell number, culturing time before stimulation, etc. the same. Additionally, we only compared results between conditions of the experiment and always used internal controls. The TGFβ pathway is a particularly interesting system for testing for fold-change detection and thus consider also the basal level because it is known that the expression levels of its components vary considerably from cell to cell (Zieba *et al*, 2012).

However, the average response of our single-cell measurements match with biochemical analyses in previous studies (Inman *et al*, 2002b; Clarke *et al*, 2009; Zi *et al*, 2011; Vizán *et al*, 2013). Currently CRISPR/ Cas9-mediated gene knock-in would be used to prevent any influence of SMAD overexpression in our reporter cells. However, validation experiments showed comparable dynamics of endogenous and tagged proteins and our system did not alter the cellular response to TGFβ stimulus. Therefore the SMAD2 and SMAD4 reporter faithfully represents the activity of the pathway. Moreover, as expected the TGFβ response of the reporter cell lines was at all time points receptor-dependent and corresponded with studies using the inhibitor SB431542 (Inman *et al*, 2002a). The authors showed that inhibiting the pathway at the receptor level causes export of both R-SMADs and SMAD4 (Inman *et al*, 2002a).

Furthermore, the average SMAD2 and SMAD4 dynamics in MCF10A cells were TGFβ dose dependent, since I observed that a decrease in the TGFβ concentration lowered the peak amplitude, rendered signaling more transient and led to rapid adaptation to the pre-stimulus level. This is consistent with experimental and modeling analyses that showed that SMAD signal amplitude gradually increases with the increments of TGFβ doses (Chung *et al*, 2009; Melke *et al*, 2006; Goumans *et al*, 2002). More in detail, Zi *et al* showed that TGFβ signaling responses display different sensitivities to ligand doses at different time scales (Zi *et al*, 2011). Modeling simulations and experimental results showed that while short-term P-SMAD2 is graded, long-term P-SMAD2 response is switch-like to changes in TGFβ doses, since a small change of TGFβ dose within a certain range results in a large change in P-SMAD2 response. In contrast to other signaling pathways such as NF-κB that display binary on/off responses (Tay *et al*, 2010) the TGFβ response was graded. The linear relationship between receptor activity and nuclear ERK activity is lost during several enzymatic amplification steps, also ERK signaling can elicit a binary, switch-like response. It seems that the ERK activation amplitude is a non-linear function of active EGF-receptor levels (Schoeberl *et al*, 2002). Obviously, the kinetic pathways of ERK signaling and SMAD signaling have differing properties. ERK signaling peaks very sharp and fades within an hour (Schmierer & Hill, 2007). Nevertheless, long-term response of ERK signaling has been reported in MCF10A cells (Albeck *et al*, 2013).

By analyzing the median nuc/cyto SMAD2 and SMAD4 ratio of the cell population, one synchronous initial response of SMAD translocation at 1h, followed by adaptation and a second signaling phase with temporally less defined periods of nuclear translocation could be monitored. However, our results conflict with a previous study in single cells that reported a different behavior of SMAD2 nuclear accumulation upon TGFβ stimulation using a clonal cell line of mouse myoblast C2C12 cells stably expressing an RFP-SMAD2 fusion protein (Warmflash *et al*, 2012). SMAD4 reveals similar results. The response to ligand was detectable within 10 min and peaked at 1–2 h, followed by adaptation. But,

Warmflash *et al* observed sustained SMAD2 accumulation, since SMAD2 exhibits stable nuclear accumulation upon continuous TGFβ1 stimulation without early adaptation. In addition to cell-type differences, a noticeable distinction in the experimental setup that may explain the contrasting results is the higher level of overexpression of tagged SMAD2 in the previous study (> 2× vs. 0.5× compared to endogenous levels) (Strasen *et al*, 2018). Furthermore, the reported cells were analyzed only 10 -12 hours by live cell imaging. In addition, this data also contradicts their data shown in the Western Blot, where clearly a peak at 1h and subsequent adaptation was shown. Furthermore, only a few timepoints in immunofluorescence were shown, and especially the time points after the peak were omitted. Their model postulates that the duration of SMAD4 nuclear localization is independent of that for R-SMADs and the model in which activated, nuclear-localized R-SMADs are synonymous with pathway activation need to be refined. My results, which are backed up by additional studies from the literature, point in another direction. The prevailing model is that R-SMADs carry pathway information with SMAD4 mirroring their activity (Schmierer & Hill, 2005; Liu *et al*, 1997). Nevertheless, future studies should include more cell lines to exclude cell type specific differences. A recent study using proximity ligation assay in fixed cells revealed that the levels of SMAD3/4 and SMAD2/4 complexes vary by more than 40-fold across cells (Zieba *et al*, 2012). Moreover I showed that SMAD2 and SMAD4 dynamics were coupled and co-regulated using fluorescent reporter cell lines simultaneously visualizing the response of both SMADs.

Moreover, as published, R-SMAD phosphorylation is necessary for the nuclear accumulation and transcriptional activity of both the R-SMADs and SMAD4 (Schmierer & Hill, 2005; Liu *et al*, 1997). I could show that the expression of TGFβ target genes were dose-dependent like the median response in the time-lapse data. While the first peak of target genes appeared to be strongly TGFβ concentration-dependent in a graded manner, the enhanced induction with increasing TGFβ concentration at later time points slightly diminished over time. Thus, target gene expression 24h after the 100pM TGFβ stimuli showed clear differences in comparison to lower doses. In particular PAI-1 represented a more switch-like behavior. However, Warmflash *et al* also examined the kinetics of endogenous target gene expression by qRT-PCR in unmodified C2C12 cells. The response of all three target genes they studied was transient, rising over the first 2 h after stimulation and returning to baseline within 4–6 h. But they have only looked at the first 12 hours and PAI1, SMAD7 and TIEG in my experiments were well above baseline at 14h and 24h with high TGFβ concentrations. Zi *et al* supports my results since they also found that the short-term SMAD7 gene expression is graded and induction of PAI-1 expression by TGFβ is considerably delayed and can be measured at 24 h post TGFβ treatment and is switch- like (Zi *et al*, 2011). However, a general switch-like response for TGFβ induced long-term gene expression should be validated carefully with further concentrations in between and more target

genes in future experiments. In addition, I observed that target genes were not only TGFβ quantity but also stimulation period dependent. Cells reacted to the current TGFβ state and needed long-term stimulation and continued SMAD signaling to achieve full target gene transcription 24 hours post TGFβ. Many studies focused on signaling responses to continuous TGFβ stimulations, thus little is known about cell responses to short pulses of TGFβ stimulations. Zi *et al* showed in model simulations that short-term TGF-β pulse stimulation results in transient P-Smad2, whereas serial pulses result in sustained P-Smad2, similar to that seen with continuous stimulation (Zi *et al*, 2011). The functional significance of pulses of TGFβ has yet to be shown *in vivo*, but is theoretically occurring within tissues, where the extracellular volume and local secretion of TGFβ is extremely small in magnitude, resulting in a largely noisy extracellular level of TGFβ (Zi *et al,* 2012).

However, median trajectories only monitor average dynamics across the population. Analysis of the SMAD2 and SMAD4 reporter cell lines revealed, that the extent and duration of SMAD nuclear accumulation was highly variable and cells showed a broad variability of dynamics, although they were genetically identical. These complex and heterogeneous dynamics were not limited to saturating TGFβ concentrations, as I also noticed pronounced variability when treating the cells with lower ligand concentrations. Likewise, Warmflash *et al* observed that in low-density cultures, nuclear localization of SMADs was heterogeneous, treatment with TGFβ1 did not synchronize the cells and SMAD4 remained heterogeneous. Zi *et al* questioned whether there are oscillations in TGFβ network because no oscillations of TGFβ signaling have yet been observed in cells (Zi *et al*, 2012). Averaging signaling dynamics at cell population levels can mask dynamic signaling mechanisms within individual cells (Spiller *et al*, 2010). The suspected oscillatory responses may appear at the single cell level in a variety of cell lines and culture conditions upon TGFβ stimulation. Oscillations of signaling responses have been observed in some pathways with negative feedbacks, for example, NF-κB, p53 and ERK systems (Shankaran *et al*, 2009; Hoffmann *et al*, 2002; Geva-Zatorsky *et al*, 2006). However, only few examples showed oscillatory SMAD dynamics in MCF10A cells. One reason could be that the negative feedback regulations of TGFβ network may not be strong enough at the endogenous level. Moreover, the time-delay between negative feedback and SMAD activation might not be coupled in a proper time scale (Zi *et al*, 2012).

In collaboration with Marcel Jentsch I extracted single cell features to analyze the complex heterogeneous dynamics in detail. We detected features that are robust, change in a dose and time dependent manner, and those that vary across individual cells. Mainly the length of the first increase was robust over all conditions, as well as the time of the maximum amplitude. However, the maximum amplitude increased with rising TGFβ concentrations and showed saturation for 25pM ligand concentration. Furthermore, the mean ratio value 5 hours after the first response increased until 25pM

TGFβ and only for 100pM TGFβ was the final value 24 hours of imaging significantly above the basal level. Interestingly, almost all SMAD2 reporter cells treated with 5pM - 100pM TGFβ ligand reacted to the stimulus, which underlines that it is not a binary on/ off system and cells sensitively respond to extracellular TGFβ concentration with SMAD specific dynamics. The variability in the level of SMAD proteins from cell to cell raises the question as to how cells and tissue can reliably sense information about their external environment through the TGFβ pathway (Frick *et al*, 2017). Some of the ideas that have been proposed are integration of responses from multiple signaling pathways (Cheong *et al*, 2011), compensate via cross-talk with other pathways (Uda *et al*, 2013), average responses across neighboring cells (Cheong *et al*, 2011), use negative feedbacks (Voliotis *et al*, 2014), or measuring signal dynamics (Selimkhanov *et al*, 2014) and interpreting signaling relative to background by detecting fold changes (Goentoro *et al*, 2009). Indeed, Frick *et al*, analyzed the response distributions across doses and found that measuring fold change in SMAD3 confers higher information transduction capacity to the TGFβ pathway. The fact that the fold change relative to background is the driving factor here also means that a high level of nuclear Smad complex alone does not necessarily indicate a high level of signaling. This finding may have implications for understanding the context-dependent outcomes of the TGFβ pathway (Frick *et al*, 2017). However, displaying the absolute nuc/cyto ratio fluorescent intensities revealed stable dynamics.

To understand how phenotypic responses and cell fates of TGFβ signaling can be specifically encoded by SMAD dynamics we used a clustering approach to achieve a better separation in more homogenous groups. Marcel Jentsch established a method based on dynamic time warping as a tool for non-linear alignment of time series data. Cells were re-sorted in six clusters of signaling classes according to their dynamic behavior, which provided a better separation than sorting to different TGFβ ligand concentration. Although signaling classes represented mathematically identifiable clusters of time courses, it is important to note that SMAD dynamics in each class were not sharp but rather gradual (Strasen *et al*, 2018). The definition of six classes is a heuristic choice to classify the observed heterogeneity. In future studies, it may be interesting to use other approaches established in the context of single-cell sequencing such as diffusion maps to reduce dimensionality of their high-dimensional observations (Haghverdi *et al*, 2016). Interestingly, a recent study proposed that the response of MCF10A cells to extracellular ATP can be similarly grouped in three classes corresponding to distinct cellular states (Yao *et al*, 2016). Moreover, phenotypic responses and cell fate decisions were correlated with signaling classes of distinct dynamic behavior. Interestingly, this data suggests that migration and proliferation may be controlled by different aspects of the dynamical SMAD signaling response. Migration tended to be affected by a transient peak of SMAD translocation, whereas the anti-proliferative effects seemed to require sustained SMAD signaling. It needs to be

highlighted that a clear shift to migration, EMT and cell cycle arrest required a strong and sustained second signaling phase rather than a high first amplitude. Therefore, signaling classes of distinct long-term dynamic behavior determine the cell fate. Thus, cells are able to translate various dynamics of the same signaling molecule into specific outcomes.

Previous studies indicated that cellular responses to TGFβ superfamily ligands depend on the quantity to which the cells are exposed. In development, TGFβ superfamily members form morphogen gradients to determine the fates of cells (Rogers and Schier, 2011). Cells read the TGFβ concentration with high precision, as they can distinguish subtle differences in the concentration gradients and orchestrate different cell fates (Green *et al*, 1992). Strict regulation of the duration and strength of the morphogenic signal itself, but also of the response evoked, are key for embryonic pattern formation (Schmierer & Hill, 2007). In addition to its role in development, TGFβ is dysregulated in a variety of cancers (Padua & Massagué, 2009), and the timing of signaling also plays an important role. For example, TGFβ is transiently upregulated in metastasizing breast cancer cells (Giampieri *et al*, 2009) and consistent with our findings, transient SMAD activation in cancer cell lines was sufficient to alter cellular motility and induce EMT–like processes, while sustained signaling was required to influence proliferation (Nicola´ s & Hill, 2003; Giampieri *et al*, 2009). Moreover, Zi *et al* found that most cell fate decisions regulated by TGFβ-related molecules are switch-like and irreversible (e.g. cell differentiation and apoptosis) (Zi *et al*, 2011). Some of the most common and well-characterized 'all-or-none' responses are found in the mitotic trigger and the MAP kinase signaling cascade during Xenopus oocyte maturation (Ferrell, 2008). Positive and double negative feedback loops are critical for the irreversible switch of these processes (Ferrell, 2008).

Interestingly, He *et al* identified TIF1g, also known as Ectodermin, as a transcriptional partner of activated R-SMADs in competition with SMAD4 (He *et al*, 2006). Whereas the R-SMAD/TIF1g complex stimulates erythrocyte differentiation, the R-SMAD/SMAD4 complex inhibits hematopoietic stem cell proliferation. Thus, the balance between R-SMAD/TIF1g- and R-SMAD/ SMAD4-mediated TGFβ signaling in hematopoietic stem cells is critical for cell fate. TIF1g acts as an inhibitor of SMAD4 function by inducing ubiquitin-induced SMAD4 degradation (Dupont *et al*, 2005).

Furthermore, the role of the transcription factor SMAD3 and its complex binding with SMAD4 is unclear. Although structurally similar, SMAD2 and SMAD3 affect distinct genes (Brown *et al*, 2007), and it is also known that SMAD3 can bind directly to DNA, whereas the predominant isoform of SMAD2 does not (Gaarenstroom *et al*, 2014).

Dynamic information encoding thus may be conserved from the level of cell lines to the level of heterogeneous single-cell signaling. It reflects regulatory potential of the pathway: The sensitivity to TGFβ inputs of individual cells can be adjusted within tissue (Strasen *et al*, 2018).

A better understanding of how signaling dynamics are regulated and how they affect cellular responses may provide new insights for manipulating them in a controlled way, like modulating the levels or enzymatic activities of selected proteins to switch the response from EMT-like processes to proliferation control. In turn, this may enable new pharmacological strategies for altering cell fate in cancer therapies.

However, changes in downstream responses are not just triggered by dynamics, but by a combination of additional factors such as posttranslational modifications, spatial localization or identity and strength of other pathway components. Thus, dynamics represent only one layer of regulation within a complex signaling response that leads to different cellular outcomes. In fact, different dynamical patterns arise because of differences in network structure or the kinetics of individual molecular interactions (Purvis & Lahav, 2013).

When considering the functional role of dynamics, the question how cell fate is encoded in these different dynamical patterns arises. Identifying the mechanisms that are necessary to detect time-dependent features and translate these patterns into distinct phenotypic responses remains one of the most challenging goals for the field.

For example, ERK dynamics are decoded by a finely tuned spatiotemporal network controlling cell fate decisions with a persistence detector for the duration of ERK activation. Thus, when ERK activation is transient, gene products such as c-Fos are induced but then undergo rapid degradation. When ERK levels are persistent, however, newly synthesized c-Fos is directly phosphorylated by the still-active kinase, which stabilizes c-Fos in the nucleus (Purvis & Lahav, 2013, Murphy *et al*, 2002, 2004).

Decoding mechanisms promise to provide critical answers about the function of temporal signals because they represent the link between signal patterns and functional cellular outcome (Behar and Hoffmann, 2010). In order to gain a better understanding of the decoding of SMAD dynamics on the RNA level, I correlated the single-cell target gene expression of PAI- 1 with single- cell SMAD signaling by combining 3 hours and 14 hours live- cell imaging of the SMAD2- reporter cell line stimulated with 25pM TGFβ with subsequent smFISH. First of all, the absolute RNA counts per cell at basal level, 3 hours and 14 hours post TGFβ stimulation showed pronounced cell-to- cell variability. The heterogeneous SMAD2 dynamics were not correlated with PAI-1 expression 3 hours post stimulation. However, considering 14 hours of individual SMAD signaling, I observed correlation of long-term SMAD2 dynamics to the PAI-1 target gene expression. This fits with experimental and computational population studies by Zi *et al.* They showed a switch- like long-term PAI-1 gene expression connected with long-term growth inhibitory response (Zi *et al*, 2011). To determine how different dynamics of the same molecule are interpreted by downstream components, a detailed analysis of the dynamic features is necessary. Also Frick *et al* observed variability in the mRNA expression of the target genes,

which may be due to variability in cell size, chromatin state, cell-cycle phase, other extrinsic variables, or stochastic noise. Using also smFISH, they observed that expression of SMAD3 target genes (*ctgf, snai1*, and *wnt9a*) correlated more strongly with the fold change, rather than the level, of nuclear SMAD3. They suspected some target genes sense SMAD3 levels relative to background, as a strategy for coping with cellular noise. However, no features of long-term dynamics were evaluated. Moreover, Hill and Levy identified in large-scale microarray analysis two populations of TGFβ- target genes that are distinguished by their dependency on SMAD4, since some genes absolutely require SMAD4 for their regulation, while others do not. Functional analysis also indicates a differential SMAD4 requirement for TGFβ -induced cell fates. Moreover, the intrinsic DNA affinity of SMADs is relatively low and SMADs themselves are not sufficient to drive transcription. They require other DNA-binding transcription factors to efficiently bind to promoters and recruit transcriptional co-activators. Thus, interfering with SMAD–DNA binding or the recruitment of co-activators or co-repressors has an effect on specific SMAD-induced gene responses. For example, SMAD partner C/EBPb plays a critical role in TGFβ-induced activation of cell cycle inhibitor p15INK4b promoter, a pivotal target gene in the cytostatic response to TGFβ (Itoh & ten Dijke, 2007).

My results demonstrate that SMAD dynamics play a functional role in driving cellular responses, but further research is needed to answer the question of how dynamics are interpreted at the molecular level.

4.2 Regulatory and adaption mechanisms

In the next step I investigated how dynamics are regulated and analyzed what molecular mechanisms give rise to specific dynamical patterns. I studied the dynamics of signaling molecules by inhibiting key components through either small molecule inhibitors or genetic manipulation. Through these perturbation experiments I showed several molecular mechanisms that contribute to the observed dynamics.

I investigated how complete adaptation of the signaling pathway is connected to TGFβ ligand depletion by cellular uptake and lysosomal degradation. By measuring extracellular TGFβ ligand concentration, we concluded that the full ligand depletion mainly affected signaling termination in time-lapse imaging experiments. As long as extracellular TGFβ was present, SMADs accumulated into the nucleus. Computational analyzes by Zi *et al* indicated that the half-life of TGFβ in the medium was also dose dependent. The low doses of TGFβ stimulations had shorter half-lives and were depleted over time, resulting in very low levels of long-term cellular responses. On the other hand, when the TGFβ dose is above a certain threshold, the half-life of TGFβ in the medium is significantly increased and the TGFβ remaining in the medium after long time periods led to a saturated response (Zi *et al*, 2011). Indeed,

we found that the estimated ligand decay of an initial TGFβ concentration of 25pM was completed within 20 hours with a half-life of around 6 hours. These findings corresponded with the complete adaptation of the signaling pathway to basal pre-stimulation level in the microscopy experiments. Furthermore, cells stimulated with 100pM TGFβ revealed an extracellular ligand concentration of around 20pM after 24 hours, which corresponded to a half- life around 9 hours. This agreed with the non-complete adaptation to basal level for 100pM TGFβ stimulation within 24 hours. Interestingly, theoretical approaches found that ligand depletion speed is affected by LRC formation, which is proportional to the concentration of ligand and cell surface receptors. The rate of ligand depletion can be adjusted by varying the volume of the media while keeping the ratio of TGFβ molecule per cell constant (Zi *et al*, 2011). Their model simulation predicts that slowing down ligand depletion by increasing medium volume should decrease the ultrasensitivity of long-term P-SMAD2 dose response with 24h treatment. Their modeling and experimental analyses also suggest that ligand depletion is an important mechanism for terminating transient signaling and generating a long-term switch-like response, since the rate of ligand depletion controls the duration of SMAD2 phosphorylation (Zi *et al*, 2011). Also predominant hypothesized mechanisms for terminating the response are loss of SMAD2 function through negative feedback and phosphorylated SMAD2 degradation, promoted by secondary phosphorylation of SMAD2 in the nucleus (Alarcón *et al*, 2009, Itoh & ten Dijke, 2007). Receptors are downregulated at the cell surface in the presence of TGFβ (Wakefield *et al*, 1987, Zwaagstra *et al*, 1999). Receptors are constitutively degraded via the lysosomal and ubiquitin-proteosome pathways, depending on whether the receptors are internalized in clathrin-coated pits or caveolae (Di Guglielmo *et al*, 2003; Kavsak *et al*, 2000; Mitchell *et al*, 2004).

In accordance with our results that the complete adaptation is mainly due to ligand depletion, Clarke *et al* concluded that TGFβ depletion principally determines SMAD signal kinetics. TGFβRII defective, but not TGFβRI defective, cell lines lost their ability to deplete TGFβ from the medium, thus TGFβ depletion most likely occurs through TGFβRII-mediated endocytosis (Clarke *et al*, 2009). In this aspect, TGFβ degradation shares many similarities with EGF or TGFα (Reddy *et al*, 1996; Shankaran *et al*, 2009). The ligand-induced endocytosis does not merely serve as a mechanism for “down- regulation” of signaling, but also provides a mechanism whereby the receptor can continuously track the changes in the secretion of TGFβ by nearby cells.

Furthermore, negative feedback in a signal transduction cascade is one of the major mechanisms for desensitization of sustained ligand stimulation and generation of transient, sometimes oscillating signaling outputs (Brandman & Meyer, 2008). Negative feedback in the TGFβ superfamily signaling pathways is mediated by induction of the inhibitory SMADs (I-SMADs) SMAD6 and SMAD7, and is thought to function in signal termination. SMAD7, a TGFβ-inducible early response gene (Nakao *et al*,

1997; Hayashi *et al*, 1997), antagonizes TGFβ signaling through multiple mechanisms, both in the cytosol and the nucleus. Despite the complex mechanisms, the question remains what is the role of negative feedback loops in regulating TGFβ dynamics? I systematically investigated the role of feedback loops in shaping SMAD dynamics by combining smFISH of SMAD7 with time-lapse imaging of the SMAD2-reporter 1.5h and 14h post 100pM TGFβ stimulation. Obviously, the first peak amplitude of SMAD2 dynamics was correlated to the absolute RNA amount. Thus, early SMAD7 transcription reflected strongly SMAD2 signaling, but for long-term dynamics the correlation was not obvious. Further experiments are needed to get conclusive results. Finally, I showed that transcriptional negative feedback loops attenuated early adaptation, by blocking these feedbacks by the general transcription inhibitor DRB, which efficiently inhibits transcription at the early elongation stage by inhibiting CDK7, 8 and 9 kinases and preventing RNA polymerase II to proceed after initiation. The amplitude was increased and the TGFβ response was amplified, but nevertheless early adaptation took place. In conclusion these results indicate that transcriptional feedbacks like SMAD7 have an impact on the early adaptation of SMAD2 signaling, but other regulatory mechanisms are apparently involved since early adaptation was attenuated and not prevented. Moreover, Vizán *et al* showed that the TGFβ pathway fully attenuates even in the presence of protein synthesis inhibitors, such as cycloheximide indicating that the mechanism governing attenuation relies on proteins constitutively present in the cells before they receive the signal (Vizán *et al*, 2013; Pierreux *et al*, 2000).

This is in contrast to Warmflash *et al*, who showed that inhibiting protein synthesis decreased the duration of SMAD2 nuclear accumulation but prolonged SMAD4 nuclear accumulation without early adaptation. Therefore, they concluded that SMAD4 adaptation requires new protein synthesis, and transcriptional dynamics correlate with SMAD4 but not SMAD2 nuclear accumulation. Since I question the SMAD2 cell line from Warmflash *et al*, I would conclude that early adaptation is only limitedly depended on transcriptional negative feedback loops and other regulatory mechanisms are involved.

In order to investigate the role of the main transcriptional negative feedback regulator SMAD7 on the dynamics of SMAD2 more specifically, I generated a *SMAD7* CRISPR Cas9 knockout cell line. First, I made clonal cell lines and validated selected clones by determining the mutation state of the *SMAD7* gene locus. Fortunately, clone 12 showed a deletion on both alleles, leading to an open reading frame shift and an early stop codon and therefore to a complete *SMAD7* knock out.

Next, I determined how *SMAD7* knock out affects the SMAD2 dynamics measured by live cell imaging. The amplitude was significantly increased compared to the control cell line. In accordance with my DRB experiments, the early adaptation rose to a higher plateau level. Furthermore, the fraction of dividing cells was reduced and the movement over the period of 21 hours was increased. This confirmed that a strong sustained SMAD2 response shifted cells to migration, EMT and cell cycle arrest

and was regulated by the negative feedback regulator SMAD7. Thus, *SMAD7* knock out led not only to a stronger SMAD2 response, but also in case of PAI1 to an enhanced downstream response. Since the homozygous *SMAD7* CRISPR Cas9 knock out clone 12 had a sustained knock out with possible compensatory mechanisms, I investigated how a transient *SMAD7* knock out affected the SMAD2 dynamics.

In conclusion, the results were similar to clone 12, basal levels were increased, the amplitude of nuclear SMAD2 was not necessarily increased, but the early adaptation was weakened with a higher nuclear SMAD2 plateau level afterwards. Using Western blot experiments, I was able to confirm live cell imaging results. Interestingly, SMAD7 is affected by post-translational modifications, which could affect SMAD dynamics. SMAD7 interacts with the transcriptional co-activator p300, which can stimulate the acetylation of two lysine residues in the N-terminus of SMAD7, the same residues targeted by SMURF1-induced ubiquitination (Itoh & ten Dijke, 2007). Importantly, acetylation prevents SMAD7 ubiquitination and protects SMAD7 from degradation [ten Dijke & Hill, 2004]. Interestingly, post-translational modifications are reversible processes. Class 1 HDAC1 and class III histone deacetylase SIRT1 can reverse p300- mediated SMAD7 acetylation and thereby accelerate SMAD7 ubiquitination and degradation (Simonsson *et al*, 2005; Kume *et al*, 2007). The deubiquitinating enzyme UCH37/UCHL5 interacts with SMAD7 and counteracts the SMURF2-induced ubiquitination of TGFβ type I receptor (Wicks *et al*, 2005). As our experimental study was limited to SMAD7, it would be interesting to investigate the contribution of the remaining negative feedbacks on SMAD dynamics.

Furthermore, TGFβ binding to its receptors initiates the degradation of several key components of the signaling pathway. The degradation of these components, including both positive and negative transducers, is mediated by the ubiquitin-proteasome system. Inhibition of the proteasome activity controls the levels of SMADs posttranslationally and modulates TGFβ signaling in a time-dependent and gene-specific manner (Zi *et al*, 2012).

R-SMADs have been found to be ubiquitinated and targeted for proteasomal degradation by various classes of ubiquitin ligases (Itoh & ten Dijke, 2007). This ensures low basal levels of non- activated SMADs, thereby decreasing cellular competence to sense TGFβ family members. Degradation of activated SMADs leads to attenuation or termination of signaling responses. The HECT family E3 ubiquitin ligases, SMURF1 and SMURF2, antagonize TGFβ family signaling by interacting with R-SMADs and targeting them for degradation (Arora & Warrior, 2001). While SMURF1 specifically targets SMAD1/5, thereby affecting BMP responses, whereas SMURF2 interacts more broadly with different R-SMADs, allowing interference with BMP and TGFβ signaling (Zhu *et al*, 1999; Arora & Warrior, 2001; Zhang *et al*, 2001; Bonni *et al*, 2001, Izzi *et al*, 2004). Interestingly, while SMURF2 binds to both SMAD2

and 3, it does not degrade SMAD3 (Lin *et al*, 2000), instead it induces the degradation of proteins such as SnoN that interact with the SMAD3–SMURF2 complex (Bonni *et al*, 2001).

SMURF-like molecule WWP1/Tiul1 binds SMAD2 in a TGFβ-dependent manner, and interaction of Tiul1/WWP1 with TGIF is required for poly-ubiquitination and degradation of SMAD2 (Seo *et al*, 2004; Komuro *et al*, 2004). Furthermore, the SMURF-like protein NEDD4-2 polyubiquinate SMAD2 and induces SMAD2 proteasomal degradation (Kuratomi *et al*, 2005; Bai *et al*, 2004]. The C-terminus of Hsc70 interacting protein (CHIP), which belongs to the U-box E3 ligase family, mediates ubiquitination and degradation of SMAD3 independently of TGFβ stimulation (Xin *et al* 2005). Alternatively, SMAD3 can be downregulated by the SCF/Roc1 ubiquitin ligase complex (ten Dijke *et al*, 2004; Izzi *et al*, 2004]. SMAD4 can be polyubiquinated and proteasomally degraded by direct binding of the E3 ligases SCFbTrCP1, Jab1 or CHIP (ten Dijke et al, 2004; Izzi et al, 2004; Li et al, 2004; Wan et al, 2004). In addition, SMURF1 and 2, Tiul1/WWP1 and NEDD4-2 also have the ability to degrade SMAD4 via a SMAD7-mediated interaction (Morén *et al*, 2005). In general proteasomal degradation also regulates the R-SMAD levels after translocation into the nucleus. Thus, C-terminally phosphorylated SMAD2 can undergo ubiquitination, and inhibition of proteasomal degradation enhances its nuclear accumulation (Lo *et al*, 1999). However, only a small fraction of SMAD2 and SMAD3, in the absence or presence of TGFβ, is ubiquitinated. Thus, the bulk of nuclear SMAD2 or SMAD3 is not targeted for degradation, but dephosphorylated and relocated to the cytoplasm (Inman *et al*, 2002b; Xu *et al*, 2002). Moreover, SMURF1 and 2 also mediate ubiquitination of activated TGFβ- receptors, leading to their degradation in the proteasome (Ebisawa *et al*, 2001; Tajima *et al*, 2003). Thus, to test whether Ubiquitin-dependent degradation plays a role in shaping the dynamics of SMADs I treated the cells with the proteasome inhibitor MG132. Inhibition of proteasomal degradation led to strongly enhanced TGFβ signaling due to enhanced SMAD2 and SMAD4 levels in the nucleus and stabilized receptors. Treatment with the inhibitor prevented the early adaptation and shifted the adaptation to later time points. Therefore, proteasomal degradation plays a strong role for the adaptation process. Western Blot experiments verified the time-lapse microscopy results and revealed more phosphorylated SMAD2, total SMAD2, SMAD4, TGFβ Receptor I and interestingly p21 was significantly enhanced.

In addition, as expected enhanced SMAD2 and SMAD4 accumulation into the nucleus through MG132 led to increased target gene expression, shown for Snail, SnoN and SARA. In particular, SARA contributes to the adaptation process. If there is less SARA, fewer R-SMADs are guided to the receptors. SnoN antagonizes TGFβ- signaling through direct interactions with SMAD4 and the R-SMADs (Liu *et al*, 2001; Wang *et al*, 2000). SnoN-mediated negative regulation on the SMAD proteins is removed during TGFβ- signaling by at least two distinct ways. In the presence of TGFβ- signaling, SMAD2 interacts with both SnoN and SMURF2, allowing the HECT domain of SMURF2 to target SnoN

for ubiquitin-mediated degradation by the proteasome (Bonni *et al*, 2001). SMAD2 and SMAD3 can also recruit the E3 ubiquitin ligase anaphase promoting complex (APC), resulting in the ubiquitination and degradation of SMAD bound SnoN (Stroschein *et al*, 2001; Wan *et al*, 2001).

My result matches observations in population studies where ubiquitin-dependent degradation has been shown to modulate the extent of SMAD2 retention in the nucleus (Lo & Massagué, 1999). Also Vizán *et al* suggested that pSMAD2 was not directly degraded, but that rather receptor turnover was affected by MG132 (Vizán *et al*, 2013). Warmflash *et al* showed that after inhibition of the proteasome with MG132 the amount of SMAD2 in the cell nucleus increased throughout the period of observation (15 h). However, it had very little effect on the dynamics of SMAD4 nuclear localization and did not prolong the time of expression of TGFβ target genes. These differences could be due to the different cell types or different experimental setup. The accelerated degradation of TGFβ signaling components via the proteasome system has been found in a number of tumors, indicating that dysregulated proteasomal degradation is a novel pathway how tumor cells silence TGFβ signaling (Zi *et al*, 2012). Thus, Dupont *et al* identified a RING-type E3 ubiquitin ligase Ectodermin that catalyzes poly-ubiquitination of SMAD4, which leads to SMAD4 degradation. Importantly, Ecto is overexpressed in intestinal tumors and thus may play a role in attenuating the antiproliferative effects of SMAD4 in tumor cells (Dupont *et al*, 2005).

Endocytosis of TGF receptors and its kinetics are expected to be important for sensing the duration and strength of signaling, and thus for reading and interpreting gradients of TGF superfamily members (Schmierer & Hill, 2007). The level of nuclear SMAD complexes must not only increase upon increasing receptor activity, but must also decrease as soon as receptor activity falls (when the receptors are degraded and/or dephosphorylated) (Kavsak *et al*, 2000; Shi *et al*, 2004). Balancing SMAD activation and SMAD inactivation ensures that the level of active nuclear SMADs is strictly proportional to receptor activity (Schmierer & Hill, 2007). Receptor internalization and degradation are a major regulatory event in signal transduction and are regulated by two distinct, competing routes (Baass *et al*, 1995; Di Fiore & De Camilli, 2001; McPherson, Kay & Hussain, 2001, Di Guglielmo *et al*, 2003). Clathrin-dependent internalization targets receptor proteins to the early endosome antigen-1 (EEA1)-positive endosome, where the SMAD2 anchor SARA is enriched, and promotes TGFβ signaling through recycling or receptors enter the late endosome-lysosome for degradation (Di Guglielmo *et al*, 2003; Hayes *et al*, 2002; Itoh *et al*, 2002; Panopoulou *et al*, 2002). Whereas the clathrin-independent, lipid raft- caveolar internalization pathway contains the SMAD7-SMURF2 bound receptor and is required for rapid receptor turnover and degradation. The I-SMAD–SMURF complex is first formed in the nucleus and is subsequently targeted to lipid raft vesicles via the C2 domains of SMURFs. Upon association of the SMAD7–SMURF2 complex with an active TGFβ receptor, both SMAD7 and the

receptor are ubiquitinated and destined for proteasomal and lysosomal degradation (Di Guglielmo *et al*, 2003; Ebisawa *et al*, 2001; Kavsak *et al*, 2000). SMURF1- deficient mice do not show any enhancement of TGFβ signaling (Yamashita *et al*, 2005), probably because of the redundant functions of SMURF1 and 2 in TGFβ signaling. My immunofluorescence experiments showed that TGFβ receptor II is stabilized in MCF10A WT cells 0.75h post 100pM TGFβ stimulation und subsequently degraded to less than the basal level. An early study from Wrana *et al* shows that the phosphorylation of TGFβRI in the receptor complex peaks at about 2 minutes after TGFβ stimulation (Wrana *et al*, 1994). The signal is relayed to the activation of SMAD proteins, which arrive at their maximal levels in about 30-60 minutes. The time delay between ligand receptor complex and R-SMAD activation may be due to intermediate processes, including receptor endocytosis, the recruitment of SMADs to receptor complex and SMAD activation (Zi *et al*, 2012). After 30-60 minutes, the phosphorylation of SMADs correlates with the degree of TGFβ-receptor complex level, which might be due to continuous nucleocytoplasmic shuttling of the SMADs, but this shuttling fails to explain why there is a prominent delay following receptor activation and prior to SMAD phosphorylation (Schmierer *et al*, 2008; Inman *et al*, 2002a & b).

To address the question how the distinct receptor internalization and degradation processes affect SMAD2 dynamics I inhibited the endocytic pathways with dynasore or nystatin respectively and performed time-lapse microscopy experiments. Treatment with nystatin disrupts the lipid raft-caveolar endocytic pathway and shifts receptors into the non-raft compartment EEA1. Therefore the inhibitor stabilizes the receptors and slightly enhances signaling and SMAD2 activation (Di Guglielmo *et al*, 2003). I showed that inhibiting the caveolar endocytic pathway enhanced the maximum amplitude and the mean intensity within 5h after the first response. Thus, SMAD2 accumulated strongly into the nucleus, but with an early adaptation and an extenuated late adaptation, so that SMAD2 remained at a high nuclear level. Interestingly, the increased nuclear SMAD2 values led to an increased mobility of the cells. Therefore, receptor internalization and degradation play a crucial role in the cell-fate decision.

Inhibiting clathrin-dependent endocytosis with dynasore 0.75h before 100pM TGFβ stimulation led to increased nuclear and cytosolic SMAD2 values, while the ratio is almost unchanged. The maximum amplitude and the mean intensity within 5h after response were slightly increased, so that SMAD2 accumulated slightly more into the nucleus, whereas the time of the maximal amplitude, increase and the end time of the first response remained unchanged.

Taken together these results suggest that TGFβ receptor signaling and turnover play a huge role for the adaptation process of SMAD2 dynamics, especially for the late adaptation. Since early adaptation was attenuated and not prevented, other regulatory mechanisms are apparently involved. Even

though there is little debate about whether the TGFβ receptors undergo endocytosis, the precise role of receptor endocytosis in signaling remains controversial (Chen, 2009). Several lines of evidence support a positive role of endocytosis on R-SMAD phosphorylation (Di Guglielmo *et al*, 2003; Penheiter *et al*, 2002; Runyan *et al*, 2005; Hayes *et al*, 2002), while there are several reports describing SMAD activation immediately at the cell surface without need of receptor endocytosis (Lu *et al*, 2002, Zhou *et al*, 2004; Meyer *et al*, 2011).

In addition, currently unknown regulatory mechanisms are likely to exist that target TGFβ receptors preferentially to one or the other endocytic compartment, thus promoting either signaling or receptor degradation (Schmierer & Hill, 2007). Interfering with one route inhibits or shifts the internalization towards the other route, respectively, indicating that partitioning is a dynamic and balanced process. The varying impact of receptor trafficking on signaling could be attributed to different experimental systems and cell types, which may have different ratio of clathrin-dependent to clathrin-independent endocytosis. In addition, in cells that are deficient in caveolin, TGFβ signaling can occur in the absence of clathrin-dependent endocytosis (Lu *et al*, 2002). Moreover, the inhibitors of endocytosis may not be very specific and could have some off-target effects. Multiple protein interactions are likely to control subcellular receptor localization and cell-surface receptor availability.

Thus, like SMURFs, TGIF interacting ubiquitin ligase (Tiul)1/WWP1 and NEDD4-2 also associate with SMAD7 and can promote degradation of activated TGFβ type I receptors (Seo *et al*, 2004; Komuro *et al*, 2004; Kuratomi *et al*, 2005). Dapper2, a PDZ-binding protein, inhibits mesoderm formation by promoting lysosomal degradation of TGFβ receptors in mammals (Su *et al*, 2007). Furthermore, protein phosphatase PP1a was shown to be recruited in a SMAD7-dependent manner to ALK1 in endothelial cells and to targ*et* ALK1 for dephosphorylation (Valdimarsdottir *et al*, 2006). In addition to the positive role it plays in signaling by recruiting SMAD2 and 3 to the activated TGFβ receptor, the assembly of PP1c with SMAD7–GADD34 complex in mammalian cells is enhanced by SARA, resulting in more efficient dephosphorylation of the TGFβ type I receptor (Shi *et al*, 2004). Moreover, receptor and SMAD kinetics are influenced by SARA. At steady state, the bulk of SARA and SARA bound SMAD2 are located in early endosomes. Receptor-mediated phosphorylation of SARA bound SMAD2 occurs at the plasma membrane but is more efficient in SARA-rich early endosomes to which the activated receptor complex is internalized via clathrin-coated pits (Di Guglielmo *et al*, 2003; Hayes *et al*, 2002; Lu *et al*, 2002). All these different parameters may in turn control the duration of SMAD phosphorylation and activation, and thus give rise to qualitatively different responses resulting from different signaling thresholds. Despite the variable effects of receptor endocytosis on SMAD phosphorylation, activation of non-SMAD signaling pathways by TGFβ appears to require receptor internalization (Meyer *et al*, 2011; Zuo *et al*, 2009).

Since TGFβ is not recycled, internalization of TGFβ by endocytosis is the primary means of removing active TGFβ from the cell surface, and lysosomal degradation is the primary means of termination of TGFβ signaling (Clarke *et al* 2009; Zi *et al*, 2011). In agreement with my results, TGFβ signaling amplitude and duration can be regulated through the control of receptor trafficking (Zi *et al*, 2012). However in contrast, it has also been shown that receptors are internalized constitutively with similar efficiencies in the absence and presence of a signal (Di Guglielmo *et al*, 2003).Thus, TGFβ does not appear to alter TGFβ receptor trafficking. The latter is compatible with the action of TGFβ family ligands as morphogens that allow a cell to continuously sense the concentrations of active ligand. In addition, studies in Xenopus have shown that the retention of activated activin receptors within the endocytic pathway is required for cellular memory of activin signaling. Such memory is needed for correct cell fate decisions by morphogens (Jullien *et al*, 2005). To understand the role of receptor endocytosis on TGFβ signaling, diverse mathematical models were established. *Vilar et al* assumed that TGFβ signaling activity is proportional to the level of ligand-receptor complexes in the internalized endosomes. In addition, ligand-receptor complexes between type I and type II receptors have the same constitutive degradation rate. However, the model lumps the processes including non-clathrin dependent internalization, recycling and the degradation of the receptors into one reaction as "the ligand-induced receptor degradation from plasma membrane" (Zi *et al*, 2012). Thus, Zi and Klipp developed a mathematical model, including two major types of TGFβ receptor endocytosis (Zi & Klipp, 2007b). In agreement with my results, the model simulations suggest that SMAD activation is regulated by the balance between clathrin dependent endocytosis and caveolar/lipid-raft mediated (clathrin-independent) endocytosis. If clathrin-dependent internalization is dominant, SMAD activation becomes a sustained response. On the other hand, if clathrin- independent endocytosis is dominant, SMAD activation displays a transient response. Interestingly, the simulation results suggest that changing the balance between the two branches of endocytosis has relatively little effect on the early SMAD signal, and has larger effect in reshaping long term SMAD activity. In addition, Vizán *et al* found that TGFβ binding triggered the rapid depletion of signaling-competent receptors from the cell surface, with the type I and type II receptors exhibiting different degradation and trafficking kinetics (Vizán *et al*, 2013). A computational model of TGFβ signal transduction from the membrane to the nucleus that incorporates their experimental findings predicts that autocrine signaling, such as that associated with tumorigenesis, severely compromises the TGFβ response. They showed that the long-term signaling behavior of the TGFβ pathway is determined by receptor dynamics, but does not require TGFβ–induced expression of feedback regulators. In the future, a detailed systems biology approach can be useful to clarify this issue by combining mathematical models with quantitative experimental data of receptors and SMAD kinetics. In further studies, systematic analysis of the dynamic receptor

localization according to different input strengths and duration would be necessary. Combined live-cell reporters for SMAD translocation and receptor localization may provide deeper insights regarding the molecular mechanisms of pathway activation. Moreover, inhibition of both endocytic pathways would provide information about the entire role of receptor endocytosis in TGFβ signaling. As the downregulation of TGFβ levels and/or TGFβ responsiveness has been implicated in other disease processes, such as autoimmune disease, potent TGFβ- enhancers such as dynasore or dynasore-like compounds are potential therapeutic compounds for treating such diseases (Li and Flavell 2008).

Finally, receptor internalization and slow recovery of the receptor at the surface, in conjunction with increased receptor degradation upon TGFβ stimulation, could influence both signal attenuation and the refractory behavior (Vizán *et al*, 2013). I showed that TGFβ signaling revealed a refractory period depending on the signaling state due to adaptation mechanisms. I examined the refractory time to understand which mechanisms restrict reactivation of the pathway and constitute the refractory time, by performing time-lapse microscopy experiments of SMAD2 reporter cells stimulated repeatedly with different TGFβ concentrations at various time points. Within the monitored 24 hours the system stimulated with high TGFβ concentrations (100pM TGFβ) was incapable of responding again to stimulation. In conclusion cells could only be completely re-stimulated after the terminal adaptation has been completed. Transcriptional negative feedback loops contributed to the refractory period of the system, at least for small concentrations. This is in accordance with Vizán *et al*, who also showed a period in which cells are unresponsive to further acute ligand stimulation. Such as different concepts for the terminal adaptation of TGFβ signaling are discussed, there are different concepts how the refractory period is influenced. In particular, the TGFβ strength and duration must be considered. Thus, Vizán *et al* assumed that cells enter a refractory state because surface receptors were rapidly occupied and internalized, whereas replenishment of the receptors at the cell surface was very slow. The refractory state was induced by TGFβ binding to receptors, but depended not on receptor activity and did not require negative feedback through TGFβ target genes. However, SMAD7 and other negative feedback loops also affect receptor endocytosis and indirectly TGFβ binding to receptors. In further experiments, the restimulation behavior should be investigated together with inhibition of the distinct receptor endocytosis pathways. Cell-dependent depletion of TGFβ from the medium (Clarke *et al*, 2009) was essential for the ability of the cells to regain response competence after the refractory period (Vizán *et al*, 2013). In accordance with my results, once the ligand was depleted or consumed, cell surface receptor levels were slowly restored and the cells became once more fully competent to respond to an acute stimulation (Vizán *et al*, 2013). For example, this concept is in contrast with signaling downstream of the erythropoietin receptor (EpoR). The amount of unoccupied cell surface EpoR recovers very quickly after ligand stimulation and the system never reaches a refractory state

(Becker *et al*, 2010). In conclusion, ligand activation mechanisms may be important *in vivo* to limit the exposure of cells to high concentrations of mature TGFβ that would provoke a refractory state (Vizán *et al*, 2013). Indeed, high TGFβ exposure is associated with disease states, for example, during wound healing, fibrosis, or in tumorigenesis (Blobe *et al*, 2000; Massagué, 2008). The consequence of exposure to high concentrations of TGFβ is not only acute pathway activation but also desensitization. Therefore, a tumor that receives a constant supply of TGFβ, for instance because of autocrine signaling, would maintain only a low level of signaling.

Thus, taken together, the results reported in this section suggest that adaptation mechanisms are a combinatorial effect of ligand degradation, proteasomal degradation, receptor endocytosis and feedback strength, which act at different time scales and doses. Positive and negative signals are equally important in controlling TGFβ signaling responses. Moreover a designation of TGFβ signaling components as having either negative or positive effects on signaling is often too simplistic. The future focus must be on how the various adaptation mechanisms change SMAD dynamics, and how this correlates precisely with cell fate. Thus, a balance between all regulatory mechanisms guarantees that the level of nuclear SMAD complexes reflects receptor activity at any time throughout the signaling period. The dynamically maintained concentration of nuclear SMAD complexes will then determine which SMAD target genes are activated, according to promoter binding-site affinity, co-repressors, co-activators, but also through more complex mechanisms (Schmierer & Hill, 2007).

4.3 Source of variability

Next, I investigated which sources influence the heterogeneity of the SMAD response to a given TGFβ stimulus in individual and genetically identical cells. To this end, I examined how the initial state of the cell, such as cell cycle state, cell density or cell location, contribute to the observed heterogeneity in dynamical behavior (Loewer & Lahav, 2011; Snijder & Pelkmans, 2011). However, cell cycle state was not the main cause of heterogeneity. No obvious correlation between cell cycle phase and TGFβ response was observed for all different TGFβ concentrations. In addition, there were no significant differences in the distributions of the cell divisions of the respective signaling classes. Furthermore, synchronized cells in G2 showed no impact on the TGFβ response.

By seeding a different number of cells 48 hours prior to 100pM TGFβ stimulation, I examined how the individual TGFβ response depends on cell density. However, the ratio TGFβ response was largely independent of cell density, but the amount of SMADs in the nucleus increased with lower cell density. This applied to the basal level, amplitude and the late SMAD response. The question is what is critical for the cellular outcome, ratio SMAD2 level or the absolute nuclear level? In addition, what are the triggering factors that the nuclear and cytoplasmic basal levels were already altered by varying cell

density? Since the cell density in this experimental setup determined by many factors, like cell contacts, cell volume, available number of receptors and/or TGFβ molecules per cell, in another experiment Marcel Jentsch and I considered the influence of the local cell density on the TGFβ response. However, local cell density was not sufficient to explain signaling heterogeneity. In summary, the cell density explains minor differences between different experiments, but not the heterogeneity within the cells in one experiment. This is also supported by a paper demonstrating that activation of the cell density sensing YAP/TAZ pathway does not attenuate SMAD signaling (Nallet-Staub *et al*, 2015). Furthermore, a mathematical model has shown that cell density affects signaling dynamics in response to the same concentration of ligand. Cells have distinct signaling durations and signaling persists longer when cell density is decreased (Zi & Klipp, 2007b). Thus the authors argued, that the key parameter for experimental design cannot be "concentration of ligand", but rather must be "molecules of ligand per cell", which takes into account the number of cells in the experiment. Therefore, we kept the cell number, time of TGFβ stimulation, size of dishes or medium volume constant for all experiments.

Interestingly, recent single-cell transcriptomic studies revealed that cell volume contribute to phenotypic and functional cell heterogeneity even in monoclonal cell lines (Buettner *et al*, 2015; Padovan-Merhar *et al*, 2005). How cell volume influences SMAD heterogeneity could be investigated in future experiments. Moreover, subcellular structures and organelle size, shape and distribution contribute to phenotypic heterogeneity (Rafelski and Marshall, 2008; Marshall, 2011; Chan and Marshall, 2010).

In addition, the stochastic nature of gene expression can lead to highly variable behaviors across genetically identical populations of cells, commonly referred to as noise. Expression noise can be disadvantageous, by affecting the precision of performing biological functions, but it may also be advantageous by enabling heterogeneous stress-response programs to environmental changes (Eldar & Elowitz, 2010). Importantly, gene expression is a multi-step process and the stochasticity of its individual steps, including transcription and translation, contributes to the resulting variability. In addition, protein level variations represent a combination of fluctuations caused by the stochastic nature of biochemical reactions (Bar-Even *et al*, 2006; Pedraza & Paulsson, 2008; Lestas *et al*, 2010), cell-specific activity of regulatory processes (Colman-Lerner *et al*, 2005) and influences from population microenvironment (Snijder *et al*, 2009; Snijder & Pelkmans, 2011). Thus, individual cells are likely to express different amounts of receptors at the cell surface. Model simulations indicated that signaling responses are regulated by the ratio of ligand to cell surface receptor number (Zi & Klipp, 2007b). When all cells are exposed to the same amount of ligand, the ratio of ligand to cell surface

receptor number in each cell will be different, which might cause heterogeneous signaling responses at single cell level. Number of receptors could also be correlated with cell volume.

To further test whether protein level variations may cause SMAD signaling heterogeneity and decomposition into signaling classes, we developed a modeling approach in cooperation with Stefan Legewie and Uddipan Sarma (Strasen *et al*, 2018). The modeling simulations provide evidence that feedback expression is a main determinant of signaling classes. In addition to stochastic gene expression, cell-specific activation of signaling pathways controlling *SMAD7* expression could contribute to the observed cell-to-cell variability. Such pathways may include IFN-c/ Stat1 (Ulloa *et al*, 1999), PKC (Tsunobuchi *et al*, 2004), hepatocyte growth factor (Shukla *et al*, 2009) or mir21 (Li *et al*, 2013). Further experiments are needed to clarify sources of heterogeneous feedback expression.

The question of the mechanisms and consequences of intercellular heterogeneity is not purely academic since cell-to-cell heterogeneity is a major driver of cancer evolution, immune responses and disease progression. The treatment of many diseases is complicated by heterogeneity that renders some cells more resistant to treatment than others. Furthermore, it has been argued that neglecting cell heterogeneity is one of the major causes of error in disease classification (Marko *et al*, 2011).

4.4 The activity of MAP kinases determines long-term dynamics of SMAD signaling

The TGFβ/SMAD pathway does not function in isolation, but is part of a signaling network in which cross-talk between pathways occurs. Therefore, it is interesting to investigate how coordinate regulation of multiple pathways is achieved by changes in activity of common pathway components. Especially noncanonical signaling pathways including the mitogen-activated protein kinase (MAPK), NF-κB or PI3 kinase/ AKT pathways, can either be induced by TGFβ, or can modulate the outcome of TGFβ-induced SMAD signaling (Massagué and Chen, 2000; Lutz and Knaus, 2002; Derynck and Zhang, 2003). SMAD proteins are also capable of physically interacting with transcription factors, themselves substrates of MAPKs, adding more complexity to the intricate relationship between MAPKs and the SMAD pathway. Although the canonical pathway tends to be treated as the more important, recent studies suggest that the SMAD-independent TGFβ signaling plays a more significant role *in vivo* than previously thought (Holm *et al*, 2011; Iwata *et al*, 2012). In a mouse model of Marfan's syndrome in which TGFβ signaling is elevated, the aortic aneurysm phenotypes are made worse by reducing the canonical pathway component SMAD4, and the phenotypes are made less severe by attenuation of noncanonical pathways (Holm *et al*, 2011). These results show not only that the noncanonical pathway is of importance in disease mechanisms but also that the two pathways somehow interact with one another. Indeed, evidence exists for a tight integration of SMAD signaling within a complex network of

cross-talks with noncanonical TGFβ pathways that largely contribute to modify the initial SMAD signals and allow the pleiotropic activities of TGFβ (Javelaud & Mauviel, 2005). Therefore, we investigated systematically how the dynamic response of SMADs is influenced by cross-talk of non-canonical TGFβ signaling and other signaling networks.

First of all, I examined the influence of the JNK pathway on SMAD2 and SMAD4 dynamics in MCF10A cells. Crosstalk between the JNK1 and SMAD pathways in RPMCs has been described as JNK–mediated phosphorylation of SMAD3 enhances its activation and nuclear translocation (Liu, 2012). In addition, the JNK pathway may contribute to regulate autocrine TGFβ1 expression, as JNK-deficient fibroblasts constitutively express TGFβ1, an expression that can be repressed by complementation of the cells with JNK (Ventura *et al*, 2004). Nevertheless, using JNK inhibitors neither the nuclear nor cytoplasmic levels of SMAD2 and SMAD4 have changed in time-lapse microscopy experiments. Clearly, the crosstalk between these two pathways depends on the physiological cell context, a general theme in TGFβ signaling.

Further on, I investigated how the p38 pathway influences SMAD2 and SMAD4 dynamics. TGFβ receptors activate MAP3Ks (MEKKs) like TAK1, which in turn activates MKKs like 3, 4, 6 and finally phosphorylate p38 (Zhang, 2009, Figure 2A). Interestingly a study by Gui *et al* showed that prolonged and sustained activation of the p38 MAPK pathway requires SMAD signaling, which is observed in hepatocytes, osteoblasts and pancreatic carcinoma cells. SMAD activation induces the expression of GADD45β, an upstream activator of MKK4, and thus promotes the prolonged activation of p38 MAPK (Gui *et al,* 2012). Additionally, treatment of JEG-3 cells with a p38 MAPK inhibitor (SB203580) attenuated TGFβ1-induced SMAD3 protein expression and suppressed the activation of SMAD3 (Xu *et al,* 2013). These results suggested that there is crosstalk between p38 MAPK and SMAD3 through TGFβ signaling in human choriocarcinoma. Indeed, I observed that inhibition of p38 activity with p38 inhibitors BIRB 796 and SB202190 modulated the dynamics and localization of SMAD2 upon TGFβ stimulation by diminishing the amplitude of the first peak and preventing nuclear accumulation of SMAD2 at all later time points. The results were also transferable for lower TGFβ concentrations. Increasing concentrations of SB202190 and BIRB 796 also increased the p38 effect on the late SMAD2 response, respectively. Immunofluorescence experiments confirmed the microscopy results. In addition, SMAD4 showed no long-term dynamics, too. Interestingly, adding the inhibitors 6 hours after TGFβ treatment terminated further activation fast, but obviously termination was slightly slower and not as strong as with TGFβ receptor inhibitors. In conclusion long-term dynamics of SMAD2 and SMAD4 were p38 kinase activity dependent. Furthermore, p38 inhibition resulted in less phosphorylation of SMAD2 and SMAD3 while total SMAD2 and total SMAD3 levels remained unchanged. Inhibition efficiency was demonstrated by the phosphorylation status of HSP27. Evidence of cross-talk between

SMADs and p38 has been controversial, some studies previously demonstrated that loss of p38 activity decreased SMAD2/3 nuclear localization in the presence of TGFβ (Hayes *et al*, 2003), and knockout of SMAD3 showed decreased phosphorylation of p38 by TGFβ (Li *et al*, 2010). Also, inhibition of p38 MAPK with a specific inhibitor, SB202190, abolished TGFβ-inducible activation of SMAD-dependent promoter and decreased SMAD2 phosphorylation. This suggests an interaction between SMAD and p38 MAPK pathways in TGFβ1-induced signaling in T98G glioblastoma cell (Dziembowska *et al*, 2007). In addition, p38 MAPK inhibitors can attenuate TGFβ1-induced SMAD3 transcriptional levels (Tan *et al*, 2014).

While other studies have shown that inhibition of p38 was not required to phosphorylate SMAD2 (Zhang *et al*, 2006), and over-expression of dominant negative SMAD3 did not inhibit TGFβ mediated activation of p38 (Yu *et al*, 2002). Likewise, TGFβ1-dependent phosphorylation of SMAD2/3 was unaffected by the inhibitor of p38 MAP kinase SB203580 in confluent growth-arrested HK-2 cells and SB203580 had no effect on the phosphorylation of SMAD2 and SMAD3 in rat peritoneal mesothelial cells stimulated with TGFβ1 (Wang *et al*, 2013). However, only short time periods were considered. Thus, I investigated the impact of this late SMAD dynamic remodeling on gene expression and cell fate. The negative feedback loops SnoN and SMAD7 were somewhat less expressed, while TIEG and SARA remained unchanged. In addition p21, which plays a role in proliferation and cell cycle arrest, was unaltered by p38 inhibition. Interestingly, Snail, a key regulator of TGFβ-induced EMT (Naber *et al*, 2013), was clearly less expressed at later time points and in accordance with this finding, cells moved significantly slower and thus probably EMT was decreased. In conclusion, p38 kinase activity was necessary for the second response of SMAD2 and SMAD4 as well as for inducing probably EMT. This could be exploited by therapeutic approaches to cancer, so that the protective TGFβ-induced cell cycle arrest persists, but EMT is suppressed and cancer progression, invasion, and tumor metastasis is no longer supported. Wu *et al* also showed that using the p38 inhibitor SB203580 resulted in decreased metastasis, indicating that p38 inhibitors can be used as potential treatment for advanced breast cancer. In addition, Bakin *et al* considered this pathway as a potential target of therapeutic interventions in neoplastic and inflammatory disorders associated with TGFβ-mediated EMT. They also found, in accordance with my results, evidence that the p38 MAPK pathway is required for TGFβ-mediated EMT and cell migration in NMuMG mouse mammary epithelial cells. Inhibition of the p38 MAPK pathway affected TGFβ-mediated phosphorylation of ATF2, but did not inhibit phosphorylation of SMAD2. The SB202190 inhibitor impaired TGFβ-mediated changes in cell shape and reorganization of the actin cytoskeleton. In addition, dominant-negative Rac1N17 blocked TGFβ-induced activation of the p38 MAPK pathway and EMT, suggesting that Rac1 mediates activation of the p38 MAPK pathway (Bakin *et al*, 2002). Furthermore, also a study by Daroqui *et al* demonstrated that p38 MAPK and MEK

contribute to TGFβ stimulation of cell motility and invasion by analyzing signal transduction mediators (Daroqui *et al*, 2012). A study by Ohshima showed that mutant TGFβI did not affect activation of the SMAD pathway, but retained signaling via the MAP kinase pathway (Ohshima & Shimotohno, 2003). They also suggested that TGFβ receptor-activated p38 is involved in TGFβ-induced apoptosis but not growth arrest in mouse mammary gland epithelial cells. In accordance with this, it was published that TGFβ-induced apoptosis is mediated by SMAD-dependent expression of GADD45b through p38 activation. They demonstrated that ectopic expression of GADD45b in AML12 murine hepatocytes is sufficient to activate p38 and to trigger apoptotic cell death, whereas antisense inhibition of *Gadd45b* expression blocks TGFβ-dependent p38 activation and apoptosis. Previous studies have shown that transcriptional activation of target genes by TGFβ, including the collagenase-3 and biglycan genes, requires the activation of both the MAP kinase and SMAD pathways (Leivonen *et al*, 2002; Ungefroren *et al*, 2003). Moreover, it was shown that TGFβ-mediated phosphorylation and stabilization of Sox9 are dependent on p38 activity in chondrocytes. Wang *et al* showed that, TGFβ1 significantly upregulated the expression of MCP-1 at both the protein and mRNA level in a time-dependent manner and SB203580 markedly inhibited the expression in rat peritoneal mesothelial cells (Wang *et al*, 2013). Next, in order to examine the upstream components of the p38 pathway that influences the dynamics and localization of SMADs in more detail, I focused on TAK1. Therefore I used the inhibitor (5Z)-7-Oxozeaenol, that inhibits both the kinase and the ATPase activity of TAK1 (Wu *et al*, 2013) and investigated how dynamics of SMAD2 and SMAD4 change. It is known that there are notable differences in the mechanism of SMAD2/3 and TAK1 activation. TGFβ1-induced TAK1 activation occurs independent of TGFβRI kinase activity, whereas activation of SMAD2/3 involves recruitment and phosphorylation by TGFβRI and requires kinase activity of TGFβRI (Wu *et al*, 2000; Chen *et al*, 1998; Kim *et al*, 2009; Sorrentino *et al*, 2008). I could show that with increasing inhibitor concentration SMAD2 translocation decreased and the first response disappeared. (5Z)-7-Oxozeaenol alone did not lead to translocation of SMAD2. Immunofluorescence experiments confirmed the results of time-lapse microscopy. As a conclusion, TAK1 activity seemed essential for SMAD2 signaling. I could show that SMAD4 accumulated strongly from the cytoplasm into the nucleus with increasing TAK1 inhibitor concentration. Furthermore, (5Z)-7-Oxozeaenol alone led to a strong translocation of SMAD4. And surprisingly adding (5Z) -7-Oxozeaenol 6 hours post TGFβ stimulation resulted in an immediate import of SMAD4. In conclusion TAK1 inhibition enhanced SMAD4 signaling independent of SMAD2 and TGFβ. These observations suggest that TAK1 might be the point of convergence in various signaling pathways activated by a variety of stimuli and play a pivotal role in regulating cellular responses (Choi *et al*, 2012). Nevertheless, another MAP3K, MEKK4 (MAP3K4), has also been proposed to mediate the TGFβ-induced phosphorylation of p38 MAPK through SMAD-dependent expression of GADD45b, which

associates with and activates MAP3K4 (Takekawa *et al*, 2002). Also, the depletion of MLK2 (MAP3K10) in cells with homozygous knock-in of catalytically inactive MEKK4 (MAP3K4) results in a complete loss of the TGFβ-induced phosphorylation of p38 MAPK, implying that MEKK4 and MLK2 mediate the TGFβ-induced phosphorylation and activation of p38 MAPK in MEFs and HaCaT keratinocytes. However, many reports implying a role for TAK1 in mediating the TGFβ-induced phosphorylation of p38 MAPK (Kim *et al*, 2009; Yamaguchi *et al*, 1995; Walsh *et al*, 2008). More recent reports have focused mainly on TRAF6 as an upstream activator of TAK1 (Sorrentino *et al*, 2008; Yamashita *et al*, 2008). It is therefore likely that TRAF6 could mediate the TGFβ-induced phosphorylation of p38 MAPK through another MAP3K (Sapkota, 2013).

In addition I confirmed the microscopy results and assumed underlying mechanisms. I showed in western blot experiments that the first response of SMAD2 and SMAD3 phosphorylation disappeared when TAK1 was inhibited. Thus, the accumulation of SMAD4 was also independent of pSMAD3. Furthermore, TAK1 inhibition stabilized TGFβ receptor 1 suggesting a remodeling of the receptors so that pSMAD2 may not bind and phosphorylation was prevented. This assumption is supported by another time-lapse movie, where cells inhibited 6 hours post TGFβ stimulation with the (5Z)-7-Oxozeaenol or TGFβR1 inhibitor showed the same signaling termination rates for SMAD2 translocation into the nucleus. Furthermore, although SMAD4 translocated into the nucleus decoupled from pSMAD2, pSMAD3 and TGFβ, I proved that the accumulation was also independent of BMP signaling. Studies indicate that TAK1 can regulate TGFβ-induced activation of SMAD signaling by inducing SMAD7 expression (Dowdy *et al*, 2003). Interestingly, a study by Yumoto *et al* showed that TAK1 is required for appropriate activation of both the noncanonical p38 pathway and canonical SMAD pathway in the neural crest-derived craniofacial ecto-mesenchyme. They show that TAK1 deficiency results in attenuated TGFβ R-SMAD linker region phosphorylation (SMAD2 at Thr-220, which has been shown to be critical for full transcriptional activity of SMAD2) and that TAK1 kinase mediates both distinct and overlapping agonist-induced transcriptional responses (Yumoto *et al*, 2013). Linker regions in R-SMADs are Ser/ Thr-rich and are known to be phosphorylated by several different kinases, *e.g.* GSK, MAPKs, and CDKs, and it has been suggested that these post-translational modifications have both activatory and inhibitory regulatory functions in TGFβ signaling. More research in this direction is necessary. My western blot experiments did not yield any clear results. Nevertheless, in conclusion TAK1 mediates both canonical and noncanonical arms of the TGFβ signaling and affects SMAD2 and SMAD4 dynamics. Furthermore, I could show that this dynamic remodeling had an impact on gene expression. The strong first response of SnoN, SMAD7, TIEG, Snail and PAI1 were gone and they were less expressed at later time points. This confirmed that TAK1 activity was probably needed for EMT and although the SMAD4 response was enhanced, SMAD2 accumulation was essential for the expression of TGFβ target genes.

In addition to the role of TAK1 in the regulation of SMAD function, there is cross-talk between the SMAD and downstream targets of TAK1 such as ATF2 in regulation of certain TGFβ1 target gene expression (Hanafusa *et al*, 1999; Sano *et al*, 1999; Abécassis *et al*, 2004).

TGFβ activates the TAK1-MKK6-p38 kinase cascade leading to the phosphorylation of ATF-2, and ATF-2 associates with SMAD4 in response to TGFβ. Therefore, SMAD complexes and phosphorylated ATF-2 may interact in a nucleoprotein complex that associates with DNA and activates transcription of TGFβ-responsive genes (Hanafusa *et al*, 1999). In accordance with my results, knocking down TRAF6 expression also inhibits TGFβ-mediated EMT (Yamashita *et al*, 2008). Thus, activation of the TRAF6-TAK1-p38 pathway is another obligatory requirement for TGFβ-induced EMT. Also, the TRAF6-TAK1-p38 pathway is essential for TGFβ- induced apoptosis. Overexpression of TAK1 caused cells or Xenopus embryo to undergo apoptosis, whereas cells expressing the kinase-inactive TAK1 were protected from TGFβ-induced apoptosis (Shibuya *et al*, 1998; Kimura *et al*, 2000; Edlund *et al*, 2003). As well abrogation of TAK1 activation inhibits TGFβ-induced apoptosis in embryonic fibroblasts, prostate cancer cells, and AML12 liver cells, indicating that TAK1 also acts as a mediator of apoptosis (Sorrentino *et al*, 2008; Yamashita *et al*, 2008). In contrast knockdown of TAK1 expression or inhibition of TAK1 activation augments cell apoptosis induced by TGFβ1 in various cell types in vitro and in vivo, including the kidney, indicating that TAK1 is required for prevention of apoptosis and plays a role as a cell survival factor (Ma *et al*, 2011; Omori *et al*, 2010). Moreover, TGFβ-induced fibronectin expression in fibroblasts is mediated by TAK1 through MKK4-JNK signaling cascade and TAK1-deficient fibroblasts exhibited reduced profibrotic response to TGFβ1 stimulation (Shi-wen *et al*, 2009; Hocevar *et al*, 2005). In vitro studies show that TAK1 mediates TGFβ-induced expression of types I and IV collagens and fibronectin in cultured mesangial cells (Ono *et al*, 2003). In conclusion, a combination of the canonical and non-canonical signaling outputs, as well as context-dependent crosstalk inputs from other signaling networks, probably define the nature of cellular responses to TGFβ ligands.

In order to investigate the underlying mechanisms of p38 activity and SMAD cross-talk, I focused first on the participation of SMAD7. TAB1 (TGFβ-activated kinase-binding protein-1) is able to associate with SMAD7, a phenomenon that may lead to inhibition of TAK-1-dependent p38 activation (Edlund *et al*, 2003). Alternatively, it has also been suggested that SMAD7 could act as a scaffolding protein to provide structural support for MKK3/p38 activation by TAK1 (Edlund *et al*, 2003). Additionally, the ability of SMAD7 to interact with TGFβR1 using two modes—a three-finger-like structure in the MH2 domain and a basic groove in the MH2 domain, in contrast to only one mode for SMAD6, the other I-SMAD, suggests a dual role for SMAD7: inhibition of TGFβ-SMAD signaling and promotion of TGFβ-induced activation of p38 MAPK pathway. Nevertheless, using a *SMAD7* knock out cell line with p38 inhibitors did not show an SMAD7 influence on the effect of p38 inhibition of long-term SMAD

dynamics. Interestingly, it was shown recently that SMAD6 is immediately induced in response to TGFβ1 in AML-12 and primary hepatocytes and inhibits TGFβ1-induced TRAF6 polyubiquitination through recruiting the A20 deubiquitinating enzyme, thereby suppressing subsequent TAK1-p38 MAPK activation (Jung *et al*, 2013). In future experiments, the role of SMAD6 could be examined in more detail. As a further approach I considered that SMAD2 is less phosphorylated due to modified receptor trafficking. However, by using Nystatin and p38 inhibitors I showed that p38 inhibition did not shift receptors to degradation. Interestingly, a study from Tan *et al* showed that p38 MAPK inhibitors can attenuate TGFβ1-induced TGFβRI and TGFβRII transcriptional levels. They assumed that the blockade of the p38 MAPK pathway can downregulate the activated TGFβRI and TGFβRII (Tan *et al*, 2014). Correlation of receptor activation and p38 activity in future experiments would be interesting. Next, by using the proteasome inhibitor MG132, I showed that the p38 effect was not mediated by alteration of the ubiquitin-dependent degradation. Interestingly, the p38 effect was also evident when the cells were treated with MG132 and p38 inhibitor compared to treatment with only MG132, hence independent of TGFβ stimulation.

To further understand the mechanism how the p38 kinase influences the long-term dynamics of SMADs, I focused on phosphatases. By using Okadaic acid, a phosphatase inhibitor particularly of type 1 (PP1) and 2A (PP2A), and p38 inhibitors I showed that inhibition of PP1 and PP2A did not alter the p38-mediated SMAD2 response. But inhibiting another phosphatase group PP2C with Sanguinarine chloride abrogated the p38 effect on SMAD2 and SMAD4 dynamics. Since phosphatase inhibition could also result in more pp38 and the p38 inhibitors function possibly incompletely, I could also show that the p38 effect disappeared with Sanguinarine chloride even at high p38 inhibitor concentrations. In conclusion inhibition of PP2C abrogated the p38- mediated SMAD response and therefore a PP2C family member is involved in the p38- SMAD-crosstalk. But the link between activated p38 and the phosphatase remain unclear.

Since PPM1A (PP2Cα) was identified as a nuclear R-SMAD phosphatase that directly dephosphorylates C-terminal phosphorylated SMAD1, 2 and 3, I focused on this candidate. PPM1A limits the activation state of SMAD2/3 and promotes nuclear export and depletion of cellular PPM1A expression enhances TGFβ responses. PPM1A is not specific for SMADs but has many other substrates like phosphatidylinositol-3 kinase, axin, CDK2 and CDK6 (Lin *et al*, 2006; Duan *et al*, 2006; Yoshizaki *et al*, 2004; Strovel *et al*, 2000; Cheng *et al*, 2000). Interestingly, PPM1A is not induced by TGFβ signaling, neither in terms of activity nor in terms of subcellular distribution (Lin *et al*, 2006). In accordance I could show that knockdown of PPM1A enhanced nuclear SMAD2 translocation in microscopy experiments. Nevertheless, even after PPM1A siRNA transfection and p38 inhibition was the p38 effect

recognizable. Therefore, PPM1A is probably not involved in the p38-mediated TGFβ response. However, compensation mechanisms and incomplete knock down can obscure the result.

Interestingly as an outlook, the p38 pathway is involved in the control of posttranslational modification of SMADs. Specifically, it has been demonstrated that p38 regulates the sumoylation of SMAD4 by proteins of the PIAS family of E3 ligases, contributing to an enhancement of SMAD4-dependent transcription. Sumoylation of SMAD4 mainly occurs at lysine 159, located in the linker region (Ohshima and Shimotohno, 2003). In another exciting study Zhang *et al* demonstrated, that inhibition of p38 MAP kinase inhibited *de novo* TGFβ1 protein synthesis without interfering with SMAD activation (Zhang *et al*, 2006). What that has to do with changing SMAD dynamics needs to be explored in future experiments. A useful approach would be to use kinase translocation reporters (KTRs), which enable multiplexed measurements of the dynamics of kinase activity at single-cell level (Regot, 2014). This would allow to track p38 kinase activity and SMAD dynamics in the same cell. These KTRs are composed of an engineered construct in which a kinase substrate is fused to a bipartite nuclear localization signal (bNLS) and nuclear export signal (NES), as well as to a fluorescent protein for microscopy-based detection of its localization. The relative cytoplasmic versus nuclear fluorescence of the KTR construct (the C/N ratio) is used as a proxy for the kinase activity in living, single cells (Kudo *et al*, 2018). Unfortunately, microscopy experiments with an established KTR cell line resulted in a weak p38 signal after TGFβ stimulation. Which role substrates of p38, such as MAPK-activated protein kinase 2 (MK2) play could also be investigated in further experiments.

Numerous small molecule inhibitors of p38 MAPK, including VX745, have been developed and have entered clinical trials. Given the critical roles of p38 MAPK in mediating TGFβ-induced CREB phosphorylation and transcription, as well as EMT (Bakin *et al*, 2002) and cell death (Yoo *et al*, 2003; van der Heide *et al*, 2011), the use of these inhibitors in a clinical context may have consequences on the TGFβ responses as well. Depending on different biological contexts, p38 MAPK inhibitors may prove to be useful as inhibitors of TGFβ-induced metastasis or may prove less useful by promoting tumor proliferation through blocking TGFβ-induced apoptosis (Sapkota, 2013).

Finally I investigated the influence of the ERK pathway, another non-canonical MAP Kinase pathway of TGFβ activation, on SMAD dynamics. According to a study by Huang and Chen, TGFβRII alone is able to mediate TGFβ signaling to ERK1/2, and differences in the level of TGFβRII expression determine whether or not TGFβ activates or inhibits ERK1/2 (Huang & Chen, 2012). The kinetics of ERK phosphorylation induced by TGFβ varies with cell types and culture conditions. The ShcA/Grb2/Sos complex is capable of activating Ras at the plasma membrane, leading to sequential activation of c-Raf, MEK, and ERK (Zhang, 2009). I showed that inhibition of the kinase activity of p38 and TGFβ stimulation led to enhanced ERK signaling in MCF10A WT cells. However, inhibition of ERK signaling

could not abrogate the p38 effect. Nevertheless, I examined the impact of ERK signaling on SMAD dynamics in live cell time-lapse microscopy experiments.

With increasing EGF concentrations the maximum amplitude and the second response rose. Thus, cells without EGF in the media before stimulating with TGFβ showed extremely low SMAD2 activation. Interestingly, already the basal nuclear and cytoplasmic SMAD2 levels increased with increasing EGF concentrations. In addition, the increasing TGFβ response by rising EGF concentrations was not due to a changed proportion of responders. With Western blot analysis I confirmed the results, as without EGF only a very weak phosphorylation of SMAD2 and SMAD3 has been measured. Furthermore, cells without EGF almost did not divide. But the different EGF concentrations had no influence on the proportion of dividing cells. But I found that cells moved more with increasing EGF concentrations and therefore both ERK and TGFβ signaling may important for EMT.

Moreover, inhibiting the ERK signaling through Gefitinib, a tyrosine kinase inhibitor of the epidermal growth factor receptor (EGFR), led to reduced nuclear SMAD2 accumulation at later time points through an enhanced adaptation, while the amplitude of the initial response remained unchanged. Western blot analysis also confirmed the results and the late phosphorylation of SMAD2 and SMAD3 was diminished. Even if the cascade was inhibited downstream of the receptors, such as the Raf kinase with Sorafenib (Wilhelm *et al*, 2004; Adnane *et al*, 2006), MEK1 and 2 with AZD6244 and UO126, another dual MEK1 and MEK2 inhibitor (Davies *et al*, 2007) a diminished late SMAD2 and SMAD4 response due to a stronger adaptation was observed which confirmed the results with Gefitinib.

Furthermore, I analyzed the impact of this dynamic remodeling on gene expression and cell fate. I showed that Gefitinib prevented the late activation of Snail. This supports the hypothesis that the long-term dynamics of SMAD2 are probably responsible for EMT and the balance between SMAD activation and ERK signaling defines cellular responses to TGFβ. ERK1/2 activation has been linked to a number of TGFβ-regulated cellular events, including CKIs p21Cip1 and p27Kip1 gene expression and growth arrest (Hartsough *et al*, 1996; Frey and Mulder, 1997), EMT (Zavadil *et al*, 2001) and breast cancer cell motility (Dumont *et al*, 2003). Moreover, activation of ERK was necessary for TGFβ induced fibroblast replication (Hough *et al*, 2012). Finally, ERK substrates, such as AP-1 family members, can interact and function in conjunction with SMADs to regulate gene expression (Davies *et al*, 2005; Zhang *et al*, 1998; Hall *et al*, 2003). Interestingly, it was shown that in HK2 cells TGFβ1 mRNA autoinduction was inhibited by the ERK MAP kinase inhibitor PD98059 (Zhang *et al*, 2006). In addition, Zhang *et al*, showed that TGFβ1 activates NF-κB via ERK MAP kinase and that this is also required for transcriptional autoinduction of TGFβ. An alternative signaling pathway was described, where by activating phosphotidylinositol 3-kinase (PI3K), TGFβ stimulates p21-activated kinase2 (Pak2) to phosphorylate

c-Raf, ultimately resulting in ERK activation. The TGFβ/PI3K/Pak2/Raf/MEK/ERK pathway regulates SMAD signaling and is critical for TGFβ-induced growth (Hough *et al*, 2012).

Furthermore, since ERK signaling had an enormous impact on the long-term dynamics of SMAD2 and SMAD4 and affected TGFβ cell fate decisions, I investigated the underlying mechanisms of this cross-talk.

First of all, by using the *SMAD7* CRISPR Cas9 knock out cell line I showed that SMAD7 played no role for the gefitinib effect. In addition, by using Okadaic acid, I observed that inhibition of PP1 and PP2A phosphatases did not abrogate the modulated SMAD2 response due to inhibition of ERK signaling. Finally, I found out that the phosphatase group PP2C interfered with ERK signaling to modulate the long-term dynamics of SMADs. Inhibition of PP2C with Sanguinarine chloride abrogated the effect of inhibition of the ERK cascade on SMAD2 and SMAD4 and all cells showed a strong SMAD response. Also I demonstrated that adding Sanguinarine chloride 3 hours post stimulation to Gefitinib pretreated cells immediately enhanced the SMAD2 accumulation into the nucleus. Moreover I confirmed that Gefitinib worked efficiently and the ERK cascade was also interrupted when treated with Sanguinarine and Gefitinib and ERKs remained unphosphorylated in Western blot analyzes. In conclusion a PP2C family member was involved in the ERK- SMAD-crosstalk, but the link between ERK signaling and the phosphatase remains unclear. Thus, I investigated that after PPM1A siRNA transfection and gefitinib inhibition, the gefitinib effect was almost gone. By clustering on the first 45 minutes of the cytoplasmic response to separate cells with a very good PPM1A knock down from those with worse or none knock down, I gathered evidence that PPM1A was involved in the ERK-mediated TGFβ response. Gefitinib-treated cells with a very good PPM1A knock down showed the same or even stronger response after TGFβ addition. In conclusion, without PPM1A the Gefitinib effect disappeared and thus late SMAD2 nuclear translocation was PPM1A-dependent. In addition, Gefitinib slightly increased the expression of PPM1A, but this was only slightly reflected in Western experiments. Therefore, modifications of PPM1A must be investigated in further experiments. Because the receptor kinase is located in the membrane compartment and R-SMAD phosphatases such as PPM1A are nuclear, the dynamic equilibrium between phosphorylation and dephosphorylation must be closely coupled to the nucleocytoplasmic transport of SMADs (Schmierer & Hill, 2007).

In addition to C-terminal phosphorylation at a conserved SS*X*S sequence, more recent research has shown that R-SMADs can also be phosphorylated in the linker region between their Mad homology domains, which is important for both full activation and cessation of activation (Alarcón *et al*, 2009; Matsuzaki *et al*, 2009). ERK phosphorylates the linker region of nuclear localized SMADs, resulting in increased half-life of C-terminal pSMAD2 and 3 (Ser465/467) and increased duration of SMAD target gene transcription (Hough *et al*, 2012). ERK signaling has also been proposed to inhibit TGFβ signaling

since ERK phosphorylates serine or threonine residues in the PX(S/T)P or (S/T)P motif of the linker regions in receptor SMADs (SMAD1,2,3,5,8) which then cannot migrate into the nucleus, thus inhibiting TGFβ-SMAD signaling (Kretzschmar *et al*, 1999). This mechanism might explain why in some cells with hyperactive Ras signaling the response to TGFβ is inhibited (Calonge *et al*, 1999; Kretzschmar *et al*, 1999). But other studies have not reported impaired nuclear translocation of SMADs in Ras-transformed cells or in cells with activated MAP kinase signaling (Engel *et al*, 1999; Lehmann *et al*, 2000).

Thus, Ras and TGFβ-signals act cooperatively as well as antagonistically during development and in oncogenesis. Although TGFβ can override the proliferative effects of EGF and other Ras-activating mitogens in normal epithelial cells, oncogenic activation of Ras suppresses the cytostatic effects of TGFβ. As Ras has diverse effectors and targets in the cell, its interplay with TGFβ- signaling is likely to occur at multiple levels, many of which involve indirect molecular interaction. Oncogenic Ras also appeared to induce degradation of SMAD4 (Saha *et al*, 2001). Interestingly, Ras/MAP kinase signaling also induces expression of TGFβ1 thereby amplifying the TGFβ response and inducing secondary TGFβ responses and thus may explain the often-observed increase in expression of TGFβ1 by tumor cells. (Yue & Mulder, 2000b; Owen *et al*, 1990; Geiser *et al*, 1991; Van Obberghen-Schilling *et al*, 1988).

Thus, in the context of cancer, the crosstalk between ERK, TGFβRs and SMADs has been shown to directly and indirectly promote cancer growth in the early stages of cancer resulting in metastasis (Corn *et al*, 2008; Fu *et al*, 2009; Giehl *et al*, 2007).

Also here, kinase translocation reporters (KTRs) could help to shed light on the cross-talk between SMAD and ERK signaling. Unfortunately, microscopy experiments with an established KTR cell line resulted in only a weak ERK signal after TGFβ stimulation. An evaluation was not possible. Furthermore, in future experiments the impact of PPM1A on the ERK-mediated SMAD2 response could be validated with a CRISPR/ CAS9 PPM1A knock out cell line. In addition, PPM1A is one of the phosphatases responsible for the removal of phosphate residues from cyclin dependent protein kinases (Cheng *et al*, 2000). Since CDKs are also involved in the linker phosphorylation of R-SMADs, one could examine the link in further experiments. Moreover, PPM1A dephosphorylates RanBP3 to enable efficient nuclear export of SMAD2 and SMAD3. PPM1A directly interacts with and dephosphorylates RanBP3 at Ser 58 in vitro and in vivo. Dephosphorylation of RanBP3 at Ser 58 promoted its ability to export SMAD2/3 and terminate TGFβ responses (Dai *et al*, 2011). In contrast RSKs (ribosomal S6 kinases) phosphorylate Serine 58 of RanBP3 (Yoon *et al*, 2008). Since activated ERKs phosphorylate and activate downstream RSKs, in further experiments one could investigate the link between SMAD dynamics, RanBP3, RSK and PPM1A.

In addition, at present, modeling efforts have been focused on the canonical TGFβ signaling cascade, but it is imperative to develop mathematical models that comprise also non-canonical pathways in order to accurately predict overall TGFβ signaling and cellular outcome. Interestingly, in an automated high-throughput interaction mapping, more than 100 proteins associated with the TGFβ receptor complex were identified (Barrios-Rodiles *et al*, 2005). Many of these proteins are either themselves signaling molecules or are signaling adaptors, which suggest a tremendous extent of cross-talk. In conclusion, further clarification of the mechanisms of the cross-talk between the TGFβ, MAPK pathways and other signaling pathways may offer novel breakthroughs and potential applications in the field of therapeutic approaches.

5 CONCLUSION AND OUTLOOK

In this study, I provided a quantitative understanding of how cells encode and decode information about the identity and quantity of a TGFβ stimulus. I followed pathway activation at the single-cell level by monitoring the translocation of SMADs from the cytoplasm to the nucleus with high temporal and spatial resolution. By analyzing the median nuc/cyto SMAD2 and SMAD4 ratio of the cell population with live-cell microscopy, one synchronous initial response of SMAD translocation at 1h, followed by adaptation and a second signaling phase with temporally less defined periods of nuclear translocation could be monitored. Adaptation mechanisms are a combinatorial effect of ligand degradation, proteasomal degradation, receptor endocytosis and feedback strength, which act at different time scales and doses. The future focus must be on how the various adaptation mechanisms change SMAD dynamics, and how this correlates precisely with cell fate. Analysis of the SMAD2 and SMAD4 reporter cell lines revealed, that the extent and duration of SMAD nuclear accumulation was highly variable and cells showed a broad variability of dynamics, although they were clonal cells. I showed that phenotypic responses and cell fate decisions were correlated with distinct dynamic behavior. One of the most challenging goals will be identifying the molecular mechanisms that are necessary to translate the different dynamical patterns into distinct phenotypic responses. Furthermore, the TGFβ/SMAD pathway does not function in isolation, but is one part of a signaling network in which cross-talk between pathways occurs. Indeed, the dynamic response of SMADs is influenced by cross-talk of non-canonical p38 and ERK MAPK signaling and especially the long-term dynamics define the nature of cellular responses to TGFβ ligands . The dynamic remodeling of SMADs through the impact of p38 and ERK signaling is mediated by phosphatases of the PP2C family member. Future research should focus on the link between p38 or ERK signaling and the phosphatases. Moreover, I gathered evidence that PPM1A is involved in the ERK-mediated TGFβ response. Thus, modifications of PPM1A must be investigated in further experiments. In general, future studies should include more cell lines to exclude cell type specific differences. In conclusion, further clarification of the mechanisms of the cross-talk between the TGFβ, MAPK pathways and other signaling pathways may offer novel breakthroughs and potential applications in the field of therapeutic approaches. Modeling simulations could help uncover these mechanisms.

6 MATERIALS AND METHODS

6.1 Cloning

6.1.1 Genomic DNA isolation

For the isolation and purification of genomic DNA from cultured MCF10A cells, the QIAamp Mini DNA Kit (Qiagen) was used. The isolation was performed according to the manufacturers protocol. The DNA was eluted with 200µl elution buffer (EB, Qiagen).

6.1.2 Polymerase chain reaction

The polymerase chain reaction (PCR) is a method to amplify DNA fragments using specific primers. *Taq* (NEB), Phusion High-Fidelity (NEB) or Q5 High-Fidelity DNA polymerase (NEB) were used with the following reaction setup and programs (**Table 1 and 2**):

Phusion High-Fidelity DNA polymerase
10 µl 5× GC-Buffer
1 µl dNTP mix (10 mM)
1.5 µl Forward primer (10 pmol/µl)
1.5 µl Reverse primer (10 pmol/µl)
10 µl Betaine
0.5 µl Phusion DNA polymerase
10-200 ng Template
up to 50µl ddH_2O

Q5 High-Fidelity DNA polymerase:
10 µl 5× Q5-Buffer
1 µl dNTP mix (10 mM)
1 µl Forward primer (10 pmol/µl)
1 µl Reverse primer (10 pmol/µl)
0.5 µl Q5 DNA polymerase
10-200 ng Template
up to 50µl ddH_2O

Taq DNA polymerase:

5 µl 10× *Taq*-Buffer

1 µl dNTP mix (10 mM)

1 µl Forward primer (10 pmol/µl)

1 µl Reverse primer (10 pmol/µl)

0.5 µl *Taq* DNA polymerase

10 ng Template

up to 50 µl dd H_2O

Step	Temperature	Time	Cycles
Initial denaturation	98 °C	1.50 min	1
Denaturation	98 °C	10s	15
Annealing	65 °C	30s	15
Elongation	72 °C	1.05 min	15
Denaturation	98 °C	10s	20
Annealing	60 °C	30s	20
Elongation	72 °C	1.05 min	20
Final elongation	72 °C	7.00 min	1

Table 1. Program used for Phusion or Q5 polymerase.

Step	Temperature	Time	Cycles
Initial denaturation	95 °C	5.00 min	1
Denaturation	95 °C	10 s	35
Annealing	60 °C	30 s	35
Elongation	72 °C	1.05 min	35
Final Elongation	72 °C	7.00 min	1

Table 2. Program used for *Taq* polymerase.

6.1.3 DNA analysis and purification by agarose electrophoresis

For separation and purification of DNA fragments, 1% - 2% agarose gel with ethidium bromide (EtBr, 1:20000, ROTH) were prepared. For a 1% (w/v) agarose gel, 1 g of agarose was dissolved in 100 ml 1× TAE buffer by heating in a microwave, until the solution appeared totally clear. EtBr was added after the solution had cooled down to approximately 40°C. Gel was loaded with either 3 µl (for DNA verification) or total sample volume (for later DNA extraction) mixed with respective volume of 6× DNA loading dye, along with 5µl 2-log DNA ladder mix (NEB). Running time was dependent on gel size and preferred degree of separation, as well as used voltage (approximately 40 - 70 min/80-100 V). For purification after detection, DNA bands were cut out of the gel and Gel Extraction kit (Qiagen) was used according to manufacturers manual. DNA was eluted in 30 µl elution buffer (EB, Qiagen) and concentration was measured with Nanodrop 2000c Spectrophotometer (Thermo Fisher Scientific).

-1xTAE buffer:

40 mM Tris, 20 mM Acetic Acid, 1 mM EDTA

-2Log DNA Ladder mix:

1/6 2Log DNA Ladder (NEB), 1/6 TriTrack DNA loading dye, 4/6 H_2O

6.1.4 Electroporation and chemical transformation of *Escherichia coli*

Cloning of plasmid constructs was carried out either in chemical (DH5α E.coli, NEB) or electro competent cells (Top10 E.coli, Thermo Fisher Scientific). Shortly before transformation cells were thawed on ice and either 15 µl of chemical competent or 50 µl of electro competent cells were gently mixed with 1 µl plasmid solution. Electro competent cells were then transferred to an electro-shock cuvette (ROTH) and electroporation (Eppendorf) was carried out. LB or SOC medium (1 ml) was used for resuspending the cells and transferring them to a new tube for incubation at 37°C/250 rpm for 1 hour. To grow single colonies, 30 µl of the cells were spread on LB-Kanamycin plates (50 µg/ml, AppliChem) or LB-Ampicillin plates (100 µg/ml, AppliChem) and placed in an incubator at 37°C over night. The mix of chemical competent cells and plasmid was incubated on ice for 30 minutes, before heat-shock was applied. Thus the cells were incubated at 42°C for 45 seconds and quickly placed on ice for 2 minutes. 200 µl prewarmed LB or SOC media was added and cells were incubated 1 hour at 37°C and 250 rpm. Finally 70 µl of the cell suspension was spread on LB-Kanamycin plates or LB-Ampicillin plates and incubated over night at 37°C. The next day single colonies were picked, transferred to 4 ml LB-medium containing either Kanamycin or Ampicillin and incubated at 37°C/200rpm overnight. Cells from overnight cultures were then pelleted in new 2 ml tubes by centrifuging 5 minutes at 6000 rpm and discarding the supernatant. Pellets were resuspended in 250 µl buffer P1, mixed (by inverting) with 250 µl Buffer P2 and incubated for 5 minutes. Addition of 250 µl buffer P3 was followed by vortexing the solution and incubation for 10 minutes on ice. To separate cell debris from DNA, centrifugation was carried out for 20 minutes at 13000 rpm/4°C and supernatant was mixed with 80% sample volume of isopropyl alcohol. After incubation of 5 minutes, a second centrifugation step of 20 minutes was performed to pellet plasmid DNA. Supernatant was discarded and the pellet washed with 500 µl 70% ethanol, by centrifuging 10 minutes. Again, the supernatant was discarded and the pellet was dried at 37°C for 10-20 minutes, before resuspending the DNA pellet in 40 µl EB buffer (Qiagen).

-Buffer P1:

50mM Tris-HCL pH 8.0, 10mM EDTA, 100ug/ml RNaseA (AppliChem)

-Buffer P2:

200mM NaOH, 1% SDS (ROTH)

-Buffer P3:

3M potassium acetate pH 5.5

-LB broth with agar:

15 g/l Agar, 10 g/l Tryptone, 5 g/l Yeast Extract, 5 g/l NaCl

-LB broth:

10 g/l Tryptone, 5 g/l Yeast extract, 5 g/l NaCl

-SOC medium:

2% Vegetable Peptone, 0.5% Yeast Extract, 10 mM NaCl, 2.5 mM KCl, 10 mM $MgCl_2$, 10 mM $MgSO_4$, 20 mM Glucose

6.1.5 Plasmid DNA isolation

For the isolation and purification of plasmid DNA from overnight cultures, the QIAprep Spin Miniprep Kit (Qiagen) was used. The isolation was performed according to the manufacturers protocol. The DNA was eluted with 30µl EB buffer (Qiagen).

6.1.6 Determination of DNA and RNA concentration

DNA and RNA concentrations were measured at a spectrophotometer (NanoDrop 2000c, Thermo Fisher Scientific). The samples with the DNA or RNA were exposed to ultraviolet light with a spectral range of 190-840nm. To verify the purity of the DNA and RNA samples, the ratio of absorbances at 260 nm and 280 nm was calculated. A_{260}/A_{280} ratios above 1.8 for DNA and 2.0 for RNA indicate pure samples. Due to protein contamination, the ratio decreases.

6.1.7 Digestion of DNA samples

To verify the insertion of the desired DNA fragments in plasmids or to prepare the DNA for other cloning processes, a restriction digest was performed. By using appropriate restriction enzymes and associated buffers (NEB) DNA molecules were cleaved at selected sites. The reaction mixture was set up as follows: 10 µl DNA (200-1000 ng), 2 µl 10× CutSmart Buffer, 0.5 µl *Enzyme* I (10 U/µl), 0.5 µl *Enzyme* II (10 U/µl) and filled up to 20 µl with nuclease-free water. The reactions were incubated at 37 °C for 1 hour.

6.1.8 Sequencing

Plasmids were diluted to 100ng/µl in 15 µl and sequenced at LGC genomics.

6.2 MCF10A WT and SMAD2/SMAD4 reporter cell lines

Human breast epithelial MCF10A cells were cultured in DMEM/F-12 medium (Thermo Fisher Scientific) supplemented with 5% horse serum (PAN-Biotech), 20 ng/ml epidermal growth factor (EGF, PeproTech), 0.5 µg/ml hydrocortisone (Sigma-Aldrich), 100 ng/ml cholera toxin (Sigma-Aldrich) and 10 µg/ml insulin (Sigma-Aldrich), penicillin and streptomycin (Thermo Fisher Scientific) at 37 °C and 5% CO_2 (Debnath *et al,* 2003). When required, the medium was supplemented with selective antibiotics to maintain transgene expression (400 µg/ml geneticin disulphate (G418, ROTH), 50µg/ml hygromycin B (Thermo Fisher Scientific), 5 µg/ml blasticidin S hydrochloride (ROTH) or 0.5 µg/ml puromycin dihydrochloride (ROTH). We generated lentiviral reporter constructs for SMAD2 and SMAD4 using the MultiSite-Gateway recombination system (Invitrogen) by fusing the protein coding sequence to the yellow fluorescent protein Venus (YFP) under the control of a constitutive human Ubiquitin C promoter (UbCp). We infected MCF10A cells with corresponding lentiviral particles together with viruses expressing histone 2B fused to cyan fluorescent protein (H2B-CFP) under the control of UbCp as a nuclear marker. Furthermore, I generated a combined fluorescent reporter cell line (E9) by fusing SMAD4 to YFP and SMAD2 to the red fluorescent protein mCherry under the control of UbCp. As an inverse variant I generated a combined cell line (A3) by fusing SMAD2 to YFP and SMAD4 to mCherry. In addition, both cell lines also stably express the nuclear marker histone H2B-CFP to enable automated image analysis. Subsequently, stable clonal cell lines were established and validated.

6.3 *SMAD7* transient knock down cell line

A clonal cell line (F10) with inducible shRNA expression for SMAD7 gene silencing in the background of the SMAD2-YFP reporter cell line (6.2) was generated (transient *SMAD7* knock down cell line). Therefor the SMAD2-YFP cell line was infected with pTRIPZ lentiviral inducible vectors which are engineered to be TET-ON and produce induction of shRNA expression in the presence of doxycycline (2µg/ml) (Thermo Scientific Open Biosystems Expression Arrest TRIPZ Lentiviral shRNAmir). Four different TRIPZ inducible lentiviral shRNA (RHS201904993, 201904238, 201903626 and 201902033) for regulatable *SMAD7* gene silencing were applied together. Since the vector contain a puromycin drug resistance marker, 0.5 µg/ml puromycin dihydrochloride (ROTH) was used to select stable cell lines. Subsequently, stable clonal cell lines were established and validated. For time-lapse microscopy experiments 0,5 x 10^5 cells (F10) were plated in 35mm poly-D-lysine-coated glass bottom plates

(MatTek Corporation) two days before experiments, whereby doxycycline (2µg/ml) was added to the medium and the horse serum (PAN-Biotech) was replaced by BSA (Sigma-Aldrich) for all conditions.

6.4 *SMAD7* knock out in MCF10A using CRISPR/Cas9

A *SMAD7* knock out cell line in MCF10A was created utilizing the CRISPR/Cas9 system. The knock out of *SMAD7* affects both alleles of the gene to ensure a complete loss of the corresponding protein. To this end, we first infected SMAD2-YFP reporter cells (6.2) with lentiviruses expressing *Cas9* under control of a doxycycline-inducible promoter (Wang *et al,* 2014). A clonal SMAD2-YFP Cas9 reporter cell line was generated and acted as a new control cell line. This clonal cell line was further infected with viruses expressing a single guide RNA (sgRNA) targeting exon 2 of SMAD7 (TCCTTACTCCAGATACCCGA) (Shalem *et al,* 2014) and cultured for 11 days in the presence of doxycycline (1µg/ml, Sigma-Aldrich) to create a polyclonal *SMAD7* knock down cell line. By annealing two oligos and utilizing Gibson Assembly the final sgRNA was cloned by Caibin Cheng. The sgRNA is a noncoding RNA which directs the Cas9 endonuclease to the desired genomic locus and exon 2 of the endogenous *SMAD7* gene was targeted and cleaved. Multiple rounds of target sequence cleavage induced DNA double-stranded breaks (DSBs) which are mainly repaired by nonhomologous end joining (NHEJ). Because NHEJ is an error prone mechanism, it facilitates the occurrence of nucleotide deletions or insertions (indels) at the site of cleavage, which can lead to frameshift mutations or premature stop codons (Ran *et al*, 2013). Next step was to determine from the resulting polyclonal cell line the mutation status of the genomic loci by using T7 endonuclease assay.

T7 endonuclease recognizes and cleaves non-perfectly matched DNA that results from annealing DNA strands that have been modified after a sgRNA/Cas9 mediated cut to DNA strands without modifications. This assay was used to get a first estimate of whether our targeting was effective or not. The assay consisted of three steps: 1. Isolation of genomic DNA (6.1.1) and amplification of *SMAD7* gen region by PCR (6.1.2) 2. Denaturation and annealing of DNA fragments 3. Digestion with T7 Endonuclease and gel-analysis (6.1.3). 200 ng of genomic DNA of MCF10A clones were obtained according to section 6.1.1 and PCR was performed with SMAD7EXON2_fwd 5´TCC CGA GTG CGC TAG GAA TG 3´ and SMAD7EXON2_rev 5´CCC CAA GCC TTT GCC TAC AC 3´ primer and Phusion DNA polymerase (NEB) (6.1.2) and the desired Exon 2 locus was amplified. The PCR product was run on a 1% gel, DNA was extracted and purified according to section 6.1.3. In preparation for the T7 Endonuclease digest, 175 ng extracted DNA of SMAD7 clones was mixed with equal amounts of SMAD2-YFP Cas9 reporter cell line, 2 µl of NEB buffer 2 and Elution buffer (Qiagen) up to 19 µl were added. Using a touchdown PCR program (starting at 95°C and gradually decreasing down to 25°C) DNA was denatured and annealed. 1 µl T7 Endonuclease (NEB) was added directly to the DNA mix and

incubated at 37°C for 1 hour. Whole sample volume was then applied on a 2% gel and extend of cleavage was analyzed (6.1.3). The results of the PCR products of the SMAD7 locus around exon2 according to the T7 endonuclease assay are shown in **Figure 51**. While the SMAD2-YFP Cas9 reporter cell line reveals just one band, three bands are identified for the polyclonal *SMAD7* knock out SMAD2-YFP Cas9/sgRNA cell line after cleavage of the DNA due to mutations in the *SMAD7* gene. Since a large portion of the original PCR product band 1 is no longer present, it indicates a high level of mutated genomic DNA.

Figure 51

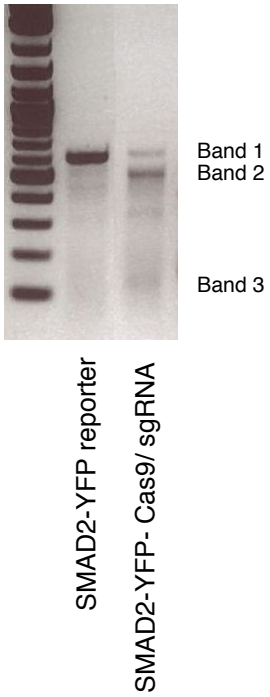

6.4 Figure 51. T7 endonuclease assay.
Results of T7 endonuclease assay analyzed on an agarose gel. While the SMAD2-YFP reporter cell line reveals one band, three bands are identified for the polyclonal SMAD7 knock out SMAD2-YFP Cas9/sgRNA cell line after cleavage of the DNA due to mutations in the SMAD7 gene.

Finally, I established and screened clonal cell lines for alterations of the *SMAD7* locus by sequencing and I selected a cell line with non-sense mutations in both alleles. Genomic DNA of MCF10A clones were obtained and (6.1.1) PCR was performed by using the primer SMAD7 EXON2 fwd and rev (6.1.2). The product was used for TA- Cloning with the pGEM-T Vector (Stratagene). For A-tailing 5µl of PCR product was then mixed with 1 µl 10x Taq-buffer, 0.2 µl dNTP and 1 µl Taq polymerase and incubated for 20 minutes at 70°C. Subsequently, 5µl of 2x rapid ligation buffer, 1µl pGEM-T vector (50ng), 2µl of A-tailing product, 1µl of T4 DNA ligase and 1 µl H_2O were mixed and incubated for 1h at room temperature. 1µl of the reaction was transformed in chemical competent *E. coli* cells (DH5α, NEB) (6.4). 70 µl of the transformed bacteria were plated on X-Gal (ROTH) and IPTG (Isopropyl β-D-1-

thiogalactopyranoside, ROTH) added LB- ampicillin (AppliChem) plates. If β-galactosidase is produced, X-gal is hydrolyzed to form 5-bromo-4-chloro-indoxyl, which spontaneously dimerizes to produce an insoluble blue pigment called 5,5'-dibromo-4,4'-dichloro-indigo. The colonies formed by non-recombinant cells, therefore appear blue in color while the recombinant ones appear white. The white colonies were picked and cultured. Isopropyl β-D-1-thiogalactopyranoside (IPTG) is used along with X-gal for blue-white screening. IPTG is a non-metabolizable analog of galactose that induces the expression of lacZ gene of the pGEM-T vector. A test digest with ScaI or BsaI (NEB, positive fragment 3600bp, negative 3000bp) was performed (6.1.7) and then sent for sequencing (6.1.8).

6.5 TGFβ and inhibitor and treatments

Suspended cells were stained with trypan blue (Sigma-Aldrich) and then counted in an automated TC10TM cell counter (Bio-Rad) and depending on the experiment seeded 48h prior to TGFβ treatment. Recombinant human TGFβ 1 was obtained from R&D Systems (#240-B-002) and stored at -80°C in 4mM HCl, 1mg/ml bovine serum albumin (Sigma-Aldrich) at 390nM. In Western blot, RT-qPCR and immunofluorescence experiments media were replaced with fresh ones containing DMSO (control condition, Sigma-Aldrich) or the inhibitors shown in **Table 3**, 45 minutes before TGFβ treatment (usually 100pM TGFβ). For microscopy experiments media were replaced with fresh ones (6.2) and the inhibitors or DMSO (Sigma-Aldrich) were added after one unstimulated round of images 45 minutes before TGFβ treatment (usually 100pM TGFβ). TGFβ 1 was prepared in 500µl media and added after one unstimulated round of images or in addition to inhibitors to achieve the final concentration in 2.5ml media. Re-stimulations were carried out by aspirating old medium and changing to new medium with desired TGFβ concentration, while leaving the plates in the incubator.

Inhibitor	**Final concentration**	**Supplier**
AZD6244	1µM	Axon Medchem
BIRB796	5µM	Axon Medchem
Dorsomorphin	2µM	Selleckchem
DRB (5,6-Dichlorobenzimidazole 1-β-D-ribofuranoside)	100µM	Cayman
Dynamin Inhibitor, Dynasore	50µM	Santa Cruz
Gefitinib	3µM	Cayman
JNK Inhibitor VIII	0.5-20µM	Cayman
LDN 193189	100nM	Selleckchem
MG132	10µM	Calbiochem
Noggin	10ng/ml	Biomol
Nystatin	50µg/ml	Sigma-Aldrich
Okadaic acid	25nM	Sigma-Aldrich
RO3306	3µM	Axon Medchem
SB202190	10µM	Axon Medchem

Sanguinarine chloride	1µM	TOCRIS
Sorafenib	10µM	LC Laboratories
TGF-β RI Kinase inhibitor VI SB431542	10µM	Calbiochem
UO126	10µM	NEB
5Z-7-Oxozeaenol	2µM	Sigma-Aldrich

Table 3. Inhibitors used in experiments.

6.6 Time-lapse microscopy

For live-cell time-lapse microscopy, $2x10^5$ reporter cells were plated in 35mm poly-D-lysine-coated glass bottom plates (MatTek Corporation) two days before experiments. Before starting the experiment, cells were washed twice with 1xPBS and media was changed to RPMI 1640 lacking phenol red and riboflavin (PAN-Biotech) supplemented with all growth factors (6.2), 5% horse serum (PAN-Biotech) and antibiotics. In addition the media contained HEPES buffer (10 mM) and GlutaMAX (2 mM) (both from Thermo Fisher Scientific). Six glass bottom plates fit in the tray of the movable microscope stage, which made it possible to observe six conditions during one time-lapse experiment. Per plate ten positions were selected using transmitted light to prevent bleaching or stressing the cells. Lids of the plates were replaced by glass discs to prevent evaporation, while making it easy to access the plates for further additions. The microscope was surrounded by a custom enclosure to maintain constant temperature (37°C), CO_2 concentration (5%), and humidity. Cells were imaged on a Nikon Ti inverted fluorescence microscope with a Hamamatsu Orca R2 or Nikon DS-Qi2 camera and a 20x plan apo objective (NA 0.75) using appropriate filter sets (Venus: 500/20 nm excitation (EX), 515 nm dichroic beam splitter (BS), 535/30 nm emission (EM); CFP: 436/20 nm EM, 455 nm BS, 480/40 nm EX). Images were acquired every 5 minutes for the duration of the experiment (usually 24 hours) using Nikon Elements software. To calibrate raw images, eliminate background noise from the camera and normalize differences of fluorescence illumination, flat field images were acquired after each experiment. To this end, 2.5 ml DMEM/F-12 medium were imaged with increasing exposure times, starting with 0 ms, until the signal saturated. From these images the offset and gain for every pixel was calculated. This information was then used to correct images, which were taken during time lapse experiments.

6.7 Cell tracking and image analysis

Cells were tracked throughout the duration of the experiment using custom-written Matlab (MathWorks) scripts based on code developed by the Alon lab (Cohen *et al*, 2008) and the CellProfiler project (Carpenter *et al*, 2006). In brief, we applied flat field correction and background subtraction to raw images before segmenting individual nuclei from nuclear marker images using adaptive thresholding and seeded watershed algorithms. Segmented cells were then assigned to corresponding

cells in following images using a greedy match algorithm. Only cells tracked from the first to last time point were considered. Upon division, we followed the daughter cell closest to the last position of the mother and merged tracks from mothers and offspring. We quantified nuclear fluorescence intensity and measured the fluorescence intensity in the cytoplasm using a 4-pixel wide annulus around the nucleus. The results of the automated image analysis were further processed and normalized. If all cells of a certain time point show spikes simultaneously, it indicates that the flickering of the fluorescent lamp is the reason. Therefore, all spikes were removed by interpolation. Another factor, which can influence the analysis is cell division. To identify cell divisions, we normalized for each cell the nuclear area and the integrated fluorescence intensity of the nuclear marker to their respective means, smoothed them and combined the two trajectories by averaging. In the next step, the median fluorescence for nuclear and cytoplasmic measurements were calculated, which are more robust against fluctuations than the mean intensity. Finally we estimated the nuc/cyt ratio for each cell over time and analyzed the resulting single-cell trajectories computationally (Strasen *et al*, 2018).

Figure 52

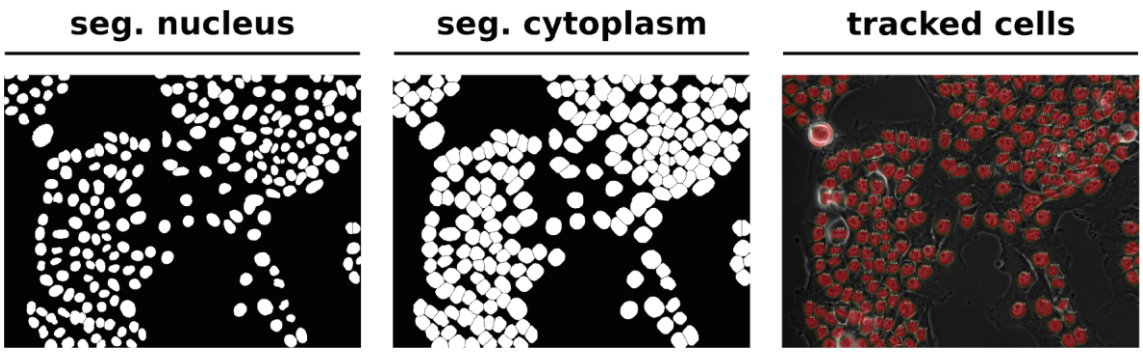

6.7 Figure 52. Image analysis example.
Cells were segmented according to the nuclear marker and cytoplasm was segmented using a 4-pixel wide annulus around the nucleus. The cells were assigned to corresponding cells at following time points. The nucleus of tracked cells is colored in red (Images by Lennart Schnirch, 2015).

6.8 Clustering approach

To compare single cell trajectories a measure for similarity/dissimilarity must be established. Therefore, Marcel Jentsch used Dynamic Time Warping (DTW), a standard method to address the temporal alignment (Sakoe & Chiba, 1978; Berndt & Clifford, 1994; Keogh & Pazzani, 2000, Strasen *et al*, 2018). DTW results in a non-linear mapping of one trajectory to another by warping the time axis iteratively until an optimal match between the two trajectories with respect to the used metric is found. DTW takes into account that distinct patterns within trajectories may differ in frequency and length and affect the shape of an individual time courses. He then used DTW to generate a dissimilarity matrix by computing pairwise dissimilarities between single cells. Based on the pairwise dissimilarity matrix estimated by DTW he applied clustering to group cells with similar dynamic patterns. In

addition, he used the *silhouette* method (Rousseeuw, 1987) for visualizing clustering quality. The *silhouette* method quantifies how similar an object is to objects within its own cluster compared to objects from other clusters and gives a useful graphical representation to assess allocation quality. The silhouette coefficient can range from -1 to 1. The higher the silhouette coefficient for all objects the better the clusters are separated. The assignment of single cell trajectories to signaling classes provides a different separation than grouping cells according to ligand dose.

6.9 Western blot analysis

For western blot experiments 5 x 10^5 MCF10A WT cells were seeded on 5 cm tissue culture plates in 5 ml medium two days before experiments. After stimulation, cells were harvested at the indicated time points after treatment. We kept the cells on ice for the whole process, while the medium was aspirated and cells were washed once with 4 ml cold phosphate-buffered saline (PBS), before adding a final volume of 2 ml PBS. Using a cell scraper cells were detached from the tissue culture plate and centrifuged during 5 minutes at 6000 rpm at 4°C. Subsequently the supernatant was aspirated. Samples were then shock frozen in liquid nitrogen and stored at -80°C. Cell pellets were resuspended in 40-50µl of lysis buffer in the presence of protease and phosphatase inhibitors by vortexing 10 seconds and incubated 20 minutes on ice and centrifuged at 4°C during 20 minutes at 14000 rpm. The supernatant was transferred to a new tube. From here on samples could be stored at -20°C. Total protein concentrations were measured by BCA assay (Thermo Fisher Scientific). The concentration was determined in technical duplicates using a bovine serum albumin (BSA) standard curve (2, 1, 0.5, 0.25, 0.125, 0.0625 and 0 mg/ml). 25 µl of each standard or 2.5 µl of each sample (diluted to 25 µl in H_2O) and 200 µl of Working Reagent (50:1, Reagent A:B) were transferred to a 96-well plate, followed by incubation of 25 minutes at 37°C and 5 minutes at room temperature (RT). The absorbance was measured at 595 nm in a microplate reader (EL800 Universal Microplate Reader) and concentration calculated by Bio-Tek Instruments software. Equal protein amounts (15-20 µg depending on protein concentration) obtained from MCF10A WT whole cell lysate were denatured in sample buffer (NuPAGE LDS Sample Buffer (4X), Thermo Fisher Scientific) and dithiothreitol (DTT) by heating for 10 minutes at 70°C. Proteins were separated by electrophoreses for 35 minutes at 200 V on 4–12% NuPAGE Bis-Tris gradient Mini Gels (Thermo Fisher Scientific) in SDS Running Buffer (NuPAGE, Thermo Fisher Scientific) in a Novex Mini-Cell chamber (Thermo Fisher Scientific) with 5 µl Precision Plus Protein Dual Color marker (Bio-Rad). Subsequently proteins were transferred to nitrocellulose membranes (Roti NC, 0.2 m, ROTH) by electroblotting (Trans-Blot Turbo Transfer System, Bio-Rad). A blotting sandwich was assembled from the anode to cathode as follows: three layers of 3 mm Whatman paper, nitrocellulose membrane, SDS gel, three layers of 3 mm Whatman paper. The papers as well as the gel and membrane

were pre-incubated in 1x Transfer Buffer. Semi-dry blotting was carried out for 30 minutes at 25 V. We blocked membranes for one hour with 5% non-fat dried milk or 5% bovine serum albumin (ROTH) in tris-buffered saline with Tween20 (TBST) according to the antibodies manufacturer's recommendations, incubated them overnight with primary antibody **(Table 4)** at 4°C and shaking with 12 rpm, washed them in TBST, incubated them for one hour at RT with secondary antibody coupled to horseradish peroxidase (HRP, **Table 5**) in 5% non-fat dried milk in TBST, washed again and detected protein levels using Amersham ECL Prime Western Blotting Detection Reagent (GE Healthcare Life Sciences) according to manufactures manual. Chemiluminescent images were captured with ChemiDoc XRS System and Image Lab Software was used for the analysis (Bio-Rad).

Buffers used (all reagents from ROTH, unless otherwise stated):

- PBS

10 mM sodium hydrogen phosphate + 2 mM monopotassium phosphate + 137 mM sodium chloride + 2.7 mM potassium chloride, pH 7.4

- Lysis buffer

50 mM Tris pH 7.5 + 100 mM sodium chloride + 1% Triton X-100 + 0.5% sodium deoxycholate + 0.1% SDS + 50 mM sodium fluoride + 1 mM sodium orthovanadate + 1:100 Protease Inhibitor Cocktail Plus + 1:100 Phosphatase Inhibitor Cocktail (Sigma-Aldrich)

- Transfer buffer

25 mM Tris + 192 mM glycine + 20% methanol

- TBST

50 mM Tris pH 7.5 + 150 mM sodium chloride + 0.1% Tween-20

Primary antibody	**Dilution**	**Supplier**
SMAD2 (D43B4) XP® Rabbit mAb #5339S	1:1000	Cell Signaling
Phospho-SMAD2 (Ser465/467) (138D4) Rabbit mAb #3108	1:1000	Cell Signaling
SMAD4 (B-8) #sc-7966	1:500	Santa Cruz
GAPDH #G9545	1:10000	Sigma-Aldrich
TGFβ Receptor I Antibody (H-100) #sc9048	1:500	Santa Cruz
PP2C-alpha (PPM1A, D18C10) XP® Rabbit mAb #3549P	1:1000	Cell Signaling
SMAD3 (C67H9) Rabbit mAB #9523	1:1000	Cell Signaling
Phospho-SMAD3 (Ser423/425) (C25A9) Rabbit mAB #9520	1:1000	Cell Signaling
SMURF2 (H50) #sc-25511	1:200	Santa Cruz
Phospho-HSP27 (Ser82) (D1H2) XP rabbit mAB #9709	1:1000	Cell Signaling
anti-p21WAF1 (Ab-1) Mouse mAb (EA10)	1:500	Merck Millipore
Phospho-p44/42 MAPK (Erk1/2) (Thr202/Tyr204) Antibody #9101	1:1000	Cell Signaling

Table 4. Primary antibodies for western blot analysis.

Secondary antibody	Dilution	Supplier
Goat anti-Rabbit IgG Secondary Antibody, HRP conjugate	1:10000	Thermo Fisher Scientific
Goat anti-Mouse IgG Secondary Antibody, HRP conjugate	1:10000	Thermo Fisher Scientific

Table 5. Secondary antibodies for western blot analysis.

6.10 RT-qPCR

For Real-Time qPCR (RT-qPCR) experiments 5 x 10^5 MCF10A WT cells were seeded on 5 cm tissue culture plates in 5 ml medium two days before experiments. After stimulation, cells were harvested at the indicated time points after treatment. Total RNA was extracted using High Pure RNA Isolation kit (Roche) according to manufactures manual and concentration was determined by using a photospectrometer (6.1.6, NanoDrop 2000c, Thermo Fisher Scientific) and stored at -80°C. Afterwards, complementary DNA (cDNA) was synthesized via reverse transcription. The following components were mixed and heated for 5 minutes at 70°C in a thermocycler (PEQLAB, VWR):

-1 µg of total RNA
-2 µl of Oligo $d(T)_{23}$ VN (50 µM) (New England Biolabs)
-1 µl of dNTP solution mix (10 mM) (New England Biolabs)
-Up to 10 µl of DEPC-treated H_2O (ROTH)

Next, the following reagents (all from New England Biolabs) were added, and the resulting mix was incubated at 42°C for one hour:

-4 µl of 5X ProtoScript II Buffer
-2 µl of DTT (0.1 M)
-1 µl of ProtoScript II Reverse Transcriptase
-1 µl of RNase Inhibitor, Murine
The resulting cDNA was stored at -20 °C or diluted 1:10 and quantitative PCR was performed. 3 µl of cDNA were mixed with 9.5 µl of primer mix and 12.5 µl of SYBR Green reagent (Roche).
Primer mix:
6.4 µl forward primer (100 µM) + 6.4 µl reverse primer (100 µM) + 987.2 µl DEPC-treated H_2O
The final concentration of each primer in the reaction mix was 243.2nM.
Quantitative PCR was performed in triplicates on a StepOnePlus PCR machine (Applied Biosystems) with the following thermal profile:
1) 95°C for 10 minutes
2) 40 cycles: 95 °C for 15 seconds, 60 °C for one minute

To determine the level of expression for each gene of interest the comparative C_T ($\Delta\Delta C_T$) method was used. First, the difference between the C_T value of a housekeeping gene (β-actin) and the C_T value of the gene of interest was calculated resulting in the ΔC_T value. Then, the difference in the ΔC_T values between the experimental and control samples is calculated resulting in the $\Delta\Delta C_T$ value.

β-Actin forward:	GGC ACC CAG CAC AAT GAA GAT CAA
β-Actin reverse:	TAG AAG CAT TTG CGG TGG ACG ATG
SnoN forward:	GGC TGA ATA TGC AGG ACA G
SnoN reverse:	TGA GTT CAT CTT GGA GTT CTT G
SMAD7 forward:	ACC CGA TGG ATT TTC TCA AAC C
SMAD7 reverse:	GCC AGA TAA TTC GTT CCC CCT
PAI1 forward:	GGC TGA CTT CAC GAG TCT TTC A
PAI1 reverse:	ATG CGG GCT GAG ACT ATG ACA
Snail forward:	GCT CGA AAG GCC TTC AAC TGC AAA
Snail reverse:	AGG CAG AGG ACA CAG AAC CAG AAA
PPM1A forward:	TAC GGC TGT GAT CGG TTT GC
PPM1A reverse:	ATA CAG CCA GAG AGC CAT TCA C
TIEG forward:	GCC AAC CAT GCT CAA CTT CG
TIEG reverse:	TGC AGT TTT GTT CCA GGA ATA CAT
SMAD2 forward:	GGA GCA GAA TAC CGA AGG CA
SMAD2 reverse:	CTT GAG CAA CGC ACT GAA GG
SMAD4 forward:	GAC TGA GGT CTT TTA CCG TTG G
SMAD4 reverse:	CTT CAA GCT CTG AGC CAT GC
p21 forward:	TGG ACC TGT CAC TGT CTT GT
p21 reverse:	TCC TGT GGG CGG ATT AG
SARA forward:	TGG TTT GCT GAT GGG ATC TT
SARA reverse:	TTC CAA CAG GAC TTC CAA CC
SMAD6 forward:	CAA GCC ACT GGA TCT GTC CGA
SMAD6 reverse:	TTG CTG AGC AGG ATG CCG AAG

Table 6. Primers used in RT-qPCR.
Oligonucleotide primers used in SYBR green RT-qPCR for several human genes. β-actin was used as reference gene. All primers were from Eurofins Genomics.

6.11 TGFβ measurement

We used in collaboration with Prof. Dr. Petra Knaus and Dr. Daniel Horbelt (Institute for Chemistry and Biochemistry, Freie Universität Berlin) Mink lung epithelial cells (MLECs) stably transfected with a

reporter containing a truncated PAI-1 promoter (3TP promoter with three consecutive TPA response elements) fused to the firefly luciferase gene (Abe *et al,* 1994). MLECs were plated at 10000 cells/well in 96 well plates. MCF10A SMAD2 reporter cells were seeded two days before stimulation with 25 pM or 100 pM and supernatants from live-cell microscopy experiments (6.6) were collected 1, 2, 3, 4, 5, 6, 7, 8, 9, 10, 13, 14, 16, 18 and 24 h post stimulation. Samples were frozen at -80°C and transported on dry ice. 50 µl were added in triplicates to MLEC reporter cells together with 50 µl DMEM/0% FCS per well. To create a standard curve, triplicate measurements were performed for different TGFβ concentrations (0, 5, 10, 20 40, 60, 80, 100 and 200 pM) in RPMI 1640 lacking phenol red and riboflavin (PAN-Biotech) supplemented with all growth factors (6.2), 5% horse serum (PAN-Biotech), HEPES, Glutamax (both from Thermo Fisher Scientific) and antibiotics (6.6). After incubation overnight, cells were lysed and thawed. Luciferase activity was measured by 10-second well readings on a Berthold Mithras LB940 plate luminometer using the Promega dual luciferase reporter gene assay kit by Dr. Daniel Horbelt. Marcel Jentsch did further final analysis by using the Hill equation to also reflect nonlinear parts of the calibration curve. The fit to the standard curve was used to convert measured relative luciferase activities into absolute TGFβ concentrations. The estimated TGFβ concentrations at different time points post stimulation were assembled into time courses and fitted using an exponential decay model to estimate the TGFβ decay and half-life for the different initial concentrations (Strasen *et al*, 2018).

6.12 Single molecule RNA fluorescence in situ hybridization (smFISH)

For smFISH experiments 2 x 10^5 reporter cells were seeded in 35mm glass bottom plates with a 500 µM relocation grid (Grid-500 glass bottom dish, Ibidi) with 2,5 ml medium one day before live-cell time-lapse microscopy experiments were performed (6.6). For basal smFISH measurements cells were fixed with 2% paraformaldehyde for 10 min at room temperature before TGFβ stimulation and the time-lapse microscopy experiments started. Otherwise cells were fixed at appropriated time points, washed and permeabilized over night with 70% Ethanol at 4°C. Custom probe sets for single molecule FISH (Raj & Tyagi, 2010) labeled with CalFluor-610 were designed using Stellaris RNA FISH probe designer (Biosearch Technologies) on the reference sequences NM_005904.3 (SMAD7) and NM_000602.4 (PAI1). Hybridization was performed at a final concentration of 0.1 µM probe following manufacturers instructions (Stellaris RNA FISH Protocols - Adherent cells). Coverslips were mounted using Prolong Gold Antifade (Thermo Fisher Scientific). For single molecule RNA quantification, 17 z-stacks of each cell were acquired with 300 nm step size. With Image J the maximum projection was calculated and quantification of RNA counts per cell was performed using the *Star Search* analysis tool for spot detection (http://rajlab.seas.upenn.edu/StarSearch/launch.html). Tracked cells from the microscopy

experiments were manually matched to cells analyzed in *StarSearch.* The coefficient of variation (CV) is defined as the ratio of the standard deviation to the mean and was calculated.

6.13 Immunofluorescence

For immunofluorescence experiments 2,5 x 10^5 MCF10A WT cells were seeded on coverslips coated with poly-L-lysine (Sigma-Aldrich) in 6-well plates two days before experiments. Cells were fixed at indicated time points with 2% paraformaldehyde in PBS for 10 minutes after washing with PBS. Cells were washed again in PBS and permeabilized with 0.1% Triton X-100 in PBS for 20 minutes, blocked with 10% goat serum (PAN-Biotech) in PBS for 30 minutes, incubated with primary antibody in 1% BSA in PBS overnight at 4°C **(Table 7)**, washed with 0.1% Triton X-100 in PBS, and incubated with secondary antibody conjugated with Alexa Fluor 488 or Alexa Fluor 647 (Thermo Fisher Scientific, **Table 8**) in 1% BSA in PBS for 30 minutes. After washing with 0.1% Triton X-100, cells were stained with 2µg/ml Hoechst 33342 (Thermo Fisher Scientific) in 0.1% Triton X-100/PBS for 5 minutes and embedded in Prolong Antifade (Thermo Fisher Scientific). Images were acquired with a 20x plan apo objective (NA 0.75) using appropriate filter sets. Automated segmentation was performed in Matlab (MathWorks) with algorithms from CellProfiler (Carpenter *et al,* 2006).

Primary antibody	Dilution	Supplier
SMAD4 (B-8) #sc-7966	1:50	Santa Cruz
SMAD2 (D43B4) XP® Rabbit mAb #5339S	1:200	Cell Signaling
TGFb RII #sc-17792	1:50	Santa Cruz

Table 7. Primary antibodies for immunofluorescence.

Secondary antibody	Dilution	Supplier
Alexa Fluor™ 488 NHS Ester (Succinimidyl Ester)	1:500	Thermo Fisher Scientific
Dextran, Alexa Fluor™ 647	1:500	Thermo Fisher Scientific

Table 8. Secondary antibodies for immunofluorescence.

6.14 siRNA treatment

For siRNA experiments 2 x 10^5 reporter cells were seeded in 6-well plates one day before siRNA treatment for RT-qPCR knock-down tests and in parallel 2 x 10^5 reporter cells were seeded in 35mm poly-D-lysine-coated glass bottom plates (MatTek Corporation) for time-lapse microscopy experiments. For siRNA treatment, co-transfection complexes were prepared by adding 6.8 µl of a 10 µM siRNA stock solution and 7.5 µl of TransIT-X2 Dynamic Delivery System (Mirus Bio LLC) to 250 µl of Opti-MEM I Reduced Serum Media (Thermo Fisher Scientific). This mix was incubated for 15-30 minutes at room temperature. Then, it was added drop-wise to different areas of the well, and the plate was gently rocked for homogeneous distribution. Two days after siRNA treatment the cells for

the knock-down tests were harvested (RT-qPCR, 6.10) or used for time-lapse microscopy (6.6), respectively. The transfection with scrambled siRNA was done the same way. The sequence of the silencer select validated siRNA PPM1A (ID: s10919, Ambion/Thermo Fisher Scientific) was sense 5´-3´GAC UUG AAG UCA CUG AUG tt, antisense 5´-3´UCA UCA GUG ACU UCA AGU C tg and of the control siRNA was CGU ACG CGG AAU ACU UCG ATT (Zheng *et al*, 2013) ordered from Eurofins Genomics.

7 APPENDIX

7.1 Appendix figures

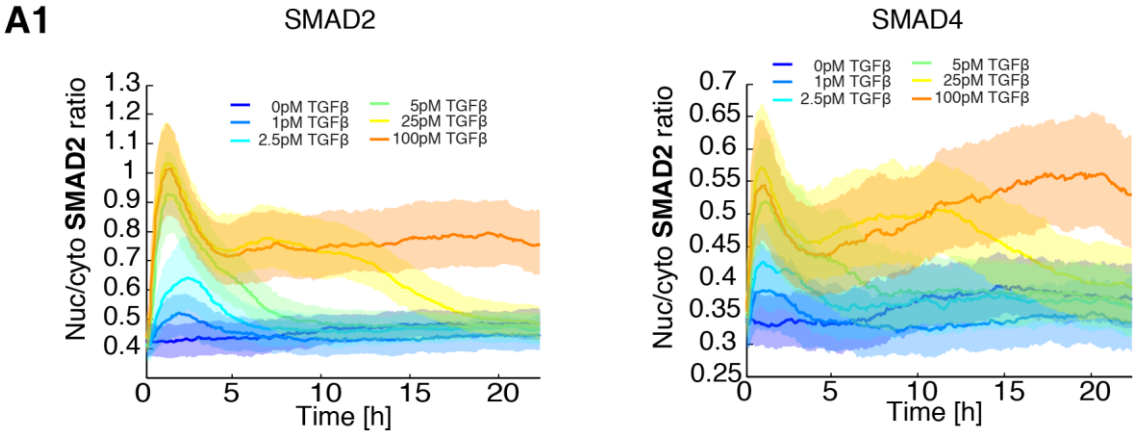

7.1 Figure A1. SMAD2 and SMAD4 show similar dynamics in the same individual cell.
Median nuc/cyto SMAD2 and SMAD4 ratio of the combined SMAD2-YFP- SMAD4-mCherry (A3) reporter cell line stimulated with 0, 1, 2.5, 5, 25 or 100pM TGFβ and tracked over 24h. Shaded area represent data between 25th and 75th percentiles.

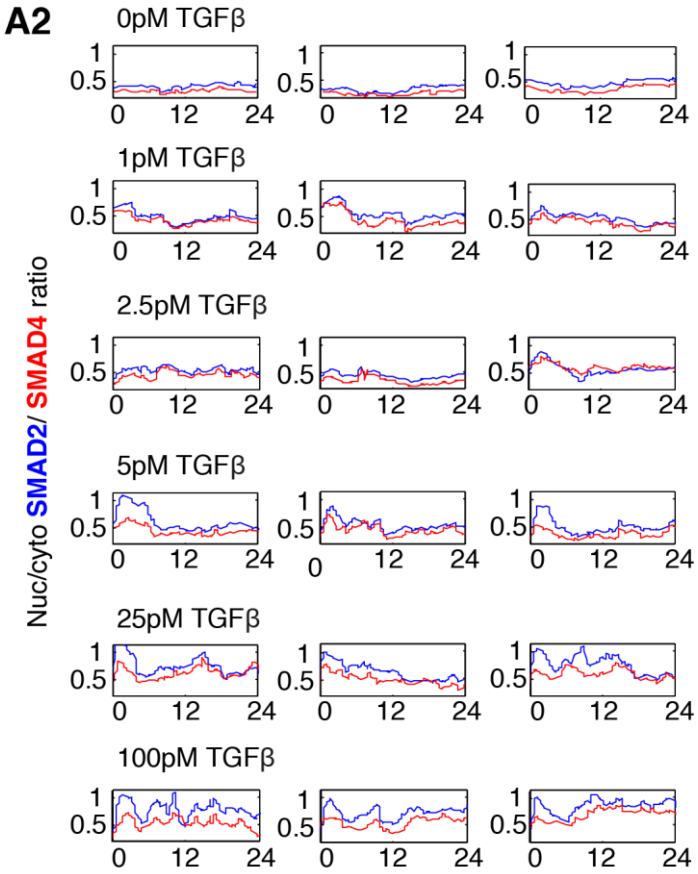

7.1 Figure A2. SMAD2 and SMAD4 show similar dynamics in the same individual cell.
Time-resolved analysis of SMAD2 (blue lines) and SMAD4 (red lines) translocation in the same individual (A3) reporter cells stimulated with varying concentrations of TGFβ.

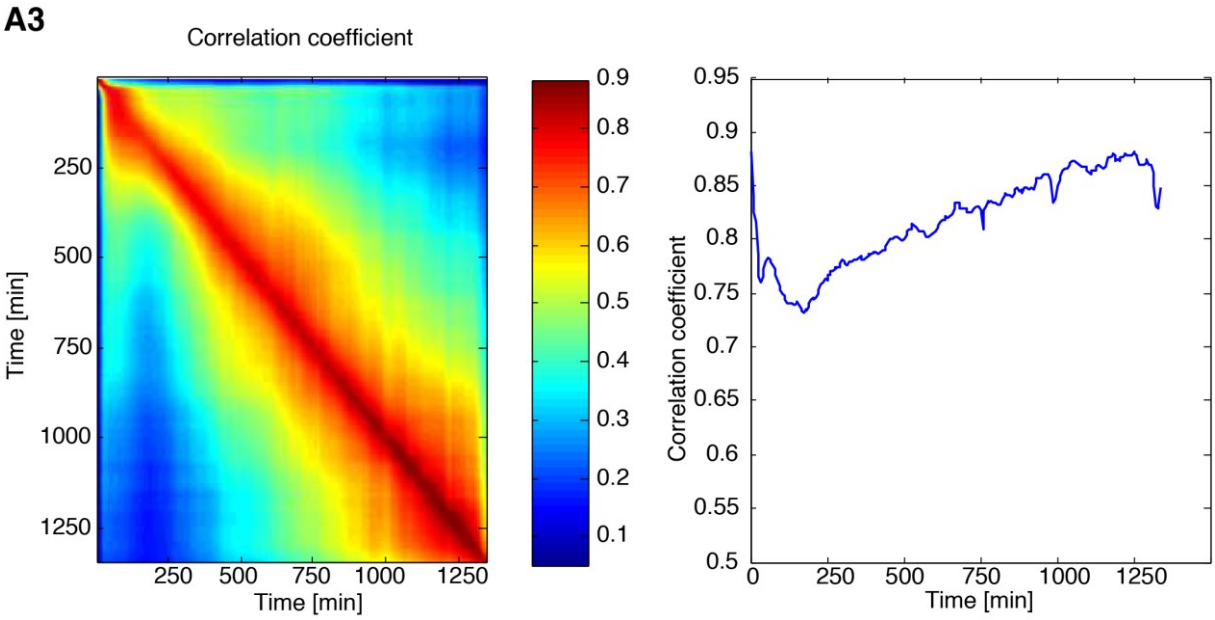

7.1 Figure A3. SMAD2 and SMAD4 show similar dynamics in the same individual cell.
Heat map of correlation coefficient of SMAD2 and SMAD4 translocation in (A3) reporter cells is shown as indicated in the legend (left panel) and correlation coefficient over 24h (right panel).

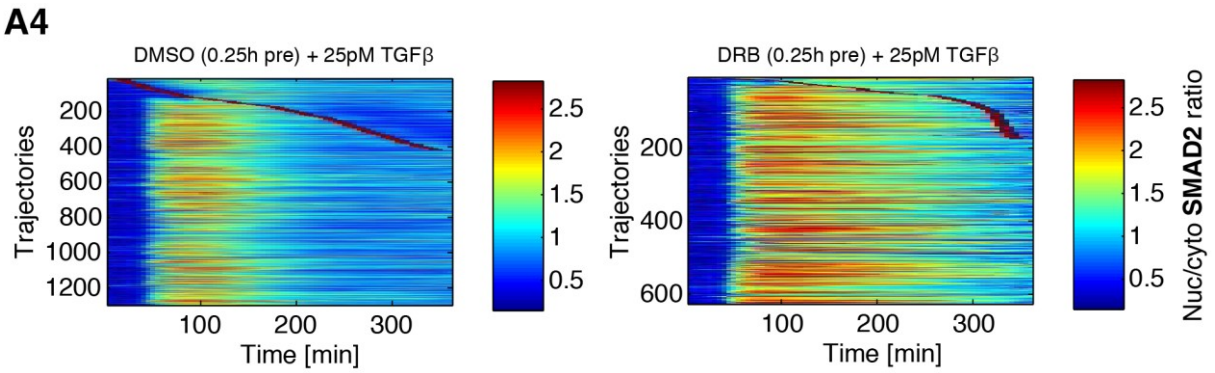

7.1 Figure A4. Inhibition of transcription by DRB attenuates early adaptation.
Heat maps of SMAD2 translocation in individual cells over 24h. Cells were stimulated with 25pM TGFβ and treated with DMSO or DRB 0.25h pre TGFβ stimulus. Each horizontal line represents a single cell and the nuc/cyto ratio is shown as indicated in the legend. Cells were sorted by the time of the first division as indicated by red marks.

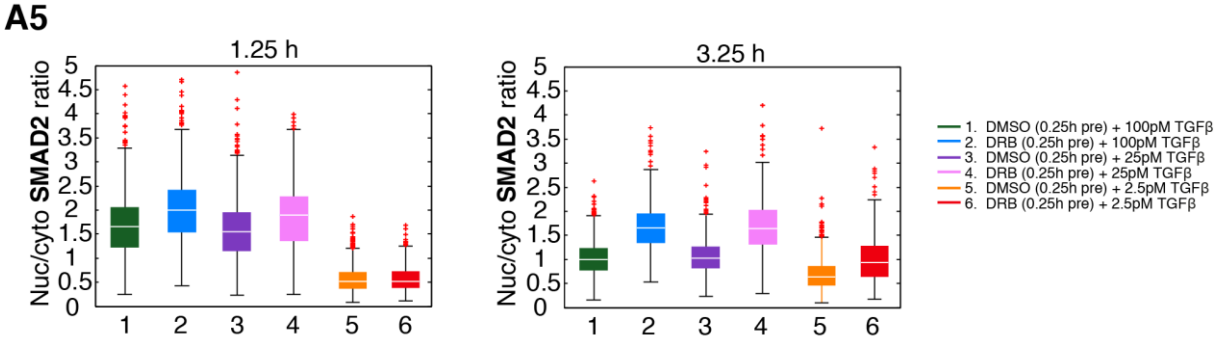

7.1 Figure A5. Inhibition of transcription by DRB attenuates early adaptation.
Signaling features for the SMAD2 reporter cells at 1.25h and 3.25h stimulated with 2.5, 25 or 100pM TGFβ and treated with DRB at indicated time points. White lines indicate median; boxes include data between the 25th and 75th percentiles; whiskers extend to maximum values within 1.5× the interquartile range; crosses represent outliers.

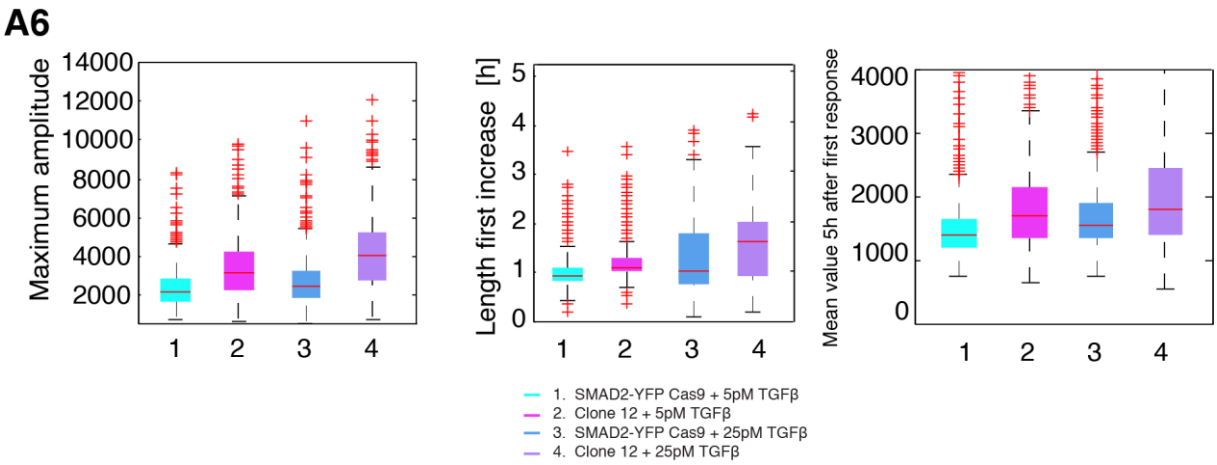

7.1 Figure A6. Sustained *SMAD7* knock out affects SMAD2 dynamics.
Signaling features for nuclear SMAD2 level in the reporter cells stimulated with 5 or 25pM TGFβ as indicated. Red lines indicate median; boxes include data between the 25th and 75th percentiles; whiskers extend to maximum values within 1.5× the interquartile range; crosses represent outliers.

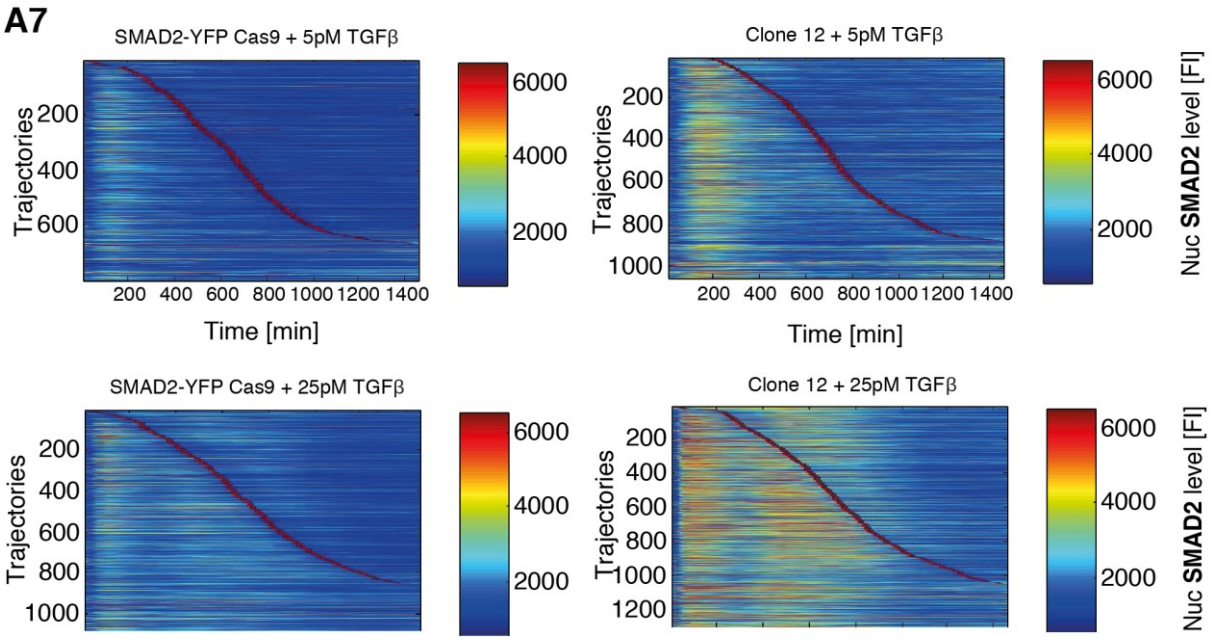

7.1 Figure A7. Sustained *SMAD7* knock out affects SMAD2 dynamics.
Heat maps of nuclear SMAD2 translocation in the reporter cells stimulated with 5 or 25pM TGFβ as indicated over 24h. Cells were stimulated with varying concentrations of TGFβ. Each horizontal line represents a single cell and the nuc/cyto ratio is shown as indicated in the legend. Cells were sorted by the time of the first division as indicated by red marks.

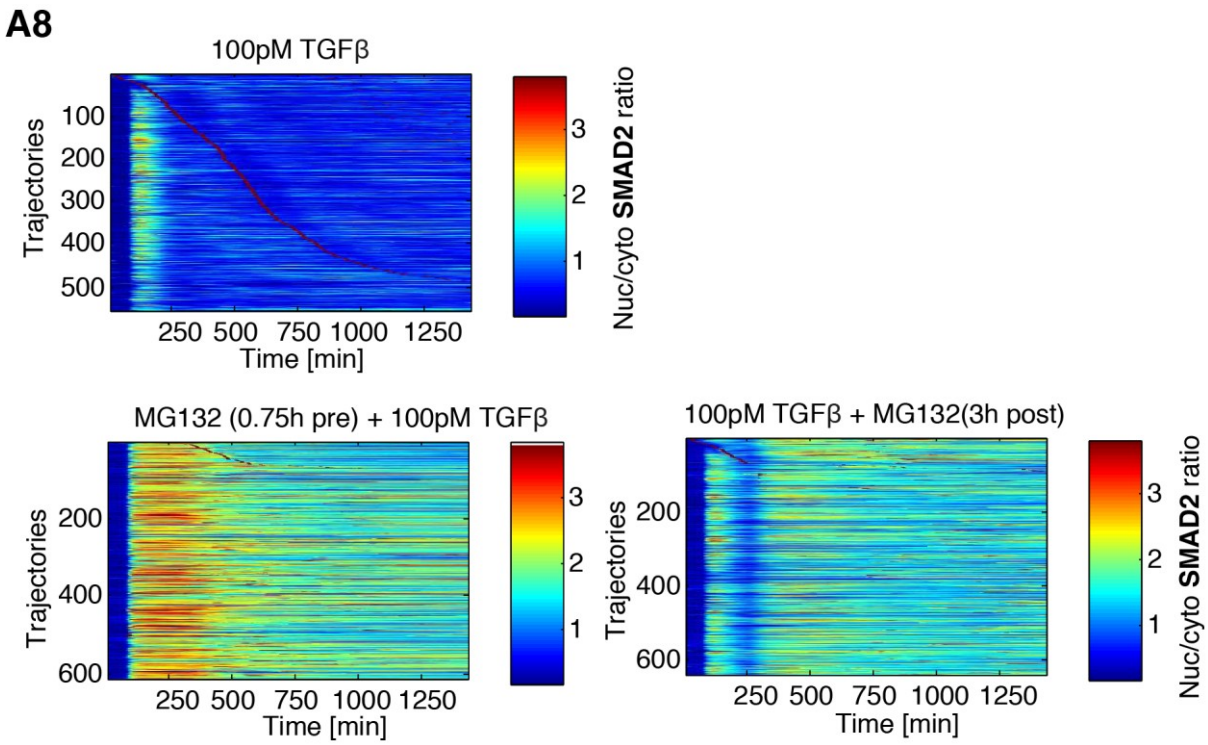

7.1 Figure A8. Inhibition of proteasomal degradation boost nuclear SMAD accumulation.
Heat maps of SMAD2 translocation in individual cells over 24h. Cells were stimulated with 100pM TGFβ and treated with MG132 at indicated time points. Cells were sorted by the time of the first division as indicated by red marks.

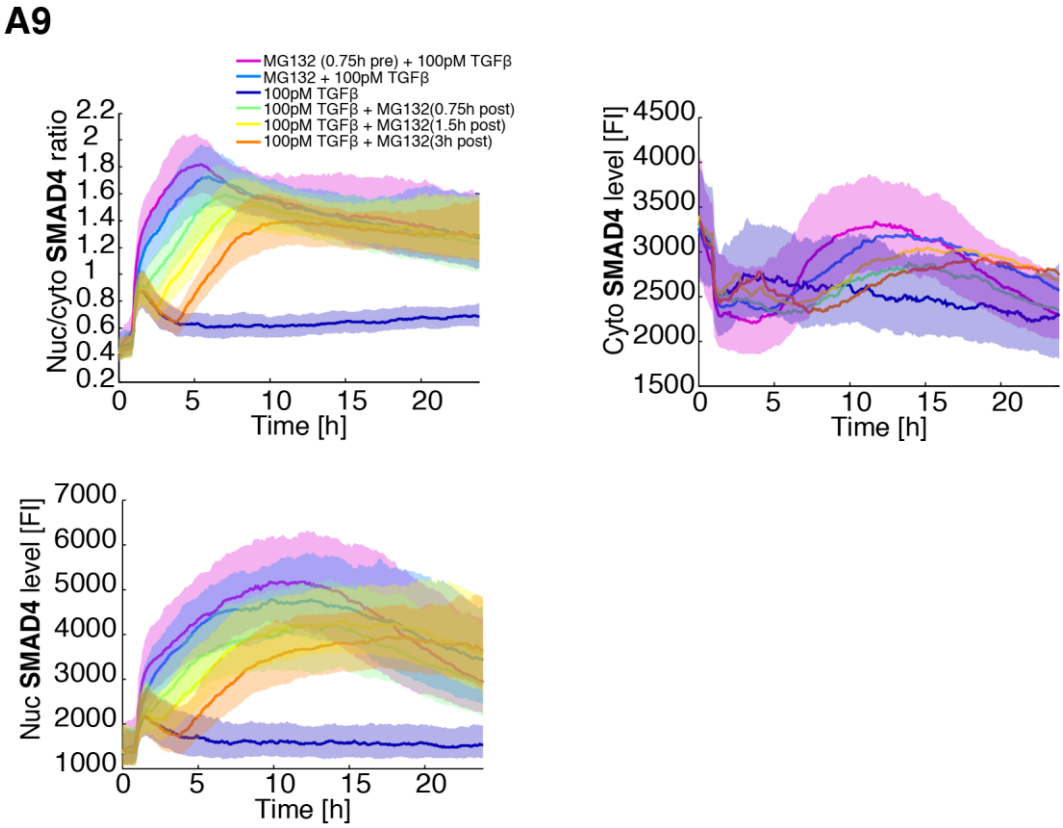

7.1 Figure A9. Inhibition of proteasomal degradation boost nuclear SMAD accumulation.
Median nuc/cyto SMAD4 ratio, median cytoplasmic and nuclear SMAD4 level of the SMAD4-YFP reporter cells stimulated with 100pM TGFβ and treated with the proteasome inhibitor. MG132 at indicated time points. Shaded area represent data between 25th and 75th percentiles.

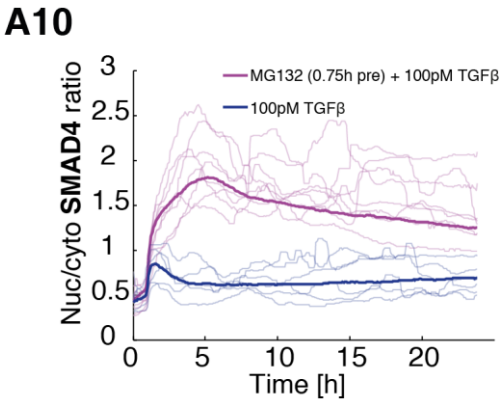

7.1 Figure A10. Inhibition of proteasomal degradation boost nuclear SMAD accumulation.
Exemplary individual nuc/cyto SMAD4 ratio trajectories (thin lines) for the SMAD4-YFP reporter cells stimulated with 100pM TGFβ and treated with MG132 0.75h pre 100pM TGFβ compared to the median nuc/cyto SMAD4 ratio of the entire population (thick line).

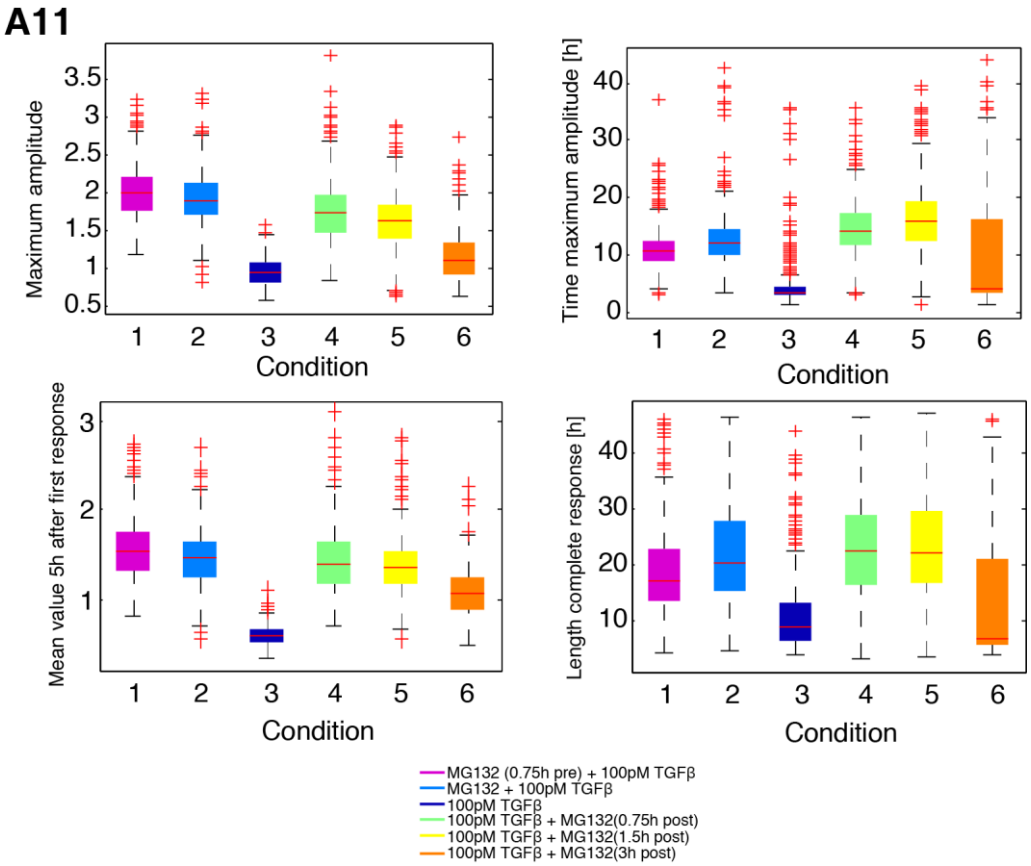

7.1 Figure A11. Inhibition of proteasomal degradation boost nuclear SMAD accumulation.
Signaling features for the nuc/cyto SMAD4 ratio in the SMAD4 reporter cells stimulated with 100pM TGFβ and treated with MG132 at indicated time points. Red lines indicate median; boxes include data between the 25th and 75th percentiles; whiskers extend to maximum values within 1.5× the interquartile range; crosses represent outliers.

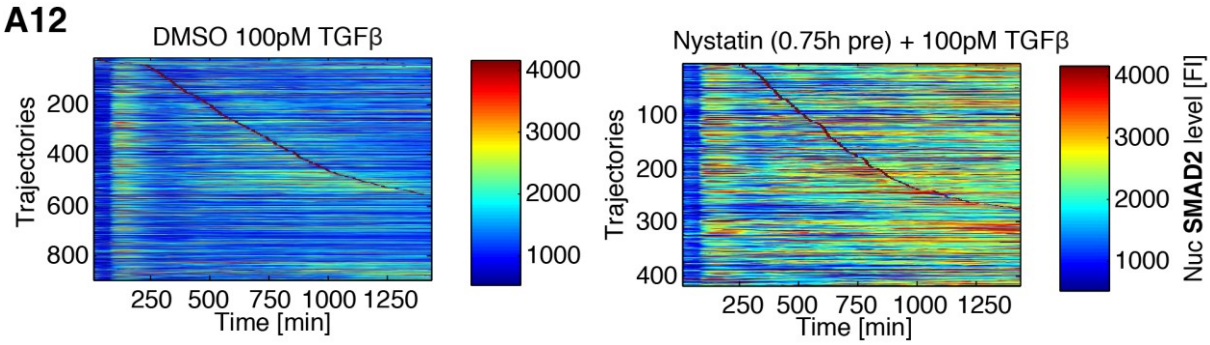

7.1 Figure A12. Receptor internalization and degradation: Endocytotic pathways.
Heat maps of SMAD2 translocation in individual cells over 24h. Cells were stimulated with 100pM TGFβ and 0.75h pretreated with Nystatin. Cells were sorted by the time of the first division as indicated by red marks.

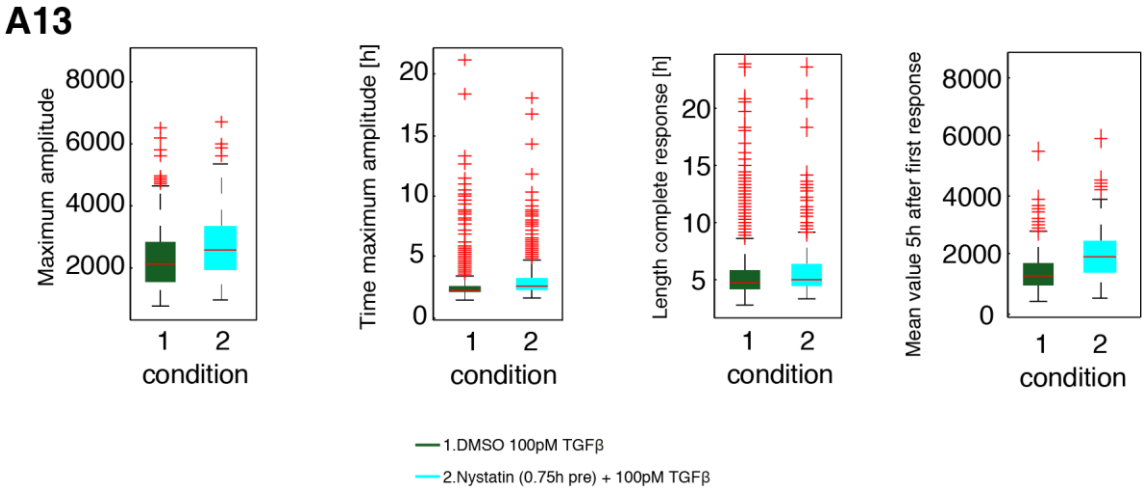

7.1 Figure A13. Receptor internalization and degradation: Endocytotic pathways.
Signaling features for the nuclear SMAD2 level in the SMAD2 reporter cells stimulated with 100pM TGFβ and 0.75h pretreated with Nystatin. Red lines indicate median; boxes include data between the 25th and 75th percentiles; whiskers extend to maximum values within 1.5× the interquartile range; crosses represent outliers.

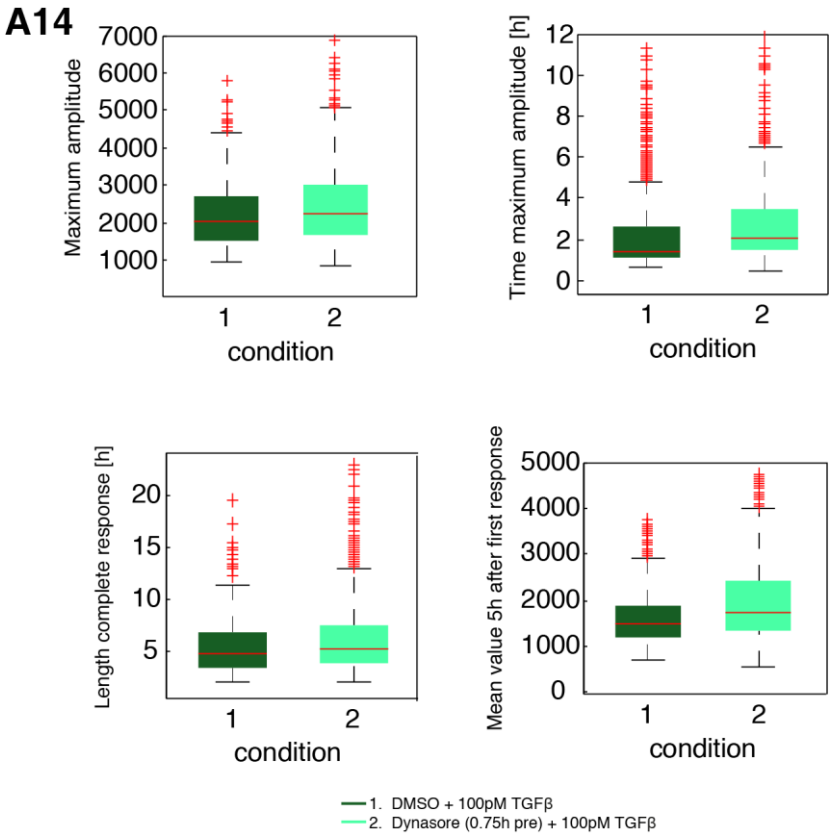

7.1 Figure A14. Receptor internalization and degradation: Endocytotic pathways.
Signaling features for the nuclear SMAD2 level in the SMAD2 reporter cells stimulated with 100pM TGFβ and 0.75h pretreated with Dynasore. Red lines indicate median; boxes include data between the 25th and 75th percentiles; whiskers extend to maximum values within 1.5× the interquartile range; crosses represent outliers.

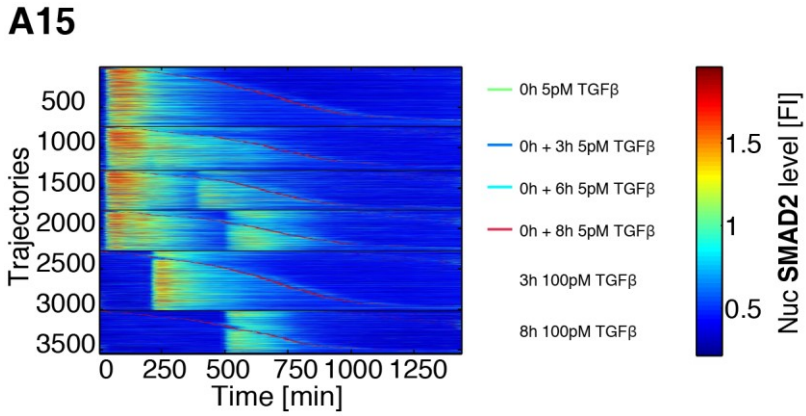

7.1 Figure A15. TGFβ signaling shows a refractory period.
Heat maps of SMAD2 translocation in individual cells over 24h. Cells were stimulated with 5pM TGFβ and restimulated with 5pM TGFβ at indicated time points. Cells were sorted by the time of the first division as indicated by red marks.

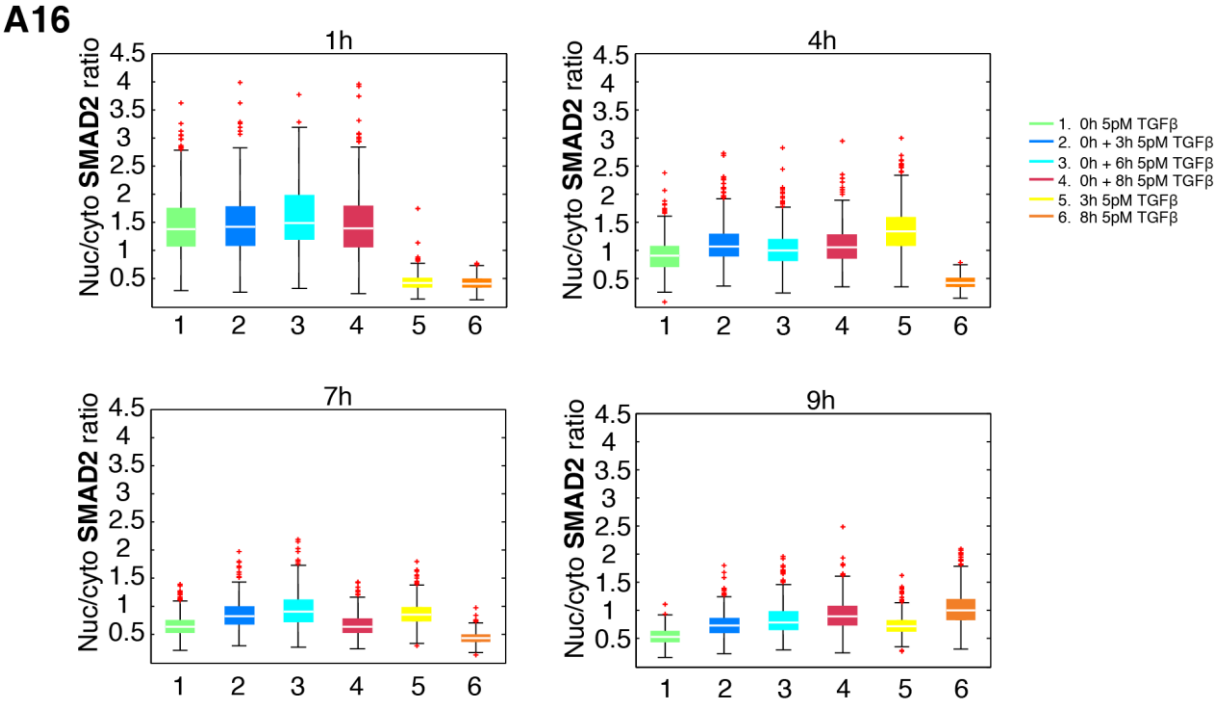

7.1 Figure A16. TGFβ signaling shows a refractory period.
Nuc/cyto SMAD2 ratio of the SMAD2 reporter cells stimulated with 5pM TGFβ and restimulated with 5pM TGFβ at indicated time points at 1, 4, 7 and 9h. White lines indicate median; boxes include data between the 25th and 75th percentiles; whiskers extend to maximum values within 1.5× the interquartile range; crosses represent outliers.

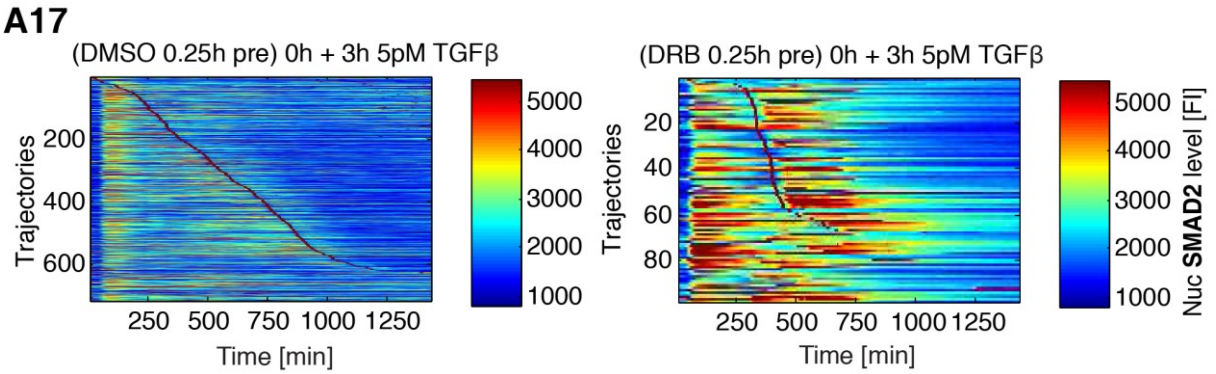

7.1 Figure A17. TGFβ signaling shows a refractory period.
Heat maps of SMAD2 translocation in individual cells over 24h. Cells were stimulated with 5pM TGFβ and restimulated 3h post with 5pM TGFβ and 0.25h pretreated with DRB. Cells were sorted by the time of the first division as indicated by red marks.

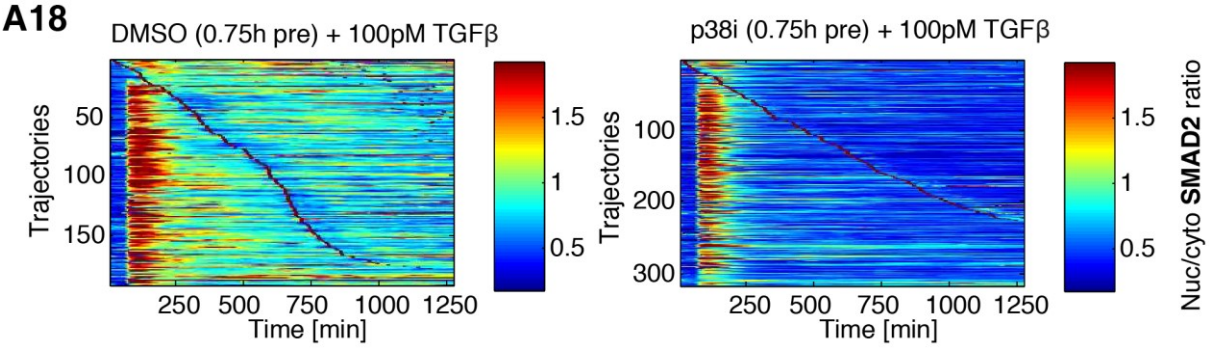

7.1 Figure A18. Inhibition of p38 modulates the dynamics and localization of SMADs.
Heat maps of SMAD2 translocation in individual cells over 24h. Cells were stimulated with 100pM TGFβ and 0.75h pretreated with p38 inhibitors. Cells were sorted by the time of the first division as indicated by red marks.

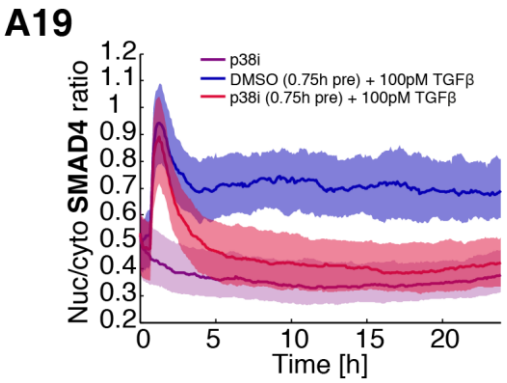

7.1 Figure A19. Inhibition of p38 modulates the dynamics and localization of SMADs.
Median nuc/cyto SMAD4 ratio of the SMAD4-YFP reporter cells stimulated with 100pM TGFβ and 0.75h pretreated with p38 inhibitors (SB202190 & BIRB796). DMSO and only p38 inhibitors were used as controls. Shaded area represent data between 25th and 75th percentiles.

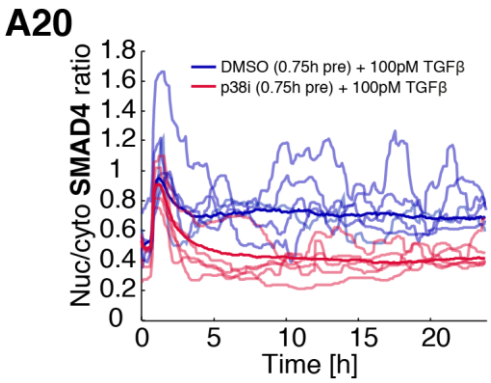

7.1 Figure A20. Inhibition of p38 modulates the dynamics and localization of SMADs.
Exemplary individual nuc/cyto SMAD4 ratio trajectories (thin lines) for the SMAD4-YFP reporter cells stimulated with 100pM TGFβ and 0.75h pretreated with p38 inhibitors compared to the median nuc/cyto SMAD4 ratio of the entire population (thick line).

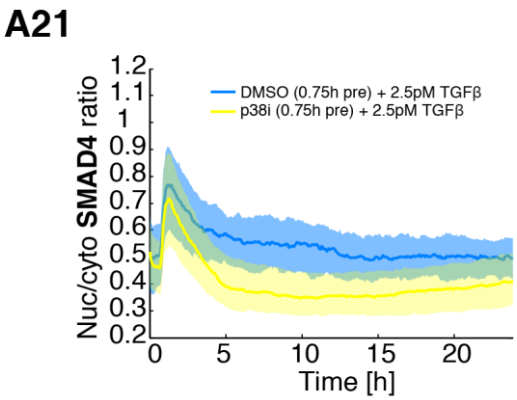

7.1 Figure A21. Inhibition of p38 modulates the dynamics and localization of SMADs.
Median nuc/cyto SMAD4 ratio of the SMAD4-YFP reporter cells stimulated with 2.5pM TGFβ and 0.75h pretreated with p38 inhibitors. Shaded area represent data between 25th and 75th percentiles.

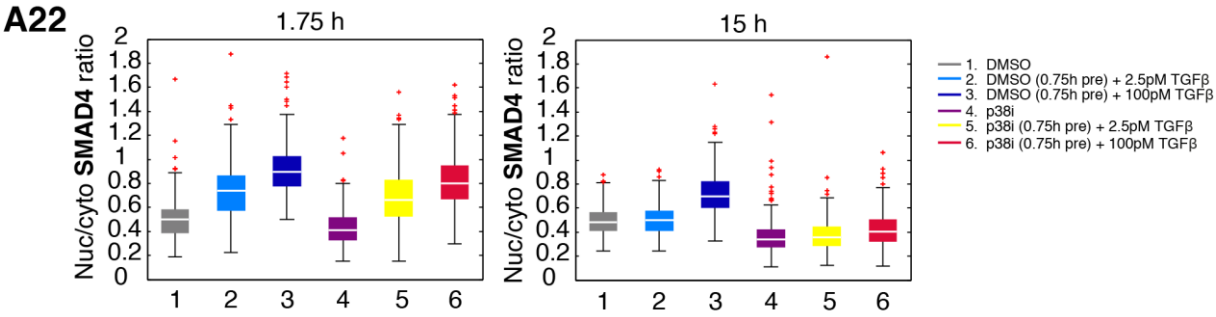

7.1 Figure A22. Inhibition of p38 modulates the dynamics and localization of SMADs.
Nuc/cyto SMAD4 ratio of the SMAD4 reporter cells stimulated with 2.5 or 100pM TGFβ and 0.75h pretreated with p38 inhibitors at time points 1.75 and 15h. White lines indicate median; boxes include data between the 25th and 75th percentiles; whiskers extend to maximum values within 1.5× the interquartile range; crosses represent outliers.

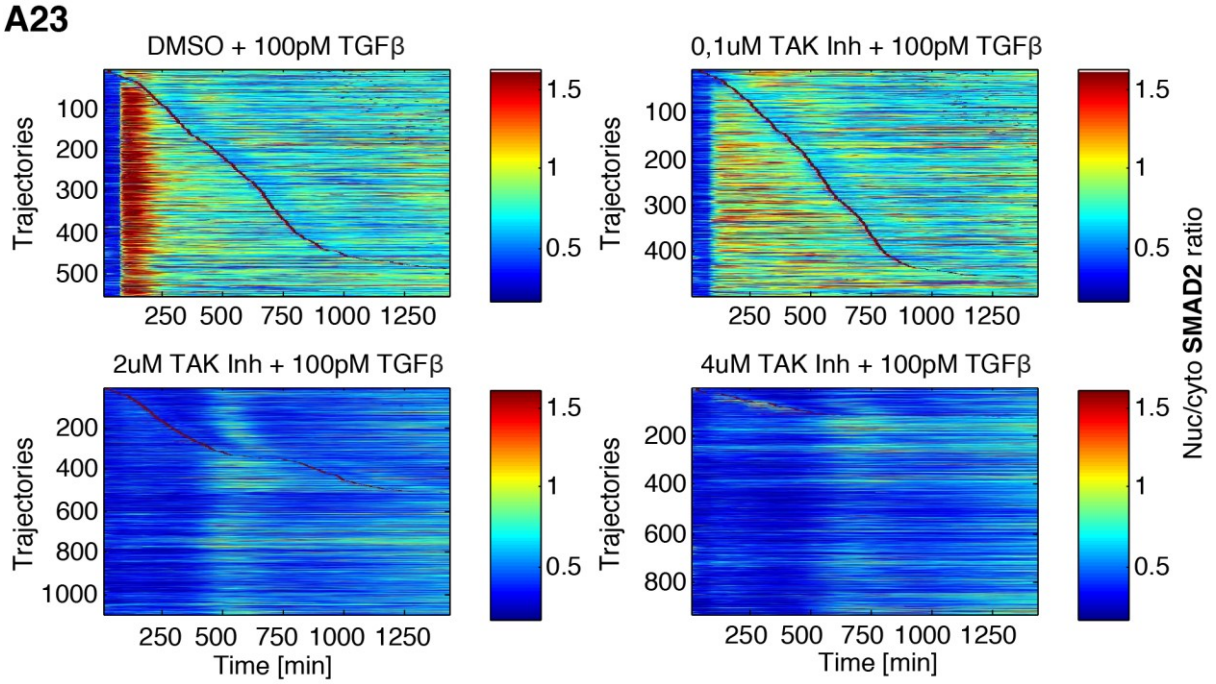

7.1 Figure A23. TAK1 Inhibition modulates the dynamics and localization of SMADs.
Heat maps of SMAD2 translocation in individual cells over 24h. Cells were stimulated with 100pM TGFβ and 0.75h pretreated with 5Z-7-Oxozeaenol (TAKi) at indicated concentrations. Cells were sorted by the time of the first division as indicated by red marks.

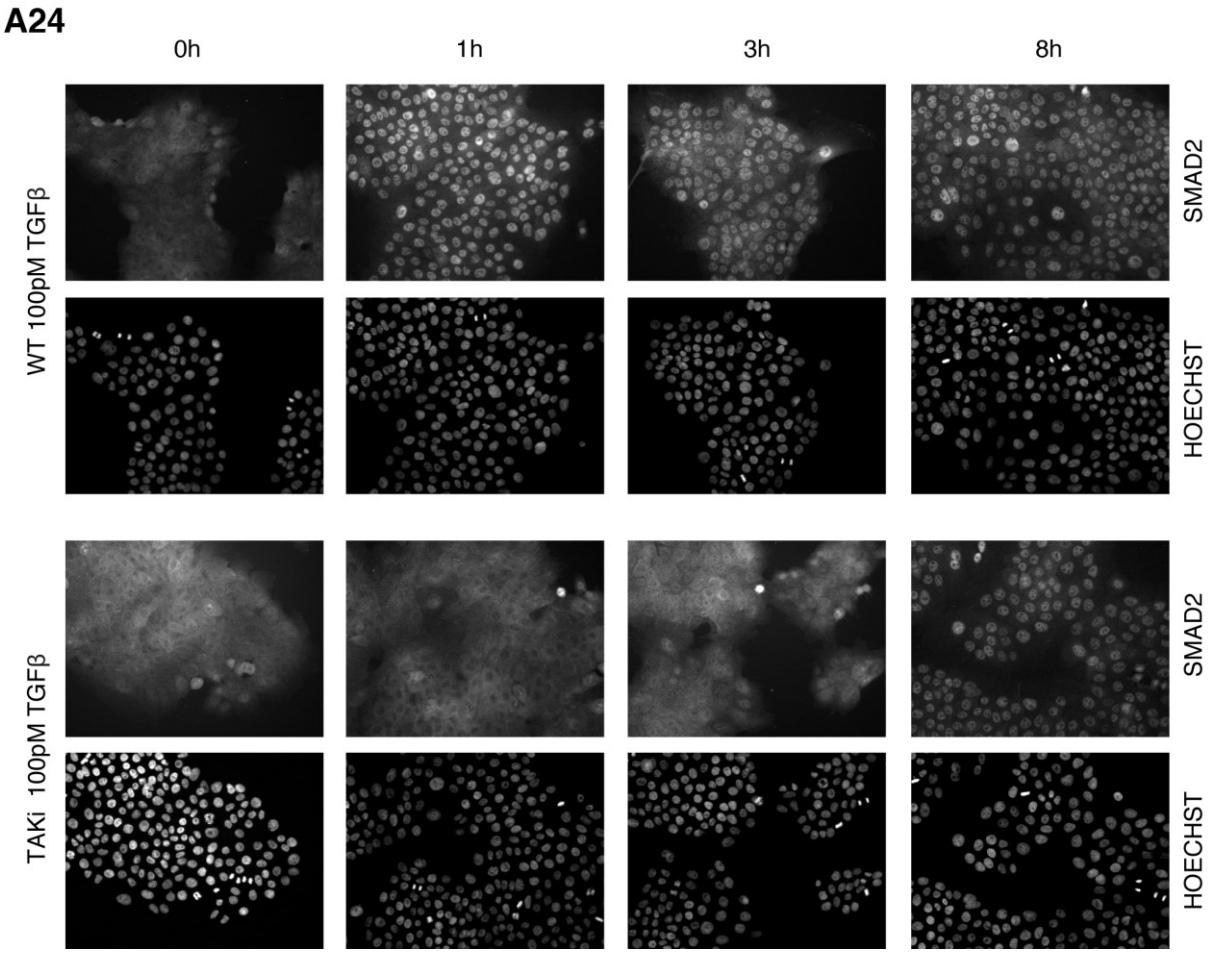

7.1 Figure A24. TAK1 Inhibition modulates the dynamics and localization of SMADs.
Exemplary pictures of SMAD2 fluorescence intensities in MCF10A WT cells stimulated with 100pM TGFβ and 0.75h pretreated with 5Z-7-Oxozeaenol (TAKi) by immunofluorescence at 1, 3 and 8h. Nuclear staining was carried out with Hoechst 33342.

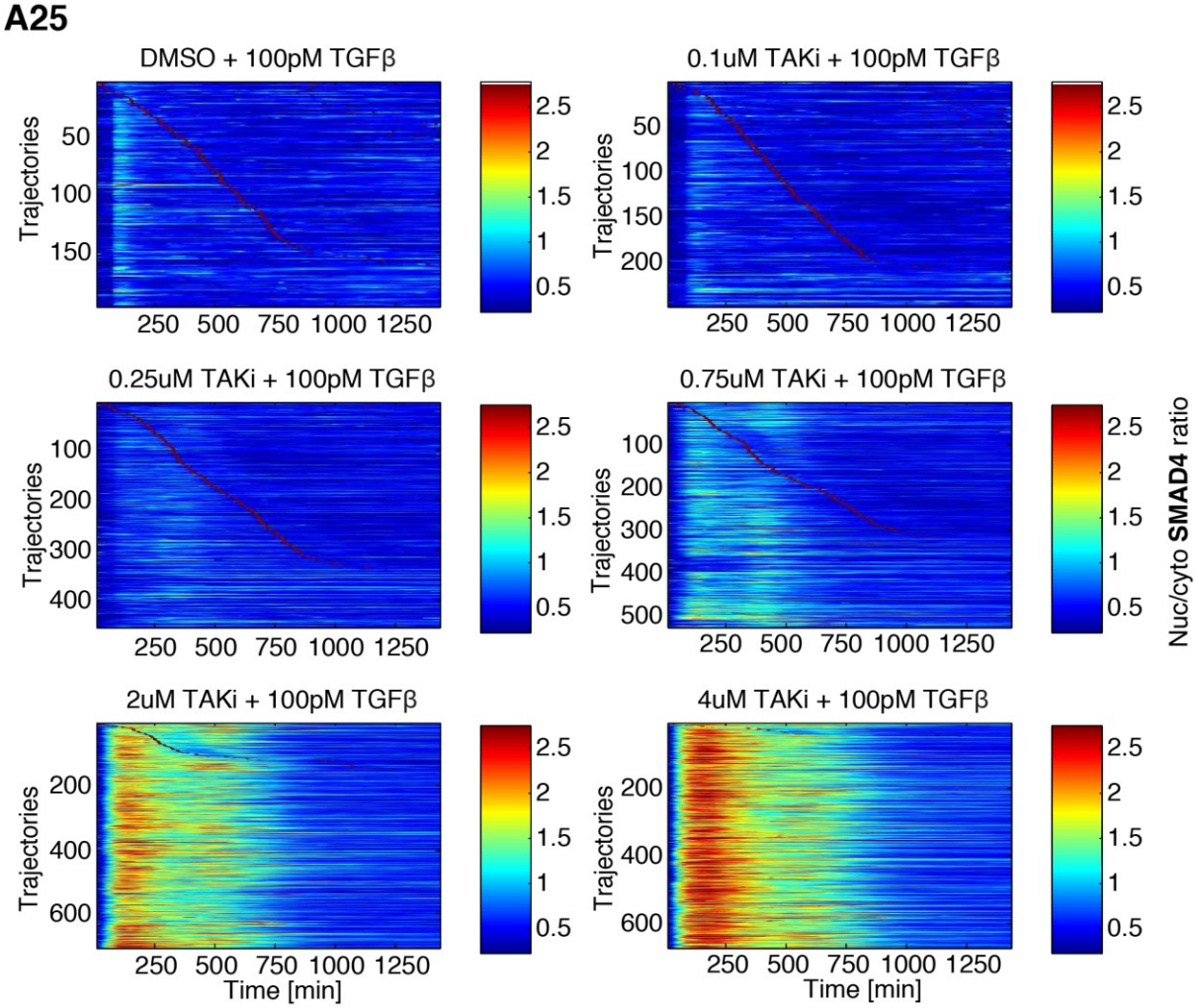

7.1 Figure A25. TAK1 Inhibition modulates the dynamics and localization of SMADs.
Heat maps of SMAD4 translocation in individual cells over 24h. Cells were stimulated with 100pM TGFβ and 0.75h pretreated with 5Z-7-Oxozeaenol (TAKi) at indicated concentrations. Cells were sorted by the time of the first division as indicated by red marks.

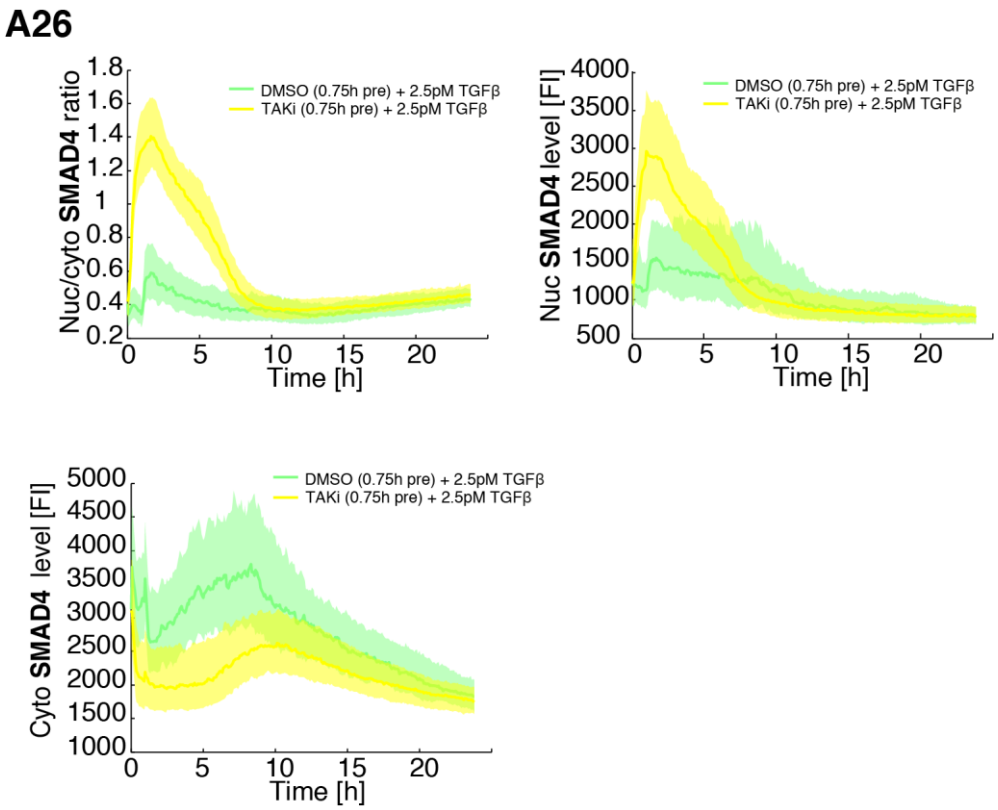

7.1 Figure A26. TAK1 Inhibition modulates the dynamics and localization of SMADs.
Median nuc/cyto SMAD4 ratio, nuclear and cytoplasmic level of the SMAD4-YFP reporter cells stimulated with 2.5pM TGFβ and 0.75h pretreated with 5Z-7-Oxozeaenol (TAKi). Shaded area represent data between 25th and 75th percentiles.

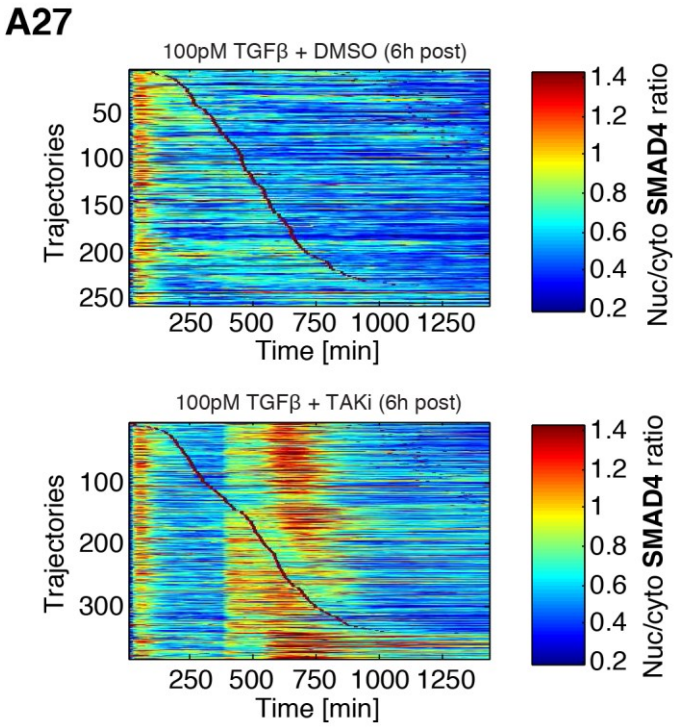

7.1 Figure A27. TAK1 Inhibition modulates the dynamics and localization of SMADs.
Heat maps of SMAD4 translocation in individual cells over 24h. Cells were stimulated with 100pM TGFβ and 6h post TAKi. Cells were sorted by the time of the first division as indicated by red marks.

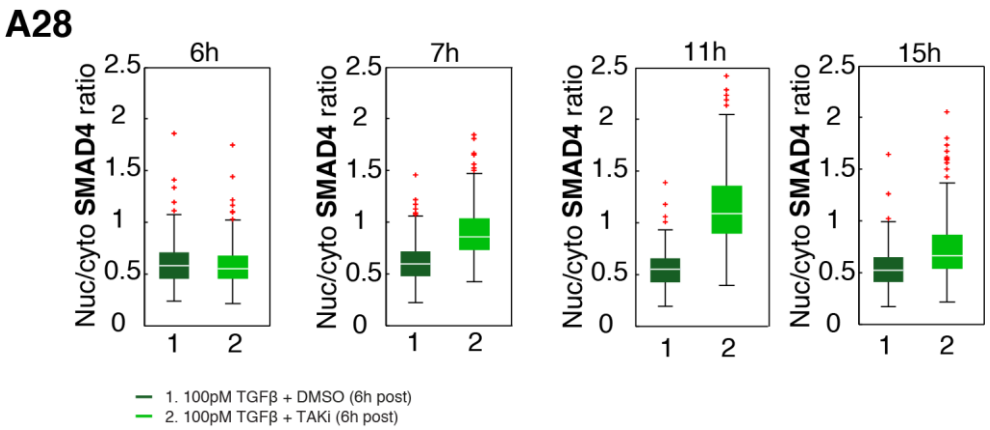

7.1 Figure A28. TAK1 Inhibition modulates the dynamics and localization of SMADs.
Nuc/cyto SMAD4 ratio of the SMAD4 reporter cells stimulated with 100pM TGFβ and 6h post TAKi at indicated time points. White lines indicate median; boxes include data between the 25th and 75th percentiles; whiskers extend to maximum values within 1.5× the interquartile range; crosses represent outliers.

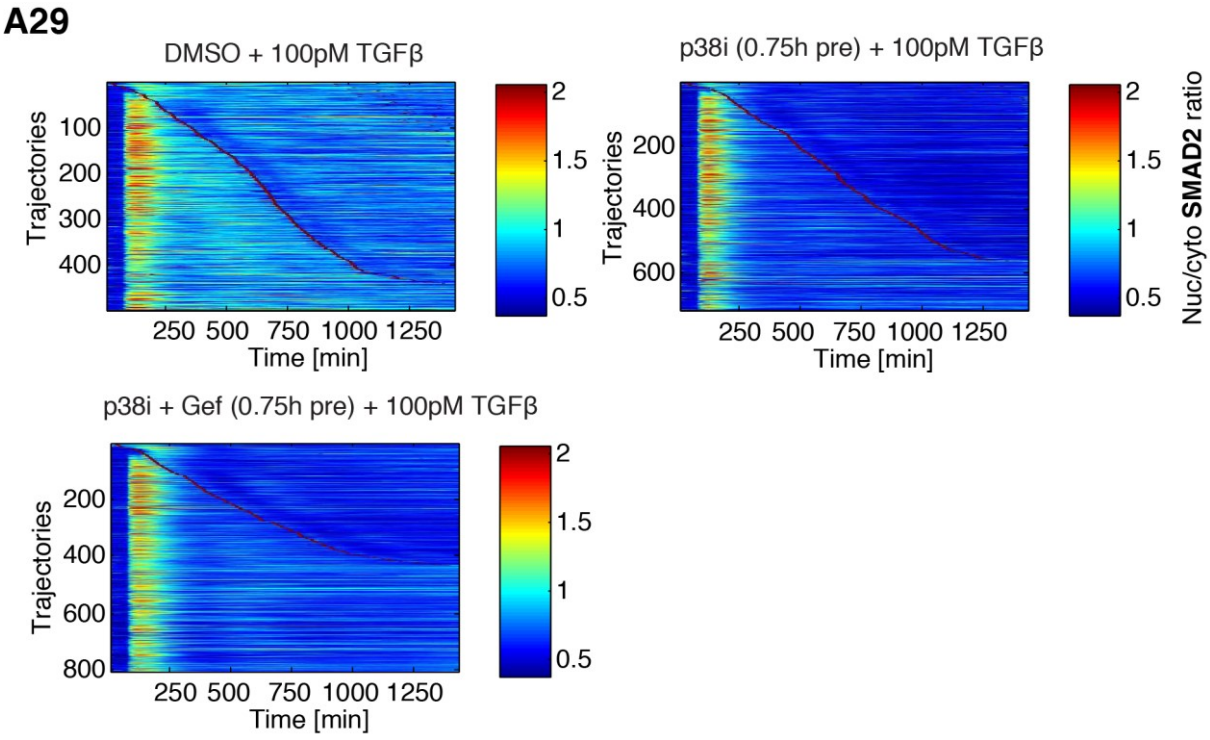

7.1 Figure A29. Inhibition of ERK signaling alters long-term SMAD dynamics.
Heat maps of nuc/cyto SMAD2 ratio in individual cells over 24h. Cells were stimulated with 100pM TGFβ and 0.75h pretreated with p38 inhibitors and/ or Gefitinib (Gef). Cells were sorted by the time of the first division as indicated by red marks.

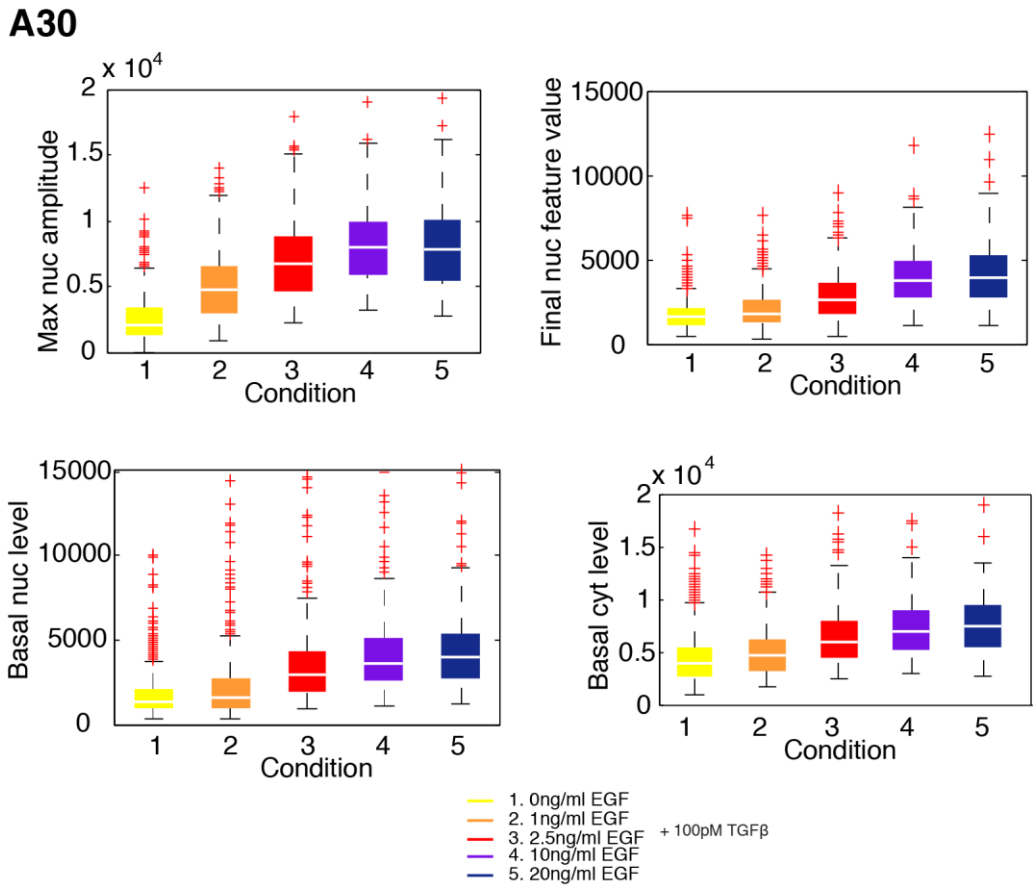

7.1 Figure A30. TGFβ response depends on EGF concentration.
Signaling features for nuclear SMAD2 level of the SMAD2 reporter cells stimulated with 100pM at varying EGF concentrations. White lines indicate median; boxes include data between the 25th and 75th percentiles; whiskers extend to maximum values within 1.5× the interquartile range; crosses represent outliers.

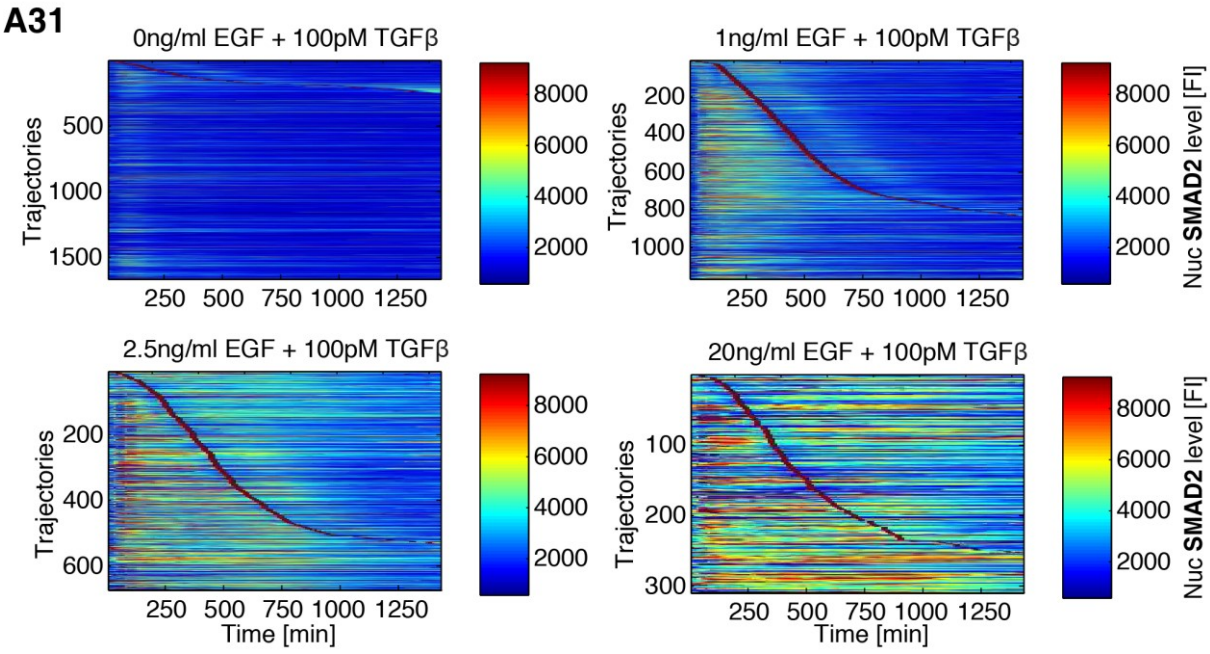

7.1 Figure A31. TGFβ response depends on EGF concentration.
Heat maps of nuclear SMAD2 level in individual cells over 24h. Cells were stimulated with 100pM TGFβ at varying EGF concentrations as indicated. Cells were sorted by the time of the first division as indicated by red marks.

A32

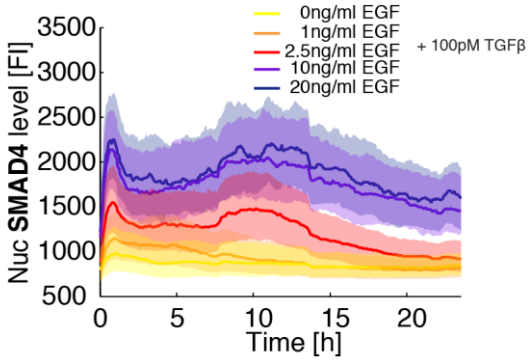

7.1 Figure A32. TGFβ response depends on EGF concentration.
Median nuclear SMAD4 level of the SMAD4-YFP reporter cells stimulated with 100pM TGFβ at varying EGF concentrations.

A33

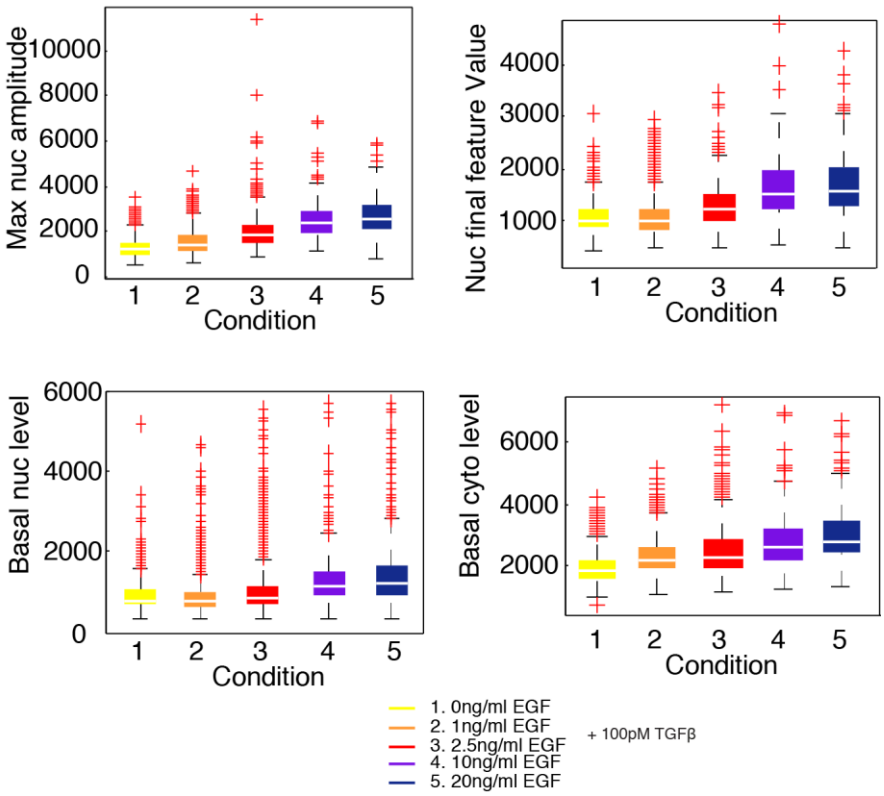

7.1 Figure A33. TGFβ response depends on EGF concentration.
Signaling features for nuclear SMAD4 level of the SMAD4 reporter cells stimulated with 100pM at varying EGF concentrations. White lines indicate median; boxes include data between the 25th and 75th percentiles; whiskers extend to maximum values within 1.5× the interquartile range; crosses represent outliers.

A34

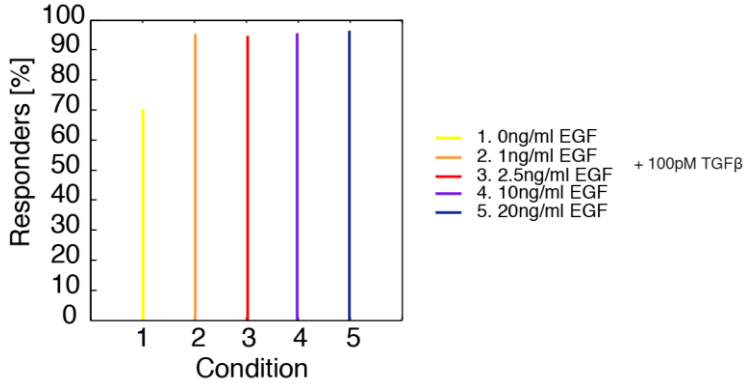

7.1 Figure A34. TGFβ response depends on EGF concentration.
Responders in % of the SMAD4-YFP reporter cells stimulated with 100pM TGFβ at varying EGF concentrations.

A35

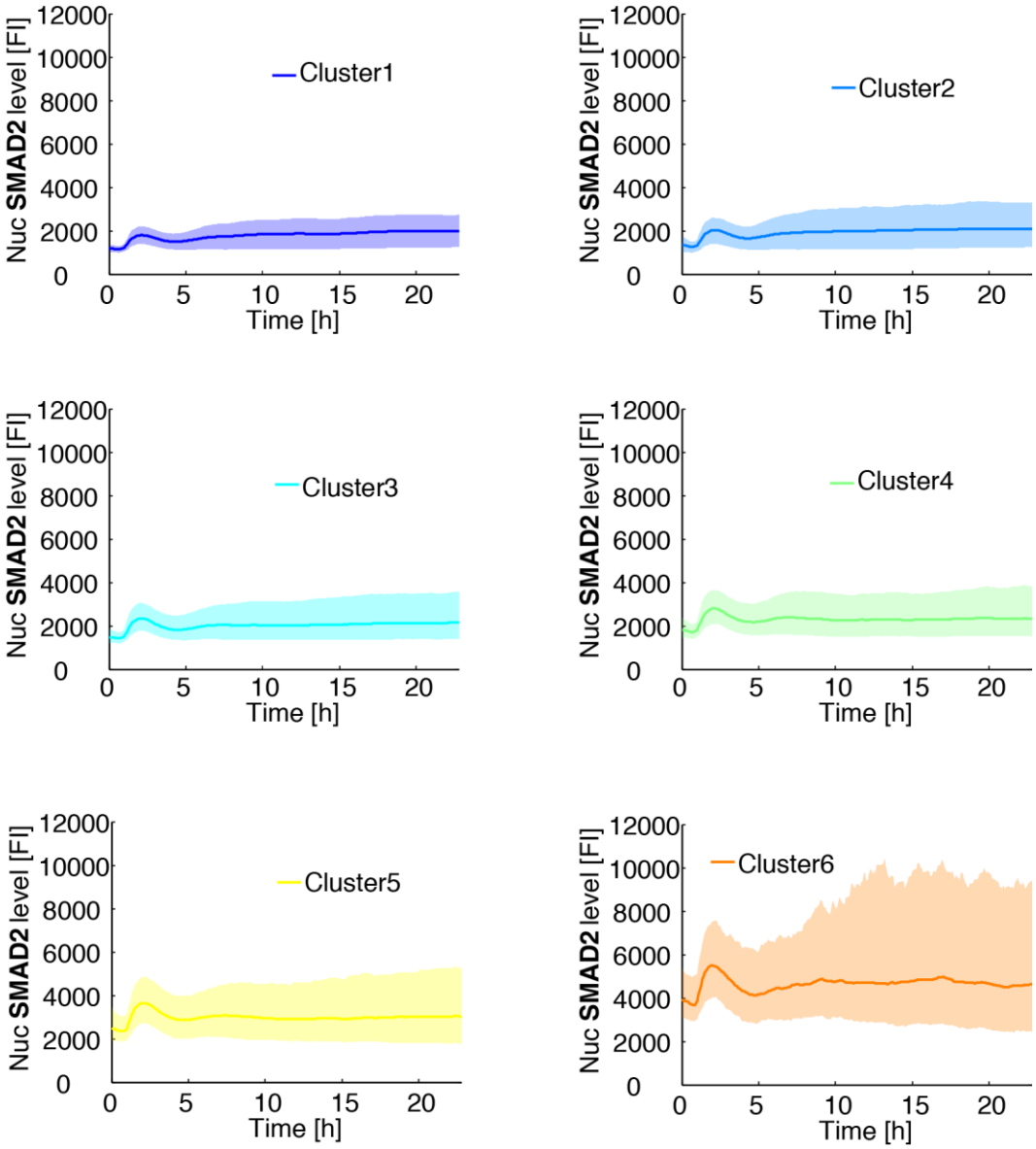

7.1 Figure A35. PPM1A is probably involved in the ERK-mediated TGFβ response.
Individual cells were clustered into six cluster (Figure 50 G) and the corresponding median nuclear SMAD2 level over 24h are shown for the individual cluster. Shaded area represent data between 25th and 75th percentiles.

7.2 List of abbreviations

BMP	bone morphogenetic protein
CFP	cyan fluorescent protein
CV	coefficient of variation
DRB	5,6-dichloro-1--D-ribofuranosylbenzimidazole
DTW	dynamic time warping
EEA1	early endosome antigen-1
EGF	epidermal growth factor
EGFR	epidermal growth factor receptor
EMT	epithelial -mesenchymal transition
ERK	extracellular signal-regulated kinase
EtBr	ethidium bromide
Fucci	fluorescent, ubiquitination-based cell cycle indicator
I-SMADs	inhibitory SMADs
IPTG	Isopropyl β-D-1-thiogalactopyranoside
JNK	c-Jun N-terminal kinase
KTR	kinase translocation reporter
MAPK	mitogen-activated protein kinase
MKK	MAP kinase kinase
MLEC	mink lung epithelial cells
NEB	New England Biolabs
NF-κB	nuclear factor kappa B
nuc/cyto	nuclear/ cytoplasmic
PAI-1	plasminogen activator inhibitor 1
R-SMADs	receptor-regulated SMADs
RPMCs	rat peritoneal mast cells
RT	room temperature
SARA	SMAD anchor for receptor activation
smFISH	single molecule fluorescent in situ hybridization
TAK1	TGFβ-activated kinase 1
TGFβ	transforming growth factor beta
TGFβRi	TGFβReceptor I Kinase inhibitor SB431542

TGFβRI	TGFβ type I receptors
TGFβRII	TGFβ type II receptors
WT	wild type
YFP	yellow fluorescent protein

7.3 List of figures

7.4 List of tables

8 REFERENCES

A

Abe M, Harpel JG, Metz CN, Nunes I, Loskutoff DJ, Rifkin DB. An assay for transforming growth factor-beta using cells transfected with a plasminogen activator inhibitor-1 promoter-luciferase construct. Anal Biochem. 1994 Feb 1;216(2):276-84.

Abécassis L, Rogier E, Vazquez A, Atfi A, Bourgeade MF. Evidence for a role of MSK1 in transforming growth factor-beta-mediated responses through p38alpha and Smad signaling pathways. J Biol Chem. 2004 Jul 16;279(29):30474-9.

Aburai N, Yoshida M, Ohnishi M, Kimura K. Sanguinarine as a potent and specific inhibitor of protein phosphatase 2C in vitro and induces apoptosis via phosphorylation of p38 in HL60 cells. Biosci Biotechnol Biochem. 2010;74(3):548-52.

Adnane L, Trail PA, Taylor I, Wilhelm SM. Sorafenib (BAY 43-9006, Nexavar), a dual-action inhibitor that targets RAF/MEK/ERK pathway in tumor cells and tyrosine kinases VEGFR/PDGFR in tumor vasculature. Methods Enzymol. 2006; 407:597-612.

Ahn JY, Kim MH, Lim MJ, Park S, Lee SL, Yun YS, Song JY. The inhibitory effect of ginsan on TGF-beta mediated fibrotic process. Journal of cellular physiology. 2011; 226:1241–7.

Akiyoshi S, Inoue H, Hanai J, Kusanagi K, Nemoto N, Miyazono K, Kawabata M. c-Ski acts as a transcriptional co-repressor in transforming growth factor-beta signaling through interaction with smads. J Biol Chem. 1999 Dec 3;274(49):35269-77.

Albeck JG, Mills GB, Brugge JS. Frequency-modulated pulses of ERK activity transmit quantitative proliferation signals. Mol Cell. 2013 Jan 24;49(2):249-61.

Alarcón C, Zaromytidou AI, Xi Q, Gao S, Yu J, Fujisawa S, Barlas A, Miller AN, Manova-Todorova K, Macias MJ, Sapkota G, Pan D, Massagué J. Nuclear CDKs drive Smad transcriptional activation and turnover in BMP and TGF-beta pathways. Cell. 2009 Nov 13;139(4):757-69.

Annes JP, Munger JS, Rifkin DB. Making sense of latent TGFbeta activation. J Cell Sci. 2003 Jan 15;116(Pt 2):217-24.

Aragón E, Goerner N, Zaromytidou AI, Xi Q, Escobedo A, Massagué J, Macias MJ. A Smad action turnover switch operated by WW domain readers of a phosphoserine code. Genes Dev. 2011 Jun 15;25(12):1275-88.

Arora K, Warrior R. A new Smurf in the village. Dev Cell. 2001 Oct;1(4):441-2.

Ashall L, Horton CA, Nelson DE, Paszek P, Harper CV, Sillitoe K, Ryan S, Spiller DG, Unitt JF, Broomhead DS, Kell DB, Rand DA, Sée V, White MR. Pulsatile stimulation determines timing and specificity of NF-kappaB-dependent transcription. Science. 2009 Apr 10;324(5924):242-6.

B

Baass PC, Di Guglielmo GM, Authier F, Posner BI, Bergeron JJ. Compartmentalized signal transduction by receptor tyrosine kinases. Trends Cell Biol. 1995 Dec;5(12):465-70.

Bai Y, Yang C, Hu K, Elly C, Liu YC. Itch E3 ligase-mediated regulation of TGF-beta signaling by modulating smad2 phosphorylation. Mol Cell. 2004 Sep 10;15(5):825-31.

Bakin AV, Rinehart C, Tomlinson AK, Arteaga CL. p38 mitogen-activated protein kinase is required for TGFbeta-mediated fibroblastic transdifferentiation and cell migration. J Cell Sci. 2002 Aug 1;115(Pt 15):3193-206.

Bar-Even A, Paulsson J, Maheshri N, Carmi M, O'Shea E, Pilpel Y, Barkai N. Noise in protein expression scales with natural protein abundance. Nat Genet. 2006 Jun;38(6):636-43.

Barrios-Rodiles M, Brown KR, Ozdamar B, Bose R, Liu Z, Donovan RS, Shinjo F, Liu Y, Dembowy J, Taylor IW, Luga V, Przulj N, Robinson M, Suzuki H, Hayashizaki Y, Jurisica I, Wrana JL. High-throughput mapping of a dynamic signaling network in mammalian cells. Science. 2005 Mar 11;307(5715):1621-5.

Batchelor E, Loewer A, Lahav G. The ups and downs of p53: understanding protein dynamics in single cells. Nat Rev Cancer. 2009 May;9(5):371-7.

Batchelor E, Loewer A, Mock C, Lahav G. Stimulus-dependent dynamics of p53 in single cells. Mol. Syst. Biol. 2011;7:488.

Baum B, Settleman J, Quinlan MP. Transitions between epithelial and mesenchymal states in development and disease. Semin Cell Dev Biol. 2008 Jun;19(3):294-308.

Becker V, Schilling M, Bachmann J, Baumann U, Raue A, Maiwald T, Timmer J, Klingmüller U. Covering a broad dynamic range: information processing at the erythropoietin receptor. Science. 2010 Jun 11;328(5984):1404-8.

Behar M, Hoffmann A. Understanding the temporal codes of intra-cellular signals. Curr Opin Genet Dev. 2010 Dec;20(6):684-93.

Berndt DJ & Clifford J. Using dynamic time warping to find patterns in time series. Proc. 3rd Int. Conf. Knowl. Discov. Data Min. 1994 359–370

Bialojan C, Takai A. Inhibitory effect of a marine-sponge toxin, okadaic acid, on protein phosphatases. Specificity and kinetics. Biochem J. 1988 Nov 15;256(1):283-90.

Blobe GC, Schiemann WP, Lodish HF. Role of transforming growth factor beta in human disease. N Engl J Med. 2000 May 4;342(18):1350-8.

Boehm JR, Kutz SM, Sage EH, Staiano-Coico L, Higgins PJ. Growth state-dependent regulation of plasminogen activator inhibitor type-1 gene expression during epithelial cell stimulation by serum and transforming growth factor-beta1. J Cell Physiol. 1999 Oct;181(1):96-106.

Bonni S, Wang HR, Causing CG, Kavsak P, Stroschein SL, Luo K, Wrana JL. TGF-beta induces assembly of a Smad2-Smurf2 ubiquitin ligase complex that targets SnoN for degradation. Nat Cell Biol. 2001 Jun;3(6):587-95.

Brandman O, Meyer T. Feedback loops shape cellular signals in space and time. Science. 2008 Oct 17;322(5900):390-5.

Brown KA, Pietenpol JA, Moses HL. A tale of two proteins: differential roles and regulation of Smad2 and Smad3 in TGF-beta signaling. J Cell Biochem. 2007 May 1;101(1):9-33.

Buettner F, Natarajan KN, Casale FP, Proserpio V, Scialdone A, Theis FJ, Teichmann SA, Marioni JC, Stegle O. Computational analysis of cell-to-cell heterogeneity in single-cell RNA-sequencing data revealshidden subpopulations of cells. Nat Biotechnol. 2015 Feb;33(2):155-60.

C

Calonge MJ, Massagué J. Smad4/DPC4 silencing and hyperactive Ras jointly disrupt transforming growth factor-betaantiproliferative responses in colon cancer cells. J Biol Chem. 1999 Nov 19;274(47):33637-43.

Carpenter AE, Jones TR, Lamprecht MR, Clarke C, Kang IH, Friman O, Guertin DA, Chang JH, Lindquist RA, Moffat J, Golland P, Sabatini DM. CellProfiler: image analysis software for identifying and quantifying cell phenotypes. Genome Biol. 2006;7(10):R100.

Chai J, Wu JW, Yan N, Massagué J, Pavletich NP, Shi Y. Features of a Smad3 MH1-DNA complex. Roles of water and zinc in DNA binding. J Biol Chem. 2003 May 30;278(22):20327-31.

Chan YH, Marshall WF. Scaling properties of cell and organelle size. Organogenesis. 2010 Apr-Jun;6(2):88-96.

Chang HH, Hemberg M, Barahona M, Ingber DE, Huang S. Transcriptome-wide noise controls lineage choice in mammalian progenitor cells. Nature. 2008 May 22;453(7194):544-7.

Chang L, Karin M. Mammalian MAP kinase signalling cascades. Nature. 2001 Mar 1;410(6824):37-40.

Chen YG, Hata A, Lo RS, Wotton D, Shi Y, Pavletich N, Massagué J. Determinants of specificity in TGF-beta signal transduction. Genes Dev. 1998 Jul 15;12(14):2144-52.

Chen YG. Endocytic regulation of TGF-beta signaling. Cell Res. 2009 Jan;19(1):58-70.

Cheng A, Kaldis P, Solomon MJ. Dephosphorylation of human cyclin-dependent kinases by protein phosphatase type 2C alpha and beta 2 isoforms. J Biol Chem. 2000 Nov 3;275(44):34744-9.

Cheong R, Bergmann A, Werner SL, Regal J, Hoffmann A, Levchenko A. Transient IkappaB kinase activity mediates temporal NF-kappaB dynamics in response to a widerange of tumor necrosis factor-alpha doses. J Biol Chem. 2006 Feb 3;281(5):2945-50.

Cheong R, Rhee A, Wang CJ, Nemenman I, Levchenko A. Information transduction capacity of noisy biochemical signaling networks. Science. 2011 Oct 21;334(6054):354-8.

Chodosh LA, Fire A, Samuels M, Sharp PA. 5,6-Dichloro-1-beta-D-ribofuranosylbenzimidazole inhibits transcription elongation by RNA polymerase II in vitro. J Biol Chem. 1989 Feb 5;264(4):2250-7.

Choi ME, Ding Y, Kim SI. TGF-β signaling via TAK1 pathway: role in kidney fibrosis. Semin Nephrol. 2012 May;32(3):244-52.

Chung SW, Miles FL, Sikes RA, Cooper CR, Farach-Carson MC, Ogunnaike BA. Quantitative modeling and analysis of the transforming growth factor beta signaling pathway. Biophys J. 2009 Mar 4;96(5):1733-50.

Chun-Lin Chen, Wei-Hsien Hou, I-Hua Liu, George Hsiao, Shuan Shian Huang and Jung San Huang. Inhibitors of clathrin-dependent endocytosis enhance TGFβ signaling and responses. J Cell Sci. 2009 Jun 1; 122(11): 1863–1871.

Clarke DC, Brown ML, Erickson RA, Shi Y, Liu X. Transforming growth factor beta depletion is the primary determinant of Smad signaling kinetics. Mol Cell Biol. 2009 May;29(9):2443-55.

Clarke DC, Liu X. Decoding the quantitative nature of TGF-beta/Smad signaling. Trends Cell Biol. 2008 Sep;18(9):430-42.

Cohen AA, Geva-Zatorsky N, Eden E, Frenkel-Morgenstern M, Issaeva I, Sigal A, Milo R, Cohen-Saidon C, Liron Y, Kam Z, Cohen L, Danon T, Perzov N, Alon U. Dynamic proteomics of individual cancer cells in response to a drug. Science. 2008 Dec 5;322(5907):1511-6.

Cohen P. Targeting protein kinases for the development of anti-inflammatory drugs. Curr Opin Cell Biol. 2009 Apr;21(2):317-24.

Colman-Lerner A, Gordon A, Serra E, Chin T, Resnekov O, Endy D, Pesce CG, Brent R. Regulated cell-to-cell variation in a cell-fate decision system. Nature. 2005 Sep 29;437(7059):699-706.

Connolly EC, Freimuth J, Akhurst RJ. Complexities of TGF-β targeted cancer therapy. Int J Biol Sci. 2012;8(7):964-78.

Corn BW, Kovner F, Bek S, Wexler I, Lifschits B, Seger R. ERK signaling in colorectal cancer: a preliminary report on the expression of phosphorylated ERKand the effects of radiation therapy. Am J Clin Oncol. 2008 Jun;31(3):255-8.

Covert MW, Leung TH, Gaston JE, Baltimore D. Achieving stability of lipopolysaccharide-induced NF-kappaB activation. Science. 2005 Sep 16;309(5742):1854-7.

Cuenda A, Rouse J, Doza YN, Meier R, Cohen P, Gallagher TF, Young PR, Lee JC. SB 203580 is a specific inhibitor of a MAP kinase homologue which is stimulated by cellular stresses and interleukin-1. FEBS Lett. 1995 May 8;364(2):229-33.

Cuenda A, Rousseau S. p38 MAP-kinases pathway regulation, function and role in human diseases. Biochim Biophys Acta. 2007 Aug;1773(8):1358-75.

D

Dai F, Shen T, Li Z, Lin X, Feng XH. PPM1A dephosphorylates RanBP3 to enable efficient nuclear export of SMAD2 and SMAD3. EMBO Rep. 2011 Oct 28;12(11):1175-81.

Dalal BI, Keown PA, Greenberg AH. Immunocytochemical localization of secreted transforming growth factor-beta 1 to the advancingedges of primary tumors and to lymph node metastases of human mammary carcinoma. Am J Pathol. 1993 Aug;143(2):381-9.

Daroqui MC, Vazquez P, Bal de Kier Joffe E, Bakin AV, Puricelli LI. TGF-β autocrine pathway and MAPK signaling promote cell invasiveness and in vivo mammary adenocarcinoma tumor progression. Oncol Rep. 2012 Aug; 28(2): 567–575.

Datto MB, Li Y, Panus JF, Howe DJ, Xiong Y, Wang XF. Transforming growth factor beta induces the cyclin-dependent kinase inhibitor p21 through a p53-independent mechanism. Proc Natl Acad Sci U S A. 1995 Jun 6;92(12):5545-9.

Davies BR, Logie A, McKay JS, Martin P, Steele S, Jenkins R, Cockerill M, Cartlidge S, Smith PD. AZD6244 (ARRY-142886), a potent inhibitor of mitogen-activated protein kinase/extracellular signal-regulated kinase kinase 1/2 kinases: mechanism of action in vivo, pharmacokinetic/pharmacodynamic relationship, and potential for combination in preclinical models. Mol Cancer Ther. 2007 Aug;6(8):2209-19.

Davies M, Robinson M, Smith E, Huntley S, Prime S, Paterson I. Induction of an epithelial to mesenchymal transition in human immortal and malignant keratinocytes by TGF-beta1 involves MAPK, Smad and AP-1 signalling pathways. J Cell Biochem. 2005 Aug 1;95(5):918-31.

Davies SP, Reddy H, Caivano M, Cohen P. Specificity and mechanism of action of some commonly used protein kinase inhibitors. Biochem J. 2000 Oct 1;351(Pt 1):95-105.

de Caestecker MP, Hemmati P, Larisch-Bloch S, Ajmera R, Roberts AB, Lechleider RJ. Characterization of functional domains within Smad4/DPC4. J Biol Chem. 1997 May 23;272(21):13690-6.

de Caestecker MP, Parks WT, Frank CJ, Castagnino P, Bottaro DP, Roberts AB, Lechleider RJ. Smad2 transduces common signals from receptor serine-threonine and tyrosine kinases. Genes Dev. 1998 Jun 1;12(11):1587-92.

de Caestecker MP, Yahata T, Wang D, Parks WT, Huang S, Hill CS, Shioda T, Roberts AB, Lechleider RJ. The Smad4 activation domain (SAD) is a proline-rich, p300-dependent transcriptional activationdomain. J Biol Chem. 2000 Jan 21;275(3):2115-22.

Debnath J, Muthuswamy SK, Brugge JS. Morphogenesis and oncogenesis of MCF-10A mammary epithelial acini grown in three-dimensional basement membrane cultures. Methods. 2003 Jul;30(3):256-68.

Deheuninck J and Luo K. Ski and SnoN, potent negative regulators of TGF-β signaling. Cell Res. 2009 Jan; 19(1): 47–57.

Derynck R, Akhurst RJ, Balmain A. TGF-beta signaling in tumor suppression and cancer progression. Nat Genet. 2001 Oct;29(2):117-29.

Derynck R, Zhang YE. Smad-dependent and Smad-independent pathways in TGF-beta family signalling. Nature. 2003 Oct 9;425(6958):577-84.

Di Fiore PP, De Camilli P. Endocytosis and signaling. an inseparable partnership. Cell. 2001 Jul 13;106(1):1-4.

Di Guglielmo GM, Le Roy C, Goodfellow AF, Wrana JL. Distinct endocytic pathways regulate TGF-beta receptor signalling and turnover. Nat Cell Biol. 2003 May;5(5):410-21.

Dowdy SC, Mariani A, Janknecht R. HER2/Neu- and TAK1-mediated up-regulation of the transforming growth factor beta inhibitor Smad7 via the ETS protein ER81. J Biol Chem. 2003 Nov 7;278(45):44377-84.

Duan X, Liang YY, Feng XH, Lin X. Protein serine/threonine phosphatase PPM1A dephosphorylates Smad1 in the bonemorphogenetic protein signaling pathway. J Biol Chem. 2006 Dec 1;281(48):36526-32.

Dumont N, Bakin AV, Arteaga CL. Autocrine transforming growth factor-beta signaling mediates Smad-independent motility in human cancer cells. J Biol Chem. 2003 Jan 31;278(5):3275-85.

Dupont S, Zacchigna L, Cordenonsi M, Soligo S, Adorno M, Rugge M, Piccolo S. Germ-layer specification and control of cell growth by Ectodermin, a Smad4 ubiquitin ligase. Cell. 2005 Apr 8;121(1):87-99.

Dziembowska M, Danilkiewicz M, Wesolowska A, Zupanska A, Chouaib S, Kaminska B. Cross-talk between SMAD and p38 MAPK signaling in transforming growth factor beta signal transduction in human glioblastoma cells. Biochem Biophys Res Commun. 2007 Mar 23;354(4):1101-6.

E

Ebisawa T, Fukuchi M, Murakami G, Chiba T, Tanaka K, Imamura T, Miyazono K. Smurf1 interacts with transforming growth factor-beta type I receptor through Smad7 and induces receptor degradation. J Biol Chem. 2001 Apr 20;276(16):12477-80.

Edlund S, Bu S, Schuster N, Aspenström P, Heuchel R, Heldin NE, ten Dijke P, Heldin CH, Landström M. Transforming growth factor-beta1 (TGF-beta)-induced apoptosis of prostate cancer cells involvesSmad7-dependent activation of p38 by TGF-beta-activated kinase 1 and mitogen-activated protein kinase kinase 3. Mol Biol Cell. 2003 Feb;14(2):529-44.

Eldar A, Elowitz MB. Functional roles for noise in genetic circuits. Nature. 2010 Sep 9;467(7312):167-73.

Engel ME, McDonnell MA, Law BK, Moses HL. Interdependent SMAD and JNK signaling in transforming growth factor-beta-mediated transcription. J Biol Chem. 1999 Dec 24;274(52):37413-20.

F

Fang JY, Richardson BC. The MAPK signalling pathways and colorectal cancer. Lancet Oncol. 2005 May;6(5):322-7.

Favata MF, Horiuchi KY, Manos EJ, Daulerio AJ, Stradley DA, Feeser WS, Van Dyk DE, Pitts WJ, Earl RA, Hobbs F, Copeland RA, Magolda RL, Scherle PA, Trzaskos JM. Identification of a novel inhibitor of mitogen-activated protein kinase kinase. J Biol Chem. 1998 Jul 17;273(29):18623-32.

Feng XH, Derynck R. Specificity and versatility in tgf-beta signaling through Smads. Annu Rev Cell Dev Biol. 2005;21:659-93.

Ferrell JE Jr. Feedback regulation of opposing enzymes generates robust, all-or-none bistable responses. Curr Biol. 2008 Mar 25;18(6):R244-5.

Fox T, Coll JT, Xie X, Ford PJ, Germann UA, Porter MD, Pazhanisamy S, Fleming MA, Galullo V, Su MS, Wilson KP. A single amino acid substitution makes ERK2 susceptible to pyridinyl imidazole inhibitors of p38MAP kinase. Protein Sci. 1998 Nov;7(11):2249-55.

Frantz B, Klatt T, Pang M, Parsons J, Rolando A, Williams H, Tocci MJ, O'Keefe SJ, O'Neill EA. The activation state of p38 mitogen-activated protein kinase determines the efficiency of ATP competition for pyridinylimidazole inhibitor binding. Biochemistry. 1998 Sep 29;37(39):13846-53.

Freshney NW, Rawlinson L, Guesdon F, Jones E, Cowley S, Hsuan J, Saklatvala J. Interleukin-1 activates a novel protein kinase cascade that results in the phosphorylation of Hsp27. Cell. 1994 Sep 23;78(6):1039-49.

Frey RS, Mulder KM. TGFbeta regulation of mitogen-activated protein kinases in human breast cancer cells. Cancer Lett. 1997 Jul 15;117(1):41-50.

Frick CL, Yarka C, Nunns H, Goentoro L. Sensing relative signal in the Tgf-β/Smad pathway. Proc Natl Acad Sci U S A. 2017 Apr 4;114(14):E2975-E2982.

Fu H, Hu Z, Wen J, Wang K, Liu Y. TGF-beta promotes invasion and metastasis of gastric cancer cells by increasing fascin1expression via ERK and JNK signal pathways. Acta Biochim Biophys Sin (Shanghai). 2009 Aug;41(8):648-56.

Funaba M, Zimmerman CM, Mathews LS. Modulation of Smad2-mediated signaling by extracellular signal-regulated kinase. J Biol Chem. 2002 Nov 1;277(44):41361-8.

G

Gaarenstroom T, Hill CS2. TGF-β signaling to chromatin: how Smads regulate transcription during self-renewal and differentiation. Semin Cell Dev Biol. 2014 Aug;32:107-18.

Gao S, Alarcón C, Sapkota G, Rahman S, Chen PY, Goerner N, Macias MJ, Erdjument-Bromage H, Tempst P, Massagué J. Ubiquitin ligase Nedd4L targets activated Smad2/3 to limit TGF-beta signaling. Mol Cell. 2009 Nov 13;36(3):457-68.

Geiser AG, Kim SJ, Roberts AB, Sporn MB. Characterization of the mouse transforming growth factor-beta 1 promoter and activation by the Ha-ras oncogene. Mol Cell Biol. 1991 Jan;11(1):84-92.

Geva-Zatorsky N, Rosenfeld N, Itzkovitz S, Milo R, Sigal A, Dekel E, Yarnitzky T, Liron Y, Polak P, Lahav G, Alon U. Oscillations and variability in the p53 system. Mol Syst Biol. 2006;2:2006.0033.

Giampieri S, Manning C, Hooper S, Jones L, Hill CS, Sahai E. Localized and reversible TGFbeta signalling switches breast cancer cells from cohesive to single cell motility. Nat Cell Biol. 2009 Nov;11(11):1287-96.

Giehl K, Imamichi Y, Menke A. Smad4-independent TGF-beta signaling in tumor cell migration. Cells Tissues Organs. 2007;185(1-3):123-30.

Goentoro L, Kirschner MW. Evidence that fold-change, and not absolute level, of beta-catenin dictates Wnt signaling. Mol Cell. 2009 Dec 11;36(5):872-84.

Gorelik L, Flavell RA. Abrogation of TGFbeta signaling in T cells leads to spontaneous T cell differentiation and autoimmune disease. Immunity. 2000 Feb;12(2):171-81.

Goumans MJ, Valdimarsdottir G, Itoh S, Rosendahl A, Sideras P, ten Dijke P. Balancing the activation state of the endothelium via two distinct TGF-beta type I receptors. EMBO J. 2002 Apr 2;21(7):1743-53.

Groppe J, Greenwald J, Wiater E, Rodriguez-Leon J, Economides AN, Kwiatkowski W, Affolter M, Vale WW, Izpisua Belmonte JC, Choe S. Structural basis of BMP signalling inhibition by the cystine knot protein Noggin. Nature. 2002 Dec 12;420(6916):636-42.

Groppe J, Greenwald J, Wiater E, Rodriguez-Leon J, Economides AN, Kwiatkowski W, Baban K, Affolter M, Vale WW, Izpisua Belmonte JC, Choe S. Structural basis of BMP signaling inhibition by Noggin, a novel twelve-membered cystine knot protein. J Bone Joint Surg Am. 2003;85-A Suppl 3:52-8.

Guan F, Handa K, Hakomori SI. Specific glycosphingolipids mediate epithelial-to-mesenchymal transition of human and mouse epithelial cell lines. Proc Natl Acad Sci U S A. 2009 May 5;106(18):7461-6.

Gui T, Sun Y, Shimokado A, Muragaki Y. The Roles of Mitogen-Activated Protein Kinase Pathways in TGF-β-Induced Epithelial-Mesenchymal Transition. J Signal Transduct. 2012;2012:289243.

H

Hachim IY, Hachim MY, López-Ozuna VM, Ali S, Lebrun JJ. A dual prognostic role for the TGFβ receptors in human breast cancer. Hum Pathol. 2016 Nov;57:140-151.

Haghverdi L, Büttner M, Wolf FA, Buettner F, Theis FJ. Diffusion pseudotime robustly reconstructs lineage branching. Nat Methods. 2016 Oct;13(10):845-8.

Hall JP, Davis RJ. Inhibition of the p38 pathway upregulates macrophage JNK and ERK activities, and the ERK, JNK, and p38 MAP kinase pathways are reprogrammed during differentiation of the murine myeloid M1 cell line. J Cell Biochem. 2002;86(1):1-11.

Hall MC, Young DA, Waters JG, Rowan AD, Chantry A, Edwards DR, Clark IM. The comparative role of activator protein 1 and Smad factors in the regulation of Timp-1 and MMP-1 gene expression by transforming growth factor-beta 1. J Biol Chem. 2003 Mar 21;278(12):10304-13.

Hanafusa H, Ninomiya-Tsuji J, Masuyama N, Nishita M, Fujisawa J, Shibuya H, Matsumoto K, Nishida E. Involvement of the p38 mitogen-activated protein kinase pathway in transforming growth factor-beta-induced gene expression. J Biol Chem. 1999 Sep 17;274(38):27161-7.

Hannon GJ, Beach D. p15INK4B is a potential effector of TGF-beta-induced cell cycle arrest. Nature. 1994 Sep 15;371(6494):257-61.

Harish RC, Abidali M, David IC, Sock HT, Edouard C, Mark SB.Transforming growth factor-β, MAPK and Wnt signaling interactions in colorectal cancer. EuPA Open Proteomics. Sep 2015 (8):104:115.

Hartsough MT, Frey RS, Zipfel PA, Buard A, Cook SJ, McCormick F, Mulder KM. Altered transforming growth factor signaling in epithelial cells when ras activation is blocked. J Biol Chem. 1996 Sep 13;271(37):22368-75.

Hartsough MT, Mulder KM. Transforming growth factor beta activation of p44mapk in proliferating cultures of epithelial cells. J Biol Chem. 1995 Mar 31;270(13):7117-24.

Hay ED. An overview of epithelio-mesenchymal transformation. Acta Anat (Basel). 1995;154(1):8-20.

Hayashi H, Abdollah S, Qiu Y, Cai J, Xu YY, Grinnell BW, Richardson MA, Topper JN, Gimbrone MA Jr, Wrana JL, Falb D. The MAD-related protein Smad7 associates with the TGFbeta receptor and functions as an antagonist of TGFbeta signaling. Cell. 1997 Jun 27;89(7):1165-73.

Hayes S, Chawla A, Corvera S. TGF beta receptor internalization into EEA1-enriched early endosomes: role in signaling to Smad2. J Cell Biol. 2002 Sep 30;158(7):1239-49.

Hayes SA, Huang X, Kambhampati S, Platanias LC, Bergan RC. p38 MAP kinase modulates SMAD-dependent changes in human prostate celladhesion. Oncogene. 2003 Jul 31;22(31):4841-50.

He W, Dorn DC, Erdjument-Bromage H, Tempst P, Moore MA, Massagué J. Hematopoiesis controlled by distinct TIF1gamma and Smad4 branches of the TGFbeta pathway. Cell. 2006 Jun 2;125(5):929-41.

Heldin CH, Miyazono K, ten Dijke P. TGF-beta signalling from cell membrane to nucleus through SMAD proteins. Nature. 1997 Dec 4;390(6659):465-71.

Herzer K, Ganten TM, Schulze-Bergkamen H, Grosse-Wilde A, Koschny R, Krammer PH, Walczak H. Transforming growth factor beta can mediate apoptosis via the expression of TRAIL in human hepatoma cells. Hepatology. 2005 Jul;42(1):183-92.

Hocevar BA, Howe PH. Mechanisms of TGF-beta-induced cell cycle arrest. Miner Electrolyte Metab. 1998;24(2-3):131-5.

Hocevar BA, Prunier C, Howe PH. Disabled-2 (Dab2) mediates transforming growth factor beta (TGFbeta)-stimulated fibronectin synthesis through TGFbeta-activated kinase 1 and activation of the JNK pathway. J Biol Chem. 2005 Jul 8;280(27):25920-7.

Hocevar BA, Smine A, Xu XX, Howe PH. The adaptor molecule Disabled-2 links the transforming growth factor beta receptors to the Smad pathway. EMBO J. 2001 Jun 1;20(11):2789-801.

Hoffmann A, Levchenko A, Scott ML, Baltimore D. The IkappaB-NF-kappaB signaling module: temporal control and selective gene activation. Science. 2002 Nov 8;298(5596):1241-5.

Holm TM, Habashi JP, Doyle JJ, Bedja D, Chen Y, van Erp C, Lindsay ME, Kim D, Schoenhoff F, Cohn RD, Loeys BL, Thomas CJ, Patnaik S, Marugan JJ, Judge DP, Dietz HC. Noncanonical TGFβ signaling contributes to aortic aneurysm progression in Marfan syndrome mice. Science. 2011 Apr 15;332(6027):358-61.

Hough C, Radu M, Doré JJ. Tgf-beta induced Erk phosphorylation of smad linker region regulates smad signaling. PLoS One. 2012;7(8):e42513.

Huang F, Chen YG. Regulation of TGF-β receptor activity. Cell Biosci. 2012 Mar 15;2:9.

Huang T, David L, Mendoza V, Yang Y, Villarreal M, De K, Sun L, Fang X, López-Casillas F, Wrana JL, Hinck AP. TGF-β signalling is mediated by two autonomously functioning TβRI:TβRII pairs. EMBO J. 2011 Apr 6;30(7):1263-76.

I

Inman GJ, Nicolás FJ, Callahan JF, Harling JD, Gaster LM, Reith AD, Laping NJ, Hill CS. SB-431542 is a potent and specific inhibitor of transforming growth factor-beta superfamily type I activin receptor-like kinase (ALK) receptors ALK4, ALK5, and ALK7. Mol Pharmacol. 2002a Jul;62(1):65-74.

Inman GJ, Nicolás FJ, Hill CS. Nucleocytoplasmic shuttling of Smads 2, 3, and 4 permits sensing of TGF-beta receptor activity. Mol Cell. 2002b Aug;10(2):283-94.

Itoh F, Divecha N, Brocks L, Oomen L, Janssen H, Calafat J, Itoh S, Dijke Pt Pt. The FYVE domain in Smad anchor for receptor activation (SARA) is sufficient for localization of SARA in early endosomes and regulates TGF-beta/Smad signalling. Genes Cells. 2002 Mar;7(3):321-31.

Itoh S, ten Dijke P. Negative regulation of TGF-beta receptor/Smad signal transduction. Curr Opin Cell Biol. 2007 Apr;19(2):176-84.

Iwata J, Hacia JG, Suzuki A, Sanchez-Lara PA, Urata M, Chai Y. Modulation of noncanonical TGF-β signaling prevents cleft palate in Tgfbr2 mutant mice. J Clin Invest. 2012 Mar;122(3):873-85.

Izzi L, Attisano L. Regulation of the TGFbeta signalling pathway by ubiquitin-mediated degradation. Oncogene. 2004 Mar 15;23(11):2071-8.

J

Javelaud D, Mauviel A. Crosstalk mechanisms between the mitogen-activated protein kinase pathways and SMAD signaling downstream of TGFβeta: implications for carcinogenesis. Oncogene. 2005 Aug 29;24(37):5742-50.

Jullien J, Gurdon J. Morphogen gradient interpretation by a regulated trafficking step during ligand-receptortransduction. Genes Dev. 2005 Nov 15;19(22):2682-94.

Jung SM, Lee JH, Park J, Oh YS, Lee SK, Park JS, Lee YS, Kim JH, Lee JY, Bae YS, Koo SH, Kim SJ, Park SH. Smad6 inhibits non-canonical TGF-β1 signalling by recruiting the deubiquitinase A20 to TRAF6. Nat Commun. 2013;4:2562.

K

Kamaraju AK, Roberts AB. Role of Rho/ROCK and p38 MAP kinase pathways in transforming growth factor-beta-mediated Smad-dependent growth inhibition of human breast carcinoma cells in vivo. J Biol Chem. 2005 Jan 14;280(2):1024-36.

Katsuno Y1, Lamouille S, Derynck R. TGF-β signaling and epithelial-mesenchymal transition in cancer progression. Curr Opin Oncol. 2013 Jan;25(1):76-84.

Kavsak P, Rasmussen RK, Causing CG, Bonni S, Zhu H, Thomsen GH, Wrana JL. Smad7 binds to Smurf2 to form an E3 ubiquitin ligase that targets the TGF beta receptor for degradation. Mol Cell. 2000 Dec;6(6):1365-75.

Keogh EJ & Pazzani MJ. Scaling up dynamic time warping for datamining applications. In Proceedings of the sixth ACM SIGKDD international conference on Knowledge discovery and data mining - New York, New York, USA: ACM Press. 2000 KDD ’00 pp 285–289.

Kim SG, Jong HS, Kim TY, Lee JW, Kim NK, Hong SH, Bang YJ. Transforming growth factor-beta 1 induces apoptosis through Fas ligand-independent activationof the Fas death pathway in human gastric SNU-620 carcinoma cells. Mol Biol Cell. 2004 Feb;15(2):420-34.

Kim SI, Kwak JH, Na HJ, Kim JK, Ding Y, Choi ME. Transforming growth factor-beta (TGF-beta1) activates TAK1 via TAB1-mediated autophosphorylation, independent of TGF-beta receptor kinase activity in mesangial cells. J Biol Chem. 2009 Aug 14;284(33):22285-96.

Kimura N, Matsuo R, Shibuya H, Nakashima K, Taga T. BMP2-induced apoptosis is mediated by activation of the TAK1-p38 kinase pathway that is negatively regulated by Smad6. J Biol Chem. 2000 Jun 9;275(23):17647-52.

Kolosova I, Nethery D, Kern JA. Role of Smad2/3 and p38 MAP kinase in TGF-β1-induced epithelial-mesenchymal transition of pulmonary epithelial cells. J Cell Physiol. 2011 May;226(5):1248-54.

Komuro A, Imamura T, Saitoh M, Yoshida Y, Yamori T, Miyazono K, Miyazawa K. Negative regulation of transforming growth factor-beta (TGF-beta) signaling by WW domain-containing protein 1 (WWP1). Oncogene. 2004 Sep 9;23(41):6914-23.

Koskinen PJ, Sistonen L, Bravo R, Alitalo K. Immediate early gene responses of NIH 3T3 fibroblasts and NMuMG epithelial cells to TGF beta-1. Growth Factors. 1991;5(4):283-93.

Kretzschmar M, Doody J, Massagué J. Opposing BMP and EGF signalling pathways converge on the TGF-beta family mediator Smad1. Nature. 1997 Oct 9;389(6651):618-22.

Kretzschmar M, Doody J, Timokhina I, Massagué J. A mechanism of repression of TGFbeta/ Smad signaling by oncogenic Ras. Genes Dev. 1999 Apr 1;13(7):804-16.

Kudo T, Jeknić S, Macklin DN, Akhter S, Hughey JJ, Regot S, Covert MW. Live-cell measurements of kinase activity in single cells using translocation reporters. Nat Protoc. 2018 Jan;13(1):155-169

Kuma Y, Sabio G, Bain J, Shpiro N, Márquez R, Cuenda A. BIRB796 inhibits all p38 MAPK isoforms in vitro and in vivo. J Biol Chem. 2005 May 20;280(20):19472-9.

Kume S, Haneda M, Kanasaki K, Sugimoto T, Araki S, Isshiki K, Isono M, Uzu T, Guarente L, Kashiwagi A, Koya D. SIRT1 inhibits transforming growth factor beta-induced apoptosis in glomerular mesangial cells via Smad7 deacetylation. J Biol Chem. 2007 Jan 5;282(1):151-8.

Kuratomi G, Komuro A, Goto K, Shinozaki M, Miyazawa K, Miyazono K, Imamura T. NEDD4-2 (neural precursor cell expressed, developmentally down-regulated 4-2) negativelyregulates TGF-beta

(transforming growth factor-beta) signalling by inducing ubiquitin-mediateddegradation of Smad2 and TGF-beta type I receptor. Biochem J. 2005 Mar 15;386(Pt 3):461-70.

L

Lahav G, Rosenfeld N, Sigal A, Geva-Zatorsky N, Levine AJ, Elowitz MB, Alon U. Dynamics of the p53-Mdm2 feedback loop in individual cells. Nat Genet. 2004 Feb;36(2):147-50.

Lammers T, Lavi S. Role of type 2C protein phosphatases in growth regulation and in cellular stress signaling. Crit Rev Biochem Mol Biol. 2007 Nov-Dec;42(6):437-61.

Lee DH, Goldberg AL. Proteasome inhibitors: valuable new tools for cell biologists. Trends Cell Biol. 1998 Oct;8(10):397-403.

Lee J, Choi JH, Joo CK. TGF-β1 regulates cell fate during epithelial-mesenchymal transition by upregulating survivin. Cell Death Dis. 2013 Jul 4;4:e714.

Lee MK, Pardoux C, Hall MC, Lee PS, Warburton D, Qing J, Smith SM, Derynck R. TGF-beta activates Erk MAP kinase signalling through direct phosphorylation of ShcA. EMBO J. 2007 Sep 5;26(17):3957-67.

Lee PS, Chang C, Liu D, Derynck R. Sumoylation of Smad4, the common Smad mediator of transforming growth factor-beta familysignaling. J Biol Chem. 2003 Jul 25;278(30):27853-63.

Lee TK, Denny EM, Sanghvi JC, Gaston JE, Maynard ND, Hughey JJ, Covert MW. A noisy paracrine signal determines the cellular NF-kappaB response to lipopolysaccharide. Sci Signal. 2009 Oct 20;2(93):ra65.

Lehmann K, Janda E, Pierreux CE, Rytömaa M, Schulze A, McMahon M, Hill CS, Beug H, Downward J. Raf induces TGFbeta production while blocking its apoptotic but not invasive responses: a mechanism leading to increased malignancy in epithelial cells. Genes Dev. 2000 Oct 15;14(20):2610-22.

Leivonen SK, Chantry A, Hakkinen L, Han J, Kahari VM. Smad3 mediates transforming growth factor-beta-induced collagenase-3 (matrix metalloproteinase-13) expression in human gingival fibroblasts. Evidence for cross-talk between Smad3 and p38 signaling pathways. J Biol Chem. 2002 Nov 29;277(48):46338-46.

Lestas I, Vinnicombe G, Paulsson J. Fundamental limits on the suppression of molecular fluctuations. Nature. 2010 Sep 9;467(7312):174-8.

Lev Bar-Or R, Maya R, Segel LA, Alon U, Levine AJ, Oren M. Generation of oscillations by the p53-Mdm2 feedback loop: a theoretical and experimental study. Proc Natl Acad Sci U S A. 2000 Oct 10;97(21):11250-5.

Li MO, Flavell RA. Contextual regulation of inflammation: a duet by transforming growth factor-beta and interleukin-10. Immunity. 2008 Apr;28(4):468-76.

Li L, Xin H, Xu X, Huang M, Zhang X, Chen Y, Zhang S, Fu XY, Chang Z. CHIP mediates degradation of Smad proteins and potentially regulates Smad-inducedtranscription. Mol Cell Biol. 2004 Jan;24(2):856-64.

Li R, Gong Z, Pan C, Xie DD, Tang JY, Cui M, Xu YF, Yao W, Pang Q, Xu ZG, Li MY, Yu X, Sun JP. Metal-dependent protein phosphatase 1A functions as an extracellular signal-regulated kinase phosphatase. FEBS J. 2013 Jun;280(11):2700-11.

Li TF, Gao L, Sheu TJ, Sampson ER, Flick LM, Konttinen YT, Chen D, Schwarz EM, Zuscik MJ, Jonason JH, O'Keefe RJ. Aberrant hypertrophy in SMAD3-deficient murine chondrocytes is rescued by restoring transforming growth factor beta-activated kinase 1/activating transcription factor 2 signaling: a potential clinical implication for osteoarthritis. Arthritis Rheum. 2010 Aug;62(8):2359-69.

Lin X, Duan X, Liang YY, Su Y, Wrighton KH, Long J, Hu M, Davis CM, Wang J, Brunicardi FC, Shi Y, Chen YG, Meng A, Feng XH. PPM1A functions as a Smad phosphatase to terminate TGFbeta signaling. Cell. 2006 Jun 2;125(5):915-28.

Lin X, Liang M, Feng XH. Smurf2 is a ubiquitin E3 ligase mediating proteasome-dependent degradation of Smad2 in transforming growth factor-beta signaling. J Biol Chem. 2000 Nov 24;275(47):36818-22.

Liu F, Pouponnot C, Massagué J. Dual role of the Smad4/DPC4 tumor suppressor in TGFbeta-inducible transcriptional complexes. Genes Dev. 1997 Dec 1;11(23):3157-67.

Liu Q, Zhang Y, Mao H, Chen W, Luo N, Zhou Q, Chen W, Yu X. A crosstalk between the Smad and JNK signaling in the TGF-β-induced epithelial-mesenchymal transition in rat peritoneal mesothelial cells. PLoS One. 2012;7(2):e32009.

Liu X, Sun Y, Weinberg RA, Lodish HF. Ski/Sno and TGF-beta signaling. Cytokine Growth Factor Rev. 2001 Mar;12(1):1-8.

Lo RS, Massagué J. Ubiquitin-dependent degradation of TGF-beta-activated smad2. Nat Cell Biol. 1999 Dec;1(8):472-8.

Loewer A, Lahav G. We are all individuals: causes and consequences of non-genetic heterogeneity in mammalian cells. Curr Opin Genet Dev. 2011 Dec;21(6):753-8.

Louzao MC, Vieytes MR, Botana LM. Effect of okadaic acid on glucose regulation. Mini Rev Med Chem. 2005 Feb;5(2):207-15.

Lu G, Wang Y. Functional diversity of mammalian type 2C protein phosphatase isoforms: new tales from an oldfamily. Clin Exp Pharmacol Physiol. 2008 Feb;35(2):107-12.

Lu Z, Murray JT, Luo W, Li H, Wu X, Xu H, Backer JM, Chen YG. Transforming growth factor beta activates Smad2 in the absence of receptor endocytosis. J Biol Chem. 2002 Aug 16;277(33):29363-8.

Lu Z, Xu S. ERK1/2 MAP kinases in cell survival and apoptosis. IUBMB Life. 2006 Nov;58(11):621-31.

Luo K, Stroschein SL, Wang W, Chen D, Martens E, Zhou S, Zhou Q. The Ski oncoprotein interacts with the Smad proteins to repress TGFbeta signaling. Genes Dev. 1999 Sep 1;13(17):2196-206.

Lutz M, Knaus P. Integration of the TGF-beta pathway into the cellular signalling network. Cell Signal. 2002 Dec;14(12):977-88.

M

Ma FY, Tesch GH, Ozols E, Xie M, Schneider MD, Nikolic-Paterson DJ. TGF-β1-activated kinase-1 regulates inflammation and fibrosis in the obstructed kidney. Am J Physiol Renal Physiol. 2011 Jun;300(6):F1410-21.

Macia E, Ehrlich M, Massol R, Boucrot E, Brunner C, Kirchhausen T. Dynasore, a cell-permeable inhibitor of dynamin. Dev Cell. 2006 Jun;10(6):839-50.

Marko NF, Quackenbush J, Weil RJ. Why is there a lack of consensus on molecular subgroups of glioblastoma? Understanding the nature of biological and statistical variability in glioblastoma expression data. PLoS One. 2011;6(7):e20826.

Marshall CJ. Specificity of receptor tyrosine kinase signaling: transient versus sustained extracellular signal-regulated kinase activation. Cell. 1995 Jan 27;80(2):179-85.

Marshall WF. Origins of cellular geometry. BMC Biol. 2011 Aug 31;9:57.

Maryu G, Miura H, Uda Y, Komatsubara AT, Matsuda M, Aoki K. Live-cell Imaging with Genetically Encoded Protein Kinase Activity Reporters. Cell Struct Funct. 2018 Apr 25;43(1):61-74.

Massagué J, Blain SW, Lo RS. TGFbeta signaling in growth control, cancer, and heritable disorders. Cell. 2000 Oct 13;103(2):295-309.

Massagué J, Chen YG. Controlling TGF-beta signaling. Genes Dev. 2000 Mar 15;14(6):627-44.

Massagué J. TGFbeta in Cancer. Cell. 2008 Jul 25;134(2):215-30.

Massagué J. TGF-beta signal transduction. Annu Rev Biochem. 1998;67:753-91.

Matsuzaki K, Kitano C, Murata M, Sekimoto G, Yoshida K, Uemura Y, Seki T, Taketani S, Fujisawa J, Okazaki K. Smad2 and Smad3 phosphorylated at both linker and COOH-terminal regions transmit malignantTGF-beta signal in later stages of human colorectal cancer. Cancer Res. 2009 Jul 1;69(13):5321-30.

Mazars A, Lallemand F, Prunier C, Marais J, Ferrand N, Pessah M, Cherqui G, Atfi A. Evidence for a role of the JNK cascade in Smad7-mediated apoptosis. J Biol Chem. 2001 Sep 28;276(39):36797-803.

McPherson PS, Kay BK, Hussain NK. Signaling on the endocytic pathway. Traffic. 2001 Jun;2(6):375-84.

Melke P, Jönsson H, Pardali E, ten Dijke P, Peterson C. A rate equation approach to elucidate the kinetics and robustness of the TGF-beta pathway. Biophys J. 2006 Dec 15;91(12):4368-80. Epub 2006 Sep 29.

Meyer C, Godoy P, Bachmann A, Liu Y, Barzan D, Ilkavets I, Maier P, Herskind C, Hengstler JG, Dooley S. Distinct role of endocytosis for Smad and non-Smad TGF-β signaling regulation in hepatocytes. J Hepatol. 2011 Aug;55(2):369-78.

Mitchell H, Choudhury A, Pagano RE, Leof EB. Ligand-dependent and -independent transforming growth factor-beta receptor recycling regulatedby clathrin-mediated endocytosis and Rab11. Mol Biol Cell. 2004 Sep;15(9):4166-78.

Moorhead GB, Trinkle-Mulcahy L, Ulke-Lemée A. Emerging roles of nuclear protein phosphatases. Nat Rev Mol Cell Biol. 2007 Mar;8(3):234-44.

Morén A, Imamura T, Miyazono K, Heldin CH, Moustakas A. Degradation of the tumor suppressor Smad4 by WW and HECT domain ubiquitin ligases. J Biol Chem. 2005 Jun 10;280(23):22115-23.

Moustakas A, Heldin CH. Non-Smad TGF-beta signals. J Cell Sci. 2005 Aug 15;118(Pt 16):3573-84.

Moustakas A, Pardali K, Gaal A, Heldin CH. Mechanisms of TGF-beta signaling in regulation of cell growth and differentiation. Immunol Lett. 2002 Jun 3;82(1-2):85-91.

Murphy LO, MacKeigan JP, Blenis. A network of immediate early gene products propagates subtle differences in mitogen-activatedprotein kinase signal amplitude and duration. Mol Cell Biol. 2004 Jan;24(1):144-53.

Murphy LO, Smith S, Chen RH, Fingar DC, Blenis J. Molecular interpretation of ERK signal duration by immediate early gene products. Nat Cell Biol. 2002 Aug;4(8):556-64.

N

Naber HP, Drabsch Y, Snaar-Jagalska BE, ten Dijke P, van Laar T. Snail and Slug, key regulators of TGF-β-induced EMT, are sufficient for the induction of single-cell invasion. Biochem Biophys Res Commun. 2013 May 24;435(1):58-63.

Nakao A, Afrakhte M, Morén A, Nakayama T, Christian JL, Heuchel R, Itoh S, Kawabata M, Heldin NE, Heldin CH, ten Dijke P. Identification of Smad7, a TGFbeta-inducible antagonist of TGF-beta signalling. Nature. 1997 Oct 9;389(6651):631-5.

Nallet-Staub F, Yin X, Gilbert C, Marsaud V, Ben Mimoun S, Javelaud D, Leof EB, Mauviel A. Cell density sensing alters TGF-β signaling in a cell-type-specific manner, independent from Hippo pathway activation. Dev Cell. 2015 Mar 9;32(5):640-51.

Nankoe SR, Sever S. Dynasore puts a new spin on dynamin: a surprising dual role during vesicle formation. Trends Cell Biol. 2006 Dec;16(12):607-9.

Nelson DE, Ihekwaba AE, Elliott M, Johnson JR, Gibney CA, Foreman BE, Nelson G, See V, Horton CA, Spiller DG, Edwards SW, McDowell HP, Unitt JF, Sullivan E, Grimley R, Benson N, Broomhead D, Kell

DB, White MR. Oscillations in NF-kappaB signaling control the dynamics of gene expression. Science. 2004 Oct 22;306(5696):704-8.

Nicolás FJ, De Bosscher K, Schmierer B, Hill CS. Analysis of Smad nucleocytoplasmic shuttling in living cells. J Cell Sci. 2004 Aug 15;117(Pt 18):4113-25.

Nicolas FJ, Hill CS. Attenuation of the TGF-beta-Smad signaling pathway in pancreatic tumor cells confers resistance to TGF-beta-induced growth arrest. Oncogene. 2003;22:3698–711.

O

Oft M, Peli J, Rudaz C, Schwarz H, Beug H, Reichmann E. TGF-beta1 and Ha-Ras collaborate in modulating the phenotypic plasticity and invasiveness of epithelial tumor cells. Genes Dev. 1996 Oct 1;10(19):2462-77.

Ohshima T, Shimotohno K. Transforming growth factor-beta-mediated signaling via the p38 MAP kinase pathway activates Smad-dependent transcription through SUMO-1 modification of Smad4. J Biol Chem. 2003 Dec 19;278(51):50833-42.

Olsson N, Piek E, Sundstrom M, ten Dijke P, Nilsson G. Transforming growth factor-beta-mediated mast cell migration depends on mitogen-activated protein kinase activity. Cell Signal 2001;13:483– 490.

Omori E, Matsumoto K, Zhu S, Smart RC, Ninomiya-Tsuji J. Ablation of TAK1 upregulates reactive oxygen species and selectively kills tumor cells. Cancer Res. 2010 Nov 1;70(21):8417-25.

Ono K, Ohtomo T, Ninomiya-Tsuji J, Tsuchiya M. A dominant negative TAK1 inhibits cellular fibrotic responses induced by TGF-beta. Biochem Biophys Res Commun. 2003 Jul 25;307(2):332-7.

Owen RD, Ostrowski MC. Transcriptional activation of a conserved sequence element by ras requires a nuclear factordistinct from c-fos or c-jun. Proc Natl Acad Sci U S A. 1990 May;87(10):3866-70.

P

Padovan-Merhar O, Nair GP, Biaesch AG, Mayer A, Scarfone S, Foley SW, Wu AR, Churchman LS, Singh A, Raj A. Single mammalian cells compensate for differences in cellular volume and DNA copy numberthrough independent global transcriptional mechanisms. Mol Cell. 2015 Apr 16;58(2):339-52.

Padua D, Massagué J. Roles of TGFbeta in metastasis. Cell Res. 2009 Jan;19(1):89-102.

Paek AL, Liu JC, Loewer A, Forrester WC, Lahav G. Cell-to-Cell Variation in p53 Dynamics Leads to Fractional Killing. Cell. 2016 Apr 21;165(3):631-42.

Panopoulou E, Gillooly DJ, Wrana JL, Zerial M, Stenmark H, Murphy C, Fotsis T. Early endosomal regulation of Smad-dependent signaling in endothelial cells. J Biol Chem. 2002 May 17;277(20):18046-52.

Pargellis C, Tong L, Churchill L, Cirillo PF, Gilmore T, Graham AG, Grob PM, Hickey ER, Moss N, Pav S, Regan J. Inhibition of p38 MAP kinase by utilizing a novel allosteric binding site. Nat Struct Biol. 2002 Apr;9(4):268-72.

Pedraza JM, Paulsson J. Effects of molecular memory and bursting on fluctuations in gene expression. Science. 2008 Jan 18;319(5861):339-43.

Peinado H, Quintanilla M, Cano A. Transforming growth factor beta-1 induces snail transcription factor in epithelial cell lines: mechanisms for epithelial mesenchymal transitions. J Biol Chem. 2003 Jun 6;278(23):21113-23.

Penheiter SG, Mitchell H, Garamszegi N, Edens M, Doré JJ Jr, Leof EB. Internalization-dependent and -independent requirements for transforming growth factor betareceptor signaling via the Smad pathway. Mol Cell Biol. 2002 Jul;22(13):4750-9.

Perlman R, Schiemann WP, Brooks MW, Lodish HF, Weinberg RA. TGF-beta-induced apoptosis is mediated by the adapter protein Daxx that facilitates JNK activation. Nat Cell Biol. 2001 Aug;3(8):708-14.

Piek E, Moustakas A, Kurisaki A, Heldin CH, ten Dijke P. TGF-(beta) type I receptor/ALK-5 and Smad proteins mediate epithelial to mesenchymal transdifferentiation in NMuMG breast epithelial cells. J Cell Sci. 1999 Dec;112 (Pt 24):4557-68.

Pierreux CE, Nicolás FJ, Hill CS. Transforming growth factor beta-independent shuttling of Smad4 between the cytoplasm and nucleus. Mol Cell Biol. 2000 Dec;20(23):9041-54.

Purvis JE, Karhohs KW, Mock C, Batchelor E, Loewer A, Lahav G. p53 dynamics control cell fate. Science. 2012 Jun 15;336(6087):1440-4.

Purvis JE, Lahav G. Encoding and decoding cellular information through signaling dynamics. Cell. 2013 Feb 28;152(5):945-56.

Q

Qing J, Zhang Y, Derynck R. Structural and functional characterization of the transforming growth factor-beta -inducedSmad3/c-Jun transcriptional cooperativity. J Biol Chem. 2000 Dec 8;275(49):38802-12.

R

Rafelski SM, Marshall WF. Building the cell: design principles of cellular architecture. Nat Rev Mol Cell Biol. 2008 Aug;9(8):593-602.

Raj A, Tyagi S. Detection of individual endogenous RNA transcripts in situ using multiple singly labeled probes. Methods Enzymol. 2010;472:365-86.

Ran FA, Hsu PD, Wright J, Agarwala V, Scott DA, Zhang F. Genome engineering using the CRISPR-Cas9 system. Nat Protoc. 2013 Nov;8(11):2281-2308.

Reddy CC, Wells A, Lauffenburger DA. Receptor-mediated effects on ligand availability influence relative mitogenic potencies of epidermal growth factor and transforming growth factor alpha. J Cell Physiol. 1996 Mar;166(3):512-22.

Regot S, Hughey JJ, Bajar BT, Carrasco S, Covert MW. High-sensitivity measurements of multiple kinase activities in live single cells. Cell. 2014 Jun 19;157(7):1724-34.

Reynisdóttir I, Polyak K, Iavarone A, Massagué J. Kip/Cip and Ink4 Cdk inhibitors cooperate to induce cell cycle arrest in response to TGF-beta. Genes Dev. 1995 Aug 1;9(15):1831-45.

Rickert P, Corden JL, Lees E. Cyclin C/CDK8 and cyclin H/CDK7/p36 are biochemically distinct CTD kinases. Oncogene. 1999 Jan 28;18(4):1093-102.

Rogers KW, Schier AF. Morphogen gradients: from generation to interpretation. Annu Rev Cell Dev Biol. 2011;27:377-407.

Rojas A, Padidam M, Cress D, Grady WM. TGF-beta receptor levels regulate the specificity of signaling pathway activation and biologicaleffects of TGF-beta. Biochim Biophys Acta. 2009 Jul;1793(7):1165-73.

Rousseeuw PJ. Silhouettes: A graphical aid to the interpretation and validation of cluster analysis. J. Comput. Appl. Math. 1987 20: 53–65

Ruden DM, Garfinkel MD, Sollars VE, Lu X. Waddington's widget: Hsp90 and the inheritance of acquired characters. Semin Cell Dev Biol. 2003 Oct;14(5):301-10.

Runyan CE, Schnaper HW, Poncelet AC. The role of internalization in transforming growth factor beta1-induced Smad2 association with Smad anchor for receptor activation (SARA) and Smad2-dependent signaling in human mesangialcells. J Biol Chem. 2005 Mar 4;280(9):8300-8. Epub 2004 Dec 21.

S

Saha D, Datta PK, Beauchamp RD. Oncogenic ras represses transforming growth factor-beta /Smad signaling by degrading tumor suppressor Smad4. J Biol Chem. 2001 Aug 3;276(31):29531-7.

Sakaue-Sawano A, Kurokawa H, Morimura T, Hanyu A, Hama H, Osawa H, Kashiwagi S, Fukami K, Miyata T, Miyoshi H, Imamura T, Ogawa M, Masai H, Miyawaki A. Visualizing spatiotemporal dynamics of multicellular cell-cycle progression. Cell. 2008 Feb 8;132(3):487-98.

Sakoe H, Chiba S. Dynamic programming algorithm optimization for spoken word recognition. IEEE Trans Acoust Speech Signal Process. 1978 26: 43 – 49

Sang-Oh Yoon, Sejeong Shin, Yuzhen Liu, Bryan A. Ballif, Michele S. Woo, Steven P. Gygi, and John Blenis. Ran-binding protein 3 phosphorylation links the Ras and PI3-kinase pathways to nucleocytoplasmic transport. Mol Cell. 2008 Feb 15; 29(3): 362–375.

Sano Y, Harada J, Tashiro S, Gotoh-Mandeville R, Maekawa T, Ishii S. ATF-2 is a common nuclear target of Smad and TAK1 pathways in transforming growth factor-betasignaling. J Biol Chem. 1999 Mar 26;274(13):8949-57.

Sapkota GP. The TGFβ-induced phosphorylation and activation of p38 mitogen-activated protein kinase is mediated by MAP3K4 and MAP3K10 but not TAK1. Open Biol. 2013 Jun 12;3(6):130067.

Schmierer B, Hill CS. Kinetic analysis of Smad nucleocytoplasmic shuttling reveals a mechanism for transforminggrowth factor beta-dependent nuclear accumulation of Smads. Mol Cell Biol. 2005 Nov;25(22):9845-58.

Schmierer B, Hill CS. TGFbeta-SMAD signal transduction: molecular specificity and functional flexibility. Nat Rev Mol Cell Biol. 2007 Dec;8(12):970-82.

Schmierer B, Tournier AL, Bates PA, Hill CS. Mathematical modeling identifies Smad nucleocytoplasmic shuttling as a dynamic signal-interpreting system. Proc Natl Acad Sci U S A. 2008 May 6;105(18):6608-13.

Schoeberl B, Eichler-Jonsson C, Gilles ED, Müller G. Computational modeling of the dynamics of the MAP kinase cascade activated by surface and internalized EGF receptors. Nat Biotechnol. 2002 Apr;20(4):370-5.

Selimkhanov J, Taylor B, Yao J, Pilko A, Albeck J, Hoffmann A, Tsimring L, Wollman R. Systems biology. Accurate information transmission through dynamic biochemical signaling networks. Science. 2014 Dec 12;346(6215):1370-3.

Seo SR, Lallemand F, Ferrand N, Pessah M, L'Hoste S, Camonis J, Atfi A. The novel E3 ubiquitin ligase Tiul1 associates with TGIF to target Smad2 for degradation. EMBO J. 2004 Oct 1;23(19):3780-92.

Shalem O, Sanjana NE, Hartenian E, Shi X, Scott DA, Mikkelson T, Heckl D, Ebert BL, Root DE, Doench JG, Zhang F. Genome-scale CRISPR-Cas9 knockout screening in human cells. Science. 2014 Jan 3;343(6166):84-87.

Shankaran H, Ippolito DL, Chrisler WB, Resat H, Bollinger N, Opresko LK, Wiley HS. Rapid and sustained nuclear-cytoplasmic ERK oscillations induced by epidermal growth factor. Mol Syst Biol. 2009;5:332.

Shi W, Sun C, He B, Xiong W, Shi X, Yao D, Cao X. GADD34-PP1c recruited by Smad7 dephosphorylates TGFbeta type I receptor. J Cell Biol. 2004 Jan 19;164(2):291-300.

Shi Y, Massagué J. Mechanisms of TGF-beta signaling from cell membrane to the nucleus. Cell. 2003 Jun 13;113(6):685-700.

Shi Y, Wang YF, Jayaraman L, Yang H, Massagué J, Pavletich NP. Crystal structure of a Smad MH1 domain bound to DNA: insights on DNA binding in TGF-beta signaling. Cell. 1998 Sep 4;94(5):585-94.

Shi Y. Serine/threonine phosphatases: mechanism through structure. Cell. 2009 Oct 30;139(3):468-84.

Shibuya H, Iwata H, Masuyama N, Gotoh Y, Yamaguchi K, Irie K, Matsumoto K, Nishida E, Ueno N. Role of TAK1 and TAB1 in BMP signaling in early Xenopus development. EMBO J. 1998 Feb 16;17(4):1019-28.

Shioda T, Lechleider RJ, Dunwoodie SL, Li H, Yahata T, de Caestecker MP, Fenner MH, Roberts AB, Isselbacher KJ. Transcriptional activating activity of Smad4: roles of SMAD hetero-oligomerization and enhancement by an associating transactivator. Proc Natl Acad Sci U S A. 1998 Aug 18;95(17):9785-90.

Shi-wen X, Parapuram SK, Pala D, Chen Y, Carter DE, Eastwood M, Denton CP, Abraham DJ, Leask A. Requirement of transforming growth factor beta-activated kinase 1 for transforming growth factor beta-induced alpha-smooth muscle actin expression and extracellular matrix contraction in fibroblasts. Arthritis Rheum. 2009 Jan;60(1):234-41.

Shook D, Keller R. Mechanisms, mechanics and function of epithelial-mesenchymal transitions in early development. Mech Dev. 2003 Nov;120(11):1351-83.

Shukla MN, Rose JL, Ray R, Lathrop KL, Ray A, Ray P. Hepatocyte growth factor inhibits epithelial to myofibroblast transition in lung cells via Smad7. Am J Respir Cell Mol Biol. 2009 Jun;40(6):643-53.

Siegel PM, Massagué J. Cytostatic and apoptotic actions of TGF-beta in homeostasis and cancer. Nat Rev Cancer. 2003 Nov;3(11):807-21.

Simeone DM, Zhang L, Graziano K, Nicke B, Pham T, Schaefer C, Logsdon CD. Smad4 mediates activation of mitogen-activated protein kinases by TGF-beta in pancreatic acinarcells. Am J Physiol Cell Physiol. 2001 Jul;281(1):C311-9.

Simonsson M, Heldin CH, Ericsson J, Grönroos E. The balance between acetylation and deacetylation controls Smad7 stability. J Biol Chem. 2005 Jun 10;280(23):21797-803.

Snijder B, Pelkmans L. Origins of regulated cell-to-cell variability. Nat Rev Mol Cell Biol. 2011 Feb;12(2):119-25.

Snijder B, Sacher R, Rämö P, Damm EM, Liberali P, Pelkmans L. Population context determines cell-to-cell variability in endocytosis and virus infection. Nature. 2009 Sep 24;461(7263):520-3.

Sorrentino A, Thakur N, Grimsby S, Marcusson A, von Bulow V, Schuster N, Zhang S, Heldin CH, Landström M. The type I TGF-beta receptor engages TRAF6 to activate TAK1 in a receptor kinase-independent manner. Nat Cell Biol. 2008 Oct;10(10):1199-207.

Soule HD, Maloney TM, Wolman SR, Peterson WD Jr, Brenz R, McGrath CM, Russo J, Pauley RJ, Jones RF, Brooks SC. Isolation and characterization of a spontaneously immortalized humanbreast epithelial cell line, MCF-10. Cancer Res. 1990 Sep 15;50(18):6075-86.

Spiller DG, Wood CD, Rand DA, White MR. Measurement of single-cell dynamics. Nature. 2010 Jun 10;465(7299):736-45.

Sporn MB. The early history of TGF-beta, and a brief glimpse of its future. Cytokine Growth Factor Rev. 2006 Feb-Apr;17(1-2):3-7.

Stamenkovic I. Matrix metalloproteinases in tumor invasion and metastasis. Semin Cancer Biol. 2000 Dec;10(6):415-33.

Stetler-Stevenson WG, Yu AE. Proteases in invasion: matrix metalloproteinases. Semin Cancer Biol. 2001 Apr;11(2):143-52.

Strasen J, Sarma U, Jentsch M, Bohn S, Sheng C, Horbelt D, Knaus P, Legewie S, Loewer A. Cell-specific responses to the cytokine TGFβ are determined by variability in protein levels. Mol Syst Biol. 2018 Jan 25;14(1):e7733.

Stroschein SL, Bonni S, Wrana JL, Luo K. Smad3 recruits the anaphase-promoting complex for ubiquitination and degradation of SnoN. Genes Dev. 2001 Nov 1;15(21):2822-36.

Stroschein SL, Wang W, Zhou S, Zhou Q, Luo K. Negative feedback regulation of TGF-beta signaling by the SnoN oncoprotein. Science. 1999 Oct 22;286(5440):771-4.

Strovel ET, Wu D, Sussman DJ. Protein phosphatase 2Calpha dephosphorylates axin and activates LEF-1-dependent transcription. J Biol Chem. 2000 Jan 28;275(4):2399-403.

Su Y, Zhang L, Gao X, Meng F, Wen J, Zhou H, Meng A, Chen YG. The evolutionally conserved activity of Dapper2 in antagonizing TGF-beta signaling. FASEB J. 2007 Mar;21(3):682-90

Subramaniam M, Harris SA, Oursler MJ, Rasmussen K, Riggs BL, Spelsberg TC. Identification of a novel TGF-beta-regulated gene encoding a putative zinc finger protein in human osteoblasts. Nucleic Acids Res. 1995 Dec 11;23(23):4907-12.

Sung MH, Salvatore L, De Lorenzi R, Indrawan A, Pasparakis M, Hager GL, Bianchi ME, Agresti A. Sustained oscillations of NF-kappaB produce distinct genome scanning and gene expressionprofiles. PLoS One. 2009 Sep 29;4(9):e7163.

T

Taipale J, Saharinen J, Keski-Oja J. Extracellular matrix-associated transforming growth factor-beta: role in cancer cell growth and invasion. Adv Cancer Res. 1998;75:87-134.

Tajima Y, Goto K, Yoshida M, Shinomiya K, Sekimoto T, Yoneda Y, Miyazono K, Imamura T. Chromosomal region maintenance 1 (CRM1)-dependent nuclear export of Smad ubiquitin regulatory factor 1 (Smurf1) is essential for negative regulation of transforming growth factor-beta signaling by Smad7. J Biol Chem. 2003 Mar 21;278(12):10716-21.

Takekawa M, Maeda T, Saito H. Protein phosphatase 2Calpha inhibits the human stress-responsive p38 and JNK MAPK pathways. EMBO J. 1998 Aug 17;17(16):4744-52.

Takekawa M, Tatebayashi K, Itoh F, Adachi M, Imai K, Saito H. Smad-dependent GADD45beta expression mediates delayed activation of p38 MAP kinase by TGF-beta. EMBO J. 2002 Dec 2;21(23):6473-82.

Tamura K, Fukuoka M. Gefitinib in non-small cell lung cancer. Expert Opin Pharmacother. 2005 Jun;6(6):985-93.

Tan Y, Xu Q, Li Y, Mao X, Zhang K. Crosstalk between the p38 and TGFβ signaling pathways through TβRI, TβRII and SMAD3 expression in plancental choriocarcinoma JEG-3 cells. Oncol Lett. 2014 Sep;8(3):1307-1311.

Tay S, Hughey JJ, Lee TK, Lipniacki T, Quake SR, Covert MW. Single-cell NF-kappaB dynamics reveal digital activation and analogue information processing. Nature. 2010 Jul 8;466(7303):267-71.

ten Dijke P, Hill CS. New insights into TGF-beta-Smad signalling. Trends Biochem Sci. 2004 May;29(5):265-73.

Tsukazaki T, Chiang TA, Davison AF, Attisano L, Wrana JL. SARA, a FYVE domain protein that recruits Smad2 to the TGFbeta receptor. Cell. 1998 Dec 11;95(6):779-91.

Tsunobuchi H, Ishisaki A, Imamura T. Expressions of inhibitory Smads, Smad6 and Smad7, are differentially regulated by TPA in human lung fibroblast cells. Biochem Biophys Res Commun. 2004 Apr 9;316(3):712-9.

U

Uchida K, Suzuki H, Ohashi T, Nitta K, Yumura W, Nihei H. Involvement of MAP kinase cascades in Smad7 transcriptional regulation. Biochem Biophys Res Commun. 2001 Nov 30;289(2):376-81.

Uda S, Saito TH, Kudo T, Kokaji T, Tsuchiya T, Kubota H, Komori Y, Ozaki Y, Kuroda S. Robustness and compensation of information transmission of signaling pathways. Science. 2013 Aug 2;341(6145):558-61.

Ulloa L, Doody J, Massagué J. Inhibition of transforming growth factor-beta/SMAD signalling by the interferon-gamma/STAT pathway. Nature. 1999 Feb 25;397(6721):710-3.

Ungefroren H, Lenschow W, Chen WB, Faendrich F, Kalthoff H. Regulation of biglycan gene expression by transforming growth factor-beta requires MKK6-p38mitogen-activated protein Kinase signaling downstream of Smad signaling. J Biol Chem. 2003 Mar 28;278(13):11041-9.

V

Valdimarsdottir G, Goumans MJ, Itoh F, Itoh S, Heldin CH, ten Dijke P. Smad7 and protein phosphatase 1alpha are critical determinants in the duration of TGF-beta/ALK1 signaling in endothelial cells. BMC Cell Biol. 2006 Mar 29;7:16.

van der Heide LP, van Dinther M, Moustakas A, ten Dijke P. TGFbeta activates mitogen- and stress-activated protein kinase-1 (MSK1) to attenuate cell death. J Biol Chem. 2011 Feb 18;286(7):5003-11.

Van Obberghen-Schilling E, Roche NS, Flanders KC, Sporn MB, Roberts AB. Transforming growth factor beta 1 positively regulates its own expression in normal and transformed cells. J Biol Chem. 1988 Jun 5;263(16):7741-6.

Vassilev LT. Cell cycle synchronization at the G2/M phase border by reversible inhibition of CDK1. Cell Cycle. 2006 Nov;5(22):2555-6.

Ventura JJ, Kennedy NJ, Flavell RA, Davis RJ. JNK regulates autocrine expression of TGF-beta1. Mol Cell. 2004 Jul 23;15(2):269-78.

Vert G, Chory J. Crosstalk in cellular signaling: background noise or the real thing? Dev Cell. 2011 Dec 13;21(6):985-91.

Virshup DM, Shenolikar S.From promiscuity to precision: protein phosphatases get a makeover. Mol Cell. 2009 Mar 13;33(5):537-45.

Vizán P, Miller DS, Gori I, Das D, Schmierer B, Hill CS. Controlling long-term signaling: receptor dynamics determine attenuation and refractory behavior of the TGF-β pathway. Sci Signal. 2013 Dec 10;6(305):ra106.

Voliotis M, Perrett RM, McWilliams C, McArdle CA, Bowsher CG. Information transfer by leaky, heterogeneous, protein kinase signaling systems. Proc Natl Acad Sci U S A. 2014 Jan 21;111(3):E326-33.

W

Waite KA, Eng C. From developmental disorder to heritable cancer: it's all in the BMP/TGF-beta family. Nat Rev Genet. 2003 Oct;4(10):763-73.

Wakefield LM, Roberts AB. TGF-beta signaling: positive and negative effects on tumorigenesis. Curr Opin Genet Dev. 2002 Feb;12(1):22-9.

Wakefield LM, Smith DM, Masui T, Harris CC, Sporn MB. Distribution and modulation of the cellular receptor for transforming growth factor-beta. J Cell Biol. 1987 Aug;105(2):965-75.

Walker RA, Dearing SJ. Transforming growth factor beta 1 in ductal carcinoma in situ and invasive carcinomas of the breast. Eur J Cancer. 1992;28(2-3):641-4.

Walsh MC, Kim GK, Maurizio PL, Molnar EE, Choi Y. TRAF6 autoubiquitination-independent activation of the NFkappaB and MAPK pathways in response to IL-1 and RANKL. PLoS One. 2008;3(12):e4064.

Wan Y, Liu X, Kirschner MW. The anaphase-promoting complex mediates TGF-beta signaling by targeting SnoN for destruction. Mol Cell. 2001 Nov;8(5):1027-39.

Wan M, Tang Y, Tytler EM, Lu C, Jin B, Vickers SM, Yang L, Shi X, Cao X. Smad4 protein stability is regulated by ubiquitin ligase SCF beta-TrCP1. J Biol Chem. 2004 Apr 9;279(15):14484-7.

Wang J, Tucker-Kellogg L2, Ng IC3, Jia R4, Thiagarajan PS5, White JK6, Yu H7. The self-limiting dynamics of TGF-β signaling in silico and in vitro, with negative feedback through PPM1A upregulation. PLoS Comput Biol. 2014 Jun 5;10(6):e1003573.

Wang T, Wei JJ, Sabatini DM, Lander ES. Genetic screens in human cells using the CRISPR-Cas9 system. Science. 2014 Jan 3;343(6166):80-4.

Wang W, Mariani FV, Harland RM, Luo K. Ski represses bone morphogenic protein signaling in Xenopus and mammalian cells. Proc Natl Acad Sci U S A. 2000 Dec 19;97(26):14394-9.

Wang X, Li X, Ye L, Chen W, Yu X. Smad7 inhibits TGF-β1-induced MCP-1 upregulation through a MAPK/p38 pathway in rat peritoneal mesothelial cells. Int Urol Nephrol. 2013 Jun;45(3):899-907.

Warmflash A, Zhang Q, Sorre B, Vonica A, Siggia ED, Brivanlou AH. Dynamics of TGF-β signaling reveal adaptive and pulsatile behaviors reflected in the nuclearlocalization of transcription factor Smad4. Proc Natl Acad Sci U S A. 2012 Jul 10;109(28):E1947-56.

Watkins SJ, Jonker L, Arthur HM. A direct interaction between TGFbeta activated kinase 1 and the TGFbeta type II receptor: implications for TGFbeta signalling and cardiac hypertrophy. Cardiovasc Res 2006;69:432–439.

Wegner K, Bachmann A, Schad JU, Lucarelli P, Sahle S, Nickel P, Meyer C, Klingmüller U, Dooley S, Kummer U. Dynamics and feedback loops in the transforming growth factor β signaling pathway. Biophys Chem. 2012 Mar;162:22-34.

Werner SL, Barken D, Hoffmann A. Stimulus specificity of gene expression programs determined by temporal control of IKK activity. Science. 2005 Sep 16;309(5742):1857-61.

Whitman M. Smads and early developmental signaling by the TGFbeta superfamily. Genes Dev. 1998 Aug 15;12(16):2445-62.

Wicks SJ, Haros K, Maillard M, Song L, Cohen RE, Dijke PT, Chantry A. The deubiquitinating enzyme UCH37 interacts with Smads and regulates TGF-beta signalling. Oncogene. 2005 Dec 1;24(54):8080-4.

Wilhelm SM, Carter C, Tang L, Wilkie D, McNabola A, Rong H, Chen C, Zhang X, Vincent P, McHugh M, Cao Y, Shujath J, Gawlak S, Eveleigh D, Rowley B, Liu L, Adnane L, Lynch M, Auclair D, Taylor I, Gedrich R, Voznesensky A, Riedl B, Post LE, Bollag G, Trail PA. BAY 43-9006 exhibits broad spectrum oral antitumor activity and targets the RAF/MEK/ERKpathway and receptor tyrosine kinases involved in tumor progression and angiogenesis. Cancer Res. 2004 Oct 1;64(19):7099-109.

Wrana JL, Attisano L, Wieser R, Ventura F, Massagué J. Mechanism of activation of the TGF-beta receptor. Nature. 1994 Aug 4;370(6488):341-7.

Wu G, Chen YG, Ozdamar B, Gyuricza CA, Chong PA, Wrana JL, Massagué J, Shi Y. Structural basis of Smad2 recognition by the Smad anchor for receptor activation. Science. 2000 Jan 7;287(5450):92-7.

Wu J, Powell F, Larsen NA, Lai Z, Byth KF, Read J, Gu RF, Roth M, Toader D, Saeh JC, Chen H. Mechanism and in vitro pharmacology of TAK1 inhibition by (5Z)-7-Oxozeaenol. ACS Chem Biol. 2013 Mar 15;8(3):643-50.

X

Xie L, Law BK, Chytil AM, Brown KA, Aakre ME, Moses HL. Activation of the Erk pathway is required for TGF-beta1-induced EMT in vitro. Neoplasia. 2004 Sep-Oct;6(5):603-10.

Xin H, Xu X, Li L, Ning H, Rong Y, Shang Y, Wang Y, Fu XY, Chang Z. CHIP controls the sensitivity of transforming growth factor-beta signaling by modulating the basal level of Smad3 through ubiquitin-mediated degradation. J Biol Chem. 2005 May 27;280(21):20842-50.

Xu L, Kang Y, Cöl S, Massagué J. Smad2 nucleocytoplasmic shuttling by nucleoporins CAN/Nup214 and Nup153 feeds TGFbetasignaling complexes in the cytoplasm and nucleus. Mol Cell. 2002 Aug;10(2):271-82.

Xu Q, Tan Y, Zhang K, Li Y. Crosstalk between p38 and SMAD3 through TGFβ1 in JEG-3 choriocarcinoma cells. Int J Oncol. 2013 Oct;43(4):1187-93.

Y

Yagi K, Goto D, Hamamoto T, Takenoshita S, Kato M, Miyazono K. Alternatively spliced variant of Smad2 lacking exon 3. Comparison with wild-type Smad2 and Smad3. J Biol Chem. 1999 Jan 8;274(2):703-9.

Yahata T, de Caestecker MP, Lechleider RJ, Andriole S, Roberts AB, Isselbacher KJ, Shioda T. The MSG1 non-DNA-binding transactivator binds to the p300/CBP coactivators, enhancing their functional link to the Smad transcription factors. J Biol Chem. 2000 Mar 24;275(12):8825-34.

Yamaguchi K, Shirakabe K, Shibuya H, Irie K, Oishi I, Ueno N, Taniguchi T, Nishida E, Matsumoto K. Identification of a member of the MAPKKK family as a potential mediator of TGF-beta signal transduction. Science. 1995 Dec 22;270(5244):2008-11.

Yamaguchi Y, Takagi T, Wada T, Yano K, Furuya A, Sugimoto S, Hasegawa J, Handa H. NELF, a multisubunit complex containing RD, cooperates with DSIF to repress RNA polymerase IIelongation. Cell. 1999 Apr 2;97(1):41-51.

Yamaguchi Y, Wada T, Handa H. Interplay between positive and negative elongation factors: drawing a new view of DRB. Genes Cells. 1998 Jan;3(1):9-15.

Yamashita M, Fatyol K, Jin C, Wang X, Liu Z, Zhang YE. TRAF6 mediates Smad-independent activation of JNK and p38 by TGF-beta. Mol Cell. 2008 Sep 26;31(6):918-24.

Yamashita M, Ying SX, Zhang GM, Li C, Cheng SY, Deng CX, Zhang YE. Ubiquitin ligase Smurf1 controls osteoblast activity and bone homeostasis by targeting MEKK2 for degradation. Cell. 2005 Apr 8;121(1):101-13.

Yan X, Liao H, Cheng M, Shi X, Lin X, Feng XH, Chen YG. Smad7 Protein Interacts with Receptor-regulated Smads (R-Smads) to Inhibit Transforming Growth Factor-β (TGF-β)/Smad Signaling. J Biol Chem. 2016 Jan 1;291(1):382-92.

Yan X, Liu Z, Chen Y. Regulation of TGF-beta signaling by Smad7. Acta Biochim Biophys Sin (Shanghai). 2009 Apr;41(4):263-72.

Yao J, Pilko A, Wollman R. Distinct cellular states determine calcium signaling response. Mol Syst Biol. 2016 Dec 15;12(12):894.

Yoo J, Ghiassi M, Jirmanova L, Balliet AG, Hoffman B, Fornace AJ Jr, Liebermann DA, Bottinger EP, Roberts AB. Transforming growth factor-beta-induced apoptosis is mediated by Smad-dependent expression of GADD45b through p38 activation. J Biol Chem. 2003 Oct 31;278(44):43001-7.

Yoon SO, Shin S, Liu Y, Ballif BA, Woo MS, Gygi SP, Blenis J. Ran-binding protein 3 phosphorylation links the Ras and PI3-kinase pathways to nucleocytoplasmic transport. Mol Cell. 2008 Feb 15;29(3):362-75.

Yoshizaki T, Maegawa H, Egawa K, Ugi S, Nishio Y, Imamura T, Kobayashi T, Tamura S, Olefsky JM, Kashiwagi A. Protein phosphatase-2C alpha as a positive regulator of insulin sensitivity through

directactivation of phosphatidylinositol 3-kinase in 3T3-L1 adipocytes. J Biol Chem. 2004 May 21;279(21):22715-26.

Yu L, Hébert MC, Zhang YE. TGFβeta receptor-activated p38 MAP kinase mediates SMAD-independent TGFβetaresponses. EMBO J. 2002 Jul 15;21(14):3749-59.

Yu PB, Deng DY, Lai CS, Hong CC, Cuny GD, Bouxsein ML, Hong DW, McManus PM, Katagiri T, Sachidanandan C, Kamiya N, Fukuda T, Mishina Y, Peterson RT, Bloch KD. BMP type I receptor inhibition reduces heterotopic [corrected] ossification. Nat Med. 2008a Dec;14(12):1363-9.

Yu PB, Hong CC, Sachidanandan C, Babitt JL, Deng DY, Hoyng SA, Lin HY, Bloch KD, Peterson RT. Dorsomorphin inhibits BMP signals required for embryogenesis and iron metabolism. Nat Chem Biol. 2008b Jan;4(1):33-41.

Yu Q, Stamenkovic I. Cell surface-localized matrix metalloproteinase-9 proteolytically activates TGF-beta and promotestumor invasion and angiogenesis. Genes Dev. 2000 Jan 15;14(2):163-76.

Yue J and Mulder KM. Activation of the mitogen-activated protein kinase pathway by transforming growth factor-b. Methods Mol. Biol. 2000a, 142, 125–131.

Yue J, Mulder KM. Requirement of Ras/MAPK pathway activation by transforming growth factor beta for transforming growth factor beta 1 production in a Smad-dependent pathway. J Biol Chem. 2000b Oct 6;275(40):30765-73.

Yue J, Sun B, Liu G, Mulder KM. Requirement of TGF-beta receptor-dependent activation of c-Jun N-terminal kinases(JNKs)/stress-activated protein kinases (Sapks) for TGF-beta up-regulation of the urokinase-typeplasminogen activator receptor. J Cell Physiol. 2004 May;199(2):284-92.

Yumoto K, Thomas PS, Lane J, Matsuzaki K, Inagaki M, Ninomiya-Tsuji J, Scott GJ, Ray MK, Ishii M, Maxson R, Mishina Y, Kaartinen V. TGF-β-activated kinase 1 (Tak1) mediates agonist-induced Smad activation and linker region phosphorylation in embryonic craniofacial neural crest-derived cells. J Biol Chem. 2013 May 10;288(19):13467-80.

Z

Zarubin T, Han J. Activation and signaling of the p38 MAP kinase pathway. Cell Res. 2005 Jan;15(1):11-8.

Zavadil J, Bitzer M, Liang D, Yang YC, Massimi A, Kneitz S, Piek E, Bottinger EP. Genetic programs of epithelial cell plasticity directed by transforming growth factor-beta. Proc Natl Acad Sci U S A. 2001 Jun 5;98(12):6686-91.

Zhang F, Laiho M. On and off: proteasome and TGF-beta signaling. Exp Cell Res. 2003 Dec 10;291(2):275-81.

Zhang M, Fraser D, Phillips A. ERK, p38, and SMAD signaling pathways differentially regulate transforming growthfactor-beta1 autoinduction in proximal tubular epithelial cells. Am J Pathol. 2006 Oct;169(4):1282-93.

Zhang S, Fei T, Zhang L, Zhang R, Chen F, Ning Y, Han Y, Feng XH, Meng A, Chen YG. Smad7 antagonizes transforming growth factor beta signaling in the nucleus by interfering with functional Smad-DNA complex formation. Mol Cell Biol. 2007 Jun;27(12):4488-99.

Zhang Y, Chang C, Gehling): ee Hemmati-Brivanlou A, Derynck R. Regulation of Smad degradation and activity by Smurf2, an E3 ubiquitin ligase. Proc Natl Acad Sci U S A. 2001 Jan 30;98(3):974-9.

Zhang Y, Feng XH, Derynck R. Smad3 and Smad4 cooperate with c-Jun/c-Fos to mediate TGF-beta-induced transcription. Nature. 1998 Aug 27;394(6696):909-13.

Zhang Y, Musci T, Derynck R. The tumor suppressor Smad4/DPC 4 as a central mediator of Smad function. Curr Biol. 1997 Apr 1;7(4):270-6.

Zhang Y, Derynck R. Regulation of Smad signalling by protein associations and signalling crosstalk. Trends Cell Biol. 1999 Jul;9(7):274-9.

Zhang YE. Non-Smad pathways in TGF-beta signaling. Cell Res. 2009 Jan;19(1):128-39.

Zheng J, Wang J, Sun X, Hao M, Ding T, Xiong D, Wang X, Zhu Y, Xiao G, Cheng G, Zhao M, Zhang J, Wang J. HIC1 modulates prostate cancer progression by epigenetic modification. Clin Cancer Res. 2013 Mar 15;19(6):1400-10.

Zhou X, Zheng M, Chen F, Zhu Y, Yong W, Lin H, Sun Y, Han X. Gefitinib inhibits the proliferation of pancreatic cancer cells via cell cycle arrest. Anat Rec (Hoboken). 2009 Aug;292(8):1122-7.

Zhou Y, Scolavino S, Funderburk SF, Ficociello LF, Zhang X, Klibanski A. Receptor internalization-independent activation of Smad2 in activin signaling. Mol Endocrinol. 2004 Jul;18(7):1818-26.

Zhu H, Kavsak P, Abdollah S, Wrana JL, Thomsen GH. A SMAD ubiquitin ligase targets the BMP pathway and affects embryonic pattern formation. Nature. 1999 Aug 12;400(6745):687-93.

Zi Z, Chapnick DA, Liu X. Dynamics of TGF-β/Smad signaling. FEBS Lett. 2012 Jul 4;586(14):1921-8.

Zi Z, Feng Z, Chapnick DA, Dahl M, Deng D, Klipp E, Moustakas A, Liu X. Quantitative analysis of transient and sustained transforming growth factor-β signaling dynamics. Mol Syst Biol. 2011 May 24;7:492.

Zi Z, Klipp E. Cellular signaling is potentially regulated by cell density in receptor trafficking networks. FEBS Lett. 2007a Oct 2;581(24):4589-95.

Zi Z, Klipp E. Constraint-based modeling and kinetic analysis of the Smad dependent TGF-beta signaling pathway. PLoS One. 2007b Sep 26;2(9):e936.

Zieba A, Pardali K, Söderberg O, Lindbom L, Nyström E, Moustakas A, Heldin CH, Landegren U. Intercellular variation in signaling through the TGF-β pathway and its relation to cell density and cell cycle phase. Mol Cell Proteomics. 2012 Jul;11(7):M111.013482.

Zuo W, Chen YG. Specific activation of mitogen-activated protein kinase by transforming growth factor-beta receptors in lipid rafts is required for epithelial cell plasticity. Mol Biol Cell. 2009 Feb;20(3):1020-9.

Zwaagstra JC, Kassam Z, O'Connor-Mccourt MD. Down-regulation of transforming growth factor-beta receptors: cooperativity between the types I, II, and III receptors and modulation at the cell surface. Exp Cell Res. 1999 Nov 1;252(2):352-62.

9 DECLARATION OF INDEPENDENT WORK

With this statement I declare, that I have independently completed the above thesis entitled with "Dynamics and variability of SMAD signaling in single cells- The activity of MAP kinases determines long-term dynamics of SMAD signaling".
The thoughts taken directly or indirectly from external sources are properly marked as such. This thesis was not previously submitted to another academic institution and has also not yet been published.

10 ACKNOWLEDGEMENT

Eine wissenschaftliche Arbeit ist nie das Werk einer einzelnen Person, deshalb möchte ich mich hier bei all denjenigen bedanken, die mir die Erstellung meiner Dissertation ermöglicht haben.

Mein erster und ganz besonderer Dank gilt Herrn Prof. Dr. Alexander Löwer, der mir dieses spannende Forschungsthema übergeben hat. Ich danke ihm für die engagierte Betreuung, für das Vertrauen, das er mir und meiner Arbeit stets entgegengebracht hat, für die Freiheiten in der Forschungsausrichtung, für die freundschaftliche Atmosphäre und für den stets regen und konstruktiven Ideenaustausch. Insbesondere danke ich ihm für die Möglichkeit an nationalen und internationalen Konferenzen teilnehmen zu können.

Weiterhin möchte ich mich bei Prof. Dr. Andreas Herrmann bedanken, der sich bereit erklärt hat mein Betreuer an der Humboldt Universität zu Berlin zu sein und ein Gutachten zu verfassen. Insbesondere möchte ich mich bedanken für seine unkomplizierte Art auch auf spontane Promotionsverlängerungen zu reagieren.

Weiterhin möchte ich mich beim MDC- Max Delbrück-Zentrum für molekulare Medizin in der Helmholtz-Gesellschaft und insbesondere dem BIMSB- the Berlin Institute for Medical Systems Biology für die herausragenden Möglichkeiten und Strukturen, die einen breiten Forschungsaustausch gefördert haben, bedanken.

Viele Menschen haben dazu beigetragen, dass die Dissertationszeit eine glückliche und wertvolle Zeitspanne für mich darstellt. Deshalb danke ich allen Kollegen und Freunden der Arbeitsgruppe Löwer für die wunderbare Zusammenarbeit und das harmonische Miteinander- Ana Finzel Pérez, Elena Cristiano, Dhana Friedrich, Caibin Sheng, Marcel Jentsch, Andrea Katzer, Gitta Blendinger, Silke Dusatko, Ilias Nolis und Felix Hoevelmann.
Derya Guenes und Lennart Schnirch danke ich für ihr Engagement und die hervorragende Zusammenarbeit im Rahmen ihrer Bachelorarbeiten, die ich betreuen durfte und deren Ergebnisse in diese Arbeit einflossen.
Ana und Elena danke ich im Besonderen für die einzigartige Atmosphäre, die wertvollen Diskussionen, die gegenseitige Unterstützung und die fantastische Zeit bei den Konferenzen.
Dhana danke ich vor allem für die wunderbare Einführung in die smFISH- Welt und ihrer lebhaften und inspirierenden Art.

Marcel danke ich für seine bioinformatorische Unterstützung, die erst so manche Analyse möglich gemacht hat.

Bei Dr. Stefan Legewie und Uddipan Sarma vom Institute of Molecular Biology (IMB) Mainz möchte ich mich für die wissenschaftliche Zusammenarbeit und das Erstellen eines Modells auf Grundlagen meiner Experimente danken. Weiterhin bedanke ich mich bei Dr. Daniel Horbelt und Prof Dr. Petra Knaus vom Institut für Chemie und Biochemie, Freie Universität Berlin, für die erfolreiche Zusammenarbeit beim TGFβ assay.

Mein ganz besonderer Dank gilt meinen Eltern Marion & Max, meiner Schwester Rike und meiner Omi & meinem Opi für die aufmerksame, liebevolle und vielseitige Unterstützung während dem Verfassen dieser Arbeit und während meines gesamten Biologiestudiums.

Allen Freunden danke ich für das in mich gesetzte Vertrauen, den neutralen Blick von außen und dafür, dass sie mir immer Mut gemacht haben. Insbesondere Bella, Anni und Mobi danke ich für die wunderbaren Ablenkungsabende, Ausflüge, das immer offene Ohr und eure Zeit für Flora.

Mein größter Dank aber gilt Mike, für seine uneingeschränkte Unterstützung, seine Liebe und Motivation. Besonders für die unzähligen Dissertationsschreibabende und Samstage, die er auf Flora aufgepasst hat, reicht kein Dankeswort aus.

Als letztes einen Dank an Flora für die wertvollste und wunderschönste Ablenkung beim Zusammenschreiben.